Influence of Geotechnical Properties on Sediment Dynamics, Erodibility, and Geomorphodynamics in Coastal Environments Based on Field Measurements

Nicola C. Brilli

Dissertation submitted to the faculty of the Virginia Polytechnic Institute and State University in partial fulfillment of the requirements for the degree of

Doctor of Philosophy
In
Civil Engineering

Nina Stark, Chair
Alba Yerro
Jennifer Irish
Emily Eidam

April 12th, 2023
Blacksburg, VA

Keywords: Geotechnical properties, erodibility, free-fall penetrometer, field measurement techniques, beaches, Arctic nearshore environments

Influence of Geotechnical Properties on Sediment Dynamics, Erodibility, and Geomorphodynamics in Coastal Environments Based on Field Measurements

Nicola C. Brilli

Academic Abstract

Geotechnical sediment properties such as moisture content, relative density, bearing capacity, and undrained shear strength have been discussed in the context of coastal sediment dynamics. However, these properties have rarely been assessed in their respective relevance or quantitatively related to sediment transport and erodibility. Also, to date there is no framework available for collecting direct measurements of these properties for estimating initiation of motion and erosion rates. Here, it is postulated that improving the ability to measure geotechnical sediment properties in energetic foreshore environments can improve our ability to predict coastal response to climate change. Through a series of field measurements, the research presented here (1) provides a framework for conducting geotechnical measurements of beaches, (2) advances portable free fall penetrometer (PFFP) data analysis in intertidal environments through the introduction of an impact velocity dependent strain-rate correction factor, (3) relates textural and sediment strength properties derived from PFFP measurements to an erosion rate parameter and hydrodynamically driven bed-level change, and (4) uses PFFP measurements to develop a sediment classification scheme in terms of soil behavior and erosion behavior for a mixed sediment type Arctic environment. Relationships between sediment properties other than grain size, most significantly void ratio, and erodibility parameters highlight the relevance of these measurements in geomorphodynamically active sandy beach environments. For the cohesive sediments in the Arctic, undrained shear strength was also related to an erosion rate parameter, allowing for a categorical framework for erodibility classification to be developed. The cohesive framework was combined with the relationships developed for sandy sediments and used to highlight areas of active sediment transport in the context of local morphodynamic and ice gouging processes. Finally, a simple case study showed how implementing in-situ erodibility parameters was important for long-term morphological modelling. The results represent a step forward in our ability to predict and mitigate climate change related issues from coastal erosion.

Influence of Geotechnical Properties on Sediment Dynamics, Erodibility, and Geomorphodynamics in Coastal Environments Based on Field Measurements

Nicola C. Brilli

General Audience Abstract

Climate change driven impacts on coastal environments include increasing frequency and severity of storms, coastal erosion, and inundation of populated areas. Specifically for Arctic environments, warming has caused more sediment to be introduced into coastal waters as well as accelerated rates of permafrost melting and shoreline retreat and decreases in sea ice. One aspect of understanding how these changes will continue to affect coastal communities and our ability to predict climate change effects is understanding the role of sediment properties on sediment erosion and shoreline change. Physical and geomechanical (strength) properties of coastal sediments are important for a variety of coastal applications but have rarely been investigated in the context of quantifying, predicting, and assessing erosion, specifically in the context of field measurements.

Towards this end, a series of field surveys were conducted along the coast of North Carolina at a sandy beach, and in Harrison Bay, Alaska, an Arctic coastal zone with both sandy and muddy sediments. Tools for taking physical samples of the beach and seabed, measuring the sediment strength, among other properties in place were used to characterize the local sediments. Once a framework was developed for characterizing the type of sediment, the measured properties were then related to measurements of erosion rate from a series of laboratory experiments performed on physical samples taken from the sites. Finally, one of the instruments for measuring sediment strength both on land and in the water was used to develop classification schemes for seabed sediments in terms of their erodibility.

The results of this work highlight the importance of geotechnical properties for coastal sediment transport processes, reveal new relationships between sediment properties and properties quantifying erosion behavior, and offer a framework for future research to classify erodibility of coastal environments in the field with a single piece of equipment. Overall, the work presented here contributes to our ability to measure, quantify, and predict coastal response to climate change.

Acknowledgements

The past five years have truly been the adventure of a lifetime. I am incredibly grateful that I had the chance to conduct important and fascinating research, to learn from some of the most gifted minds in the geotech and coastal science communities, to make collaborations and friendships that will last far beyond my time as a student, and to travel the world. I'm proud of the research presented in this document, and all of the work that went into these pages, but I could not have done it alone. Firstly, I want to thank my advisor, Dr. Nina Stark for giving me the opportunity to join her research group back in 2017, her dedication to my development as researcher, and her guidance and willingness to go out of her way to make my job easier. I could not have asked for a better mentor, and I am forever grateful for her support. To my committee and the many collaborators I've worked with all over the years: Dr. Emily Eidam, Dr. Jen Irish, Dr. Alba Yerro, Dr. Dave Callaghan, Dr. Peter Nielsen, Dr. Bill Dally, Dr. Joe Calantoni, Dr. Celso-Castro Bolinaga, and Dan Duncan, thank you for sharing your wisdom and knowledge. To all the friends I made in the Virginia Tech geotechnical program: Reem Jaber, Tat Shing, Matthew Florence, Julie Paprocki, Dennis Kiptoo, Casey Peloquin, Collin Sweeney, Ailie Vuper, Abby Burke-Flask, Austin Flask, Sam Consolvo, Liz Smith, and Jonathan Moore, thank you for all the study sessions, the research trips, and late nights at the Cellar. To my best friends: Julia Longacre, Mary McCorkill, Andrew Phelps, Banks Vickhouse, Melissa & Darren Walters, Adam Varner, Jonathan McVicker, and Wojtek Skowronek, thanks for going on this journey with me, and for the years of memories we've made together. I wouldn't be where I am today without all of you. Finally, I want to thank my family. Mom, Dad, Genny, and the rest of my family, thank you for raising me to be man I am today, for always being there for me no matter where in the world I found myself, and for your unconditional love and support. A special thank you to our family dog, Millie, for keeping me company while I wrote most of this dissertation. I couldn't have done this without any of you, and I feel incredibly lucky to have each and every one of you in my life. I've been blessed to call Blacksburg my home for the past 9 years, and no matter where life takes me from here, I'll always be a Hokie.

This dissertation is dedicated to the late Rhonda Coston.

Preface

This manuscript is comprised of six main chapters, four of which are manuscripts that have been combined to form the main body of the dissertation. Chapter 1 represents an introduction and background, Chapters 2 through 5 are the four manuscripts, and Chapter 6 is a concluding section with future outlooks. Chapter 2 is a peer reviewed conference manuscript and Chapters 3, 4, and 5 are journal manuscripts. The beginning of each chapter describes the coauthors contribution and provides pertinent submission and/or publication information. The author of this dissertation is the lead author on all main body manuscripts.

Table of Contents

List of Figures

Chapter 1

Chapter 2

Chapter 3

Chapter 4

Chapter 5

Appendix B

Appendix D

Appendix E

Appendix F

Appendix G

List of Tables

Chapter 1: Introduction

1.1. Motivation

Climate change is expected to increase sea level, rates of sea level rise and the frequency and intensity of severe meteorological events, posing an increasing threat to coastal areas in coming years (Sallenger 2000, Bender et al. 2010, Knutson et al. 2010). Beach erosion, shoreline retreat, and coastal flooding are predicted to become more severe as a result of these changes (Zhang et al. 2004, Jones et al. 2008). In Arctic environments, climate-related changes in environmental conditions have led to decreases in seasonal sea ice and an increased sediment yield from rivers and permafrost bluff erosion (Jones et al. 2009, Overeem and Syvitski 2010, Wang and Overland 2015). Understanding the mechanics of sediment dynamics in these areas is key to predict coastal evolution and associated impacts on communities and habitats. Thus, an improved understanding of the relationship between foreshore and nearshore sediment characteristics and the driving mechanisms of erosion has the potential to improve erosion prediction and to mitigate climate-related impacts on coastal communities and habitats. To-date, foreshore sediments are often considered as a single particle problem in erosion relationships for sandy sediments, but there are bulk sediment properties that have been acknowledged but rarely considered for erosion processes (Shields 1936, National Academy of Science, Engineering, and Medicine 2019). It is hypothesized that considering geotechnical properties of foreshore sediments in the investigation of coastal erosion geomorphodynamics will improve our predictive capabilities for coastal evolution in the context of climate change.

1.2. Background

1.2.1. Geotechnical Properties and Geomorphodynamics

Local hydrodynamics serve as the driver of geomorphodynamics in coastal environments (Dalrymple 1992, Masselink and Short 1993, Dean and Dalrymple 2004, Masselink et al. 2006). The role of geotechnical sediment properties, and their relation to geomorphodynamics has been acknowledged, but is seldom a main area of research. However, some studies have highlighted their importance on sediment dynamics in subaquatic and coastal areas (Mulhearn 2001, Watts et al. 2003, Albatal and Stark 2017, Jafari et al. 2018).

The individual sediment grain has been the focus when investigating erosion, and erosion problems are often modelled as a fluid-particle interaction (Shields 1936, Briaud 2001). While particle

properties, namely grain size and particle density are important in modelling geomorphodynamics, the particle properties do not necessarily represent the behavior of the sediment as a bulk material at a beach or on the seabed (Dean 1973, Jackson et al. 2005, Gallagher et al. 2011). Interactions between individual particles and the stresses that result from interparticle interaction give the sediment unique geotechnical properties distinct from that of the particle (moisture content, friction angle, bulk density, shear strength, etc.). These properties have also been acknowledged to play a significant role in sediment dynamics (Davidson-Arnott et al. 2005, Erikson et al. 2007, Sassa and Watabe 2007, van Rijn 2007).

The packing state of granular materials can be quantified through a variety of metrics such as void ratio (e), porosity (n), density (ρ), unit weight (γ), just to name a representative few. Void ratio and porosity describe the ratios of the volume of voids (volume of air and water in the sediment matrix) to the volume of sediment and the total volume, respectively. Density gives the mass of sediment per unit volume, and unit weight give the weight of sediment per unit volume. These two properties can be expressed as dry density/unit weight (ρ_d, γ_d), where there is only air in the voids, or as bulk density/unit weight (ρ_b, γ_b), where there is some combination of air and water in the voids. Conversions between each of these metrics depending upon the engineering application can be done using weight/volume relationships of soils (see Briaud (2013), Chapter 3 for a detailed breakdown). Relative density (D_r) is another way to quantify packing state of granular materials on a scale of 0-100%. A relative density of 0% describes the loosest possible state a dry soil can attain, and D_r = 100% describes the densest possible state. These limits are found through a set of standardized laboratory procedures. D_r can be computed using unit weights or void ratio, but only the computation using unit weights will be described here for simplicity. D_r = 0% is found by determining the minimum dry unit weight (γ_{d-min}) using the "Standard Test Methods for Minimum Index Density and Unit Weight of Soils and Calculation of Relative Density" procedure (ASTM D4254). D_r = 100% is then found by determining the maximum dry density (γ_{d-max}) using the "Standard Test Methods for Maximum Index Density and Unit Weight of Soils Using a Vibratory Table" procedure (ASTM D4253). Once these limits are found, D_r can be computed for any γ_d from Equation 1.1:

$$D_r = \frac{\gamma_{d-max}}{\gamma_d} * \left(\frac{\gamma_d - \gamma_{d-min}}{\gamma_{d-max} - \gamma_{d-min}}\right) * 100\% \quad (1.1)$$

The packing state of sediments in coastal environments can be subject to high variability in both space and time, and this variability has important implications for local geomorphodynamics and sediment transport. Suction dynamics in tidal-flat sediments due to tidally driven changes in groundwater were shown to induce changes in D_r of up to 50%, and these changes in turn had strong impacts on the morphologic evolution of the tidal flats over multiple tidal cycles (Sassa and Watabe 2007). Bulk density of dune sediments has been used as an input in Rankine Earth Pressure theory, a common geotechnical earth pressure theory, to model dune recession through shear plane failure (Erikson et al. 2007). As an example of relationships between packing state metrics, Equation 1.2 gives the computation for converting ρ_{bulk} into γ_d for the purpose of calculating D_r:

$$\gamma_d = \frac{\rho_{bulk} g}{(1+w)} \quad (1.2)$$

where g is gravitational acceleration, and w is the gravimetric water content. A study by Heathershaw et al. (1981) used a simple penetrometer as a proxy for ρ_b of beach sands and found that bed level change and bulk density were inversely related. Dean and Dalrymple (2004) suggested that swash and backwash processes on a wave-to-wave basis could act to reduce porosity (increase density/unit weight/D_r). More recently, Zambrano-Cruzatty et al. (2019) attempted to include more geotechnical parameters in the formulation for determining the threshold velocity for aeolian (wind-driven) sediment transport but found that bulk density had only a slight effect on the results. Albatal et al. (2020) developed an empirical correlation between portable free-fall penetrometer measurements (PFFP, see Section 1.2.2) and D_r for nearshore sandy sediments, and found that D_r is highly spatially variable in nearshore areas with a range of 30-90%. Additional work by Albatal et al. (2019) showed that surficial sediment strength from PFFPs (and therefore D_r) was also highly variable in time, with strong transitions from loose to dense after storm events.

Moisture content (MC) is a controlling variable in aeolian sediment transport. Wind-driven sediment transport has been found to be closely linked to surface moisture content, with higher moisture contents having a higher entrainment threshold and therefore being more resistant to aeolian erosion (Davidson-Arnott et al. 2005, Darke and Neuman 2008, Bauer et al. 2009). Due to tidal fluctuations in water level as well meteorological effects, moisture content can be highly variable on beaches and other emerged coastal areas. Partial saturation due to these fluctuations in

moisture content can have an impact on surface shear strength, and impact morphology (Sassa and Watabe 2009). One way to quantify the impacts of partial saturation is through suction stresses, which is an additional source of sediment strength due to capillary action in the pores (Kim 2001, Lu and Likos 2006, Lu et al. 2009). The model for dune recession dune proposed by Erikson et al. (2007) also used moisture content by determining shear strength using a formulation that accounted for added strength due to partial saturation. Additionally, Sassa and Watabe (2007) showed that changes in suction stresses on tidal flat sediments could induce significant variations in surface shear strength, affecting bed-level change and erodibility.

The term friction angle is commonly used interchangeably in literature to encompass three terms for the same conceptual property, with different ways of being defined. The most traditional concept of the "friction angle" describes sliding object (e.g., a block) friction, or the angle at which a ramp must be inclined for the object to overcome friction and start sliding. The second is the "angle of repose" which is the natural settling angle for a mass of loosely placed sediment. This definition is common in literature to describe the angle between single sediment grains when they come to rest on a bed and can be used to define entrainment thresholds for sediment transport (Miller and Byrne 1966, Kirchner et al. 1990). The third type of friction angle is called "angle of internal friction" and has the symbol ϕ'.This is the primary term for the friction angle used in geotechnical engineering. This definition is a measure of frictional resistance to shearing stresses within the bulk sediment mass. In well-graded sediments (large range of particle sizes), gaps between larger particles can be filled with smaller one which increases frictional resistance and therefore ϕ' (de Beer 1965, Bolton 1986, Duncan et al. 2014). Other factors that control ϕ' are D_r (increases with D_r), and confining stress (decreases with confining stress) (Lee and Seed 1967, Duncan et al. (2014). Since D_r is directly related to ϕ', it follows that ϕ' should also be highly variable in coastal environments. The listed "friction angles" are connected, for example, the angle of repose describes the angle of internal friction for a loosely packed dry sand. While ϕ' by itself is not commonly found in literature pertaining to sediment transport processes, it has a controlling influence on shear strength (as will be discussed in the next section) that makes it important for these considerations (Erikson et al. 2007).

Shear strength of soil is the maximum magnitude of shear stress that can be applied to the bulk mass of sediment before inducing failure along a shear plane. In geotechnical engineering,

frictional contact between particles (effective stresses) for dry and saturated material control shear strength. (Lee and Seed 1967, Duncan et al. 2014). Since erosion processes are governed by fluid exerting a shear stress on the sediment bed surface, it follows that shear strength is an important parameter for characterizing erosion. As mentioned in the previous sections, suction stresses generated due to partial saturation can increase shear strength (Lu and Likos 2006, Briaud 2013). There are different equations to describe shear strength accounting for partial saturation (Fredlund and Rahardjo 1993, Lu et al. 2009, Briaud 2013), but all commonly attempt to quantify the effect of soil moisture on shear strength. An example by Briaud (2013) is shown in Equation 1.3:

$$\tau_f = c' + (\sigma - Su_w)tan\phi' \tag{1.3}$$

where c' is the effective stress cohesion, σ is the normal stress on the failure plane, u_w is the water pressure, and S is the degree of saturation (0-100%). In this simple example, low values of saturation will provide a higher shear strength than higher values of saturation. The properties described previously ($D_r, MC,$ and ϕ') all have a controlling influence on shear strength. These properties are highly variable at intertidal beaches, tidal flats, and other emerged coastal environments, and thus it follows that shear strength is also highly variable across temporal and spatial scales (Sassa et al. 2014, Manning and Stark 2019, Sassa and Yang 2019). Geotechnical sediment properties are highly variable and affect the sediment's erodibility. However, there is still a lack of studies quantitatively and generally connecting geotechnical sediment properties, erodibility, and coastal geomorphodynamics, particularly under a wide range of environmental conditions.

1.2.2. Portable Free-Fall Penetrometer

Coastal environments present a unique set of challenges for conducting geotechnical sediment characterization. Energetic hydrodynamics, rapidly changing water levels, and unpredictable environmental conditions make the operation of large cone penetration testing (CPT) systems and boring rigs dangerous. Additionally, traditional CPT is expensive and often lacks accuracy and sensitivity for measuring soft or loose surficial sediment properties. Specifically in Arctic environments, the presence of sea ice and limited open ocean availability in the summer months further complicates potential surveys and would be difficult without the additional expense of an icebreaker vessel, while pack-ice conditions in winter are not representative for studies of sediment dynamics.

Portable free-fall penetrometers (PFFP) have emerged as a suitable tool for conducting geotechnical characterization in these difficult environments (Stark et al. 2014, Albatal and Stark 2016, Stark et al. 2017). They provide a cost-effective complement to traditional geotechnical measurements, can be deployed under energetic hydrodynamic conditions, and focus on the uppermost sediment layer (Stoll and Akal 1999). These devices typically feature onboard accelerometers recording free-fall through the water column, impact, and penetration into the seabed. While initial work focused on rapid seabed sediment characterization, more recent work has focused relating PFFP data to more detailed geotechnical properties (Aubeny and Shi 2006, Randolph 2016) and to sediment transport processes (Stark and Kopf 2011, Stark et al. 2011, Albatal and Stark 2017, Albatal et al. 2019). They have succeeded to estimate bearing strength (Akal and Stoll 1995, Stark et al. 2011, Stark et al. 2012, Albatal et al. 2018, Dorvinen et al. 2018), relative density of sands (White et al. 2018, Albatal et al. 2020), and undrained shear strength of fine-grained sediments (Aubeny and Shi 2006, Chow and Airy 2014, Chow et al. 2017, Stark and Ziotopoulou 2017, Kiptoo et al. 2020). Additionally, when equipped with pore pressure sensors, PFFPs have been used to study pore pressure response to dynamic penetration and the subsequent effects on soil behavior (Silva et al. 2006, Seifert et al. 2008, Lucking et al. 2017, Mumtaz et al. 2018, Mumtaz and Stark 2020).

The PFFP used in this work, blueDrop, was specifically designed for use in coastal areas that provided difficulty for traditional measurements (Stark et al. 2014). Its rugged and lightweight design makes it suitable for deployment in energetic conditions from a variety of platforms. The probe features a streamlined shape, can accommodate steel tips of either conical or parabolic shape, has a mass of 7.7kg, and length of 63.1cm. Five onboard vertical accelerometers (ranging from $\pm 2g$ to $\pm 250g$, where g is gravitational acceleration) and two horizontal accelerometers ($\pm 55g$) record continuously at 2kHz. The device free-falls through the water column and impacts the seabed, with the sediment resistance ultimately bringing the probe to a stop. Impact velocity and penetration depth can be derived via single and double integration, respectively, of the deceleration-time record from impact until stop (Dayal and Allen 1973, Stoll and Akal 1999, Stark and Wever 2009). Due to the probe's streamlined shape, smooth body, and vertical impact, sediment resistance is assumed to act at the tip. Thus, the total sediment resistance force (F) can estimated via Newton's second law (Equation 1.4) and has been proposed to be considered an

estimate of tip resistance in the absence of detailed soil information to estimate soil buoyancy and soil drag in addition to buoyancy and drag in water:

$$F = m * dec \tag{1.4}$$

Where, m is the buoyant mass of the probe and dec is the measured deceleration. To convert this resistance force to a dynamic bearing strength (q_{dyn}), it is divided by the area of the tip (A) (Equation 1.5):

$$q_{dyn} = \frac{F}{A} \tag{1.5}$$

This bearing strength is considered a dynamic strength as the PFFP is impacting at a high and changing velocity (on the order of m/s), when compared to other testing methods such as a CPT, which penetrate the sediment as a much slower and constant rate (on the order of cm/s). Due to this high strain rate, the experienced bearing capacity will likely be higher than a comparable test at a lower strain rate (Stoll et al. 2007). To mitigate these effects, a strain rate correction (f_{sr}) is applied in an attempt to normalize the results to a slower, constant penetration velocity (Dayal and Allen 1973, Steiner et al. 2014). Equation 1.6 gives the logarithmic form of the strain rate correction, most commonly applied to submerged sands and other seabed sediments in the absence of complementary information about soil type and properties (Stoll et al. 2007, Stark et al. 2009, Stephan et al. 2015, Albatal et al. 2020):

$$f_{sr} = 1 + K log_{10}\left(\frac{v}{v_{ref}}\right) \tag{1.6}$$

Where K is the strain rate correction factor, v is the dynamic velocity over the course of penetration into the seabed, and v_{ref} is the reference velocity, typically taken as $2cm/s$. The empirical strain rate correction factor K, is soil dependent and highly variable (True 1976). Values ranging from K = 0-1.5 have been suggested for sands (Dayal and Allen 1975, Stoll et al. 2007, Stark et al. 2012, Stephan et al. 2015, Albatal et al. 2020) and K = 0.15 is considered a conservate estimate for clays (Aubeny and Shi 2006). Dividing the dynamic bearing capacity by the strain rate correction, gives the quasi-static bearing capacity ($qsbc$), which is the proxy for equivalent static sediment strength (Stark et al. 2012), and is given by Equation 1.7:

$$qsbc = \frac{q_{dyn}}{f_{sr}} \tag{1.7}$$

While the aforementioned studies have shown the utility of PFFPs for estimating sediment parameters in submerged environments, until recently, PFFPs have not been used for surveying of intertidal beach environments. However, it is posited to be a useful tool in this setting due to its rapid deployment and the device's capability to also measure both emerged and submerged, which can link different foreshore zones (Reeve et al. 2018). The ability to collect geotechnical information easily and rapidly in different coastal zones makes the PFFP an attractive tool for investigating relationships between erodibility, geotechnical sediment properties, and morphodynamics in coastal systems. However, the data analysis of PFFP records at beaches has only been rarely explored (Reeve et al. 2018, Paprocki et al. 2019).

1.2.3. Sediment Properties and Erodibility

Sediment dynamics (of the seabed, riverbed, beach face, etc.) is determined by the interaction between mobilizing and stabilizing forces. Mobilizing forces are mostly aero/hydrodynamics such as fluid flow and turbulence, and stabilizing forces are predominantly associated with sediment properties (Grabowski et al. 2011). If the mobilizing forces overcome the stabilizing forces, sediment motion is initiated, representing the first step to erosion. This is referred to as incipient motion. The minimum shear stress needed to initiate sediment motion is the critical shear stress (τ_{cr}). While there are several formulations for determining the critical stress (e.g., Madsen and Grant 1976, Hallermeier 1980, Soulsby and Whitehouse 1997), a most traditional and still commonly applied expression is the critical Shield's Parameter (θ_{cr}), which is a non-dimensional version of the critical shear stress (Shields 1936):

$$\theta_{cr} = \frac{\tau_{cr}}{(\rho_s - \rho) g d_{50}} \tag{1.8}$$

Where ρ_s is the sediment particle density, ρ is the density of the fluid, g is gravitational acceleration, and d_{50} is the particle diameter. For sediment beds with a range of grain sizes present, the median size of the grain size distribution (d_{50}) can be used (van Rijn 2007).

Once particle motion has been initiated, erosion may result if net sediment transport is associated with material loss. The rate at which sediment is removed from the bed per unit area during erosive processes is called the erosion rate (E). Again, there are various expressions for determining E

(see Wilson 1993, Roberts et al. 1998, Ternat et al. 2008), but most take a form similar to one presented by Grabowski et al. (2011):

$$E = M(\tau_b - \tau_{cr})^n \tag{1.9}$$

Where τ_b is the shear stress applied to bed and M is referred to as the erosion rate parameter. The fitting parameter n is set to a value of one when assuming a linear relationship between erosion rate and shear stress (Graf 1984, Parchure and Mehta 1985). Erodibility of sediment can be described by the critical shear stress (i.e., if and when sediment is mobilized) and the erosion rate (i.e., how much sediment is eroded) and exhibits high variability between sediments (Briaud 2008). Thus, sediment properties have a significant impact on erodibility (Briaud 2013). Numerous attempts have been made to correlate erodibility and sediment properties (see National Academy of Science, Engineering, and Medicine 2019 for a detailed summary), and there is a stark difference in the properties influencing erodibility between cohesive and non-cohesive sediments, as cohesive sediments have strong inter-particle attraction due to electro-chemical processes referred to as cohesion (Winterwerp and van Kesteren 2004, Grabowski et al. 2011). Sediment properties known to influence erodibility include grain size, water content, unit weight, plasticity index, undrained shear strength, void ratio, swell, fine fraction, amongst others (National Academy of Science, Engineering, and Medicine 2019).

1.2.3.1. Erodibility of Non-Cohesive Sediment

For non-cohesive sediments (sands & gravels), a controlling parameter for erodibility is particle size (Briaud 2013). Grain size was the basis of the work done by Hjulstrom (1935) and Shields (1936) as the first attempts to correlate erosion thresholds with sediment properties. Table 1.1 contains examples of existing correlations between erodibility and sediment properties for non-cohesive sediments.

Table 1.1: Examples of simple correlations between sediment properties and erosion thresholds for non-cohesive sediments.

Relationship	Erosion Parameter	Reference
$\frac{\rho v_{cr}^2}{\gamma_b D_g} = 2.50\left(\frac{D_g}{z}\right)^{-0.2}$	Critical velocity	Neill (1967)
$\tau_{cr} = 0.05\gamma_b D_{50}$	Critical shear stress	Chen and Anderson (1987)
$v_{cr}(m/s) = 0.35(D_{50})^{0.45}$	Critical velocity	Briaud (2008)
$\tau_{cr}\ (Pa) = D_{50}\ (mm)$	Critical shear stress	Briaud (2008)

where v_{cr} is the critical velocity for erosion, $D_g = \sqrt{D_{84}D_{16}}$ is the effective grain diameter from Neil (1967), z is the flow depth, and γ_b is the submerged unit weight. As seen from Table 1.1, though these are just a few examples of correlations for non-cohesive sediments, they all require a grain size, either using the median grain size (D_{50}) or the effective grain diameter (D_g). The other sediment property included in some of the relations is the submerged unit weight, γ_b which is a metric of the packing state of the material. Kirchner et al. (1990) studied relationships between critical shear stress and friction angles in the form of angle of repose (Miller and Byrne 1966) and found that critical shear stresses were highly variable functions of the sediment size, angle of repose, grain protrusion, and grain exposure. The authors suggested that a single value of critical shear stress was insufficient to describe the entrainment behavior of riverbed sediment, and that a probability distribution was a more effective method of determining entrainment (Kirchner et al. 1990). Particle sorting and shape have also been shown to be important for initiation of motion for non-cohesive sediments. Sediment beds composed of a wide range of particle sizes (well-sorted) will have selective entrainment of smaller particle sizes first based on the flow conditions, which can lead to a coarsening of the surficial particles in a process known as bed armoring (Proffitt 1980, Chin et al. 1994). This can be juxtaposed to a poorly sorted bed (similar particle sizes) which will all entrain at a similar flow regime when motion is assessed using a grain size based approach. With regard to particle shape, Lane and Carlson (1954) found that flatter particles could become "stuck" in the bed due to their shape and resist motion when compared to spherical particles, but once entrained would travel further than spherical particles due to a lower settling velocity, which was also suggested by Bridge and Bennett (1992).

A variety of sediment characteristics influence the erosion behavior of non-cohesive sediments such as grain size, shape, and sorting as well as packing state and angle of repose. However, a majority of these properties have not been studied in the context of coastal sediment transport processes. The work done using submerged unit weight by Neill (1967) focused on glass spheres and gravel sized particles, and the Chen and Anderson (1987) relation came from a study on soil erosion during dam overtopping. Further, the studies mentioned with regard to grain size, shape, and sorting were all conducted in the context of riverine environments and unidirectional flow. Studies on coastal sediment transport with regard to erodibility have focused on a Shields (1936) style approach, using grain size as the sediment property determining motion, with the difference being in how bed shear stress are computed to account for combined wave-current flows (see Nielsen 1992, Soulsby 1997, and Dean and Dalrymple 2004). As mentioned in Section 1.2.1, moisture content is an important parameter for aeolian sediment transport in emerged coastal environments such as beaches, but moisture is not a factor in water-driven erosion as the sediment are fully saturated (Davidson-Arnott et al. 2005, Darke and Neuman 2008, Bauer et al. 2009). Zambrano-Cruzatty et al. (2019) attempted to introduced bulk density into relations for critical fluid velocity for wind-driven sediment transport on beaches but found that considering density only had slight effect on the results. This lack of consideration for additional sediment properties, specifically in the context of water-driven erosion in coastal environments, is an opportunity to explore potential relationships containing more than simply the grain dimensions.

1.2.3.2. Erodibility of Cohesive Sediments

Grain size does not correlate well with erosion behavior of cohesive sediments (silts and clays) (Briaud 2013). This has led to numerous attempts to correlate other sediment properties with erodibility for fine-grained sediments, with Table 1.2 providing a brief list of examples:

Table 1.2: Examples of existing relationships between erosion threshold and sediment properties for cohesive sediments.

Relationship	Sediment Property	Reference
$\tau_{cr} = 0.0034(PI)^{0.84}$	Plasticity Index (PI)	Chen and Anderson (1987)
$\tau_{cr} = 0.0323 - 0.00653e$	Void Ratio (e)	Lyle and Smerdon (1965)
$\tau_{cr} = 0.493 * 10^{0.0182P_c}$	Percent Clay (P_c)	Smerdon and Beasley (1961)
$\tau_{cr} = 5.44 * 10^{-4}\rho_b - 0.28$	Bulk Density (ρ_b)	Amos et al. (2004)
$\tau_{cr} = 0.70\exp(0.06MC(\%))$	Moisture Content (MC)	Singh and Thompson (2015)

Additionally, as one example of the variety of sediment properties that have been used in correlations, Lyle and Smerdon (1965) provided expressions for relationships between erosion threshold and dispersion ratio, percentage of organic matter, vane shear strength, cation exchange capacity, and calcium/sodium ration. These examples serve to highlight the wide range of sediment properties that affect the erodibility of cohesive sediments. However, the use of empirical relationships and linear regression to correlate limited numbers of sediments properties with erodibility has been met with limited success (Cao et al. 2002). This is due to the complexity of the erodibility problem in general, and the influence of a large number of sediment-specific properties (Briaud 2013). Still, these types of relationships represent the state of the art for obtaining erodibility parameters from soil properties, specifically when combined with the laboratory tests discussed in the next section, and the varying degrees of success do not undermine the importance of developing such relationships for practical engineering applications. One improvement that could be made in the area of cohesive sediment erodibility in coastal environments is the introduction of direct soil strength measurements. Parameters such as vane shear strength or undrained shear strength have been considered for both the determination of τ_{cr} (Lyle and Smerdon 1965, Ghebreiyessus et al. 1994), and the erosion rate parameter M from Equation 1.9 (Winterwerp and van Kesteren 2004). However, these studies did not make in-situ measurements of shear strength, instead relying on remolded samples or laboratory testing, which has the potential to change the measured properties due to sample disturbance (Duncan et al. 2014). A tool such as the PFFP has been shown to be able to make in-situ measurement of s_u in coastal

and marine environments (Kiptoo et al. 2020, Jaber 2022). This ability to directly measure strength properties of cohesive sediments has the potential to generate new relationships between in-situ geotechnical properties and erodibility.

1.2.3.3. Measuring Erodibility

Laboratory tests such as the Jet Erosion Test (JET) and Erosion Function Apparatus (EFA) have been used to determine erosion parameters for field sediment samples and varying laboratory prepared samples (Hanson 1991, Briaud et al. 2001). The JET measures erodibility by setting a head tank to fixed height, shooting a jet of water into a sediment sample for fixed time intervals and recording the resulting depth of scour in the sample (Hanson 1991). Measured parameters are erosion rate (E) from the scour depth measurements, and the applied shear stress (τ) from head tank height and flow conditions of the jet nozzle (Hanson and Cook 2004). Erosion parameters (k_d and τ_{cr}) are obtained by iteratively solving the excess shear equation (Graf 1984), which is equivalent to Equation 1.9, with the detachment coefficient k_d replacing M. M and k_d both describe the erosion rate of a material once erosion has been initiated ($\tau > \tau_{cr}$), and a higher M/k_d indicates a higher erosion rate at a given excess shear stress. The parameter M describes erosion rate in terms of mass, and k_d is a volume based parameter, thus converting between the two can be done by knowing the sediment density (ρ_b). The EFA measures erodibility by pumping water through a rectangular flume while a Shelby tube sample (ASTM D1587) is extruded from the bottom into the flow (Briaud et al. 1999, Briaud et al. 2001). Erosion rate is measured by recording the time to reach 50 mm of erosion under a given flow velocity, and the test is repeated at different flow velocities to cover a range of shear stresses. These types of laboratory tests have led to the development of a more categorical approach to erodibility, as shown in Figure 1.1 for the EFA, whereby soils can be grouped into different classes of erodibility behavior based on laboratory measurements of erosion rate and shear stresses (Briaud 2008). Hanson and Simon (2001) developed a similar classification chart for samples tested with the JET. From this chart, fine sand is the most erodible material, with clays and rock being the most difficult to erode (Figure 1.1).

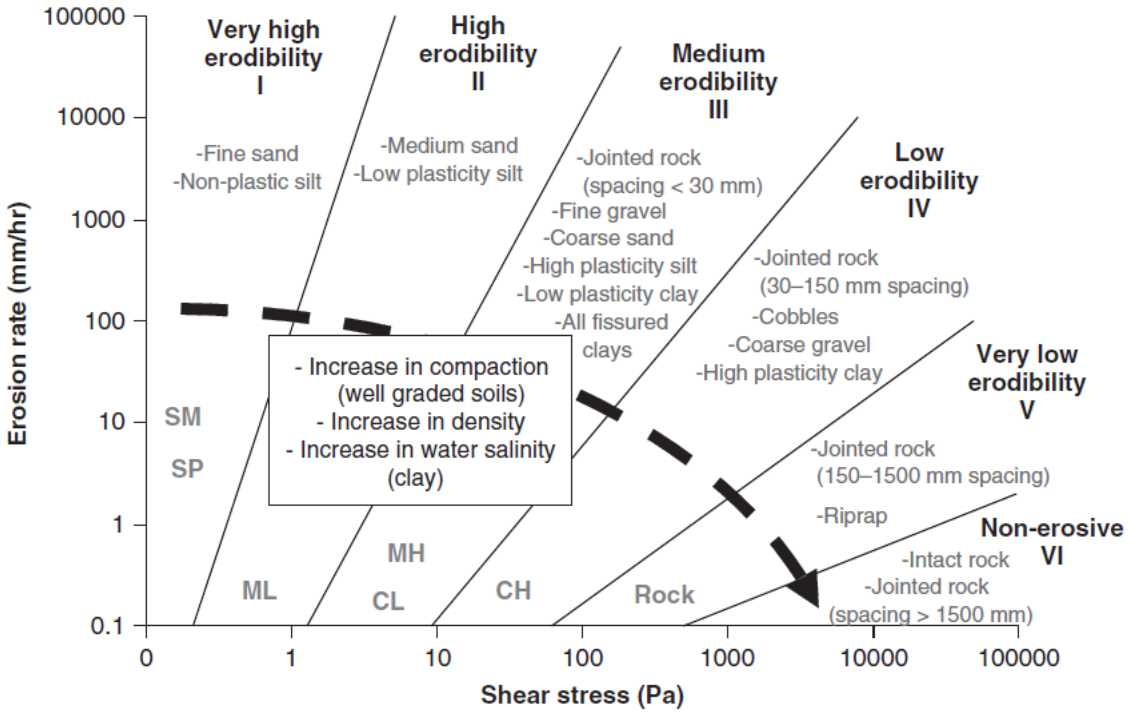

Figure 1.1: Relationship between applied shear stress and erosion rate for different of sediment types (taken from Briaud 2013). ***SM*** and ***SP*** refer to well and poorly graded sands, ***ML*** and ***MH*** refer to low and high plasticity silts, and ***CL*** and ***CH*** refer to low and high plasticity clay, respectively.

While laboratory testing provides a valuable method for obtaining erosion parameters, these tests can often be time consuming and expensive to perform, especially in field settings, and can be affected by the difficulty required to obtain undisturbed samples, specifically for coarse-grained sediments and in challenging coastal areas such beach/nearshore zones and Arctic environments (National Academy of Science, Engineering, and Medicine 2019). Measuring soil properties and strength characteristics of in-situ coastal sediments using tools such as the PFFP (see Section 1.2.2) and comparing these properties to the laboratory measures of erodibility described above has the potential to mitigate some of the issues related to obtaining soil properties during lab testing and allow for field erodibility characterization in challenging coastal settings. Based on the work detailed in Section 1.2.1 highlighting the importance of geotechnical soil properties for a variety of coastal sediment transport processes, it can be hypothesized that geotechnical parameters measurable in-situ can be correlated to coastal sediment erodibility, paving the way for accessible field measurements to predict coastal erosion more accurately.

1.2.4. Sediment Dynamics in Arctic Nearshore to Continental Shelf Systems

The Arctic has seen some of the highest rates of shoreline retreat in the world due to climate change (Jones et al. 2008, Frederick et al. 2016). Seasonal sea ice thickness and extent has decreased due to warming temperatures, resulting in more open water during the summer months and increasing fetch available to generate storm driven wind waves, which attack and erode the coastline (Aré 1988, Overeem et al. 2011, Barnhart et al. 2016). This issue is exacerbated by melting of permafrost bluffs which induces slumping and block failure (Lantuit and Pollard 2008). The drivers of these erosive processes (wave energy and ground thaw) are expected to continue increasing, leading to further increases in shoreline retreat rates and vulnerability of coastal communities (Ford et al. 2006, Jones et al. 2009). In addition to coastal erosion, increases in precipitation are expected to drive increases in river discharge, all of which point to an increase in sediment supply to Arctic marine environments (Rachold et al. 2000, Box et al. 2019). Factors impacting the transport mechanisms of this new sediment include coastal morphology, and winter/summer differences in currents generated by the presence of sea-ice. Coastal bluffs reflect wave energy, driving offshore directed currents, whereas low-lying barrier islands allow wave energy to move sediment onshore (Héquette et al. 2001). The presence of ice near the shore in the winter promotes offshore directed bottom currents, while calm conditions in the summer months promote deposition on the inner shelf, although storms during the summer increase erosion, as mentioned previously (MacDonald et al. 2015, Forest et al. 2016). While understanding the complex interactions between transport processes, climate change, and local/seasonal hydrodynamics is an area of current study (Osborne and Forest 2016), one underserved area related to the concepts presented in the previous sections is the role of sediment properties. Previous work has acknowledged the importance of geotechnical sediment properties such as grain size, packing state, and shear strength for determining erosion rates of coastal bluff and for the protection of buried pipelines from ice scour (Reimintz et al. 1985, Nematzadeh and Shiri 2020, Hashemi et al. 2022). Additionally, Arctic seabed sediments are known to be highly variable spatially as well as in vertical stratification due to reworking from ice gouging, which implies a similar degree of variability in erodibility (Barnes et al. 1980, Barnes et al. 1984, Reimintz et al. 1977). Measuring sediment properties and erodibility poses a difficult challenge in Arctic environments due to the presence of sea-ice for most of the year, and the logistics required for performing field work in remote areas. Still, these vulnerable coastal systems present a unique opportunity explore new

relationships between sediment properties and erodibility across a variety of sediment types (see Section 1.2.3). PFFPs have been successfully employed in Arctic nearshore systems for the purpose of geotechnical sediment characterization, and the challenging location provides an ideal setting for advancing PFFP measurements to directly estimate erosion parameters (Stark et al. 2015, Stark et al. 2017). Using PFFP measurements to rapidly characterize both sediment properties and erodibility in-situ would allow for more accurate values to be implemented into long-term morphodynamic models, such as in the study by Malito et al. (2022), with the goal of improving our understanding of sediment dynamics in Arctic environments, and our ability to model the response of these systems to climate change in the future.

1.3. Gaps in Knowledge

There have been numerous studies acknowledging the variability of geotechnical sediment properties in emerged coastal environments and their role in affecting local geomorphodynamics (see Section 1.2.1). Example of such properties include moisture content (Darke and Neuman 2008, Davidson-Arnott et al. 2005), shear strength (Sassa and Watabe 2007, Sassa and Yang 2019), packing state in the form of relative density or bulk density (Erikson et al. 2007, Zambrano-Cruzatty et al. 2019), and bearing capacity (Paprocki et al. 2019). However, these properties have all been studied for specific applications, and rarely in reference to their general variations in the crosshore beach profile with active geomorphodynamics (Heathershaw 1981). Improving our understanding of sediment dynamics and geomorphodynamics, and thus, of coastal erosion and shoreline change, requires a better understanding of how these properties vary across spatial and temporal scales in beach environments and how they relate to geomorphodynamics. Collecting geotechnical and geomorphodynamic data in-situ can contribute to tackling this gap in knowledge. Yet, there has been little research directed toward the direct measurement of geotechnical sediment properties in emerged beach environments. PFFPs have paved the way to obtain geotechnical information of surficial sediments in nearshore and submerged sites, but have just recently been considered to enable seamless measurements from subaerial over intertidal to subtidal cross-shore locations (Reeve et al. 2018, Paprocki et al. 2019). Developing and evaluating a strategy for PFFP measurements in partially saturated intertidal environments would enhance the ability of researchers to understand how variations in sediment properties affect and are affected by local sediment transport, hydrodynamics, and morphology at beaches.

Further, once these properties can be directly measured in an efficient and reliable manner, their connections to in-situ erodibility behavior can be investigated. Specifically for non-cohesive sandy sediments to-date, the sediment property of interest in terms of quantifying erodibility is grain size (Shields 1936, Nielsen 1992, Soulsby 1997, National Academy of Science, Engineering, and Medicine 2019). Other sediment properties such as packing state or sediment strength have been explored for non-cohesive sediments, but these relationships have not been explored in the context of coastal/nearshore environments (Neill 1967, Chen and Anderson 1987). For mixed/cohesive sediments, relations to a variety of sediment properties have been attempted with mixed results (Cao et al. 2002). Further, a majority of these studies and relationships were developed based on laboratory tests of erodibility and samples prepared to specific properties. While there are tools for in-situ measurement of erodibility (Hanson and Cook 2004), there is a lack of work pertaining to relationships between directly measured soil properties and directly measured erodibility parameters, likely due to challenges presented by measuring either set of these parameters in the field. This problem is exacerbated by the aforementioned lack of guidance on collecting geotechnical measurements of beaches and measurement challenges presented by difficult/energetic coastal and nearshore environments.

From the identified gaps in knowledge, the goal of this research is to improve geotechnical data collection techniques for surficial sediment properties relevant for erosion in coastal environments and to advance our understanding of the relationships between geotechnical sediment properties and erodibility in coastal settings. Regarding specific coastal settings, this study focuses on sandy beach environments and then stretches into Arctic coastal to shallow water environments, representing settings of particular urgency to improve of understanding of sediment dynamics in the context of climate change and of significant challenges for field data collection. This goal will be addressed by testing the following research hypotheses:

1. In-situ geotechnical properties of coastal and nearshore sediments such as relative density, moisture content, and bearing capacity can be measured safely and reliably in energetic coastal environments subject to significant geomorphodynamics and possibly shoreline erosion.
2. Geotechnical properties of foreshore and nearshore continental shelf sediments vary in response to local geomorphodynamics along crosshore beach profiles and across other

morphologic features. Quantifying these variations is key to understanding the complex relationships between sediment properties, morphology, and hydrodynamics.

3. Considering geotechnical properties as significant variables in erodibility relations can improve our understanding and prediction of coastal morphodynamics.

To address these hypotheses, the following set of tasks were completed, reflecting the contents in the main body of the dissertation (Chapters 2-5):

1. A series of field data sets of geotechnical sediment properties were collected at sandy beaches in North Carolina and Southeast Alaska. Drawbacks in the measurement techniques were assessed and local environmental conditions affecting the measurement techniques were identified. Finally, the quality and feasibility of collecting geotechnical measurements was assessed and focused on areas of improvement in data collection and processing.
2. Geotechnical properties, erodibility, geomorphodynamics, and hydrodynamic regime were related using data from the sandy beach in North Carolina. Field data collection was performed using the knowledge gained from Task #1. Laboratory erodibility testing and theoretical modelling of sediment mobility using the collected field data and physical samples from the beach were performed, and comparisons to morphological change measured using ground-based LiDAR were made.
3. Using a field data set collected in Harrison Bay, Alaska, variations in geotechnical sediment properties and erodibility across a mixed nearshore to continental shelf system were quantified. Relationships developed in Objective #2 between erodibility, sediment properties, and morphology for coarse sediments were applied to the new results. Finally, new relationships were investigated for fine sediments using the field data and further laboratory erodibility testing of gravity core samples to build a more complete picture of sediment dynamics at the site.

1.4. Contributions

This research makes the following contributions to current knowledge and data availability:

1. Advancement of geotechnical measurements of beaches. Moisture content was measured over rapid spatial and temporal scales and a calibration scheme was developed to mitigate

seawater effects on the sensors. Measurement of relative density was incorporated into beach measurements and identified to fall into the range of negative values due to partial saturation. A new PFFP data analysis method is presented, introducing a new velocity-dependent strain-rate correction factor, K_{mod} which is a function of the impact velocity.

2. Relationships between direct measurements of void ratio, bulk density, firmness factor, and $qsbc$ and laboratory derived erodibility parameter k_d which controls the erosion rate after onset of erosion. A parametric study performed using laboratory derived and empirical relations for τ_{cr} showed that motion would be initiated under most circumstances for the given hydrodynamic regime at the field site, implying that k_d (which controls erosion rate) is more important than τ_{cr} for characterizing the erodibility of sands. Additionally, a framework is proposed to explain the relationship between sediment properties prior to morphologic change and how hydrodynamics driven changes in morphology change sediment properties in-situ.

3. A regional sediment classification model for an Arctic nearshore/continental shelf system is proposed using PFFP measurements to differentiate cohesive and non-cohesive sediments. Once sediments have been grouped in this way, the framework developed by Jaber (2022) is expanded upon to create categories based on erodibility parameters. These categories are able to identify zones of high and low erodibility across small and large scale spatial areas and highlight the need for consideration of high variability in sediment properties and erodibility in morphological models.

1.5. Dissertation Structure and Content

The chapters of this dissertation are a series of paper manuscripts that are combined to make the contributions outlined in the previous section. The dissertation contains an introductory chapter, four main body manuscript chapters, and six appendices.

Chapter 2 is a peer-reviewed conference contribution which details one of the first studies on PFFP deployments in beach environment. Local variations in sediment strength were studied in relation to position in the crosshore profile, and crosshore variations in strength were studied across three hydrodynamically and morphologically distinct sites in Yakutat, AK. The results of this study further supported the first hypothesis regarding the feasibility of performing geotechnical surveying of beaches.

Chapter 3 is a journal manuscript that addresses geotechnical surveying of beaches (Objective #1). A large field data set was collected using a moisture gauge, density sampling, three penetrometers, and a vane shear. Changes in geotechnical sediment properties in the crosshore profile are shown, and their importance for surficial sediment erosion is highlighted. Additionally, the suite of field tools is assessed in terms of measurement quality and feasibility. A method for obtaining relatively undisturbed density samples is presented. PFFP measurements in emerged environments are compared to a partially saturated bearing capacity theory by Vanapalli and Mohammed (2007), and this model is used to introduce a new type of velocity dependent strain rate correction. This work was motivated by the second research hypothesis regarding the importance of measuring geotechnical properties at beaches and provided further evidence of the variability in sediment properties.

Chapter 4 is journal manuscript that builds upon the lessons from Chapter 3 to begin relating geotechnical properties to erodibility at a beach environment (Objective #2). A second field data set was collected in Duck, NC with the addition of LiDAR to measure bed change. A series of in-situ samples were collected and tested in a Jet Erosion Test setup and these results are compared to the measured sediment properties. A relationship between the erosion rate parameter and packing state is established. Initiation of motion is address through both a parametric study and with the laboratory results. Discussion is focused on how sediment properties affect changes in morphology and how morphodynamic change can lead to changes in sediment properties in a type of feedback loop. This study was a first step in support of the third research hypothesis, showing that sediment properties were indeed linked to erodibility, and had implications for geomorphodynamics at beaches.

Chapter 5 is a journal manuscript assessing relationships between sediment properties and erodibility in a mixed sediment Arctic environment (Objective #3). Specific challenges and research questions for Arctic nearshore zones due to climate change are addressed in the context of better understanding local sediment dynamics. PFFP measurements are used to create a regional sediment classification scheme, and this framework is then applied to obtain strength properties for the seabed sediments. These properties are then used in conjunction with JET tests on gravity core samples to define categories of erodibility at the site. These differences in erodibility are discussed in the context of large and small scale sediment variability at the site and for use in improving numerical models of shelf morphology. The results of this work represented further

evidence in support of the third research hypothesis, as a second dataset in differing sediment types also showed the importance of including sediment properties in erodibility relationships and using those new relationships to give insights into local sediment dynamics.

Appendix A contains the data repository information and link in addition to the readme file that describes the repository files organization and contents.

Appendix B presents a calibration method for soil moistures sensors. Seawater acts to artificially increase moisture measurements in dielectric permittivity probes. This conference submission provides a simple laboratory calibration method, as well as a comparison with a field data set to affirm the utility and necessity of such calibrations, and further addresses the goal in Objective #1 of improving geotechnical characterization methods at beaches.

Appendix C is an abstract from a conference presentation providing an overview of the measurements collected in Harrison Bay, Alaska. Emphasis is placed on the high degree of variability found in the area, both across the bay as whole and on smaller scales such as single stations or along small transects. This presentation served as introduction to the measurements and concepts detailed in Chapter 5, towards completing Objective #3.

Appendix D is an extended abstract from a conference presentation detailing differences in geotechnical properties and their potential effects on local sediment transport processes. Friction angles and relative density are determined for a series of nearshore transects on a large spit via a framework proposed by Albatal et al. (2020). Differences in strength properties are discussed in terms of different migration rates for certain areas of the spit. This work highlighted again the variability of geotechnical properties in coastal environments as well as how that variability is connected to local morphodynamics, as proposed in the second research hypothesis.

Appendix E is a conference manuscript detailing crosshore variations in moisture content and sediment strength for a field site with complex morphology in Yakutat, Alaska. Variations in these properties well as the topography are discussed in context of the dominant sediment transport processes and local hydrodynamics at the site. This contribution served as a first look at highlighting the need for collecting geotechnical properties and connecting those properties to sediment transport and mobilization processes, supporting the first two hypotheses.

Appendix F is a text version of a poster presentation given to highlight a series of long term beach measurements. A long term field study was undertaken in Yakutat, Alaska that involved topographic, moisture content, and sediment strength measurements. These measurements are discussed in terms of variations in the crosshore and present another example of the utility of performing geotechnical surveys of beach environments (Objective #1).

Appendix G provides an overview of a sensitivity analysis aimed at understanding the role of erodibility parameters in numerical models. A simple case study was performed using a Delft3D cross-shelf morphodynamic model. Erosion parameters for cohesive sediments were updated to reflect the measured in-situ values, showing a reduction in bed morphological change. Future work will continue to explore the integration of in-situ variability of erodibility in the model to better the understanding of long-term shelf evolution in response to climate change, supporting the second research hypothesis.

References

Akal, T., & Stoll, R. D. (1995). Expendable penetrometer for rapid assessment of seafloor parameters. Oceans Conference Record (IEEE), 3. https://doi.org/10.1109/oceans.1995.528858

Albatal, A., & Stark, N. (2016). *In Situ Geotechnical Early Site Assessment of a Proposed Wave Energy Converter Site in Yakutat, Alaska, Using a Portable Free-Fall Penetrometer*. https://doi.org/10.1061/9780784480137.041

Albatal, A., & Stark, N. (2017). Rapid sediment mapping and in situ geotechnical characterization in challenging aquatic areas. Limnology and Oceanography: Methods, 15(8). https://doi.org/10.1002/lom3.10192

Albatal, A., Stark, N., & Castellanos, B. (2020). Estimating in situ relative density and friction angle of nearshore sand from portable free-fall penetrometer tests. Canadian Geotechnical Journal, 57(1). https://doi.org/10.1139/cgj-2018-0267

Albatal, A., Wadman, H., Stark, N., Bilici, C., & McNinch, J. (2019). Investigation of spatial and short-term temporal nearshore sandy sediment strength using a portable free fall penetrometer. Coastal Engineering, 143. https://doi.org/10.1016/j.coastaleng.2018.10.013

Amos, C. L., Droppo, I. G., Gomez, E. A., & Murphy, T. P. (2003). The stability of a remediated bed in Hamilton Harbour, Lake Ontario, Canada. Sedimentology, 50(1). https://doi.org/10.1046/j.1365-3091.2003.00542.x

ASTM D1587. (2015). Standard Practice for Thin-Walled Tube Sampling of Fine-Grained Soils for Geotechnical Purposes. *Annual Book of ASTM Standards. West Conshohocken, PA: ASTM.*

Aré, F. E. (1988). Thermal abrasion of sea coasts (part I). *Polar Geography and Geology*, *12*(1). https://doi.org/10.1080/10889378809377343

ASTM D4254-00. (2006). Standard Test Methods for Minimum Index Density and Unit Weight of Soils and Calculation of Relative Density. *Annual Book of ASTM Standards. West Conshohocken, PA: ASTM.*

ASTM D4253-16. (2006). Standard Test Methods for Maximum Index Density and Unit Weight of Soils Using a Vibratory Table. *Annual Book of ASTM Standards. West Conshohocken, PA: ASTM.*

Aubeny, C. P., & Shi, H. (2006). Interpretation of Impact Penetration Measurements in Soft Clays. Journal of Geotechnical and Geoenvironmental Engineering, 132(6). https://doi.org/10.1061/(asce)1090-0241(2006)132:6(770)

Barnes, P. W., Rearic, D. M., & Reimnitz, E. (1984). Ice Gouging Characteristics and Processes. In *The Alaskan Beaufort Sea*. https://doi.org/10.1016/b978-0-12-079030-2.50015-0

Barnes, P. W., Reimnitz, E., Ross, R., & Survey, U. S. G. (1980). Nearshore surficial sediment textures: Beaufort Sea, Alaska. In *Open-File Report*. https://doi.org/10.3133/ofr80196

Barnhart, K. R., Miller, C. R., Overeem, I., & Kay, J. E. (2016). Mapping the future expansion of Arctic open water. *Nature Climate Change*, *6*(3). https://doi.org/10.1038/nclimate2848

Bauer, B. O., Davidson-Arnott, R. G. D., Hesp, P. A., Namikas, S. L., Ollerhead, J., & Walker, I. J. (2009). Aeolian sediment transport on a beach: Surface moisture, wind fetch, and mean transport. Geomorphology, 105(1–2). https://doi.org/10.1016/j.geomorph.2008.02.016

Bender, M. A., Knutson, T. R., Tuleya, R. E., Sirutis, J. J., Vecchi, G. A., Garner, S. T., & Held, I. M. (2010). Modeled impact of anthropogenic warming on the frequency of intense Atlantic hurricanes. Science, 327(5964). https://doi.org/10.1126/science.1180568

Bolton, M. D. (1986). The strength and dilatancy of sands. Geotechnique, 36(1). https://doi.org/10.1680/geot.1986.36.1.65

Box, J. E., Colgan, W. T., Christensen, T. R., Schmidt, N. M., Lund, M., Parmentier, F. J. W., Brown, R., Bhatt, U. S., Euskirchen, E. S., Romanovsky, V. E., Walsh, J. E., Overland, J. E., Wang, M., Corell, R. W., Meier, W. N., Wouters, B., Mernild, S., Mård, J., Pawlak, J., & Olsen, M. S. (2019). Key indicators of Arctic climate change: 1971-2017. In *Environmental Research Letters* (Vol. 14, Issue 4). https://doi.org/10.1088/1748-9326/aafc1b

Briaud, J.-L. (2008). Case Histories in Soil and Rock Erosion: Woodrow Wilson Bridge, Brazos River Meander, Normandy Cliffs, and New Orleans Levees. Journal of Geotechnical and Geoenvironmental Engineering, 134(10). https://doi.org/10.1061/(asce)1090-0241(2008)134:10(1425)

Briaud, J.-L. (2013). Geotechnical Engineering: Unsaturated and Saturated Soils. John Wiley & Sons.

Briaud, J.-L., Ting, F. C. K., Chen, H. C., Gudavalli, R., Perugu, S., & Wei, G. (1999). SRICOS: Prediction of Scour Rate in Cohesive Soils at Bridge Piers. *Journal of Geotechnical and Geoenvironmental Engineering*, *125*(4). https://doi.org/10.1061/(asce)1090-0241(1999)125:4(237)

Briaud, J. L., Ting, F. C. K., Chen, H. C., Cao, Y., Han, S. W., & Kwak, K. W. (2001). Erosion Function Apparatus for Scour Rate Predictions. Journal of Geotechnical and Geoenvironmental Engineering, 127(2). https://doi.org/10.1061/(asce)1090-0241(2001)127:2(105)

Bridge, J. S., & Bennett, S. J. (1992). A model for the entrainment and transport of sediment grains of mixed sizes, shapes, and densities. *Water Resources Research*, *28*(2). https://doi.org/10.1029/91WR02570

Brilli, N. C., & Stark, N. (2020). Variations in Sediment Strength across a Sandy Peninsula. Proceedings of Geo-Congress 2020, Minneapolis, Minnesota, 769–788. https://doi.org/10.1061/9780784482810.080

Cao, Z., Day, R., & Egashira, S. (2002). Coupled and Decoupled Numerical Modeling of Flow and Morphological Evolution in Alluvial Rivers. Journal of Hydraulic Engineering, 128(3). https://doi.org/10.1061/(asce)0733-9429(2002)128:3(306)

Chin, C. O., Melville, B. W., & Raudkivi, A. J. (1994). Streambed Armoring. *Journal of Hydraulic Engineering*, *120*(8), 899–918. https://doi.org/10.1061/(asce)0733-9429(1994)120:8(899)

Chen, Y. H., & Anderson, B. A. (1987). Methodology for Estimating Embankment Damage Caused by Flood Overtopping. Transportation Research Record, 1151.

Chow, S. H., & Airey, D. W. (2014). Free-Falling Penetrometers: A Laboratory Investigation in Clay. Journal of Geotechnical and Geoenvironmental Engineering, 140(1). https://doi.org/10.1061/(asce)gt.1943-5606.0000973

Chow, S. H., Bienen, B., & Randolph, M. F. (2018). Rapid penetration of piezocones in sand. Cone Penetration Testing 2018 - Proceedings of the 4th International Symposium on Cone Penetration Testing, CPT 2018.

Dalrymple, R. A. (1992). Prediction of Storm/Normal Beach Profiles. Journal of Waterway, Port, Coastal, and Ocean Engineering, 118(2). https://doi.org/10.1061/(asce)0733-950x(1992)118:2(193)

Darke, I., & Neuman, C. M. K. (2008). Field study of beach water content as a guide to wind erosion potential. Journal of Coastal Research, 24(5). https://doi.org/10.2112/00-000.1

Davidson-Arnott, R. G., MacQuarrie, K., & Aagaard, T. (2005). The effect of wind gusts, moisture content and fetch length on sand transport on a beach. Geomorphology, 68(1–2). https://doi.org/10.1016/j.geomorph.2004.04.008

Dayal, U., & Allen, J. H. (1973). Instrumented Impact Cone Penetrometer. Canadian Geotechnical Journal, 10(3). https://doi.org/10.1139/t73-034

Dayal, U., Allen, J. H., & Jones, J. M. (1975). Use of an impact penetrometer for the evaluation of the in-situ strength of marine sediments. Marine Geotechnology, 1(2). https://doi.org/10.1080/10641197509388155

de Beer, E. E. (1965). Bearing capacity and settlement of shallow foundations on sand. Proceedings of Symposium on Bearing Capacity and Settlement of Foundations.

de Smit, J. C., Kleinhans, M. G., Gerkema, T., & Bouma, T. J. (2021). Quantifying natural sediment erodibility using a mobile oscillatory flow channel. Estuarine, Coastal and Shelf Science, 262. https://doi.org/10.1016/j.ecss.2021.107574

Dean, R. G. (1973). Heuristic Models of Sand Transport in the Surf Zone. Proceedings of the Australian Conference on Coastal Engineering, Sydney, NSW, (MAY 14-17, 1973).

Dean, R. G., & Dalrymple, R. A. (2004). Coastal Processes with Engineering Applications. In Coastal Processes with Engineering Applications. https://doi.org/10.1017/cbo9780511754500

Dorvinen, J., Stark, N., Hatcher, B., Hatcher, M., Leys, V., & Kopf, A. (2018). In Situ Assessment of Sediment Erosion and Consolidation State Using a Free-Fall Penetrometer: Sydney Harbour, Nova Scotia. Journal of Waterway, Port, Coastal, and Ocean Engineering, 144(2). https://doi.org/10.1061/(asce)ww.1943-5460.0000423

Duncan, J. M., Wright, S. G., & Brandon, T. L. (2014). Soil Strength and Slope Stability, 2nd Edition. In John Wiley & Sons.

Erikson, L. H., Larson, M., & Hanson, H. (2007). Laboratory investigation of beach scarp and dune recession due to notching and subsequent failure. Marine Geology, 245(1–4). https://doi.org/10.1016/j.margeo.2007.04.006

Flodkvist, H., Hjulström, F., & Hjulstrom, F. (1936). Studies of the Morphological Activity of Rivers as Illustrated by the River Fyris. Geografiska Annaler, 18. https://doi.org/10.2307/519824

Ford, J. D., Smit, B., & Wandel, J. (2006). Vulnerability to climate change in the Arctic: A case study from Arctic Bay, Canada. *Global Environmental Change*, *16*(2). https://doi.org/10.1016/j.gloenvcha.2005.11.007

Forest, A., Osborne, P. D., Curtiss, G., & Lowings, M. G. (2016). Current surges and seabed erosion near the shelf break in the Canadian Beaufort Sea: A response to wind and ice motion stress. *Journal of Marine Systems*, *160*. https://doi.org/10.1016/j.jmarsys.2016.03.008

Frederick, J. M., Thomas, M. A., Bull, D. L., Jones, C. A., & Roberts, J. D. (2016). The Arctic Coastal Erosion Problem. *Sandia Report*, *SAND2016-9*.

Fredlund, D. G., & Rahardjo, H. (1993). Soil Mechanics for Unsaturated Soils. In Soil Mechanics for Unsaturated Soils. https://doi.org/10.1002/9780470172759

Gallagher, E., Wadman, H., McNinch, J., Reniers, A., & Koktas, M. (2016). A conceptual model for spatial Grain size variability on the surface of and within beaches. Journal of Marine Science and Engineering, 4(2). https://doi.org/10.3390/jmse4020038

Ghebreiyessus, Y. T., Gantzer, C. J., Alberts, E. E., & Lentz, R. W. (1994). Soil erosion by concentrated flow. Shear stress and bulk density. *Transactions of the American Society of Agricultural Engineers*, *37*(6). https://doi.org/10.13031/2013.28268

Grabowski, R. C., Droppo, I. G., & Wharton, G. (2011). Erodibility of cohesive sediment: The importance of sediment properties. In Earth-Science Reviews (Vol. 105, Issues 3–4). https://doi.org/10.1016/j.earscirev.2011.01.008

Graf, W. H. (1984). Hydraulics of sediment transport. Hydraulics of Sediment Transport. https://doi.org/10.5772/25982

Gui, M. W., & Bolton, M. D. (1998). Geometry and scale effects in CPT and pile design. In P. K. Robertson & P. W. Mayne (Eds.), 1st International Conference on Site Characterization, ISC'98 (pp. 1063–1068).

Hallermeier, R. J. (1980). A profile zonation for seasonal sand beaches from wave climate. Coastal Engineering, 4(C). https://doi.org/10.1016/0378-3839(80)90022-8

Hanson, G. J. (1991). Development of a jet index to characterize erosion resistance of soils in earthen spillways. Transactions of the American Society of Agricultural Engineers, 34(5). https://doi.org/10.13031/2013.31831

Hanson, G. J., & Cook, K. R. (2004). Apparatus, test procedures, and analytical methods to measure soil erodibility in situ. *Applied Engineering in Agriculture*, *20*(4).

Hanson, G. J., & Cook, K. R. (1997). Development of excess shear stress parameters for circular jet testing. *Paper - American Society of Agricultural Engineers*, *2*.

Hanson, G. J., & Simon, A. (2001). Erodibility of cohesive streambeds in the loess area of the Midwestern USA. *Hydrological Processes*, *15*(1). https://doi.org/10.1002/hyp.149

Hashemi, S., Shiri, H., & Dong, X. (2022). The influence of layered soil on ice-seabed interaction: Soft over stiff clay. *Applied Ocean Research*, *120*. https://doi.org/10.1016/j.apor.2021.103033

Heathershaw, A. D., Carr, A. P., Blackley, M. W. L., & Wooldridge, C. F. (1981). Tidal variations in the compaction of beach sediments. Marine Geology, 41(3–4). https://doi.org/10.1016/0025-3227(81)90082-7

Héquette, A., Desrosiers, M., Hill, P. R., & Forbes, D. L. (2001). The influence of coastal morphology on shoreface sediment transport under storm-combined flows, Canadian Beaufort Sea. *Journal of Coastal Research*, *17*(3).

Hir, P. le, Cann, P., Waeles, B., Jestin, H., & Bassoullet, P. (2008). Chapter 11 Erodibility of natural sediments: experiments on sand/mud mixtures from laboratory and field erosion tests. Proceedings in Marine Science, 9. https://doi.org/10.1016/S1568-2692(08)80013-7

Jackson, D. W. T., Cooper, J. A. G., & del Rio, L. (2005). Geological control of beach morphodynamic state. Marine Geology, 216(4). https://doi.org/10.1016/j.margeo.2005.02.021

Jafari, N. H., Harris, B. D., & Stark, T. D. (2018). Geotechnical investigations at the caminada headlands beach and dune in coastal Louisiana. Coastal Engineering, 142. https://doi.org/10.1016/j.coastaleng.2018.04.014

Jones, B. M., Arp, C. D., Jorgenson, M. T., Hinkel, K. M., Schmutz, J. A., & Flint, P. L. (2009). Increase in the rate and uniformity of coastline erosion in Arctic Alaska. Geophysical Research Letters, 36(3). https://doi.org/10.1029/2008GL036205

Jones, G. S., Stott, P. A., & Christidis, N. (2008). Human contribution to rapidly increasing frequency of very warm Northern Hemisphere summers. Journal of Geophysical Research Atmospheres, 113(2). https://doi.org/10.1029/2007JD008914

Kiptoo, D., Stark, N., Massey, G., Wright, C., & Friedrichs, C. T. (2020). Strain Rate Effects in Soft Estuarine Soils using Portable Free Fall Penetrometers. Proceedings of Ocean Science Meeting, San Diego, California.

Kim, T.-H. (2001). *Moisture-Induced Tensile Strength and Cohesion in Sand*.

Kirchner, J. W., Dietrich, W. E., Iseya, F., & Ikeda, H. (1990). The variability of critical shear stress, friction angle, and grain protrusion in water-worked sediments. Sedimentology, 37(4). https://doi.org/10.1111/j.1365-3091.1990.tb00627.x

Knutson, T. R., McBride, J. L., Chan, J., Emanuel, K., Holland, G., Landsea, C., Held, I., Kossin, J. P., Srivastava, A. K., & Sugi, M. (2010). Tropical cyclones and climate change. In Nature Geoscience (Vol. 3, Issue 3). https://doi.org/10.1038/ngeo779

Lane, E. W., & Carlson, E. J. (1954). Some observations on the effect of particle shape on the movement of coarse sediments. *Eos, Transactions American Geophysical Union*, *35*(3), 453–462. https://doi.org/10.1029/TR035i003p00453

Lantuit, H., & Pollard, W. H. (2008). Fifty years of coastal erosion and retrogressive thaw slump activity on Herschel Island, southern Beaufort Sea, Yukon Territory, Canada. *Geomorphology*, *95*(1–2). https://doi.org/10.1016/j.geomorph.2006.07.040

Lee, K. L., & Seed, H. B. (1967). Drained Strength Characteristics of Sands. Journal of the Soil Mechanics and Foundations Division, 93(6). https://doi.org/10.1061/jsfeaq.0001048

Lu, N., Kim, T.-H., Sture, S., & Likos, W. J. (2009). Tensile Strength of Unsaturated Sand. Journal of Engineering Mechanics, 135(12). https://doi.org/10.1061/(asce)em.1943-7889.0000054

Lu, N., & Likos, W. J. (2006). Suction Stress Characteristic Curve for Unsaturated Soil. Journal of Geotechnical and Geoenvironmental Engineering, 132(2). https://doi.org/10.1061/(asce)1090-0241(2006)132:2(131)

Lucking, G., Stark, N., Lippmann, T., & Smyth, S. (2017). Variability of in situ sediment strength and pore pressure behavior of tidal estuary surface sediments. Geo-Marine Letters, 37(5). https://doi.org/10.1007/s00367-017-0494-6

Lyle, W. M., & Smerdon, E. T. (1965). Relation of Compaction and Other Soil Properties to Erosion Resistance of Soils. Transactions of the ASAE, 8(3). https://doi.org/10.13031/2013.40536

Macdonald, R. W., Kuzyk, Z. Z. A., & Johannessen, S. C. (2015). The vulnerability of Arctic shelf sediments to climate change. In *Environmental Reviews* (Vol. 23, Issue 4). https://doi.org/10.1139/er-2015-0040

Madsen, O. S., & Grant, W. D. (1976). Sediment Transport in the Coastal Environment. MIT Dep Civ Eng Ralph M, Parsons Lab Water Resource Hydrodynamics Rep, 209.

Malito, J., Eidam, E., & Nienhuis, J. (2022). Increasing Wave Energy Moves Arctic Continental Shelves Toward a New Future. *Journal of Geophysical Research: Oceans*, *127*(9). https://doi.org/10.1029/2021JC018374

Manning, M., & Stark, N. (2019). Investigating moisture contents of sandy beaches in the context of a geotechnical site characterization. https://doi.org/10.1142/9789811204487_0219

Masselink, G., Kroon, A., & Davidson-Arnott, R. G. D. (2006). Morphodynamics of intertidal bars in wave-dominated coastal settings - A review. Geomorphology, 73(1–2). https://doi.org/10.1016/j.geomorph.2005.06.007

Masselink, G., & Short, A. D. (1993). The effect of tide range on beach morphodynamics and morphology: a conceptual beach model. Journal of Coastal Research, 9(3).

Miller, R. L., & Byrne, R. J. (1966). The angle of repose of a single grain on a fixed rough bed. Sedimentology, 6(4). https://doi.org/10.1111/j.1365-3091.1966.tb01897.x

Mulhearn, P. J. (2001). Methods of Obtaining Soil Strength Data for Modelling Vehicle Trafficability on Beaches.

Mulukutla, G. K., Huff, L. C., Melton, J. S., Baldwin, K. C., & Mayer, L. A. (2011). Sediment identification using free fall penetrometer acceleration-time histories. Marine Geophysical Research, 32(3). https://doi.org/10.1007/s11001-011-9116-2

Mumtaz, M. B., Stark, N., & Brizzolara, S. (2018). Pore pressure measurements using a portable free fall penetrometer. Cone Penetration Testing 2018 - Proceedings of the 4th International Symposium on Cone Penetration Testing, CPT 2018.

Mumtaz, M. B., & Stark, N. (2020). Pore Pressure Dissipation Induced by High-Velocity Impacts of a Portable Free-Fall Penetrometer in Clays. *Journal of Geotechnical and Geoenvironmental Engineering*, *146*(9). https://doi.org/10.1061/(asce)gt.1943-5606.0002273

Neill, C. (1967). Mean-Velocity Criterion for Scour of Coarse Uniform Bed-Material. 3.

Nematzadeh, A., & Shiri, H. (2020). The influence of non-linear stress-strain behavior of dense sand on seabed response to ice gouging. *Cold Regions Science and Technology*, *170*. https://doi.org/10.1016/j.coldregions.2019.102929

Osborne, P. D., & Forest, A. (2016). Sediment dynamics from coast to slope - Southern Canadian Beaufort Sea. *Journal of Coastal Research*, *1*(75). https://doi.org/10.2112/SI75-108.1

Overeem, I., & Syvitski, J. P. M. (2010). Shifting discharge peaks in arctic rivers, 1977-2007. Geografiska Annaler, Series A: Physical Geography, 92(2). https://doi.org/10.1111/j.1468-0459.2010.00395.x

Overeem, I., Anderson, R. S., Wobus, C. W., Clow, G. D., Urban, F. E., & Matell, N. (2011). Sea ice loss enhances wave action at the Arctic coast. *Geophysical Research Letters*, *38*(17). https://doi.org/10.1029/2011GL048681

Parchure, T. M., & Mehta, A. J. (1985). Erosion of Soft Cohesive Sediment Deposits. Journal of Hydraulic Engineering, 111(10). https://doi.org/10.1061/(asce)0733-9429(1985)111:10(1308)

Proffitt, G. T. (1980). *Selective Transport and Armoring of Non-Uniform Alluvial Sediments*.

Rachold, V., Grigoriev, M. N., Are, F. E., Solomon, S., Reimnitz, E., Kassens, H., & Antonow, M. (2000). Coastal erosion vs riverine sediment discharge in the Arctic shelf seas. *International Journal of Earth Sciences*, *89*(3). https://doi.org/10.1007/s005310000113

Randolph, M. F. (2016). New tools and directions in offshore site investigation. Proceedings of the 5th International Conference on Geotechnical and Geophysical Site Characterisation, ISC 2016, 1.

Reeve, B., Stark, N., & Mewis, P. (2018). Cross-shore variation in sediment strength at a sandy beach. Coastal Engineering Proceedings, 36. https://doi.org/10.9753/icce.v36.sediment.83

Reimnitz, E., Barnes, P. W., Toimil, L. J., & Melchior, J. (1977). Ice gouge recurrence and rates of sediment reworking, Beaufort Sea, Alaska. *Geology*, *5*(7). https://doi.org/10.1130/0091-7613(1977)5<405:IGRARO>2.0.CO;2

Reimnitz, E., Graves, S. M., Barnes, P. W., & Survey, U. S. G. (1985). Beaufort Sea coastal erosion, shoreline evolution, and sediment flux. In *Open-File Report*. https://doi.org/10.3133/ofr85380

Roberts, J., Jepsen, R., Gotthard, D., & Lick, W. (1998). Effects of Particle Size and Bulk Density on Erosion of Quartz Particles. Journal of Hydraulic Engineering, 124(12). https://doi.org/10.1061/(asce)0733-9429(1998)124:12(1261)

Sallenger, J. (2000). Storm impact scale for barrier islands. Journal of Coastal Research, 16(3).

Sassa, S., & Watabe, Y. (2007). Role of suction dynamics in evolution of intertidal sandy flats: Field evidence, experiments, and theoretical model. Journal of Geophysical Research: Earth Surface, 112(1). https://doi.org/10.1029/2006JF000575

Sassa, S., & Watabe, Y. (2009). Persistent sand bars explained by geodynamic effects. *Geophysical Research Letters*, *36*(1). https://doi.org/10.1029/2008GL036230

Sassa, S., & Yang, S. (2019). Role of geoenvironmental dynamics in the biodiversity of sandy beaches and sandflats: The ecohabitat chart and its ecological implications. Estuarine, Coastal and Shelf Science, 219. https://doi.org/10.1016/j.ecss.2019.02.002

Sassa, S., Yang, S., Watabe, Y., Kajihara, N., & Takada, Y. (2014). Role of suction in sandy beach habitats and the distributions of three amphipod and isopod species. Journal of Sea Research, 85. https://doi.org/10.1016/j.seares.2013.06.005

Seifert, A., Stegmann, S., Mörz, T., Lange, M., Wever, T., & Kopf, A. (2008). In situ pore-pressure evolution during dynamic CPT measurements in soft sediments of the western Baltic Sea. Geo-Marine Letters, 28(4). https://doi.org/10.1007/s00367-008-0102-x

Shafii, I., Briaud, J. L., Chen, H. C., & Shidlovskaya, A. (2016). Relationship between soil erodibility and engineering properties. Scour and Erosion - Proceedings of the 8th International Conference on Scour and Erosion, ICSE 2016. https://doi.org/10.1201/9781315375045-134

Shields, I. A. (1936). Anwendung der Aehnlichkeitsmechanik und der Turbulenzforschung auf die Geschiebebewegung. [English title: Application of similarity principles and turbulence research to bed-load movement]. Preussische Versuchsanstalt Für Wasserbau Und Schiffbau, 26.

Silva, M. F., White, D. J., & Bolton, M. D. (2006). An analytical study of the effect of penetration rate on piezocone tests in clay. International Journal for Numerical and Analytical Methods in Geomechanics, 30(6). https://doi.org/10.1002/nag.490

Singh, H. V., & Thompson, A. M. (2016). Effect of antecedent soil moisture content on soil critical shear stress in agricultural watersheds. Geoderma, 262. https://doi.org/10.1016/j.geoderma.2015.08.011

Smerdon, E., & Beasley, R. (1961). Critical tractive forces in cohesive soils. Agricultural Engineering, 42(1).

Soulsby, R. (1997). Dynamics of marine sands: a manual for practical applications. In Dynamics of marine sands: a manual for practical applications.

Soulsby, R. L., & Whitehouse, R. J. S. (1997). Threshold of sediment motion in coastal environments. Proceedings Pacific Coasts and Ports 1997 Conference, 1(c).

Stark, N., Coco, G., Bryan, K. R., & Kopf, A. (2012). In-situ geotechnical characterization of mixed-grain-size bedforms using a dynamic penetrometer. Journal of Sedimentary Research, 82(7). https://doi.org/10.2110/jsr.2012.45

Stark, N., Hanff, H., Svenson, C., Ernstsen, V. B., Lefebvre, A., Winter, C., & Kopf, A. (2011). Coupled penetrometer, MBES and ADCP assessments of tidal variations in surface sediment layer characteristics along active subaqueous dunes, Danish Wadden Sea. Geo-Marine Letters, 31(4). https://doi.org/10.1007/s00367-011-0230-6

Stark, N., & Kopf, A. (2011). Detection and quantification of sediment remobilization processes using a dynamic penetrometer. OCEANS'11 - MTS/IEEE Kona, Program Book. https://doi.org/10.23919/oceans.2011.6106914

Stark, N., Kopf, A., Hanff, H., Stegmann, S., & Wilkens, R. (2009). Geotechnical investigations of sandy seafloors using dynamic penetrometers. MTS/IEEE Biloxi - Marine Technology for Our Future: Global and Local Challenges, OCEANS 2009. https://doi.org/10.23919/oceans.2009.5422460

Stark, N., Quinn, B., Ziotopoulou, K., & Lantuit, H. (2015). Geotechnical investigation of pore pressure behavior of muddy seafloor sediments in an arctic permafrost environment. *Proceedings of the International Conference on Offshore Mechanics and Arctic Engineering - OMAE, 1*. https://doi.org/10.1115/OMAE2015-41583

Stark, N., Radosavljevic, B., Quinn, B., & Lantuit, H. (2017). Application of portable free-fall penetrometer for geotechnical investigation of arctic nearshore zone. *Canadian Geotechnical Journal*, *54*(1). https://doi.org/10.1139/cgj-2016-0087

Stark, N., & Ziotopoulou, K. (2017). Undrained Shear Strength of Offshore Sediments from Portable Free Fall Penetrometers: Theory, Field Observations and Numerical Simulations. In *Offshore Site Investigation Geotechnics 8th International Conference Proceedings.* https://doi.org/10.3723/osig17.391

Stark, N., Staelens, P., Hay, A. E., Hatcher, B., & Kopf, A. (2014). Geotechnical investigation of coastal areas with difficult access using portable free-fall penetrometers. Proceedings of the CPT, 14, 12–14.

Steiner, A., Kopf, A. J., L'Heureux, J. S., Kreiter, S., Stegmann, S., Haflidason, H., & Moerz, T. (2014). In situ dynamic piezocone penetrometer tests in natural clayey soils - a reappraisal of strain-rate corrections. Canadian Geotechnical Journal, 51(4). https://doi.org/10.1139/cgj-2013-0048

Stephan, S., Kaul, N., & Villinger, H. (2015). Validation of impact penetrometer data by cone penetration testing and shallow seismic data within the regional geology of the Southern North Sea. Geo-Marine Letters, 35(3). https://doi.org/10.1007/s00367-015-0401-y

Stoll, R. D., & Akal, T. (1999). XBP - Tool for rapid assessment of seabed sediment properties: Instrumented with accelerometers, new expendable probes measure the impact signature of the ocean bottom. In Sea Technology (Vol. 40, Issue 2).

Stoll, R. D., Sun, Y. F., & Bitte, I. (2007). Seafloor properties from penetrometer tests. IEEE Journal of Oceanic Engineering, 32(1). https://doi.org/10.1109/JOE.2007.890943

Ternat, F., Boyer, P., Anselmet, F., & Amielh, M. (2008). Erosion threshold of saturated natural cohesive sediments: Modeling and experiments. Water Resources Research, 44(11). https://doi.org/10.1029/2007WR006537

True, D. G. (1976). Undrained vertical penetration into ocean bottom soils [Ph.D Dissertation]. University of California-Berkeley.

van Rijn, L. C. (2007). Unified View of Sediment Transport by Currents and Waves. II: Suspended Transport. Journal of Hydraulic Engineering, 133(6). https://doi.org/10.1061/(asce)0733-9429(2007)133:6(668)

van Rijn, L. C. (2020). Erodibility of Mud–Sand Bed Mixtures. Journal of Hydraulic Engineering, 146(1). https://doi.org/10.1061/(asce)hy.1943-7900.0001677

Vanapalli, S. K., & Mohamed, F. M. O. (2007). Bearing Capacity of Model Footings in Unsaturated Soils. In Experimental Unsaturated Soil Mechanics. https://doi.org/10.1007/3-540-69873-6_48

Wang, M., & Overland, J. E. (2015). Projected future duration of the sea-ice-free season in the Alaskan Arctic. Progress in Oceanography, 136. https://doi.org/10.1016/j.pocean.2015.01.001

Watts, C. W., Tolhurst, T. J., Black, K. S., & Whitmore, A. P. (2003). In situ measurements of erosion shear stress and geotechnical shear strength of the intertidal sediments of the experimental managed realignment scheme at Tollesbury, Essex, UK. Estuarine, Coastal and Shelf Science, 58(3). https://doi.org/10.1016/S0272-7714(03)00139-2

White, D. J., O'Loughlin, C. D., Stark, N., & Chow, S. H. (2018). Interpretation of free fall penetrometer tests in sands : An approach to determining the equivalent static resistance. Cone Penetration Testing 2018, June.

Wilson, B. N. (1993). Evaluation of a fundamentally based detachment model. In Transactions - American Society of Agricultural Engineers (Vol. 36, Issue 4). https://doi.org/10.13031/2013.28442

Winterwerp, J. C., & van Kesteren, W. G. M. (2004). Introduction to the Physics of Cohesive Sediment in the Marine Environment. In *Journal of Materials Processing Technology* (Vol. 1, Issue 1).

Winterwerp, J. C., van Kesteren, W. G. M., van Prooijen, B., & Jacobs, W. (2012). A conceptual framework for shear flow–induced erosion of soft cohesive sediment beds. Journal of Geophysical Research: Oceans, 117. https://doi.org/10.1029/2012JC008072

Zambrano-Cruzatty, L., Yerro, A., & Stark, N. (2019). Influence of Shear Strength and Moisture Content on Aeolian Sand Erosion. Proceedings of Geo-Congress 2019, Philadelphia, Pennsylvania. https://doi.org/10.1061/9780784482155.001

Zhang, K., Douglas, B. C., & Leatherman, S. P. (2004). Global warming and coastal erosion. Climatic Change, 64(1–2). https://doi.org/10.1023/B:CLIM.0000024690.32682.48

Chapter 2: Variation in Sediment Strength Across a Sandy Peninsula

The contributions of the authors to the composition of this manuscript are delineated as follows:

Nicola Brilli:

- Participated in the field survey
- Performed literature review; processed and analyzed field data; prepared figures, tables, and draft of manuscript
- Revised manuscript based on suggestions of co-author
- Addressed comments from outside reviewers and prepared final manuscript

Nina Stark:

- Lead primary investigator of this study
- Initiated research idea and co-developed the refined research questions
- Planned, supervised, and participated in the field survey in Yakutat, Alaska
- Reviewed and edited the draft manuscript
- Reviewed and edited the response to reviewer comments and the final version of the manuscript

Variations in Sediment Strength Across a Sandy Peninsula

Nicola C. Brilli[1] and Nina Stark[2], Ph.D., M.ASCE

[1]Virginia Tech, Department of Civil and Environmental Engineering, Blacksburg, VA 24060; e-mail: nickb96@vt.edu

[2]Virginia Tech, Department of Civil and Environmental Engineering, Blacksburg, VA 24060; e-mail: ninas@vt.edu

Published by the American Society of Civil Engineers (ASCE) as part of the proceedings of Geo-Congress 2020: University of Minnesota 68th Annual Geotechnical Engineering Conference, February 25-28, 2020, Minneapolis, MN

Reference:

Brilli, N. C., & Stark, N. (2020). Variations in Sediment Strength across a Sandy Peninsula. *Proceedings of Geo-Congress 2020, Minneapolis, Minnesota*, 769–788. https://doi.org/10.1061/9780784482810.080

2.1. Abstract

Phipps Peninsula is a sandy peninsula located near the town of Yakutat, Alaska. In the summer of 2018, a field study was conducted in three areas of the peninsula. All three locations feature complex sediment remobilization processes shaping the local geomorphology. Here, variations in geotechnical properties at the three test sites are investigated. For this purpose, a portable free fall penetrometer (PFFP) was deployed along several transects at the three sites, totaling approximately 750 deployments throughout the course of the study. Since field studies using PFFP on sub-aerial and intertidal beach areas are limited, and results are highly variable, novel methods were implemented for the analysis of the PFFP data. This study represents a first step towards the use of PFFP data to characterize geotechnical properties on sub-aerial and intertidal beaches. Temporal differences in strength are discussed in the context of local physical processes, and spatial variability was related to differences in morphology and hydrodynamics.

2.2. Introduction

Sediment strength (e.g., in terms of bearing capacity and/or shear strength) is an important consideration for many coastal applications, including assessing beach trafficability and understanding local sediment transport/remobilization processes. However, coastal environments present unique challenges for measuring sediment strength. Nearshore areas are often highly energetic and beach environments can be affected by dynamic geomorphodynamics. This makes the use of the heavy equipment typical to geotechnical surveying impractical in these areas and sometimes unsuitable to test near-surface sediments. In the nearshore zone, portable free-fall penetrometers (PFFPs), which are low-cost, lightweight, and easily deployable from a small craft, enable a geotechnical characterization of surficial subaqueous sediments in energetic coastal environments (Stark et al. 2014a). For sandy nearshore sediments, analysis of PFFP data can provide an estimate of equivalent cone resistance (Akal and Stoll 1995; Stoll et al. 2007; Stark et al. 2009, 2012; Lucking et al. 2017), relative density, and friction angle (Albatal et al. 2019) using deceleration measurements. However, this work has rarely been extended onto the sub-aerial and intertidal (exposed to the air, not submerged) beach areas (Reeve et al. 2018). An added complexity of using PFFP on beaches stems mainly from the effects of partial saturation, which introduces an apparent cohesion adding to the sediment strength that may change with time (Lu and Likos 2006, 2013). Other factors affecting local sediment strength include complex groundwater-swash zone interaction (Heiss et al. 2014, 2015) and spatiotemporal variations in geomorphology and sediment

distributions in response to tidal variations and hydrodynamic forcing (Masselink et al. 2006; Sassa and Watabe 2007, 2009). As an initial step towards extending the use of PFFPs into sub-aerial and intertidal beach environments, this paper aims to examine the strength data obtained from PFFP deployments at three beaches, analyze temporal differences in strength along a crosshore transect, and discern if hydrodynamic and morphodynamic differences can explain differences in strength profiles at three distinct sites.

2.3. Regional Context

This study was performed on Phipps Peninsula, a sandy peninsula west of the town of Yakutat, Alaska. Yakutat is located about 225 miles northwest of Juneau, and Phipps Peninsula is bordered by the Gulf of Alaska to the southwest, Yakutat Bay to northwest, and Monti Bay to the northeast. Figure 2.1 shows the overall area and the location of the three study sites. The following sections will detail the local geology, geomorphology, and hydrodynamic conditions of the three different sites.

Figure 2.1: Site Geography and Study Locations, Source: “Yakutat” 59°32'33.01"N and 139°49'35.74"W. Google Earth. May 11, 2016.

2.3.1. Geology

All three test sites are composed of predominantly fine quartz sand, having a dark color due to the presence of heavy minerals. Cannon Beach was the only site characterized by an appreciable increase in median grain size (d_{50}) along a crosshore profile, increasing from 230 μm to 310 μm from the dune towards the low water line. Sediment distributions at Ocean Cape and Point Carrew were more uniform, with a median grain size of 260 μm. Ocean Cape features additionally a large boulder field located on a low-tide terrace, likely due to local erosion of the headland, which was not surveyed in this study. The Yakutat area is seismically active. Thus, the beaches have the potential for liquefaction and/or impacts of submarine landslides during earthquakes (Yehle 1971).

2.3.2. Morphology

Cannon Beach is wide (150 m) and has the most gently sloping intertidal zone (3°) of the three beaches evaluated, Ocean Cape is much narrower (80 m) and steeper (5°) and Point Carrew is a very wide sandy spit (460 m), also with a steeper intertidal zone (5°) (Table 2.1). Ridge-runnel systems (King and Williams 1949) were observed at all three sites, but the crosshore transect at Cannon Beach did not capture this feature at the time of measurements.

Table 2.1: Morphology Summary

Site	Low-Tide Beach Width (meters)	Intertidal Slope (degrees)
Cannon Beach	150	3.1
Ocean Cape	80	5.1
Point Carrew	460	5.0

2.3.3. Hydrodynamics

Exposed to swell from the Gulf of Alaska, Cannon Beach features the overall highest wave energy of the three sites, with the predominant wave direction from the south. Ocean Cape is exposed to similar hydrodynamic conditions as Cannon Beach, being located at the headland between the Gulf of Alaska and Yakutat Bay. The annual average significant wave height for these two sites is 1.9 m at the 10 m depth contour (Previsic and Bedard 2009). The wave climate drives strong longshore sediment transport along the beach to the north. Here, the waves refract around the peninsula, depositing sediment and forming the spit at Point Carrew. Point Carrew is sheltered from the ocean swell, facing northeast on Monti Bay, and has an average significant wave height of 0.5 m at 10 m depth. The average annual wave height 50 km offshore is 2.5 m (Previsic and Bedard 2009).

2.4. Methods

Two to three (eight in total) cross-shore transects were investigated at each site over a 6-day period. The PFFP *blueDrop* (Stark et al. 2014b) was deployed three times at each station along the cross-shore profiles. The device is of streamlined torpedo-like shape, 63.1 cm long, and has a mass of 7.71 kg. It is equipped with five vertical microelectromechanical systems (MEMS) accelerometers, two horizontal MEMS accelerometers, a pressure transducer, which was not utilized for this study, and a conical steel tip. The accelerometers can measure $\pm$1.7-250 g in the vertical, and $\pm$55 g (g is gravitational acceleration) in the horizontal to determine tilt. The device was released about 1 m above the sediment surface, which is high enough for the probe to obtain an impact velocity of 4-5 m/s while not tiring the operator. It fell freely through air, and then penetrated the sediment, being brought to a stop by the sediment resistance. The accelerometers, recording continuously at 2 kHz, captured the full acceleration-deceleration profile at a sub-centimeter vertical resolution once double-integrated. Using Newton's 2nd Law, the deceleration profile from impact to stop is converted into a sediment resistance force, and then into a dynamic bearing capacity or cone resistance considering the cone area. The equivalent of a quasi-static bearing capacity (*qsbc*) is then estimated by applying a strain rate correction to normalize to a constant velocity (2 cm/s) following Dayal and Allen (1973). The underlying assumptions and detailed explanation of the process to acquire a *qsbc* profile from the deceleration profile is provided in Stark et al. (2012). While there is uncertainty related to the strain rate correction factor, K, Albatal et al. (2019) found good agreement using K = 0.3 for sands from this region. This value was therefore adopted here as well. Finally, integrating the deceleration profile can provide the impact velocity, and double integration provides the penetration depth (Dayal and Allen 1973; Stoll and Akal 1999; Stark and Wever 2009). Time constraints prevented independent measurements of penetration depth at every deployment location, but the derived penetration depth was confirmed by occasional measurements and available photo materials. The pressure sensor was not utilized here due to limited penetration depths (often < 7.5 cm, thus, the pressure transducer ports have not been embedded in the soil) and a complex pore pressure response to partially saturated sediments that was out of the scope of this article. Over the course of the study, the PFFP was deployed 753 times along the eight transects.

Other field methods included: sediment sampling along each transect at PFFP deployment locations to obtain moisture contents and bulk densities, simplistic topographic profiling to

measure beach slopes and small-scale temporal morphological change, and recording of wave heights by anchoring an *RBR Solo* pressure sensor in the beach face. Over 300 sediment samples were weighed and oven-dried, and pressure sensors were deployed over several tidal cycles to accurately represent the wave climate.

2.5. Results

2.5.1. Beach Profiles

Topographic profiles measured at each location are provided as visual aid to explain the differences in morphology and as support for discussion (Figure 2.2).

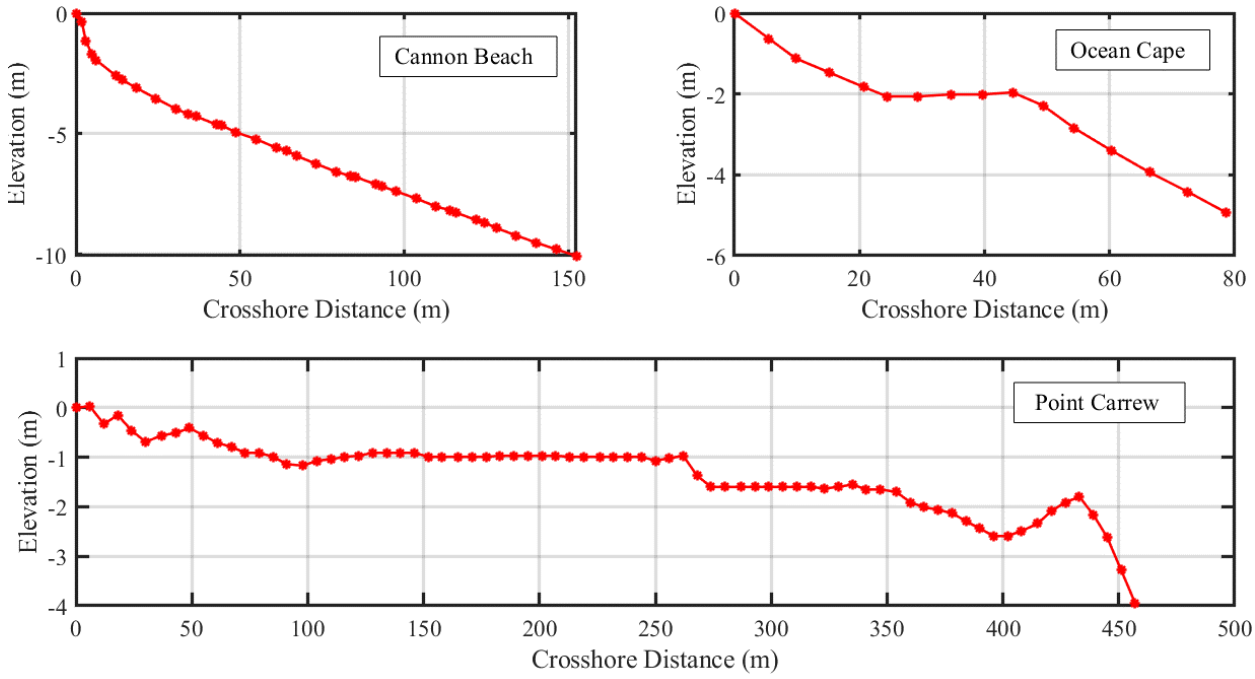

Figure 2.2: Topographic profiles at Cannon Beach (Top Left), Ocean Cape (Top Right), and Point Carrew (Bottom), Point Carrew profile adapted from Stark et al. (2019). The beginning of each profile (0m crosshore distance) corresponds to the toe of the dune.

2.5.2. Penetrometer Deployments

High variability of the PFFP profiles was observed (Figure 2.3). The profiles were grouped into three general types, based on their shape with sediment depth. Type A profiles (Figure 2.3 left) resembled the typical strength profile shape found by Albatal and Stark (2016) for sediments just offshore of Phipps Peninsula, and were seen predominantly for penetration depths greater than 10 centimeters. They feature low strengths in the upper 5 cm of the profile, followed by an increase in strength with depth until reaching a maximum, after which the decrease is due to the

penetrometer coming to a stop. Type B profiles (Figure 2.3 center) exhibited an approximately constant sediment strength with depth, lacked a well-defined maximum, and were typical of penetration depths of 7-10 centimeters (slightly deeper than the cone height). Type C (Figure 2.3 right) profiles were observed for deployments in the swash zone of the beach where the penetration depth was less than 7 centimeters (less than the cone height). The observed decrease in strength could be due to the probe falling over. It is important to note that the maximum *qsbc* increased from Type A to C, ranging from 50-500 kPa. For profiles resembling the Type A shape, the maximum *qsbc* is often compared to investigate spatiotemporal variations (Albatal and Stark 2016). However, defining a consistent strength from maximum value becomes difficult when Type A, B, & C profiles were all observed along the same transect. Therefore, it was decided to use the *qsbc* at 4 centimeters of penetration depth as a comparable sediment strength between all deployments. This depth was chosen because all deployments reached at least 4 centimeters, giving a surficial strength for every deployment, and this decision allowed for a consistent comparison between otherwise varying results. It should be noted that this choice of depth is somewhat arbitrary, and could vary for different sites, based on the range of penetration depths present in the data set.

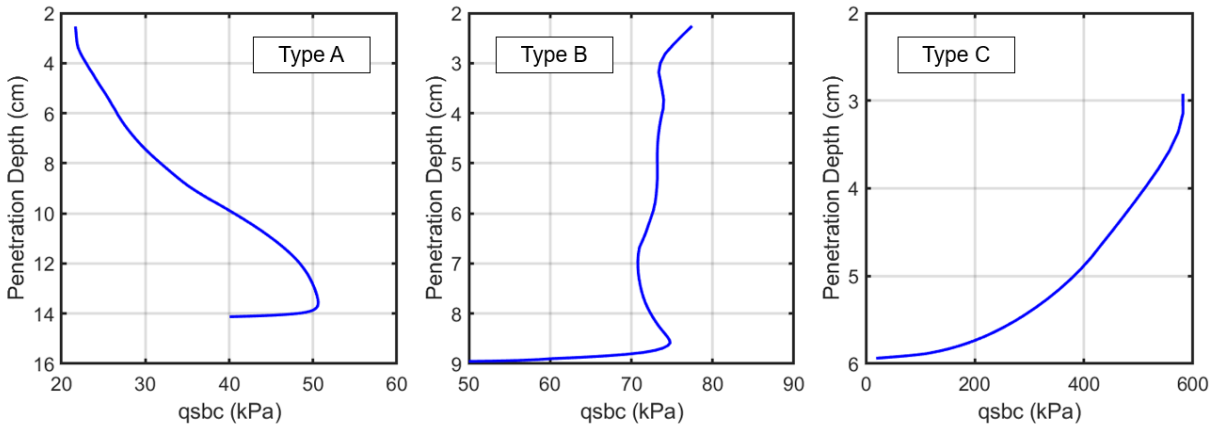

Figure 2.3: Variability in PFFP profiles: (Left) Type A – increasing strength with depth, defined maximum, & penetration > 10 cm, (Center) Type B – constant strength with depth, lack of defined maximum, penetration 7-10 cm , (Right) Type C – swash zone deployments, highest strength magnitudes, penetration < 7 cm

2.5.3. Temporal Variations at Cannon Beach

Transects were tested at Cannon Beach every twelve hours during daylight over the course of two full tidal cycles, capturing three low tides. This allowed for a temporal comparison of the strength

profiles (Figure 2.4). Within the dry zone of the beach above the high tide mark (from the dune at 0 m out to 40 m), there was little variability in the sediment strength. However, this changed drastically in the intertidal zone with profiles fluctuating from 50 – 300 kPa. The intertidal zone is the area of the beach between the high tide line and the low water line. The emerged width of this zone changes throughout the tidal cycle, being smallest at high tide and widest at low tide. All transects displayed a large increase in strength approaching the swash zone. It is important to note the order of magnitude of difference in sediment strength along the profiles, with the dry zone being on the order of tens of kPa and the intertidal/swash zone going up to hundreds of kPa.

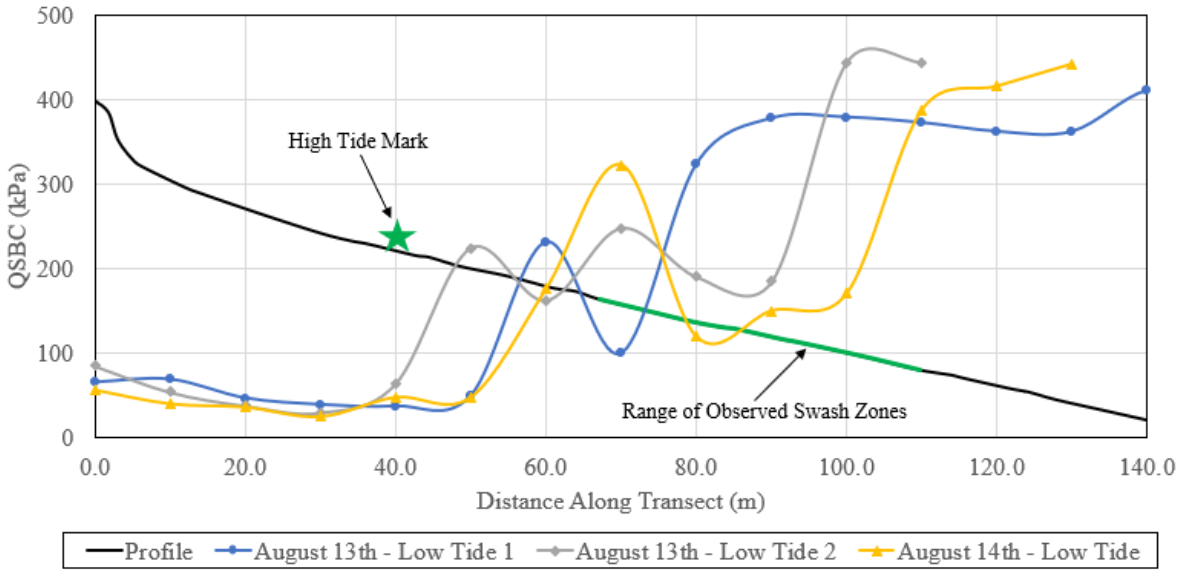

Figure 2.4: Strength profiles from 3 low tides at Cannon Beach. Green star marks the high tide line which is the extent of the dry zone. The green line on the topographic profile shows the extent of the fluctuations of the swash zone during measurements.

2.5.4. Spatial Variations between the Sites

To compare the different sites, strength profiles were selected for transects that were surveyed at the same point on the tidal cycle, just after low tide, and plotted versus the non-dimensional distance along the total transect length, *L*, to place transects of different lengths on the same scale (Figure 2.5). All three sites exhibited similar magnitudes of strength in the dry (sub-aerial) zone, and all three featured a spike in strength at the end of the profile that corresponded to the swash zone. Cannon Beach was the only site to show variability in the intertidal zone (it also has the largest intertidal zone of the three sites). Ocean Cape did not show intertidal variability but did show a similar increase in strength approaching the swash zone. Point Carrew represented a long

consistent profile, and showed a strength increase at the swash zone that was less than at the other two sites. Ocean Cape and Point Carrew each exhibited a small decrease in strength right before the increase at the swash, which was not seen on the Cannon Beach profile.

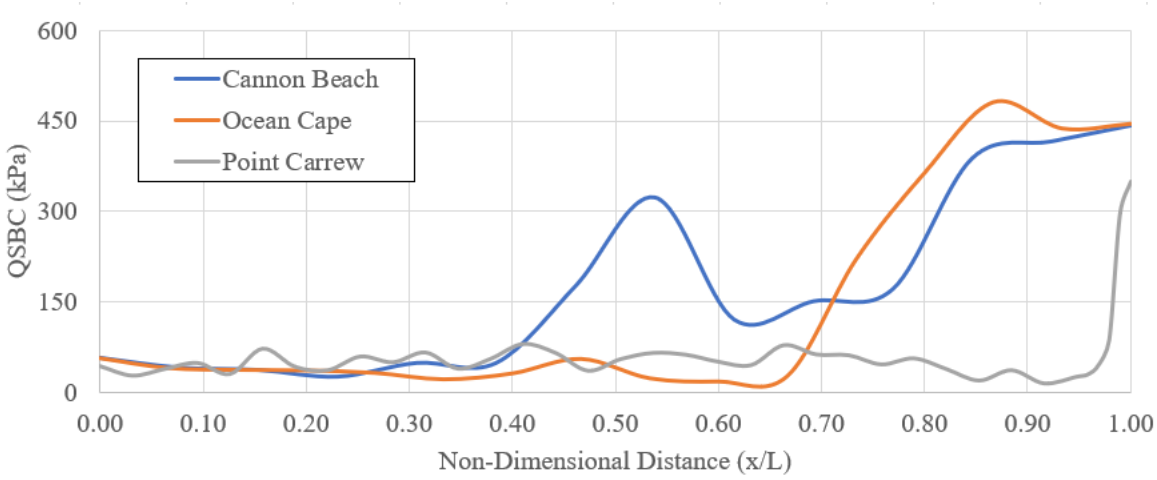

Figure 2.5: Strength profiles along transects for the three sites near low tide. Cannon Beach shows fluctuation within intertidal zone and Ocean Cape lacks this variability. Point Carrew has a very wide dry zone, but all three increase approaching the swash.

2.6. Discussion

2.6.1. Temporal Variations at Cannon Beach

The consistency of strength in the dry (sub-aerial) zone for all four measurement times matched expectations (Figure 2.4). This area is above the high tide line and the water table, and such, it is not subject to daily fluctuations in water content or density. However, it rained during all four measurement times. This introduced somewhat of water content across the beach, but this effect was consistent for all measurements, and thus, is not expected to affect the comparison. All profiles show a large increase in strength approaching the swash zone, which was also seen by Reeve et al. (2018). This increase can be tied to reworking of sediments due to swash and backwash processes and porosity reduction over time due to wave action. (Heathershaw 1981; Dean and Dalrymple 2004). As waves break and disturb the sediment bed, the induced swash could remove any loose sediments, leaving only the denser, stronger, less erodible sediments behind. Shear stresses can also contribute to particle rearrangement and densification.

The intertidal zone at Cannon Beach is very wide (~100 meters) which means that large portions of the beach are cyclically submerged and drained throughout the tidal cycle. The swash zone at

any given time during the tidal cycle appears to be subject to sediment strengthening processes mentioned previously. Yet, the entire intertidal zone does not display such high strengths, only the swash zone. Thus, the same processes that serve to strengthen the sediment in the swash zone cannot account solely for the high variability seen in the intertidal zone. As the tide goes in and out each day, sediment is constantly being moved and reworked by the waves and currents. Loose sediments eroded by the waves are deposited elsewhere on the beach, and as the location of the swash zone changes so does the location of high strength. Thus, this implies an inherent spatial variability of sediment strength in the intertidal zone. Furthermore, as sections of beach emerge as the tide retreats, the beach face must drain, leaving zones of partially saturated soil, which is another source of strength (Lu and Likos 2006, 2013, Lu et al. 2009). With the large tidal variation seen at this site (~3 meters), the effects of groundwater table fluctuations likely act to complicate drainage and partial saturation (Heiss et al. 2014, 2015).

In summary, the dry zone was temporally consistent in strength due to being above the high tide line and the groundwater table, the swash zone is consistently higher in strength due to active localized wave action and swash processes, and the intertidal zone is highly variable due to deposition/erosion throughout the tidal cycle and complex groundwater/partial saturation effects. The processes contributing to high variability in the intertidal zone are only described here as potentially causing changes in the sediment strength, and future work will need to be conducted to adequately quantify such changes.

2.6.2. Spatial Variations

In the surveyed areas of the three sites, Cannon Beach featured a slight increase in grain size towards the water, while Ocean Cape and Point Carrew were characterized by uniform grain sizes. At Ocean Cape, a large cobble and boulder field was observed below the survey site. The increase in grain size along the transect is consistent with the literature (Abuodha 2003), and Duncan, Wright, & Brandon (2014) noted an increase in shear strength with grain size of sands, gravels, and rockfills as well as between well-graded and poorly-graded sands. However, the effects of these differences unlikely explain alone the high range of strengths seen in the profiles. Thus, grain size is not a large contributor to differences in strength between the sites. The gravel and boulder field seen on the low tide terrace of Ocean Cape may have effects on the sediment transport processes between the nearshore and intertidal, which could in turn have effects on the measured

strengths, but since this area was not surveyed, such effects are outside the scope of this study, and will be considered in future work.

Cannon Beach featured no distinct morphological bedforms but an approximately constant intertidal beach slope at the time of measurements (Figure 2.2 Left). Nevertheless, it has the highest amount of intertidal variability in strength (Figure 2.5). The reason that the other two sites, which also have intertidal zones affected by the same processes, do not show such variability is tied to the morphology. The transects at Ocean Cape and Point Carrew both exhibited a ridge-runnel profile in the intertidal zone at the time of measurements (King and Williams 1949). When surveyed at low tide, the runnel is filled with water and the ridge is exposed. From the top of the ridge, the beach then again slopes back down to the swash zone and water line. (Figure 2.2, Right & Bottom). In Figure 5, there is a small decrease in strength just before the substantial increase in strength in both the Ocean Cape and Point Carrew profiles. This decrease is consistent with the location of the water-filled runnel. The sand in the runnel is fully saturated and loose due to being fully submerged and constantly reworked by flows within the channel and the morphodynamics of intertidal bar systems (Masselink et al. 2006). The subsequent increase would then be due to partial saturation effect increasing the strength on the exposed ridge, and the small intertidal zones at both sites putting the swash zone just below the ridge. Finally, the majority of the Point Carrew profile represents the sub-aerial zone. The typical increase in strength is seen at the swash zone, but to a lesser extent than the other two sites (Figure 2.5). The waves that reach Point Carrew must refract around the tip of the peninsula, causing them to become smaller and lose energy (Dean and Dalrymple 2004). Since the wave energy is lower at Point Carrew, the strength increase from densification is lessened at this site. The three sites are different morphologically, and these differences are in line with the strength differences. Still, more research is needed to quantify the effects of hydrodynamic processes on the measured sediment strengths.

2.7. Conclusions

A portable free-fall penetrometer was deployed at three sites on a sandy peninsula to explore the use of PFFP's in sub-aerial and intertidal coastal environments. Additional goals of the study were to assess the temporal and spatial differences in sediment strength between the sites, using the obtained geotechnical properties. Cannon Beach is a wide, high energy beach with no morphological features at the time of measurements, Ocean Cape is a narrow, high energy beach,

with a ridge-runnel system, and Point Carrew is a very wide spit, also with a ridge-runnel, but with low wave energy due to being on a protected bay. Lack of consistency in results of PFFP deployments along beach transects motivated using the strength at 4 centimeters of penetration depth as the sediment strength for comparison between all deployments. Temporal variations at Cannon Beach were explained by a number of interacting processes: in-situ densification from waves and swash, partial saturation over tidal cycles, and groundwater table fluctuation. Quantifying the effects of these processes will be the subject of future work. Finally, the differences in strength along transects between the sites were explained by the differences in morphology and hydrodynamics, namely the presence of ridge-runnel systems and differences in wave energy.

2.8. Acknowledgements

The authors acknowledge funding by the National Science Foundation through grant CMMI-1751463. The authors also acknowledge funding for travel support of undergraduate researchers who contributed to the data collection by Dr. Mike Duncan. Furthermore, the authors would like to thank Julie Paprocki, Dennis Kiptoo, and the undergraduate students of the Coastal Geotechnical Field Research Experience 2018 for support in the field. The authors would also like to thank the City and Borough of Yakutat, and specifically, Rhonda Coston and Irving Grass, and the Yakutat Lodge for local support.

References

Abuodha, J.O.Z. (2003). “Grain size distribution and composition of modern dune and beach sediments, Malindi Bay coast, Kenya.” *J. Afr. Earth Sci.,* 36, 41–54.

Akal, T., and Stoll, R. D. (1995). “An expendable penetrometer for rapid assessment of seafloor parameters.” OCEANS 1995. *MTS/IEEE, Challenges of Our Changing Global Environment*., IEEE, San Diego, CA, 1822–1826.

Albatal, A. and Stark, N. (2016). “In Situ Geotechnical Early Site Assessment of a Proposed Wave Energy Converter Site in Yakutat, Alaska, Using a Portable Free-Fall Penetrometer.” *Proc., Geo-Chicago 2016,* ASCE, Reston, VA ,429-438.

Albatal, A., Stark, N., and Castellanos, B. (2019). “Estimating in-situ relative density and friction angle of nearshore sand from portable free fall penetrometer tests.” *Canadian Geotechnical Journal*. 0(ja).

Dayal, U., and Allen, J. H. (1973). “Instrumented Impact Cone Penetrometer.” *Canadian Geotechnical Journal*, 10(3), 397–409.

Duncan, J. M., Wright, S. G., and Brandon, T. L. (2014). *Soil strength and slope stability*. John Wiley & Sons, Hoboken, NJ.

Dean, R. G., and Dalrymple, R. A. (2004). *Coastal processes with engineering applications*. Cambridge University Press.

Heathershaw, A.D., Carr, A.P., Blackley, M.W.L., and Wooldridge, C.F. (1981). “Tidal variations in the compaction of beach sediments.” *Marine Geology*, 41, 223 – 238.

Heiss, J. W., Ullman, W. J., & Michael, H. A. (2014). Swash zone moisture dynamics and unsaturated infiltration in two sandy beach aquifers. *Estuarine, Coastal and Shelf Science*, 143, 20-31.

Heiss, J. W., Puleo, J. A., Ullman, W. J., & Michael, H. A. (2015). Coupled surface-subsurface hydrologic measurements reveal infiltration, recharge, and discharge dynamics across the swash zone of a sandy beach. *Water Resources Research*, 51(11), 8834-8853.

King, C.A.M., and Williams, W.W. (1949). “The formation and movement of sand bars by wave action.” *Geographical Journal 113*, 70–85.

Lu, N., and Likos, W.J. (2006). “Suction Stress Characteristic Curve for Unsaturated Soil.” *Journal of Geotechnical and Geoenvironmental Engineering*, 132(2), 131-142.

Lu, N. and Likos, W.J. (2013). “Origin of Cohesion and Its Dependence on Saturation for Granular Media.” *Poromechanics V*, 669-675.

Lucking, G., Stark, N., Lippmann, T., and Smyth, S. (2017). “Variability of in situ sediment strength and pore pressure behavior of tidal estuary surface sediments.” *Geo-Marine Letters*, 37(5), 441-456.

Masselink, G., Kroon, A., and Davidson-Arnott, G.D., (2006). “Morphodynamics of intertidal bars in wave-dominated coastal settings — A review.” *Geomorphology*, 73(1), 33-49.

Previsic, M., and Bedard, R. (2009). Yakutat Conceptual Design, Performance, Cost and Economic Wave Power Feasibility Study. Tech. Report No. EPRI-WP-006-Alaska.

Reeve, B., Stark, N., and Mewis, P. (2018). "Cross-shore variations in sediment strength at a sandy beach." *Proc. Coastal Engineering*, 36.

Sassa, S., & Watabe, Y. (2007). Role of suction dynamics in evolution of intertidal sandy flats: Field evidence, experiments, and theoretical model. *Journal of Geophysical Research: Earth Surface*, 112.

Sassa, S. and Watabe, Y. (2009). "Persistent sand bars explained by geodynamic effects." *Hydrology And Land Surface Studies*, 36(1).

Stark, N., Coco, G., Bryan, K. R., and Kopf, A. (2012). "In-Situ Geotechnical Characterization of Mixed-Grain-Size Bedforms Using a Dynamic Penetrometer." *Journal of Sedimentary Research*, 82(7), 540–544.

Stark, N., Kopf, A., Hanff, H., Stegmann, S., and Wilkens, R. (2009). "Geotechnical investigations of sandy seafloors using dynamic penetrometers." *IEEE/MTS Oceans 2009*, Biloxi, MS, 1–10.

Stark N., Hay, A.E., and Trowse, G. (2014a). "Geotechnical investigation of areas of difficult access using portable free-fall penetrometers," *Proc., CPT'14*, Las Vegas, NV.

Stark N., Staelens P., Hay, A.E., Hatcher, B., and Kopf, A. (2014b). "Cost-effective Geotechnical and Sedimentological Early Site Assessment for Ocean Renewable Energies," *IEEE/MTS Oceans 2014*, St. John's, NL, 1-8.

Stoll, R. D., and Akal, T. (1999). "XBP - Tool for rapid assessment of seabed sediment properties." *Sea Technol.* (40), 47–51.

Stoll, R. D., Sun, Y.F., and Bitte, I. (2007). "Seafloor properties from penetrometer tests." *J. Ocean. Eng.* (32), 57–63.

Yehle, L.A. (1971). "Reconnaissance Engineering Geology of the Yakutat Area, Alaska, With Emphasis on Evaluation of Earthquake and Other Geologic Hazards." *Geological Survey Professional Paper 1074.* USGS.

Chapter 3: Crosshore Geotechnical Characterization of Sandy Beach Surface Sediments

The contributions of the authors to the composition of this manuscript are delineated as follows:

Nicola Brilli:

- Participated in the field survey
- Conducted all laboratory analysis
- Performed literature review; processed and analyzed field data; prepared figures, tables, and draft of manuscript
- Revised manuscript based on suggestions of co-author
- Prepared final manuscript for submission

Nina Stark:

- Lead primary investigator of this study
- Initiated research idea and co-developed the refined research questions
- Planned, supervised, and participated in the field survey in Duck, NC
- Reviewed and edited the draft manuscript
- Reviewed and edited the final version of the manuscript

Cross-shore Geotechnical Characterization of Sandy Beach Surface Sediments

Nicola C. Brilli, S.M.ASCE[1] and Nina Stark[2], Ph.D., M.ASCE

[1]Virginia Tech, Department of Civil and Environmental Engineering, Blacksburg, VA 24060; e-mail: nickb96@vt.edu

[2]Virginia Tech, Department of Civil and Environmental Engineering, Blacksburg, VA 24060; e-mail: ninas@vt.edu

The authors of the following manuscript have submitted it to Coastal Engineering.
Manuscript submitted: May 2022 (In Review)

3.1. Abstract

Geotechnical properties of surficial beach sediments affect beach erosion and shoreline changes. This study sets out to measure relative density, moisture content, friction angle, and shear strength of sandy beach surface sediments from dune to swash zone towards the goal of assessing their importance in sandy beach morphodynamics. Methods of sediment sampling, a conductivity based moisture probe, field penetrometers, and a field vane shear were deployed to collect data at the sandy Atlantic-side beach in Duck, North Carolina. The tools used were assessed based on their operability in the beach environment and data quality, and results are discussed in the context of beach morphodynamics. A digital field vane shear provided an efficient and direct method of measuring shear strength, but the difficulty of computing stresses on the failure plane, which is necessary to validate the results, ultimately reduced the usability of this instrument. The results from three penetrometers were compared to a partially-saturated bearing capacity model, where a portable free-fall penetrometer yielded the best fit. However, a modified velocity-dependent strain rate correction factor ($K = 0.31v_i$) was required to convert dynamic sediment resistance to a quasi-static resistance for the partially saturated sands. A small-scale digital push in penetrometer also achieved a positive correlation when compared to moisture content, but the small tip diameter (5 mm) coupled with the grain size at the beach (0.35 mm) raised concerns about the ability to derive an accurate measure of strength. It was determined that estimating strength parameter using a partially saturated bearing capacity model was appropriate for water contents less than 25% by volume, or anywhere in the crosshore above the swash to the dune. Relative density and moisture content were found to be closely linked, with partial saturation resulting in samples that featured negative relative densities up to -40%.

3.2. Introduction

Dynamics of surface sediments in beach environments driven by aeolian and hydrodynamic processes are complex and can lead to active geomorphodynamics, beach erosion, and shoreline change. High spatiotemporal variations in sediment dynamics also affect geotechnical properties of beach surface sediments (sediment depth < 0.2 m), which in turn may enhance or restrict local sediment dynamics. The interaction of the dominant forcing processes with the sediment depends on the location on the beach face. Sediment dynamics in the subaerial zone of the beach (above the high water line), or backbeach, are primarily driven by aeolian processes (Darke and Neuman, 2008; Davidson-Arnott et al., 2005; Zambrano-Cruzatty et al., 2019). In this zone, the interaction

between wind and sediment is the main driver for morphological change, and precipitation and humidity primarily govern the sediment's water content when not considering inundation events (Bauer et al., 2009). Conversely, the sediment in the intertidal zone (high water line to swash zone) is mobilized mainly by hydrodynamic processes. Tides and waves interact with and reorganize the local geomorphology and surface sediments. Generally, the local hydrodynamics and a representation of grain size (e.g., median grain size, particle settling velocity) serve as a predictor of beach morphology (Dalrymple, 1992; Dean and Dalrymple, 2004; Masselink et al., 2006; Masselink and Short, 1993; McNinch, 2004). The role of variations in geotechnical sediment properties (e.g., relative density, friction angle, apparent cohesion) on local sediment dynamics has been acknowledged, but rarely been studied in detail, despite their relevance for local sediment dynamics in coastal and subaquatic environments (Albatal and Stark, 2017; Jafari et al., 2018; Kirchner et al., 1990; Mulhearn, 2001; Watts et al., 2003).

Much work has been focused on the sediment as an individual particle where each grain can be described by its size and particle density, and thus, sediment mobilization/deposition processes can be modelled as a fluid-particle interaction. These studies have shown that beach sediments are highly variable on both temporal and spatial scales (Abuodha, 2003; Gallagher et al., 2016), and that sediment particle properties can be useful in modelling morphological change (Dean 1973; Medina et al. 1994; Jackson et al. 2005; Gallagher et al. 2011). However, sediment particle properties may not always reflect the behavior of the sediments as a bulk material, i.e., particle-particle interaction with stress-driven processes between the particles and a matrix of interacting particles that has unique, and possibly, spatiotemporally varying geotechnical properties. Properties such as shear strength, friction angle, moisture content, bulk density, are known to be significant for sediment transport and morphodynamics (Davidson-Arnott et al., 2005; Erikson et al., 2007; Sassa and Watabe, 2007; van Rijn, 2007; and others). Through an in-depth literature review, four geotechnical properties were selected based on the importance for sediment transport processes at a sandy beach and the ability to be measured in-situ at a sandy beach: relative density (D_r), moisture content (MC), friction angle (ϕ'), and shear strength (s).

Relative density is a measure of the packing state of granular materials. It is based on a scale of 0-100%, with 0% corresponding to the loosest possible state, and 100% corresponding to the densest possible state. The relative density of coastal sediments can be highly variable, both spatially and temporally, which can affect local sediment transport and morphological change. Sassa and

Watabe (2007) found that suction dynamics due to tide-induced groundwater level change could lead to changes in D_r up to 50% and has strong effects on bed evolution over tidal cycles. Erikson et al. (2007) found good agreement with measured data by modelling dune erosion and recession using Rankine Earth Pressure theory, a common geotechnical earth pressure theory which utilizes soil bulk density (ρ_{bulk}), a parameter directly related to relative density. Swash and backwash processes can reduce porosity over time (increase bulk density), leaving behind less erodible sediment (Dean and Dalrymple, 2004). Additionally, Heathershaw et al. (1981), using penetration resistance as a proxy for packing state, showed an inverse relationship between soil bulk density and net bed level change on beaches. Recent work by Zambrano-Cruzatty et al. (2019) suggested that bulk density had only a small effect on the threshold velocity for wind erosion.

There is general consensus about the importance of moisture content for aeolian sediment transport. The surface moisture content has significant control over the entrainment threshold for wind-blown transport with higher moisture contents reduce aeolian erosion (Bauer et al., 2009; Darke and Neuman, 2008; Davidson-Arnott et al., 2005). Other coastal erosion processes are also affected by moisture content. The work by Erikson et al. (2007) estimated the shear strength by using a modified equation for partially-saturated sediments that included matric suction ($u_a - u_w$) where u_a is the air entry pressure and u_w is the water pressure. Matric suction is tied to moisture content by a Soil Water Characteristic Curve (*SWCC*) which gives the matric suction as a function of the volumetric water content. Lastly, the study by Sassa and Watabe (2007) concluded that moisture content changes cause significant suction stresses that could alter the surface shear strength, and thus, affect erodibility.

Friction angle, or the "angle of internal friction", ϕ', and expresses the friction resistance within a bulk sediment (i.e., the shear plane is located within the bulk mass of the sediment). ϕ' increases with D_r, and decreases as confining pressure increases (Duncan et al., 2014; Lee and Seed, 1967). Also, it is typically higher for well-graded sediments versus uniformly-graded sediments as there is room for smaller particles to fill in the gaps between larger ones and generate more frictional resistance (Bolton, 1986; de Beer, 1965; Duncan et al., 2014). Referring again to the work by Erikson et al. (2007), ϕ' was a key parameter in the determination of shear strength for the study. Additionally, since D_r is known to be highly variable in beach environments, it follows that ϕ' likely exhibits such variations as well.

The shear strength of sediment describes the amount of shear stress that sediment can withstand before failure and possibly mobilization. Shear strength is controlled by effective stresses (particle contact stresses), which are denoted by the $'$ symbol. Since erosion is characterized by a fluid shearing the surface of the sediment, shear strength is a key parameter for understanding surficial sediment erosion processes. For dry and saturated sand, shear strength is supplied by soil stresses and the friction angle (Duncan et al., 2014; Lee and Seed, 1967). However, when sand becomes partially saturated, which is primarily the case in beach environments, water and air in the sediment pores can provide an additional source of shear strength through suction between particles (Briaud, 2013). Since some of the controlling properties of shear strength (D_r, MC, ϕ') are all highly variable at sandy beaches, shear strength is likely highly variable on temporal and spatial scales, which is supported by recent work (Manning and Stark, 2019; Sassa et al., 2014; Sassa and Yang, 2019; Stark et al., 2022).

Previous studies have highlighted the importance of certain geotechnical properties to sediment transport processes. Nevertheless, geotechnical parameters are still rarely implemented in morphological models of beach environments, and if so, often through unspecific and approximated values (e.g., $\phi' = 32^{\circ}$). A reason for this is that little work has been done to examine the tools and techniques to obtain field measurements of these properties. There are few tools designed for the sole purpose of collecting geotechnical measurements in coastal environments or of frequently reworked surface sediments (Stark et al., 2015; Stoll and Akal, 1999). Developing new instruments is often expensive and time-consuming, which makes it desirable to repurpose instruments not necessarily intended for use in these environments (Reeve et al., 2018; Sassa et al., 2014). This presents its own challenges, as available instruments may not be suited for the specific site conditions or collect data at the desired spatial or temporal scales (Stark and Brilli, 2021). Additionally, such improvisations often lead to a high degree of individuality and uncertainty when conducting field studies, as researchers are forced to come up with modified measurement techniques centered around the tools available. The result is a lack of a generalized, consistent framework how to conduct geotechnical field measurements of sandy beach surface sediments.

The goals of this study are to assess variations in relative density, moisture content, shear strength/friction angle across the subaerial, intertidal, and upper swash zone towards use of geotechnical properties for prediction of geomorphodynamics at sand beaches. Hand-deployed

tools that can obtain geotechnical properties were identified and included density sampling, a moisture gauge, three types of penetrometers, and a vane shear. An emphasis was set on portable and hand-deployed tools considering that beaches often represent vulnerable ecosystems where heavy equipment may require special permitting as well as that implementation for erosion and morphodynamic problems will require to establish spatial and temporal trends, i.e., will require a significant number of measurements locations and times. The suitability of these tools for beach environments as well as the quality of the resulting parameters were investigated. It is important to note that sediment strength via penetrometer measurements will be used as a proxy for friction angle, as the two are directly related. These goals will be addressed by examining a field data set collected at the U.S. Army Corp of Engineers' Field Research Facility in Duck, NC in October 2019 in the framework of the During Nearshore Event Experiment (DUNEX) pilot experiment, supplemented by geotechnical sediment characterization through laboratory testing.

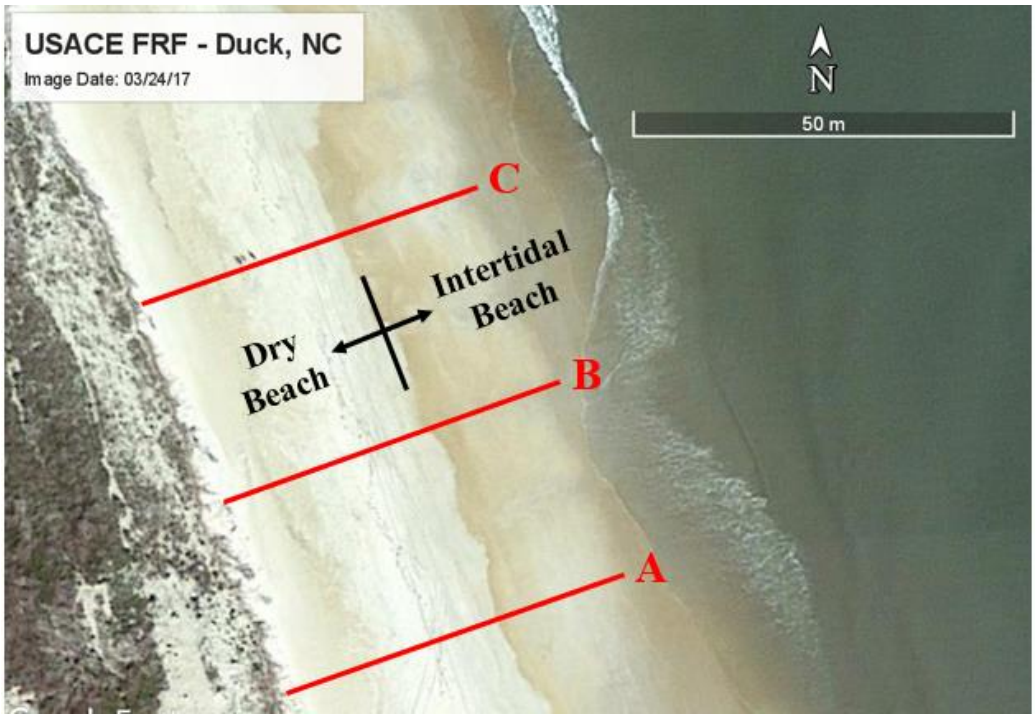

Figure 3.1: Google Earth satellite image of field site in Duck, NC, highlighting the measurement transects A,B, and C. (by Terrametrics; lower left corner: N36°10'58.61" W75°45'5.87")

3.3. Methods

Three transects (A-C) were surveyed at five meter increments, daily between October 7th and October 11th, 2019, at the Atlantic sand beach in Duck, North Carolina, USA (Figure 3.1). The

suite of field instruments and tools used in this study was comprised of density sampling through push tubes, a moisture gauge, three penetrometers with different measurement methods, and a field vane shear (Figure 3.2).

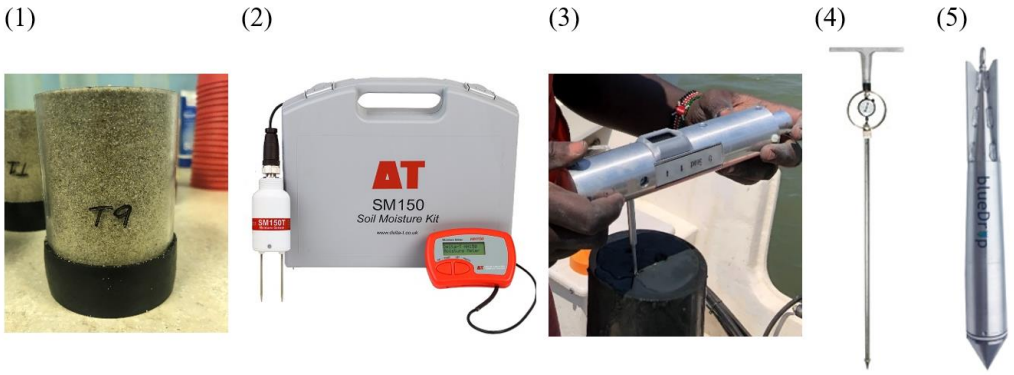

Figure 3.2: Instrument suite used for field experiments. (1) Example of sand sample extracted via sharpened push-in tubes, (2) Dynamax moisture gauge, (3) GeoTac Soil Sabre in vane shear configuration, (4) Corp of Engineers (COE) cone penetrometer, (5) blueDrop portable free-fall penetrometer (PFFP).

3.3.1. Relative Density (D_r) Sampling

Physical sediment samples were collected to determine in-situ relative density (Figure 3.2.1) at every station by pushing a 10 cm long, sharpened tube, into the sediment, trimming and capping the top, and then carefully digging the sample out and capping the bottom. Diameters and heights of each tube were measured to obtain the volume as accurately as possible, ranging between 351-353 cm^3. In the laboratory, the samples were removed from the tube, weighed, and bulk density (ρ_{bulk}) was computed via Equation 3.1. Once weighed, the sample was dried in a soil oven and weighed again to obtain dry density (ρ_{dry}) via Equation 3.2. Finally, Equation 3.3 gives the dry unit weight (γ_d) which is used to compute D_r (Equation 3.4).

$$\rho_{bulk} = \frac{M_T}{V_T} \tag{3.1}$$

$$\rho_{dry} = \frac{M_D}{V_T} \tag{3.2}$$

$$\gamma_d = g\rho_{dry} \tag{3.3}$$

where M_T is the total mass of sample (water and sediment) in the tube, V_T is the total volume of the sample tube, M_D is the dry mass of sediment, and g is gravitational acceleration. The minimum unit weight (γ_{d-min}) is found using ASTM D4254 and the maximum unit weight (γ_{d-max}) is found using ASTM D4253. Relative density is then computed using the measured dry unit weight (γ_d) and Equation 3.4.

$$D_r = \frac{\gamma_{d-max}}{\gamma_d} * \left(\frac{\gamma_d - \gamma_{d-min}}{\gamma_{d-max} - \gamma_{d-min}}\right) * 100\% \quad (3.4)$$

Additionally, grain size characteristics and classification of the samples were obtained using sieve analysis, following the "Standard Test Methods for Particle Size Distribution (G ASTM D6913.

3.3.2. Moisture Content (***MC***)

Moisture content was measured using the *Dynamax SM150T* soil moisture gauge (Delta-T Devices Ltd, Cambridge, UK). The sensor transmits an electromagnetic field into the sediment, which is influenced by the permittivity of the sediment around the sensor prongs. Since water has a much higher permittivity than quartz sand (as predominantly present in this study area), the water content dominates the measurement of the medium (higher permittivity = higher water content). The interaction with the electromagnetic field results in an output voltage to the instrument which is calibrated to a specific moisture content. This specific device (Figure 3.2.2) is handheld and allows for rapid and high density spatial measurements. Five readings at approximately 10 cm distance were taken at each station and averaged to determine the water content.

3.3.2.1. Sensor Calibration

The sensor is pre-equipped with a general mineral soil calibration. Nevertheless, an additional calibration to the local sediments and local seawater was performed. Seawater has more free ions than freshwater, increasing its permittivity. To account for the impact of seawater, a custom calibration scheme was developed. Using sediment and seawater collected from the survey site, samples were prepared, and the raw voltage output was read from the sensor. An additional freshwater calibration was also conducted. The salinity was held consistent to the field conditions at 30 PSS and tested with a *CastAway* conductivity, temperature, and depth (CTD*)* sensor. The results show an increasing difference between the two curves with increasing moisture content, which highlights the necessity of calibrating for seawater effects (Figure 3.3). Since this effect was anticipated, field data was collected in raw output voltage so that it can easily be converted to true

water content using the seawater calibration. The calibration of handheld moisture gages for the more generalized use in coastal environments is explored in greater detail in a companion study (Appendix B).

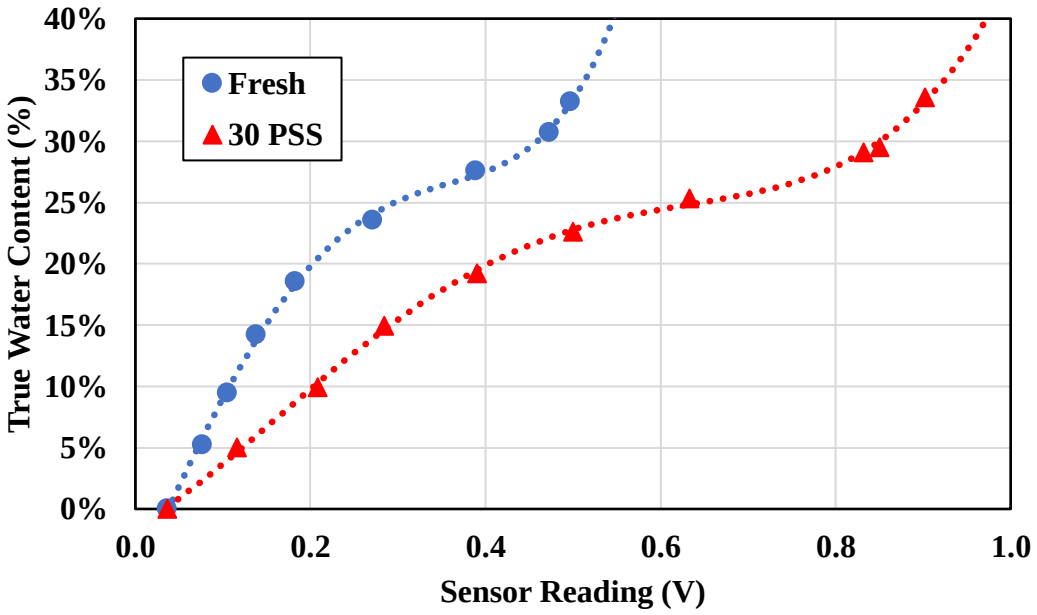

Figure 3.3: Moisture sensor calibration results for fresh (blue) and saline water (red) and performed using site specific sediments

3.3.3. Field Vane Shear and Penetrometer

One of the instruments used to measure in-situ sediment strength was the *Soil Saber* (handheld penetrometer) by Trautwein, Houston, Texas (Figure 3.2.3, Figure 3.4). The probe is equipped with an attachable penetrometer and vane shear. The vane shear (1x1 inch vane, 0.5x0.5 inch shown in Figure 3.4) is inserted into the sediment and rotated to shear the sediment. The probe measures the maximum torque, and this is converted into a shear resistance. Since the vane shear is collecting a direct measurement of shear strength, it could be possible from this alone to draw conclusions about the sediment transport processes at work. However, the device was designed to be used in cohesive sediments, assuming a circular failure plane, which is not the case for sandy sediments (Park et al., 2016). Additionally, validating the shear strength measurement via a theoretical model would require knowledge of the pore pressures to compute the effective stress on the failure plane, which is very difficult to determine in partially saturated sediments (Briaud,

2013). Thus, vane shear results will be considered in the context of similar studies using vane shear measurements in coastal environments (Sassa and Watabe, 2007; Sassa and Yang, 2019).

The penetrometer (flat, cylindric tip with 0.5 cm diameter, 4 cm long) is slowly pushed into the sediment (~1-2 cm/s), and a load cell reads the maximum resistance pressure achieved during penetration. A concern regarding this instrument is the small tip diameter (*B)*, 5 mm, compared to the predominant grain size (d_{50}), 0.35 mm, seen at the site. For the given penetrometer, the ratio of tip diameter to grain size (B/d_{50}) is approximately 14. Work by Lee (1990) and Gui and Bolton (1998) noted that CPT results would be affected by ratios smaller than 25-28 for sandy sediments, specifically, causing the measurement to be artificially increased. Additionally, de Lima and Tumay (1991) found that for the same grain size, tip resistance decreased by 15% when moving from a 10cm^2 cone to a 1.27cm^2 (Bałachowski, 2007). For field experiments, three measurements were taken at each station. The instrument is not waterproof. Therefore, measurements in the swash zone were not possible. It is important to note that the user controls the penetration and shearing rate, and that the probe digitally records the maximum resistance values over the penetration or shearing process.

Figure 3.4: GeoTac Soil Saber with penetrometer (top) & vane shear (back) attachments.

3.3.4. U.S Army Corp of Engineers (COE) Cone Penetrometer

The *COE Cone Penetrometer* (Humboldt Mfg. Co., Elgin, IL) (Figure 3.2.4) is another highly portable tool for rapidly measuring sediment strength. This instrument will be referred to as "manual penetrometer" henceforth in the text. It consists of a metal rod with a 30 degree cone at the tip (2 cm diameter) and estimates the cone index (CI) using a dial gauge and proving ring. The cone index is a measure of soil strength and has been widely used to assess the trafficability of soils. CI is a direct measurement as the bearing pressure is calibrated to the dial gauge. The

instrument is pushed into the sediment at a rate of three centimeters per second (cm/s), and the CI is read off the dial gauge in pounds per square inch (psi) at three inch intervals. The penetration rate is suggested by the manufacturer, but it is ultimately up to the care of the user to push at a constant rate. Additionally, the CI is read directly from the dial gauge by a second operator during penetration and not recorded by the instrument. Due to time constraints, the manual penetrometer was used sparingly, and only for one transect the data will be considered.

3.3.5. Portable Free-Fall Penetrometer

The *blueDrop* (blue C designs Inc., Halifax, N.S.) is a portable free-fall penetrometer (PFFP). The probe has a streamlined shape with conical tip (Figure 3.2.5), is 63.1 cm long, has a weight of 7.71 kg, and a diameter of 8.75 cm. It is characterized by a rugged design, developed for use in submerged, energetic coastal environments. It has five vertical microelectromechanical systems (MEMS) accelerometers ($\pm$1.7-250 *g*, *g* is the gravitational acceleration) and two horizontal MEMS accelerometers ($\pm$55 *g*) for tilt. The onboard accelerometers record continuously (2 kHz) and capture a profile of free-fall, impact, penetration into the sediment, rest, and recovery. The deceleration profile from impact to stop can be used to estimate geotechnical properties of seafloor sediments including equivalent cone resistance (Akal and Stoll, 1995; Lucking et al., 2017; Stark et al., 2012, 2009; Stoll et al., 2007), relative density, and friction angle (Albatal et al., 2020, White et al., 2018). The impact velocity, which is a function of the drop height, also affects the measured deceleration, particularly as sediment response can be strain rate dependent. Thus, the probe was deployed from three different drop heights at each location. The average impact velocities were: 2.0 m/s, $\pm$0.3 for the low drops (~0.25 m), 3.5 m/s, $\pm$0.2 for the medium drops (~0.5 m), and 5.0 m/s, $\pm$0.2 for the high drops (~1.0 m). Single and double integration of the deceleration profile give the impact velocity and penetration depth, respectively. PFFPs have not been used for surveying of emerged beach environments until recently, but offer an attractive means through rapid deployment and the device's capability to also measure submerged (i.e., in the swash zone and transitioning into the nearshore) (Brilli and Stark, 2020; Reeve et al., 2018; Stark et al. 2021).

The deceleration profile from the PFFP can be used to estimate the in-situ strength of the sediment. Using Newton's 2nd Law, the profile is converted into a dynamic sediment resistance force and dividing by the tip area gives a dynamic bearing pressure or cone resistance. Since the PFFP is impacting at a high velocity (~meters/second (m/s)), compared to other testing methods such as

CPT, handheld penetrometer, or manual penetrometer (~cm/s), the computed bearing capacity (q_{dyn}) is expected to be higher due to viscous effects and dilation (Stoll et al., 2007). To make the results comparable, a strain rate correction (f_{sr}) is applied to the results to normalize to a constant, slower penetration velocity (Dayal and Allen, 1973; Steiner et al., 2014). The logarithmic form of this correction has been applied for submerged (i.e., assumed to be fully saturated) sandy sediments. (Albatal et al., 2020; Stark et al., 2012, 2009; Stephan et al., 2015; Stoll et al., 2007). The correction is computed via Equation 3.5:

$$f_{sr} = 1 + K * log_{10}\left(\frac{v}{v_{ref}}\right) \tag{3.5}$$

where K is the strain rate correction factor, v is the velocity of the probe, and v_{ref} is the reference velocity (typically 2 cm/s). The correction factor, K, is an empirical coefficient dependent on soil type, and has been reported to range from 0-1.5 for sands (Albatal et al., 2020; Dayal et al., 1975; Stark et al., 2012; Stephan et al., 2015; Stoll et al., 2007). Dividing the dynamic bearing pressure by f_{sr} gives a quasi-static bearing capacity ($qsbc$), and this value is the proxy of the equivalent static sediment strength (see Stark et al., 2012) via Equation 3.6:

$$qsbc = \frac{q_{dyn}}{f_{sr}} \tag{3.6}$$

where m is the mass of the probe, dec is the measured deceleration, and A is the tip projected area.

Albatal et al. (2020) developed a method for back calculating ϕ' from $qsbc$ using bearing capacity models proposed by Durgunoglu and Mitchell (1973) and Meyerhof (1961). Results showed good agreement with laboratory triaxial and direct shear tests using $K = 1.25$, and strong correlation was found between maximum deceleration (dec)and D_r. Additionally, $K = 0.2$ and $K = 0.4$ yielded promising results when compared to an empirical equation for estimating ϕ' using D_r, grain size, and confining stress (Albatal et al., 2020, Duncan et al., 2014). Thus, these three strain rate factors will be considered for this study. It is important to note that this method was developed for saturated sands and is still dependent upon proper selection of strain rate factor K.

3.3.6. Consideration of Drainage Conditions

As each of the penetrometers has different rates of penetration and geometry, it was necessary to analyze the induced drainage conditions. The dimensionless penetration velocity (V) has been

suggested as a way to assess the drainage condition for penetrometers and is shown in Equation 3.7 (Chow et al., 2018; Finnie and Randolph, 1994; Randolph, 2004; Randolph and Hope, 2004; Steiner et al., 2014; White et al., 2018):

$$V = \frac{v_{dyn}B}{c_v} \tag{3.7}$$

Where v_{dyn} is the penetration velocity, B is the diameter of the penetrometer, and c_v is the coefficient of consolidation in the vertical direction. Values of $V > 30$ are considered an undrained response, $V < 0.3$ is considered drained, and in between denotes a partially drained response (Chow et al. 2018). The value of c_v is typically derived via pore pressure dissipation measurements from the penetrometer, but lack of adequate penetration depth and partial-saturation conditions prevented the onboard pore pressure sensor from being used for this purpose. However, Duncan et al. (2014) reported values of c_v for fine sands to be in the range of $1.075*10^{-4}$ to $1.075*10^{-2}$ meters-squared/second (m^2/s), so this range will be adopted here. Similar to analysis by Albatal et al. (2020), the known diameters, and penetration velocity ranges for each instrument, were used to determine the boundaries of the drainage regimes over the range of c_v. The high penetration velocities of the PFFP put the sediment response in the region of undrained behavior. Conversely, the slower penetration of the handheld penetrometer placed it in partial/fully drained region. However, the sediment, a medium sand, is slightly coarser than the reference fine sand for the c_v range. Since c_v increases with grain size, it can be concluded that c_v is likely approaching the higher end of the range, and thus, the handheld penetrometer is generating a fully drained response from the sediment. Finally, the same analysis was performed on the manual penetrometer, and the results plotted in the partial/fully drained range, with significantly more of the area lying in the partially drained regime.

3.3.7. Comparison to Bearing Capacity Model

In order to assess the quality of the results from the penetrometers, the data from each were compared to a partially saturated bearing capacity model. A bearing capacity theory for partially-saturated soil was suggested by Vanapalli and Mohamed (2007) based on the original theory for saturated soils from Terzaghi (1943) and is given by Equation 3.8:

$$q_u = \left[c' + (u_a - u_w)S^{\psi} tan\phi'\right] N_c \zeta_c + \frac{1}{2}\gamma B N_\gamma \zeta_\gamma \quad (3.8)$$

where q_u is the partially-saturated bearing capacity, c' is the effective stress soil cohesion, $(u_a - u_w)$ is the matric suction, S is the degree of saturation, ψ is a fitting parameter typically set to 1 for sandy soils, ϕ' is the friction angle, N_c, N_γ are bearing capacity factors (Terzaghi, 1943), , ζ_c, ζ_γ are shape factors (Vesic, 1973), γ is the unit weight of the sediment, and B is with width of the footing (penetrometer diameter). Many of these parameters are attainable via the collected measurements. The cohesion, c' is typically set equal to zero for sandy sediments. Moisture measurements as well as grain size characteristics from the density samples can be used in tandem with a SWCC to give $(u_a - u_w)$ as a function of volumetric water content (Wang et al., 2017; Wayllace and Lu, 2012). S is easily computed using the moisture content and density measurements, and γ is directly measured via the density sampling. Finally, ϕ' must be estimated for the given sediment. It is understood that ϕ' is likely variable amongst the stations due to variations in grain size and density (Duncan et al., 2014). However, laboratory testing of partially saturated sands to obtain ϕ' was outside of the scope of this work and using empirical relations for ϕ' was determined to add additional uncertainty to the model, especially given that relations for ϕ' were not developed considering the very low densities seen at these sites. Thus, it was decided to use in this initial study a constant value of $\phi' = 34°$ based on direct shear and tilt table tests conducted on dry and saturated sands from the same site by Stark et al. (2017).

3.4. Results

Surficial grain size distributions varied noticeably on the survey days (Figure 3.5) and along the three transects. Variations in grain size are known to affect the properties of interest here, but they are not focus of this study, and therefore, will only be discussed briefly. The average d_{50} for samples on October 11th was 0.35 mm, classifying as a fine sand (between 0.074 mm and 0.42 mm) based on the United Soil Classification System (USCS). From October 7th – 10th, grain size increased in the crosshore direction, with many swash zone samples classifying as a medium sand (0.42 mm – 2 mm). This trend was consistent among transects taken the same day (alongshore direction, A-C). Therefore, the data from October 11th were selected for further investigation because of their consistency in grain size along transects, lack of mixed grain sizes, and clustering around the mean distribution for all samples (black line, Figure 3.5).

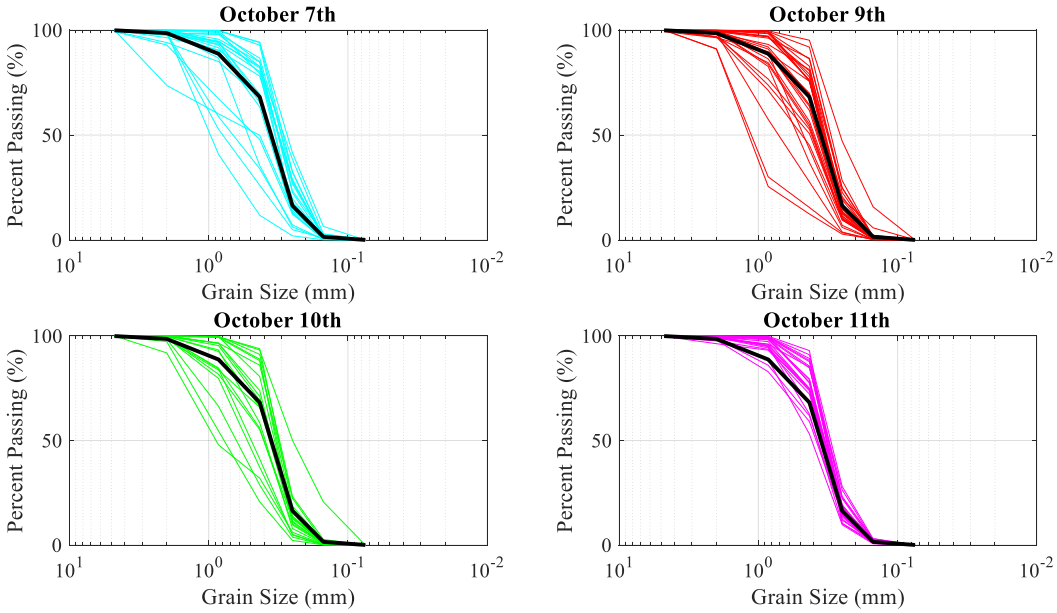

Figure 3.5: Grain size distributions for all samples taken during the study. Black line on each plot is the mean of all distributions, which was the sand used to determine the index densities.

Figure 3.6 depicts the variation of D_r determined from the samples along the three transects on October 11th. Distance is measured from dune to water line, with zero being at the dune toe (Figure 3.1). Relative density was elevated at the dune toe (0-40%) and at the water line (70%), with the highest measurements occurring at the water line (Figure 3.6). In between, the values were markedly lower, with most of the measurements falling in the negative relative density range. A value of D_r less than zero implies that the packing is less dense than the loosest packing stable for dry sand. Negative D_r can be achieved through effects of partial saturation (Martin et al. 2009).

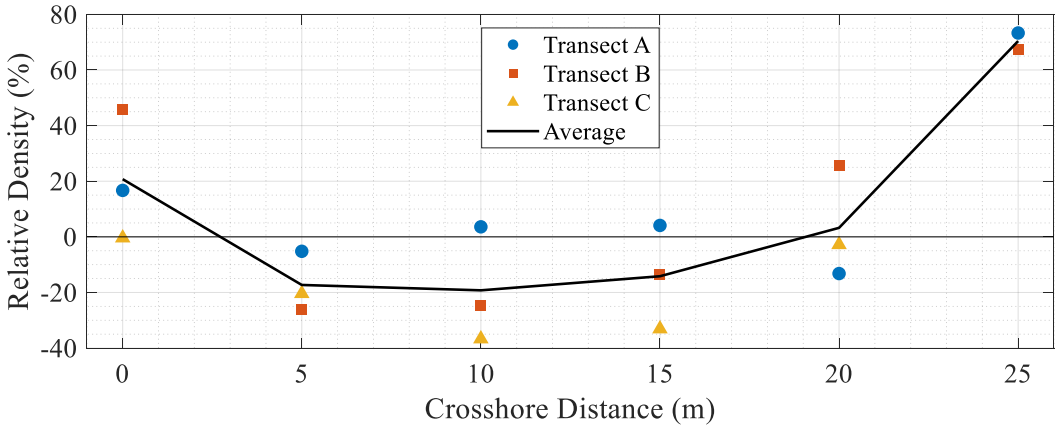

Figure 3.6: Variation of relative density along the three transects on October 11th. The data points correspond to discrete measurements on each transect and the black line is the average.

Volumetric moisture content showed a continuous increase from dune to the waterline, as expected (Figure 3.7). Variability seemed more significant at the lower beach and highest at 20 m, which was the approximate upper limit of the swash zone.

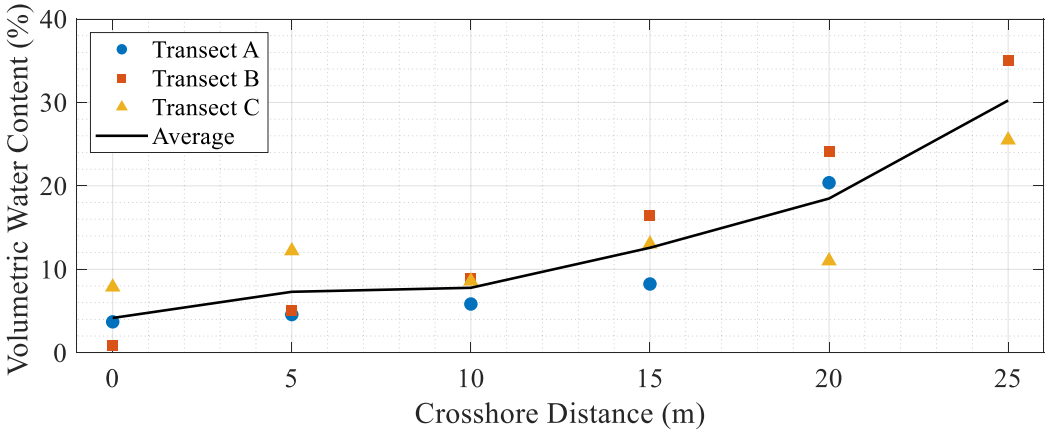

Figure 3.7: Variation of volumetric water content on October 11th. The data points correspond to discrete measurements on each transect and the black line is the average.

Measurements by the handheld penetrometer and the field vane shear followed a similar trend (Figure 3.8), however, with the vane shear suggesting strength values consistently smaller in magnitude. The strength estimates were low in the swash zone and the highest variability between transects was found at the dune toe. The latter is likely due to a high degree of site disturbance at the dune toe from continuous human activities. It is also worth noting that only Transect B included a measurement in the swash zone (25 m), since the instrument is highly vulnerable to being damaged by water and timing limitations.

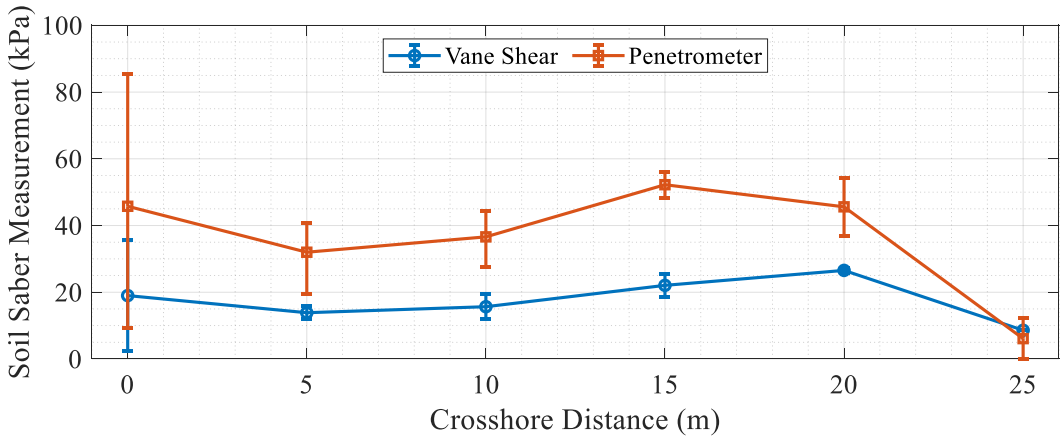

Figure 3.8: Variation of handheld penetrometer resistance and vane shear strength on October 11th. The solid line between data points represents the transect average for a given location, and the error bars correspond to the spread of the individual measurements.

Due to time constraints in field data collection, there are no measurements available from the manual penetrometer on October 11th. The instrument was only used on October 9th, and only transect B from that day contains a complete set of measurements including the manual penetrometer and the handheld penetrometer measurements. Thus, this transect will be used for comparative analysis (Figure 3.9). Both penetrometers follow nearly the exact same trend, with the handheld penetrometer being much lower in magnitude. However, it should be noted that the handheld penetrometer measurements are on the order of tens of kPa for a penetration depth of ~4 cm, while the manual penetrometer is on the order of hundreds of kPa for a penetration depth of ~9 cm.

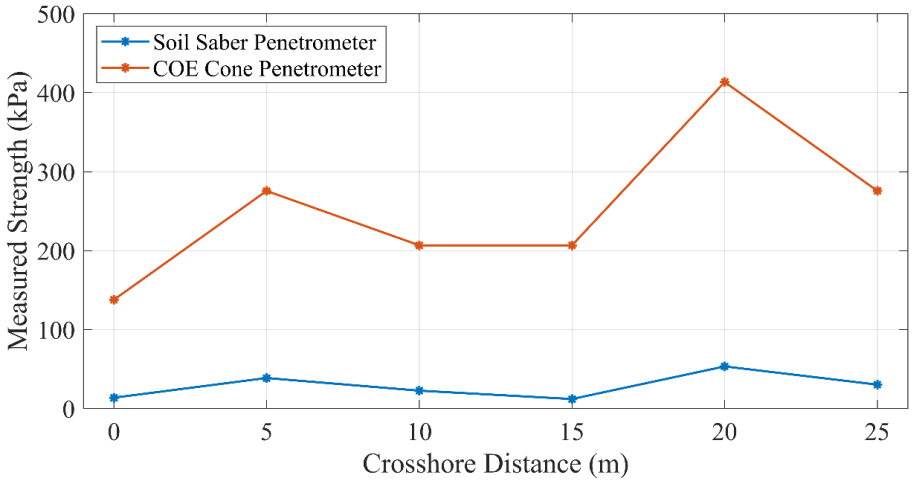

Figure 3.9: Crosshore variation of handheld and manual penetrometer measurements for October 9th, Transect B.

Figure 3.10 depicts the variation of *qsbc* determined from the PFFP along the transects using the three aforementioned strain rate correction factors $K = 0.2, 0.4, 1.25$ (Equations 3.5 & 3.6). Results from the PFFP showed similar trends between the three correction factors, with the *qsbc* increasing from dune to water line and the highest variability was seen in the swash zone.

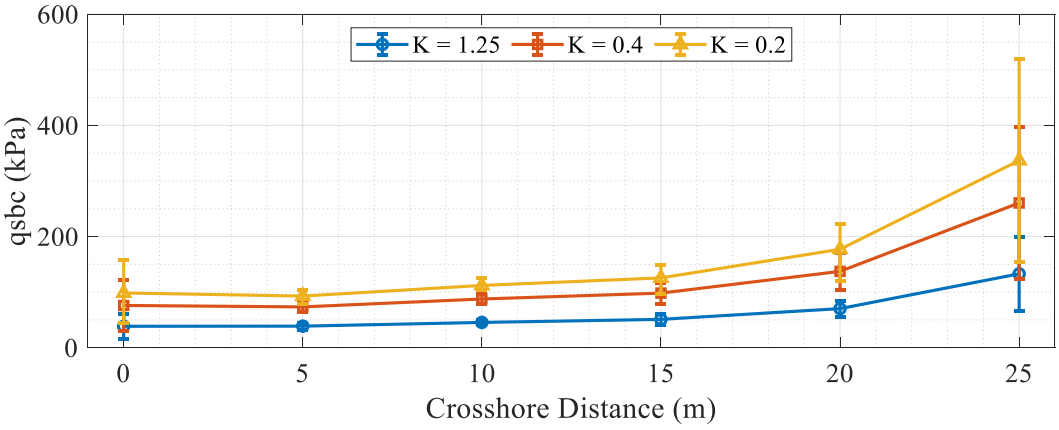

Figure 3.10: Variation of *qsbc* from the PFFP on October 11th. The solid line between data points represents the transect average for a given drop height, and the length of the error bars on the top and bottom of each data point represents the highest and lowest individual measurements, respectively. All three drop heights showed the same crosshore trend, so the medium drop height (~0.5 m) was chosen arbitrarily.

3.4.1. Comparison to Partially Saturated Bearing Capacity Model

Using Equation 3.8, q_u was computed for each station and penetrometer (i.e., different tip diameters), the results were compared to the measured values from the instruments. Since the manual and handheld penetrometers were direct measurements of tip resistance, they could be directly compared to the model. For the PFFP measurements, *qsbc* was computed using the three selected values of K for each station and drop height. The results for each penetrometer are presented in Figure 3.11. The manual penetrometer (Figure 3.11, top right) provided an overestimate compared to the model, and the handheld penetrometer (Figure 3.11, bottom) results were scattered around the one-to-one line, with a slight tendency to underestimate. The PFFP (Figure 3.11, top left) results at $K = 0.2$ and $K = 0.4$ showed a tendency to overestimate. $K = 1.25$ provided the best results, with a slight tendency to underestimate, and was the value of K used in subsequent analysis. All three instruments overall displayed unsatisfying correlations with the model with R^2 values being close to zero.

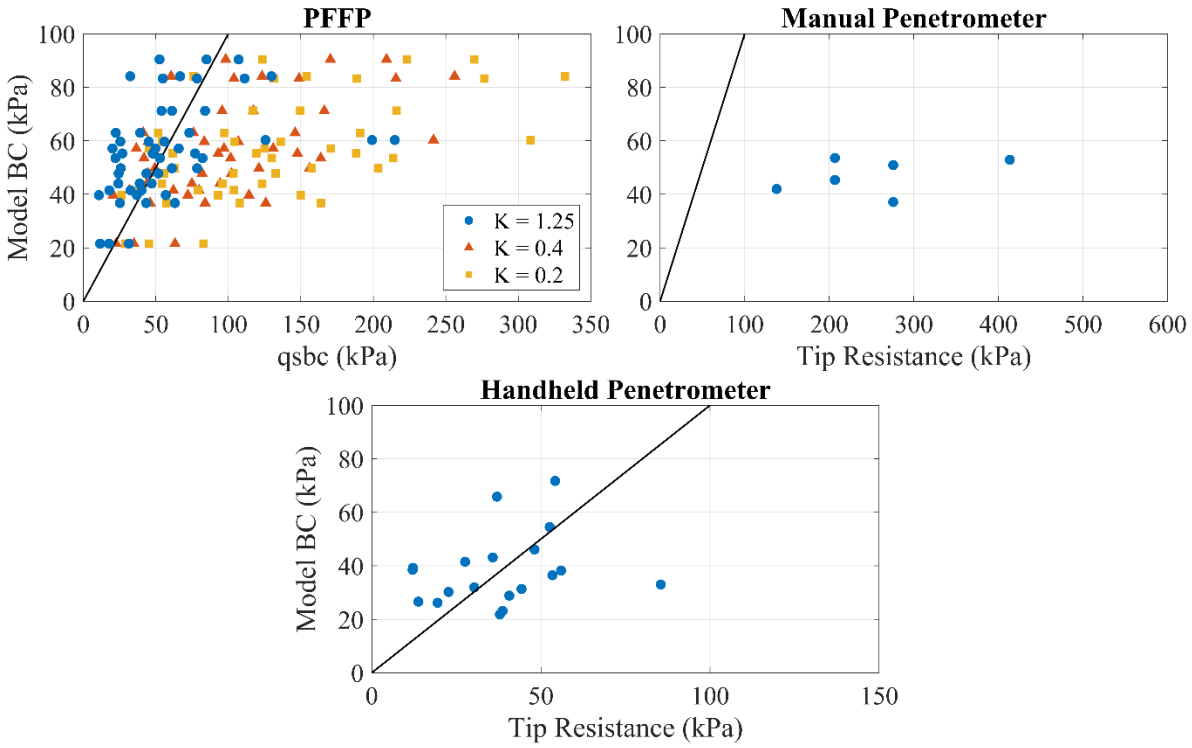

Figure 3.11: Comparison of tip resistance from the three penetrometers to the Vanapalli and Mohammed (2007) bearing capacity model. The black line on each plot represents the one-to-one line.

Figure 3.12 shows the PFFP results for $K = 1.25$, differentiated by drop height. Of the three drop heights, the medium drop height ($v_i \cong 2.5 m/s$) provided the best fit with the model. As seen from the plot, data points from the same station, with the same soil properties, do not collapse down to a single point. Since K is known to be soil-dependent (True, 1976), the strain-rate correction should theoretically collapse the $qsbc$ values to a single point for a given station, as the soil properties did not change between deployments. As seen from Figure 3.12, using a single value of K fails to reduce $qsbc$ to a single value at each station, which implies that for beach sands, in addition to being soil-dependent, the value of K is also velocity-dependent, as impact velocity increases with drop height. Also of note is the outlier station, with three data points far to the right of the plot, a large overestimation compared to the model. This outlier was a station located in the swash zone (B6) and viscous effects associated with a moisture content and undrained loading are the likely reason for this large overestimation. This data point will be discussed in later sections. Ignoring this outlier gives $R^2 = 0.38$ using $K = 1.25$.

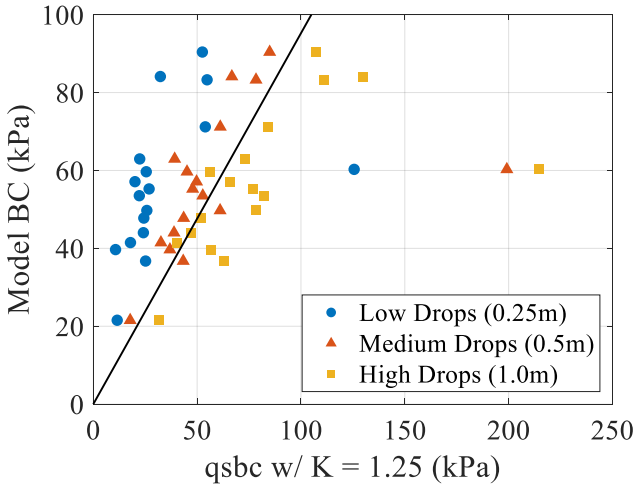

Figure 3.12: Application of strain-rate correction using K = 1.25. Results are separated by drop height. Each of the 17 individual stations is represented by three data points, with a PFFP deployment from each of the three drop heights.

3.4.2. Modified Strain-Rate Correction Factor, K_{mod}

In order to overcome the added complication of strain rate (i.e., impact velocity and here drop height), as well as to further improve the fit with the model, it was decided to modify they strain rate correction expression by relating K to impact velocity, v_i. For each deployment, the modelled value of bearing capacity, q_u, computed via Equation 3.8, was assumed to be equal to $qsbc$, and Equations 3.5 and 3.6 were used to solve for K. The resulting values of K were then compared to the known values of v_i, and the equation of the linear best-fit was taken as the modified velocity-dependent K-factor, K_{mod} (Figure 3.13). The new strain-rate correction, f_{sr-mod}, is given by Equation 3.9:

$$f_{sr-mod} = 1 + K_{mod} * log_{10}\left(\frac{v}{v_{ref}}\right) = 1 + 0.31 * v_i * log_{10}\left(\frac{v}{v_{ref}}\right) \qquad (3.9)$$

Using the modified strain-rate correction factor, new values of $qsbc$ were computed via Equations 3.6 and 3.9 and compared to the modelled values of q_u (Figure 3.14). The velocity-dependent strain rate correction improved agreement with the model by 65% ($R^2 = 0.63$ also ignoring the outlier). Between the drop heights, the medium drop from ~0.5 m height had the best individual agreement, with R^2 = 0.78. The new correction factor was still unable to collapse deployments of different heights at the same station down to a single point but did represent an improvement over the previous single value strain rate factor (Figure 3.12).

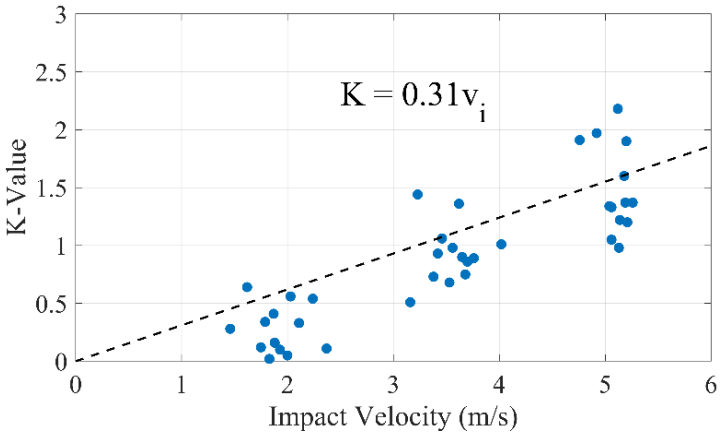

Figure 3.13: Relationship between strain-rate empirical coefficient, $\boldsymbol{K}$, and $\boldsymbol{v_i}$. Dashed line indicates the linear best-fit through the data, with the equation shown.

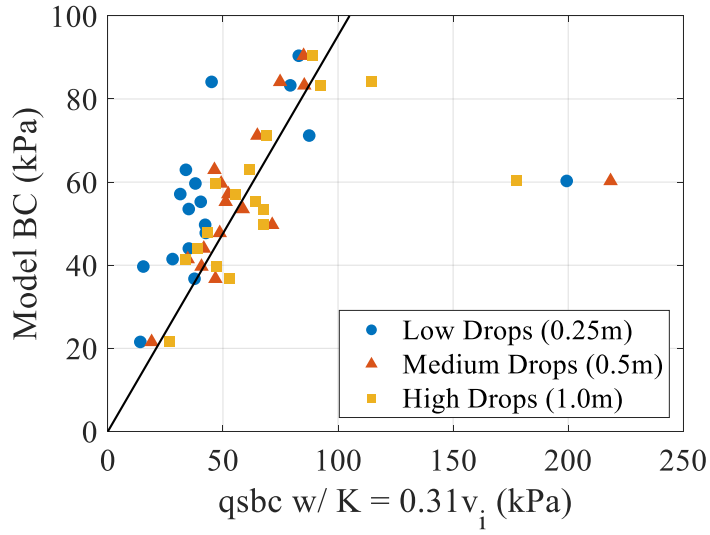

Figure 3.14: $\boldsymbol{qsbc}$ vs. modelled bearing capacity. Black line indicates one-to-one line.

3.4.3. Comparison with Other Properties

Strength estimates from the PFFP, using the medium drop height and modified strain rate correction factor, along with the measurements from the *Soil Saber* penetrometer were compared to moisture content (Figure 3.15) and relative density (Figure 3.16). A positive trend was observed between strength and moisture content for both instruments with the exception of the data points at $w_v = 35\%$. A less well-defined relationship was found between strength and relative density, however there the data points at $D_r = 75\%$ exhibited a similarly anomalous behavior as the aforementioned data points in Figure 3.15. In both plots, it can be seen that the difference between both methods was significant for high water contents or high relative densities with the magnitude of *qsbc* typically being comparatively high compared to other values (Figure 3.15 & 3.16). Both

pairs of diverging data points correspond to the same station in the swash zone as the outlier data points in Figures 3.12 & 3.14.

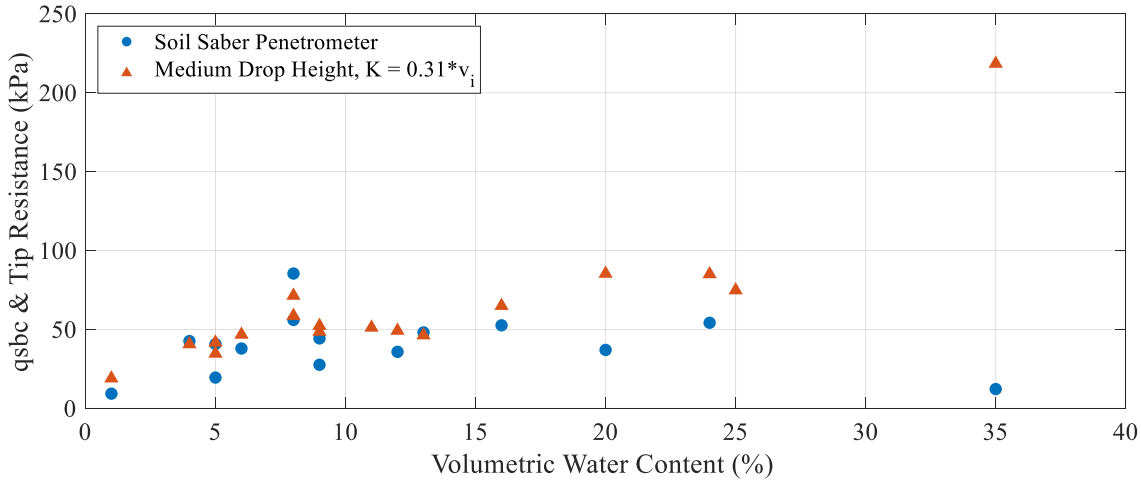

Figure 3.15: Relationship between moisture content and strength estimates from PFFP and handheld penetrometer.

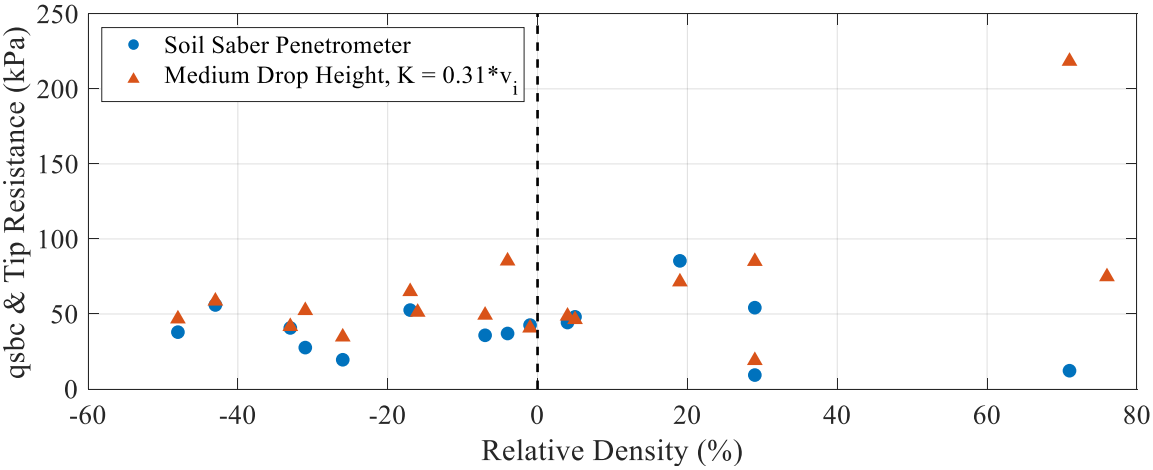

Figure 3.16: Relationship between relative density and strength estimates from PFFP and handheld penetrometer.

3.5. Discussion

Interestingly, D_r < 10%, including negative values, were observed for the entire intertidal zone. 10% < D_r < 50 % was only measured near the dune toe and near the swash, and higher D_r were only found in the swash zone (during low tide) (Figure 3.6). This seems to suggest that recent surficial sediment reorganization and partial saturation enables the creation and maintenance of extreme loose sands. Despite a significant range of D_r of these loose sands, the apparent strength

was fairly consistent and more sensitive to moisture content variations (Figures 3.15 and 3.16). The lack of apparent trends in relative density and strength runs counterintuitive to traditional geotechnical intuition (Figure 3.16). However, partially saturated sediments with a very loose packing state ($D_r < 0\%$) rely less on particle-particle stresses and more on suction stresses to support the soil skeleton (Lu and Likos, 2006). Additionally, these negative D_r sediments will have larger pore spaces, and more air in the voids. These effects would cause these sediments to undergo compression/contractive, or negative volume change, when sheared. This is consistent with knowledge of loose sediments exhibiting contractive behavior when sheared (Duncan et al., 2014). The degree of this compression and extent to which it affects the stress-strain behavior is likely a function of both the moisture content and initial density. Different moisture contents result in different suction stresses, and the initial density would control how much compression takes place before a $D_r > 0$ is achieved. More work is needed to fully understand the behavior of sediments with $D_r < 0$ and the relationship to partial saturation, but this theory may explain why the observed data did not agree with the initial expectation. This makes moisture content a key governing property controlling apparent strength as well as relative density in the intertidal zone. However, it should be noted that D_r exhibited clear differences between the intertidal zone ($D_r <$ 10%), the subaerial zone (10% < D_r < 50 %), and the swash zone around low tide ($D_r >$ 70%), making it a significant variable across different foreshore zones (Figure 3.6). Thus, measurements of relative density across the foreshore and moisture content across the intertidal zone may be important to represent sand packing and state of saturation accurately, relevant for computing bearing capacity (Equation 3.8), as well as for coastal sediment transport processes (Bauer et al., 2009; Darke and Neuman, 2008; Davidson-Arnott et al., 2005; Erikson et al., 2007; Sassa and Watabe, 2007). The methods tested in this study provided results with sufficient accuracy to depict foreshore-zone-dependent and inter-zonal variations where applicable.

Sediment strength measurements are expected to be affected by particle properties, packing, as well as state of saturation, and thus, could possible represent a rapid and efficient way to investigate variations in beach surface sediment properties relevant for engineering problems and sediment dynamics.

The vane shear results showed a similar trend to the penetrometer, with the vane shear being lower in magnitude (Figure 3.8). It is difficult to assess the validity of the vane shear strength

measurements using existing relationships due to issues surrounding the shape of the failure plane in sandy sediments and difficulty in determining effective stresses on the failure plane due to partial saturation (Briaud, 2013; Park et al., 2016). While it is acknowledged that shear strength is a key parameter for understanding surficial sediment erosion, the difficulty involved in assessing the quality of the shear strength measurements and the sparse literature available regarding vane shear measurements in partially saturated sands outweigh the potential benefits of collecting this type of information. Sassa and Yang (2019) collected vane shear measurements on sandy beaches and sandflats of similar grain size to the current site to compare the measured torque with suction measurements. The values reported as shear strength by those authors were about an order of magnitude smaller (< 5 kPa) than the measurements for this study (10-20 kPa) (Figure 3.8). Additionally, a positive correlation was observed between vane shear strength and groundwater level induced suction stresses, which are a function of the soil moisture content (Sassa and Watabe, 2007; Sassa and Yang, 2019). This result has important implications for morphologic change, as tidal fluctuations result in highly variable moisture contents, and therefore suction stresses at beach environments. Deriving and measuring suction stresses using moisture content was outside the scope of this work, and thus it is suggested that vane shear measurements on beaches be used only with proper consideration given to measurement of suction stresses and validation of the vane shear measurements.

When compared to the Vanapalli and Mohammed (2007) bearing capacity model, the tip resistance measurements from the handheld penetrometer exhibited poor correlation (Figure 3.11). This poor performance is likely due to geometry and scale effects associated to the small tip size of the penetrometer itself (5mm) compared to the d_{50} of the sediment (0.35mm). Since the tip diameter is small compared to the grain size, and the low density sediment (D_r < 0%) is already inclined to exhibit compressive behavior during penetration, it is likely that the sediment was no longer acting as a continuum, and rather as individual particles being moved out of the way during penetration. This effect would reduce the measured values, as the sediment would not be able to mobilize its available to shear strength as a bulk material. Thus, values would be considered not representative for most applications.

Despite a comparatively slow penetration velocity (~3 cm/s) and partial/fully drained shearing regime, the manual penetrometer vastly overestimated bearing capacity via the Vanapalli and Mohammed (2007) model (Figure 3.11, top right). Additionally, while handheld and manual

penetrometers exhibited similar trends in tip resistance (Figure 3.10), the manual penetrometer recorded tip resistances up to an order of magnitude larger than the handheld penetrometer. The difference between the two may be due in part to the different drainage regimes and penetration depths (9 cm vs. 5 cm, respectively), but the likely reason for consistent overestimation is the configuration of the manual penetrometer itself. The probe measures resistance from a dial gauge read by a user, in 5 psi increments from 0-300 psi. This equates to a ~35 kPa jump between increments. The modelled values of q_u for all stations are on the order of tens of kPa, suggesting that the manual penetrometer is not recording at a resolution sensitive enough to capture the low resistance of the surficial beach sediments. An additional complicating factor is that it is difficult for the user to read a moving dial gauge to the 5 psi increments, making the true resolution even lower than the increments on the gauge (on the order of 10-20 psi, or ~100kPa). It is extremely difficult to make an accurate reading for the upper 5-10 cm of sediment that is of interest for this work. These factors indicate that the manual penetrometer is not well equipped for measuring the strength of sandy surficial beach sediments.

With the development of a velocity-dependent strain rate correction (Equation 3.9), the measurements from the PFFP, specifically the medium drop height from 0.5 m, provided the best fit with the bearing capacity model (Figure 3.14). Improvements to this new analysis could be made by increasing the number of data points used to develop the empirical coefficient, or possibly looking at the shape of the deceleration profiles as a representation of the soil response instead of simply taking the maximum values. As the strain-rate empirical coefficient, K, is soil-dependent, we expect that K_{mod} will need to be calibrated for different soil types (True, 1976). The strain-rate correction used in this study was developed for fully saturated environments, and the influence of other controlling parameters, namely soil-type and bulk sediment properties (ϕ', D_r) have been addressed by previous work (True, 1976; Albatal et al., 2020). Thus, it is hypothesized that the additional sensitivity to strain-rate was introduced by the partial saturation (Atherton et al., 2001; Martin et al., 2009).

Strength measurements were not sensitive to low relative densities < 10% and lack of data prohibited any clear statement if the strength measurements related to relative densities in the range of 10-40%. However, strength measurements were related to moisture content, and it may be argued that PFFP measurements mimicked the cross-shore trends in moisture content. In the swash

zone, it may be hypothesized that viscous effects related to high pore saturation and high relative density yielded high strength measurements. Thus, it appears feasible that strength measurements could be utilized to represent impacts of soil behavior related to saturation and particle packing in beach environments. Particularly, the use of a water-proof system like the PFFP could pave the way for seamless measurements from the foreshore to the nearshore that could inform geomorphological models regarding sediment bulk properties as well as saturation properties (where appropriate).

3.6. Conclusions

Variations in relative density, moisture content, sediment strength, and their correlations were explored at a sandy beach towards the ultimate goal of using geotechnical properties for prediction of geomorphodynamics. Hand-deployed tools were chosen to measure these properties in the interest of considering methods that would be applicable for highly spatiotemporally variable environments. They were assessed based on their performance in sandy beach environments reaching from the subaerial zone into the swash. Relative density was measured from push core samples revealing a clear distinction between subaerial zone, intertidal zone, and swash zone. Negative relative densities (looser packing than loosest possible packing in a dry state) were observed in the intertidal zone and attributed to the effects of partial saturation. In the same zone, relative density did not correlate well with measured strength values. However, strength related to variations in moisture contents. The results suggested that strength measurements may serve as one representative parameter to capture sediment bulk and saturation properties in the content erosion and sediment dynamics, possibly simplifying field data collection to inform predictive models.

Of the four strength measurement methods tested, a portable free fall penetrometer performed best, yielding a satisfying correlation with a partially saturated bearing capacity model when applying a modified strain rate correction factor $K = 0.31v_i$. Other penetrometers tested were affected by issues of resolution or penetrometer diameter-grain size- ratio limitations. The vane shear provided a direct estimate of shear strength, but difficulties in validating the accuracy of the results and lack of appropriate consideration of suction stresses associated with tidal fluctuations precluded any further work with this device within the scope of the study. Further work is needed to explore the development of a possibly strength based and moisture content-dependent parameter most suited

for the implementation into geomorphodynamic models. Furthermore, the swash zone and its processes leading to sediment densification require further investigations.

3.7. Acknowledgements

The authors would like to thank Julia Paprocki, Reem Jaber, Matthew Florence, and the scientists and staff at the USACE FRF for their support in data collection efforts. This material is based upon work supported by the National Science Foundation under Grant CMMI-1751463. Any opinions, findings, and conclusions or recommendations expressed in this material are those of the author(s) and do not necessarily reflect the views of the National Science Foundation.

References

Abuodha, J.O.Z., 2003. Grain size distribution and composition of modern dune and beach sediments, Malindi Bay coast, Kenya. Journal of African Earth Sciences 36. https://doi.org/10.1016/S0899-5362(03)00016-2

Akal, T., Stoll, R.D., 1995. Expendable penetrometer for rapid assessment of seafloor parameters, in: Oceans Conference Record (IEEE). https://doi.org/10.1109/oceans.1995.528858

Albatal, A., Stark, N., 2017. Rapid sediment mapping and in situ geotechnical characterization in challenging aquatic areas. Limnology and Oceanography: Methods 15. https://doi.org/10.1002/lom3.10192

Albatal, A., Stark, N., Castellanos, B., 2020. Estimating in situ relative density and friction angle of nearshore sand from portable free-fall penetrometer tests. Canadian Geotechnical Journal 57. https://doi.org/10.1139/cgj-2018-0267

ASTM D422-63. Standard Test Method for Particle-Size Analysis of Soil. ASTM International, West Conshohocken, PA.

ASTM D2453-16. Standard Test Methods for Maximum Index Density and Unit Weight of Soils Using a Vibratory Table. ASTM International, West Conshohocken, PA.

ASTM D2454-00. Standard Test Methods for Minimum Index Density and Unit Weight of Soils and Calculation of Relative Density. ASTM International, West Conshohocken, PA.

Atherton, R., Baird, J., Wiggs, G., 2001. Inter-tidal dynamics of surface moisture content on a meso-tidal beach. Journal of Coastal Research 17(2). https://www.jstor.org/stable/4300198

Bałachowski, L., 2007. Size effect in centrifuge cone penetration tests. Archives of Hydroengineering and Environmental Mechanics 54.

Bauer, B.O., Davidson-Arnott, R.G.D., Hesp, P.A., Namikas, S.L., Ollerhead, J., Walker, I.J., 2009. Aeolian sediment transport on a beach: Surface moisture, wind fetch, and mean transport. Geomorphology 105. https://doi.org/10.1016/j.geomorph.2008.02.016

Bolton, M.D., 1986. The strength and dilatancy of sands. Geotechnique 36. https://doi.org/10.1680/geot.1986.36.1.65

Briaud, J.-L., 2013. Geotechnical Engineering: Unsaturated and Saturated Soils. Wiley.

Brilli, N.C., Stark, N., 2020. Variations in Sediment Strength across a Sandy Peninsula. https://doi.org/10.1061/9780784482810.080

Chow, S., Bienen, B., Randolph, M., 2018. Rapid penetration of piezocones in sand. Proceedings of the 4th International Symposium on Cone Penetration Testing, Delft.

Dalrymple, R.A., 1992. Prediction of Storm/Normal Beach Profiles. Journal of Waterway, Port, Coastal, and Ocean Engineering 118. https://doi.org/10.1061/(asce)0733-950x(1992)118:2(193)

Darke, I., Neuman, C.M.K., 2008. Field study of beach water content as a guide to wind erosion potential, in: Journal of Coastal Research. https://doi.org/10.2112/00-000.1

Davidson-Arnott, R.G., MacQuarrie, K., Aagaard, T., 2005. The effect of wind gusts, moisture content and fetch length on sand transport on a beach. Geomorphology 68. https://doi.org/10.1016/j.geomorph.2004.04.008

Dayal, U., Allen, J.H., 1973. Instrumented Impact Cone Penetrometer. Canadian Geotechnical Journal 10. https://doi.org/10.1139/t73-034

Dayal, U., Allen, J.H., Jones, J.M., 1975. Use of an impact penetrometer for the evaluation of the in-situ strength of marine sediments. Marine Geotechnology 1. https://doi.org/10.1080/10641197509388155

de Beer, E.E., 1965. Bearing capacity and settlement of shallow foundations on sand, in: Proceedings of Symposium on Bearing Capacity and Settlement of Foundations.

de Lima, D.C., Tumay, M.T., 1991. Scale effects in cone penetration tests, in: Geotechnical Special Publication.

Dean, R.G., Dalrymple, R.A., 2004. Coastal Processes with Engineering Applications, Coastal Processes with Engineering Applications. https://doi.org/10.1017/cbo9780511754500

Duncan, J.M., Wright, S.G., Brandon, T.L., 2014. Soil Strength and Slope Stability, 2nd Edition, John Wiley & Sons.

Durgunoglu, H.T., Mitchell, J.K., 1973. Static penetration resistance of soils. Washington, D.C.

Erikson, L.H., Larson, M., Hanson, H., 2007. Laboratory investigation of beach scarp and dune recession due to notching and subsequent failure. Marine Geology 245. https://doi.org/10.1016/j.margeo.2007.04.006

Finnie, I.M., Randolph, M., 1994. Bearing response of shallow foundations on uncemented calcareous soil, in: International Conference Centrifuge '94. CRC Press/Balkema, Singapore.

Fisher, J.S., Stauble, D.K., 1977. Impact of Hurricane Belle on Assateague Island washover. Geology 5. https://doi.org/10.1130/0091-7613(1977)5<765: IOHBOA>2.0.CO;2

Fredlund, D.G., Rahardjo, H., 1993. Soil Mechanics for Unsaturated Soils, Soil Mechanics for Unsaturated Soils. https://doi.org/10.1002/9780470172759

Gallagher, E., Wadman, H., McNinch, J., Reniers, A., Koktas, M., 2016. A conceptual model for spatial Grain size variability on the surface of and within beaches. Journal of Marine Science and Engineering 4. https://doi.org/10.3390/jmse4020038

Gui, M.W., Bolton, M.D., 1998. Geometry and scale effects in CPT and pile design, in: Robertson, P.K., Mayne, P.W. (Eds.), 1st International Conference on Site Characterization, ISC'98. Atlanta, GA, pp. 1063–1068.

Heathershaw, A.D., Carr, A.P., Blackley, M.W.L., Wooldridge, C.F., 1981. Tidal variations in the compaction of beach sediments. Marine Geology 41. https://doi.org/10.1016/0025-3227(81)90082-7

Jafari, N.H., Harris, B.D., Stark, T.D., 2018. Geotechnical investigations at the Caminada headlands beach and dune in coastal Louisiana. Coastal Engineering 142. https://doi.org/10.1016/j.coastaleng.2018.04.014

Jamiolkowski, M., Ladd, C.C., Germaine, J.T., Lancellotta, R., 1985. New developments in field and laboratory testing of soils. Proc. 11th international conference on soil mechanics and foundation engineering, San Francisco, August 1985. Vol. 1, (Balkema).

Kirchner, J.W., Dietrich, W.E., Iseya, F., Ikeda, H., 1990. The variability of critical shear stress, friction angle, and grain protrusion in water-worked sediments. Sedimentology 37. https://doi.org/10.1111/j.1365-3091.1990.tb00627.x

Kulhawy, F.H., Mayne, P.W., 1990. Manual on Estimating Soil Properties for Foundation Design. Ostigov.

Lee, K.L., Seed, H.B., 1967. Drained Strength Characteristics of Sands. Journal of the Soil Mechanics and Foundations Division 93. https://doi.org/10.1061/jsfeaq.0001048

Lee, S.Y., 1990. Centrifuge modelling of cone penetration testing in cohesionless soils. Cambridge, UK. https://doi.org/10.17863/CAM.14104

Lu, N., Kim, T.-H., Sture, S., Likos, W.J., 2009. Tensile Strength of Unsaturated Sand. Journal of Engineering Mechanics 135. https://doi.org/10.1061/(asce)em.1943-7889.0000054

Lu, N., Likos, W., 2006. Suction stress characteristic curve for unsaturated soils. Journal of Geotechnical and Geoenvironmental Engineering 132(2). https://doi.org/10.1061/(ASCE)1090-0241(2006)132:2(131)

Lucking, G., Stark, N., Lippmann, T., Smyth, S., 2017. Variability of in situ sediment strength and pore pressure behavior of tidal estuary surface sediments. Geo-Marine Letters 37. https://doi.org/10.1007/s00367-017-0494-6

Manning, M., Stark, N., 2019. Investigating moisture contents of sandy beaches in the context of a geotechnical site characterization. https://doi.org/10.1142/9789811204487_0219

Martin, B.E., Chen, W., Song, B., Akers, S.A., 2009. Moisture effects on the high strain-rate behavior of sand. Mechanics of Materials 41. https://doi.org/10.1016/j.mechmat.2009.01.014

Masselink, G., Kroon, A., Davidson-Arnott, R.G.D., 2006. Morphodynamics of intertidal bars in wave-dominated coastal settings - A review. Geomorphology 73. https://doi.org/10.1016/j.geomorph.2005.06.007

Masselink, G., Short, A.D., 1993. The effect of tide range on beach morphodynamics and morphology: a conceptual beach model. Journal of Coastal Research 9.

McNinch, J.E., 2004. Geologic control in the nearshore: Shore-oblique sandbars and shoreline erosional hotspots, Mid-Atlantic Bight, USA. Marine Geology 211. https://doi.org/10.1016/j.margeo.2004.07.006

Meyerhof, G., 1961. The ultimate bearing capacity of wedge-shaped foundations. Proceedings, 5th International Conference on Soil Mechanics and Foundation Engineering ICSMFE, Paris, 105–109.

Miller, R.L., Byrne, R.J., 1966. The angle of repose of a single grain on a fixed rough bed. Sedimentology 6. https://doi.org/10.1111/j.1365-3091.1966.tb01897

Mulhearn, P.J., 2001. Methods of Obtaining Soil Strength Data for Modelling Vehicle Trafficability on Beaches.

Park, S.-S., Zhou, A., Kim, D.-R., 2016. Vane Shear Test on Nakdong River Sand. Journal of The Korean Society of Civil Engineers 36. https://doi.org/10.12652/ksce.2016.36.3.0463

Randolph, M., 2004. Characterization of soft sediments for offshore applications. Proc. 2nd Int. Conf. on Site Characterization, Porto 1.

Randolph, M., Hope, S., 2004. Effect of cone velocity on cone resistance and excess pore pressures, in: Matsui, T., Tanaka, Y., Mimura, M. (Eds.), Proceedings of the IS Osaka - Engineering Practice and Performance of Soft Deposits. Yodogawa Kogisha Co. Ltd, Osaka, Japan.

Reeve, B., Stark, N., Mewis, P., 2018. Cross-shore variation in sediment strength at a sandy beach. Coastal Engineering Proceedings. https://doi.org/10.9753/icce.v36.sediment.83

Robertson, P.K., Campanella, R.G., 1983. Interpretation of cone penetration tests. Part I: sand. Canadian Geotechnical Journal 20. https://doi.org/10.1139/t83-078

Robertson, P.K., Robertson (Cabal), K., 2007. Guideline for Cone Penetration Testing for Geotechnical Engineering, 2nd ed., Gregg Drilling and Testing, Inc.

Salgado, R., Prezzi, M., Kim, K., Lee, W., 2013. Penetration rate effects on cone resistance measured in a calibration chamber, in: Geotechnical and Geophysical Site Characterization 4 - Proceedings of the 4th International Conference on Site Characterization 4, ISC-4.

Sassa, S., Watabe, Y., 2007. Role of suction dynamics in evolution of intertidal sandy flats: Field evidence, experiments, and theoretical model. Journal of Geophysical Research: Earth Surface 112. https://doi.org/10.1029/2006JF000575

Sassa, S., Yang, S., 2019. Role of geoenvironmental dynamics in the biodiversity of sandy beaches and sandflats: The ecohabitat chart and its ecological implications. Estuarine, Coastal and Shelf Science 219. https://doi.org/10.1016/j.ecss.2019.02.002

Sassa, S., Yang, S., Watabe, Y., Kajihara, N., Takada, Y., 2014. Role of suction in sandy beach habitats and the distributions of three amphipod and isopod species. Journal of Sea Research 85. https://doi.org/10.1016/j.seares.2013.06.005

Stark, N., Brilli, N.C., 2021. Geotechnical Investigation of Spatiotemporal Variations of Moisture Contents in Intertidal Beach Sands and Effects on Coastal Erosion Processes, in: Proceedings of the International Conference on Scour and Erosion (ICSE-10). Arlington, VA.

Stark, N., Coco, G., Bryan, K.R., Kopf, A., 2012. In-situ geotechnical characterization of mixed-grain-size bedforms using a dynamic penetrometer. Journal of Sedimentary Research 82. https://doi.org/10.2110/jsr.2012.45

Stark, N., Hay, A.E., Trowse, G., 2015. Cost-effective geotechnical and sedimentological early site assessment for ocean renewable energies, in: 2014 Oceans - St. John's, OCEANS 2014. https://doi.org/10.1109/OCEANS.2014.7003004

Stark, N., Kopf, A., Hanff, H., Stegmann, S., Wilkens, R., 2009. Geotechnical investigations of sandy seafloors using dynamic penetrometers, in: MTS/IEEE Biloxi - Marine Technology for Our Future: Global and Local Challenges, OCEANS 2009. https://doi.org/10.23919/oceans.2009.5422460

Stark, N., McNinch, J., Wadman, H., Graber, H.C., Albatal, A., Mallas, P.A., 2017. Friction angles at sandy beaches from remote imagery. Geotechnique Letters 7. https://doi.org/10.1680/jgele.17.00053

Stark, N., Mewis, P., Reeve, B., Florence, M., Piller, J., & Simon, J. (2022). Vertical pore pressure variations and geotechnical sediment properties at a sandy beach. *Coastal Engineering*, *172*. https://doi.org/10.1016/j.coastaleng.2021.104058

Stark, N., Wever, T.F., 2009. Unraveling subtle details of expendable bottom penetrometer (XBP) deceleration profiles. Geo-Marine Letters 29. https://doi.org/10.1007/s00367-008-0119-1

Steiner, A., Kopf, A.J., L'Heureux, J.S., Kreiter, S., Stegmann, S., Haflidason, H., Moerz, T., 2014. In situ dynamic piezocone penetrometer tests in natural clayey soils - a reappraisal of strain-rate corrections. Canadian Geotechnical Journal 51. https://doi.org/10.1139/cgj-2013-0048

Stephan, S., Kaul, N., Villinger, H., 2015. Validation of impact penetrometer data by cone penetration testing and shallow seismic data within the regional geology of the Southern North Sea. Geo-Marine Letters 35. https://doi.org/10.1007/s00367-015-0401-y

Stoll, R.D., Akal, T., 1999. XBP - Tool for rapid assessment of seabed sediment properties: Instrumented with accelerometers, new expendable probes measure the impact signature of the ocean bottom. Sea Technology.

Stoll, R.D., Sun, Y.F., Bitte, I., 2007. Seafloor properties from penetrometer tests. IEEE Journal of Oceanic Engineering 32. https://doi.org/10.1109/JOE.2007.890943

Terzaghi, K., 1943. Theoretical Soil Mechanics, Theoretical Soil Mechanics. https://doi.org/10.1002/9780470172766

True, D.G., 1976. Undrained vertical penetration into ocean bottom soils. Berkeley, CA.

van Rijn, L.C., 2007. Unified View of Sediment Transport by Currents and Waves. II: Suspended Transport. Journal of Hydraulic Engineering 133. https://doi.org/10.1061/(asce)0733-9429(2007)133:6(668)

Vanapalli, S.K., Mohamed, F.M.O., 2007. Bearing Capacity of Model Footings in Unsaturated Soils, in: Experimental Unsaturated Soil Mechanics. https://doi.org/10.1007/3-540-69873-6_48

Vesic, A.S., 1973. Analysis of ultimate loads of shallow foundations. ASCE J Soil Mech Found Div 99. https://doi.org/10.1061/jsfeaq.0001846

White, D., O'Loughlin, C., Stark, N., Chow, S., 2018. Free fall penetrometer tests in sand: Determining the equivalent drained resistance. Proceedings of the 4th International Symposium on Cone Penetration Testing, Delft.

Wang, J.P., Hu, N., François, B., Lambert, P., 2017. Estimating water retention curves and strength properties of unsaturated sandy soils from basic soil gradation parameters. Water Resources Research 53. https://doi.org/10.1002/2017WR020411

Watts, C.W., Tolhurst, T.J., Black, K.S., Whitmore, A.P., 2003. In situ measurements of erosion shear stress and geotechnical shear strength of the intertidal sediments of the experimental managed realignment scheme at Tollesbury, Essex, UK. Estuarine, Coastal and Shelf Science 58. https://doi.org/10.1016/S0272-7714(03)00139-2

Wayllace, A., Lu, N., 2012. Atransient water release and imbibition method for rapidly measuring wetting and drying soil water retention and hydraulic conductivity functions. Geotechnical Testing Journal 35. https://doi.org/10.1520/GTJ103596

Zambrano-Cruzatty, L., Yerro, A., Stark, N., 2019. Influence of Shear Strength and Moisture Content on Aeolian Sand Erosion. https://doi.org/10.1061/9780784482155.001

Chapter 4: Relating Geotechnical Sediment Properties and Erodibility at a Sandy Beach

The contributions of the authors to the composition of this manuscript are delineated as follows:

Nicola Brilli:

- Participated in the field survey
- Conducted all laboratory analysis
- Performed literature review; processed and analyzed field data; prepared figures, tables, and draft of manuscript
- Revised manuscript based on suggestions of co-author
- Prepared final manuscript for submission

Nina Stark:

- Lead primary investigator of this study
- Initiated research idea and co-developed the refined research questions
- Planned, supervised, and participated in the field survey in Duck, NC
- Reviewed and edited the draft manuscript
- Reviewed and edited the final version of the manuscript

Celso Castro-Bolinaga:

- Provided laboratory space and equipment for Jet Erosion Tests
- Reviewed and edited the draft manuscript
- Reviewed and edited the response to reviewer comments and the final version of the manuscript

Relating Geotechnical Sediment Properties and Erodibility at a Sandy Beach

Nicola C. Brilli, S.M.ASCE[1], Nina Stark[2], Ph.D., M.ASCE, Celso Castro-Bolinaga[3], Ph.D.

[1]Virginia Tech, Department of Civil and Environmental Engineering, Blacksburg, VA 24060; e-mail: nickb96@vt.edu

[2]Virginia Tech, Department of Civil and Environmental Engineering, Blacksburg, VA 24060; e-mail: ninas@vt.edu

[3]North Carolina State University, Dept. of Biological and Agricultural Engineering, Raleigh, NC 27606; e-mail: cfcastro@ncsu.edu

The authors of the following manuscript have submitted it to the ASCE Journal of Waterway, Port, Coastal, and Ocean Engineering.
Manuscript Submitted: March 2023

4.1. Abstract

Geotechnical sediment properties, morphological change, and hydrodynamics were measured as part of the During Nearshore Event Experiment (DUNEX) in October 2021 at the sandy Atlantic side beach in Duck, NC. Moisture content, grain size, packing state (i.e., bulk density, relative density, void ratio), and sediment strength were compared to bed-level change from ground-based LiDAR and erodibility parameters from laboratory Jet Erosion Tests (JET) along a cross-shore transect stretching from the dune toe to the lower intertidal zone. Decreases in bulk unit weight, quasi-static bearing capacity, and firmness factor (both expressions of sediment strength) correlated with areas of recent sediment deposition. Change of void ratio appeared most related to observed erosion/deposition, with increases in void ratio being observed for depositional areas and decreases in erosional areas with up to 0.5 m of bed-elevation change. Void ratio also correlated with the detachment rate coefficient from JETs, with denser sediments testing as less erodible. In-situ sediment strength measurements related – as expected – to bulk unit weight, void ratio, and water content, with increases in firmness factor tied to increases in packing state and water content.

4.2. Introduction

Coastal areas are subject to increasingly difficult challenges due to climate change. Sea level rise and increases in the frequency and severity of coastal storms are expected to lead to increasing beach erosion, shoreline retreat, and flood events (Sallenger 2000, Zhang et al. 2004, Jones et al. 2008, Bender et al. 2010, Knutson et al. 2010). Central to improving prediction and mitigation capabilities of these impacts is improving the understanding of sediment dynamics in coastal areas. Specifically, the role of sediment properties beyond grain size, for example, geotechnical sediment properties and their relationship to driving mechanisms of erosion, are still not well understood. Such relationships have the potential to improve prediction of sediment dynamics and to help with mitigating climate-related coastal change and impacts on coastal communities.

Erosion is typically modelled as a fluid-particle interaction, and thus, grain size and particle density predominantly govern the prediction of erodibility (Shields 1936, Briaud 2001). For cohesive sediments, there have been numerous attempts to correlate a wide variety of sediment properties with erodibility (National Academy of Science and Engineering 2019). Properties such as water content, unit weight, plasticity index, undrained shear strength, void ratio, swell, fines fraction, amongst others have been tested with various degrees of success (Cao et al. 2002,

National Academy of Science and Engineering 2019). For non-cohesive sediments, sands and gravels, grain size is accepted as the controlling parameter for erodibility relationships (Briaud 2013). For beach environments, sand is the predominant sediment type, and thus, sediment dynamics are predicted mostly based on grain size, if sediment properties are considered at all. However, geotechnical sediment properties such as moisture content, density, and shear strength have shown to be important for a variety of related coastal processes such as dune retreat, tidal flat evolution, and aeolian sediment transport (Davidson-Arnott et al. 2005, Erikson et al. 2007, Sassa and Watabe 2007, Zambrano-Cruzatty et al. 2019), and may be particularly important in the intertidal zone that is subject to saturation and drainage and variations in forcing conditions on different time scales (waves, tides, inundation events). While geomorphodynamics of coastal areas are driven by local hydrodynamics (Dalrymple 1992, Masselink and Short 1993, Dean and Dalrymple 2004, Masselink et al. 2006), it is hypothesized that including geotechnical sediment properties in erodibility relationships could further improve the prediction of coastal change by understanding sediment stabilizing forces better.

Challenges of conducting geotechnical measurements in energetic coastal environments have been approached in recent years. Tools such as portable free-fall penetrometers (PFFPs) have enabled conducting geotechnical surveying of energetic coastal areas (Stark and Kopf 2011, Stark et al. 2014, Albatal and Stark 2017, Albatal et al. 2019). When deployed in submerged coastal areas, PFFPs have been used for sediment characterization and for estimating bearing strength, relative density of sands, undrained shear strength, and soil behavior under dynamic loading (Akal and Stoll 1995, Chow et al. 2018, Lucking et al. 2017, Albatal et al. 2020, Kiptoo et al. 2020). More recently, PFFPs have been tested for geotechnical surveying in emerged intertidal environments (Reeve et al. 2018, Brilli and Stark 2020). The ability of a single tool to collect geotechnical measurements seamlessly from the emerged to submerged coastal zones is essential to integrate geotechnical sediment properties in sediment transport prediction and simulation at beaches. The goal of this study was to relate geotechnical sediment properties, erodibility parameters, morphodynamics, and hydrodynamic regime in a sandy beach environment. To this end, a field survey was conducted at the United States Army Corp of Engineers Field Research Facility (USACE FRF) in October 2021 in the framework of the During Nearshore Event Experiment (DUNEX). The field survey included in-situ testing and the collection of sediment samples for subsequent laboratory erodibility testing. Based on the collected field data and

physical sample analysis, sediment properties and mobility were assessed and related to bed-elevation change.

4.3. Methods

4.3.1. Field Measurements

From October 11th to October 15th, 2021, three transects (A-C) were surveyed daily on the Atlantic-side sand beach in Duck, North Carolina located on the Outer Banks barrier islands (Figure 4.1). Each transect was surveyed at five meter increments from the dune to the waterline. Measurements at each station involved moisture content measurements using a handheld moisture gauge calibrated for the effects of seawater, 10 cm push cores for bulk density and grain size analysis and estimates of sediment strength from a portable free-fall penetrometer (PFFP). Over the five day survey period, 120 individual stations were surveyed, with five PFFP deployments, moisture content readings, as well as a push core taken per station. Local morphology was surveyed via terrestrial LiDAR measured throughout the week (blue stars, Figure 4.1). LiDAR scans were collected from two sites: on the dune using a Riegl VZ-1000 LiDAR scanner (left blue star) and on the pier using a Riegl Z390 LiDAR Scanner (right blue star). Scans of the beach are performed at 30min intervals, collected at 7.1 Hz, with a 0.025° angular resolution (O'Dea et al. 2019, US Army Corp of Engineers 2022).

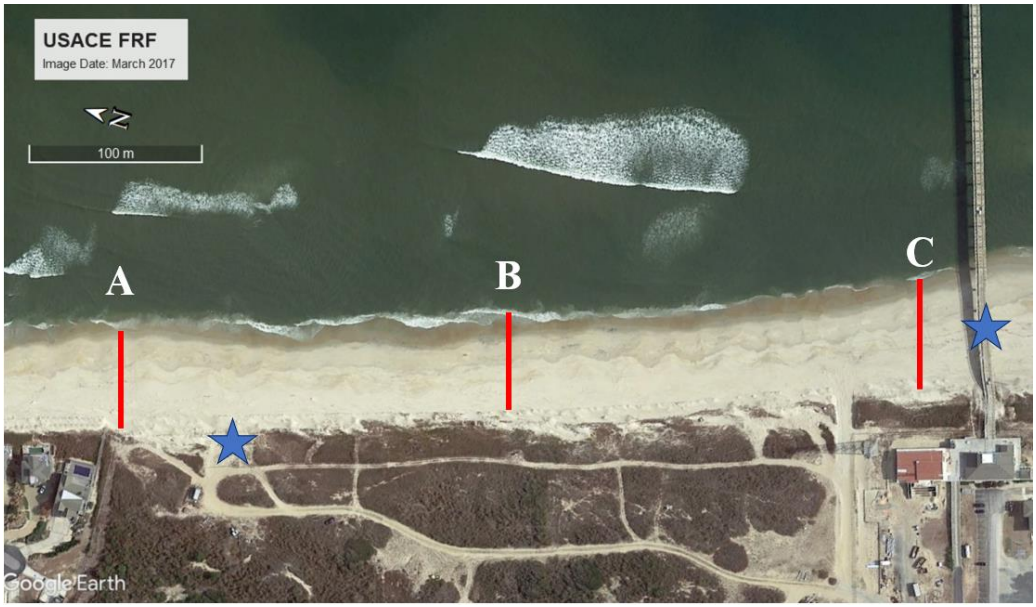

Figure 4.1: Google Earth satellite image of field site in Duck, NC, highlighting the measurement transects A, B, and C. (by Terrametrics; lower right corner: N36°10'54.13" W75°45'7.30")

Characterization of in-situ sediment strength was performed using the PFFP *blueDrop*. The instrument is approximately streamlined in shape, with a length of 63.1 cm and mass of 7.71 kg when equipped with a conical tip. Five onboard vertical accelerometers ranging from $2g$ to $250g$ (where g is gravitational acceleration) measure continuously, along with two horizontal $\pm 55g$ tilt accelerometers. The deceleration of the probe from impact with the sediment until stoppage (dec) is used with the mass of the probe (m) in Newton's second law to obtain a sediment resistance force (F_{soil}), and dividing by the area of the tip (A) gives the dynamic bearing capacity of the soil, q_{dyn} (Equation 4.1):

$$q_{dyn} = \frac{F_{soil}}{A} = \frac{m * dec}{A} \tag{4.1}$$

The deceleration profile can be single and double integrated to obtain velocity and penetration depth, respectively. In emerged environments, the probe is impacting at 2-5 m/s, which is more than 100 times faster than other standard testing methods such as CPT, which penetrate at 2 cm/s. These high strain rates can cause an increase in the measured bearing capacity when compared to results from tests at lower strain rates (Stoll et al. 2007). This effect can be mitigated by introducing a strain-rate correction (f_{sr}) to normalize the results to a constant, slower strain-rate. Equation 4.2 presents the logarithmic form of this equation, often used in submerged sandy environments (Stoll et al. 2007, Stark et al. 2009, Stephan et al. 2015, Albatal et al. 2020):

$$f_{sr} = 1 + K log_{10}\left(\frac{v}{v_{ref}}\right) \tag{4.2}$$

where K is an empirical strain-rate correction factor, v is the dynamic velocity, and v_{ref} is the reference velocity typically taken as 2 cm/s to model a CPT. K is soil dependent, and for submerged sandy environments is typically taken as 0-1.5 (True 1976, Dayal and Allen 1975, Stark et al. 2012, Stephan et al. 2015, Albatal et al. 2020). For emerged beach environments, a recent study by Brilli & Stark (*in review*), found good agreement with theoretically modelled bearing capacity using a velocity-dependent correction factor, $K_{mod} = 0.31 * v_i$, where v_i is the impact velocity in m/s. This modification of K can be used in Equation 2 to give a modified strain rate correction for emerged beach environments (f_{sr-mod}). q_{dyn} is divided by the strain rate correction to give an estimate of the equivalent static strength of the sediment, called the quasi-static bearing capacity ($qsbc$) (Stark et al. 2012), and is given by Equation 4.3 as:

$$qsbc = \frac{q_{dyn}}{f_{sr-mod}} \tag{4.3}$$

The modified strain rate correction will be used in this study, as it is presently the only strain-rate correction tested for PFFP's in emerged, partially saturated environments. An additional metric used in this study for sediment characterization from PFFP measurements is the Firmness Factor (FF), developed by Mulukutla et al. (2011) (Equation 4.4):

$$FF = \frac{a_{max}}{v_i g t_p} \tag{4.4}$$

where a_{max} is the maximum measured acceleration and t_p is the penetration time. This parameter is a proxy for soil stiffness and attempts to normalize the PFFP record for the effects of impact velocity, as the measurement is sensitive to changes in v_i. Firmness factor has been used in conjunction with $qsbc$ to successfully characterize sediment types based on PFFP deployments in submerged environments (Albatal & Stark 2017).

4.3.2. Laboratory Testing

The 10cm push cores were carefully collected at the beach and were processed in the lab to obtain grain size and density information about the samples. Bulk density (ρ_{bulk}) and bulk unit weight (γ_{bulk}) were computed using the mass of sediment and water, and the volume of the tubes (~350 cm^3), given by Equation 4.5:

$$\gamma_{bulk} = g\rho_{bulk} = g\frac{M_T}{V_T} \tag{4.5}$$

where g is gravitational acceleration, M_T is the total mass of sediment and water, and V_T is the total volume of the tube. The sample was then oven dried and weighed to obtain dry density (ρ_d) and dry unit weight (γ_d), computed via Equation 4.6, and converted to void ratio (e) using Equation 4.7:

$$\gamma_d = g\rho_d = g\frac{M_d}{V_T} \tag{4.6}$$

$$e = \frac{V_v}{V_s} = \frac{G_s\gamma_w}{\gamma_d} - 1 \tag{4.7}$$

where M_d is the dry mass of sediment, V_v is the volume of voids, V_s is the volume of solids, G_s is the specific gravity of the sediment taken as 2.65 for the quartz sand at this site, and γ_w is the unit weight of salt water. Once density testing was completed, the remaining dry sample was used to determine grain size statistics, namely the median grain size (d_{50}), via sieve analysis in accordance with the "Standard Test Methods for Particle Size Distribution (Gradation) of Soils Using Sieve Analysis" procedure (ASTM 6913).

Laboratory characterization of erodibility was performed on fifteen 25 cm push cores collected at various stations throughout the week using the Jet Erosion Test (JET) setup at North Carolina State University. The JET was developed as a field and laboratory tool for testing the erosion behavior of cohesive soils (Hanson 1990). The laboratory tests were conducted using the mini-JET device shown in Figure 4.2. The device was connected to a constant pressure head tank fed by a recirculating water system, ultimately creating a submerged jet of water through the mini-JET that impinged vertically on the sediment sample. Pressure head setting ranging between 1.2m and 2m were used in this study. Before testing, the elevation of the soil surface was recorded using the device's point gauge (Figure 4.2). During testing, the jet of water was run for given periods of time to simulate erosion, measuring the scour depth after each period. After three consecutive and approximately equal scour depth measurements, the time period was increased, and the testing procedure was repeated. The time periods used herein were 5s, 15s, 30s, 1min, 2min, and 5min. Testing ended after all time periods were completed.

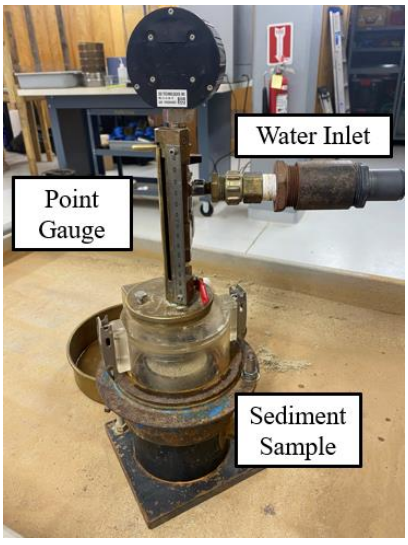

Figure 4.2: Laboratory setup of the Jet Erosion Test

The erodibility parameters that are derived from the JET are the critical shear stress (τ_{cr}) and the erodibility coefficient (k_d). The former characterizes the threshold entrainment force and the latter the detachment rate after the onset of erosion. These parameters are typically obtained by analytically solving the erosion rate equation (Equation 4.8), a linear excess shear model for scour via jet (Hanson and Cook 1997):

$$\frac{dJ}{dt} = k_d \left[\frac{\tau J_p^2}{J^2} - \tau_{cr} \right] \tag{4.8}$$

where J is the measured depth of scour, dJ/dt is the measured erosion rate, τ is the estimated shear stress from the velocity of the water jet, and J_p is the length of the jet core from the nozzle. There are multiple methods for solving this equation to obtain τ_{cr} and k_d (see Hanson and Cook 2004, Simon 2010, Daly et al. 2013, Al-Madhhachi et al. 2013, Wahl 2021). The method selected for the present study was linear regression of the raw erosion rate and shear stress data. This method was selected as it provided the best fit to the data of the four methods tested, the others being the Blaisdell method (Hanson and Cook 2004), the Iterative method (Simon 2010), and the Scour Depth method (Daly et al. 2013). Model performance for each of the methods was quantified using a Normalized Objective Function, suggested by Al-Madhhachi et al. (2013) for JET analysis.

4.3.3. Incipient Motion Modelling

In addition to the laboratory erodibility testing, analytical modelling was conducted to estimate the incipient motion criteria for the field samples under the given hydrodynamic forcing. This was accomplished by modelling the critical Shield's parameter (θ_{cr}), which provides a non-dimensionalization of the critical shear stress (τ_{cr}) for incipient motion (Shields 1936). If the in-situ Shields parameter (θ), which like θ_{cr}, is a non-dimensional shear stress due to the forcing conditions is greater than θ_{cr}, particle motion will occur, and if it is less motion will not occur. It should be noted that the only sediment property included in the estimates presented here is d_{50}. The first estimate of θ_{cr} is from Brownlie (1981), which is an analytical fit to the original Shields (1936) data in terms of the particle Reynolds number (Re_p), and is given by Equations 4.9 & 4.10:

$$\theta_{cr} = 0.22 Re_p^{-0.6} + 0.06\, exp\left(-17.77 Re_p^{-0.6}\right) \tag{4.9}$$

$$Re_p = \frac{\sqrt{(G_s - 1) g d_{50}}\, d_{50}}{\nu} \tag{4.10}$$

where ν is the kinematic viscosity of the fluid. The second estimate is from Soulsby and Whitehouse (1997), which also fits the Shields data with the addition of data points under waves, and mixed wave/current regimes, and is a function of the dimensionless grain size (D_*) (Equations 4.11 & 4.12):

$$\theta_{cr} = \frac{0.3}{1 + 1.2D_*} + 0.055(1 - exp(-0.02D_*)) \tag{4.11}$$

$$D_* = \left[\frac{g(G_s - 1)}{\nu^2}\right]^{\frac{1}{3}} d_{50} \tag{4.12}$$

In order to characterize θ under the in-situ hydrodynamic forcing, a relation by Madsen and Grant (1976) for sediment mobility under waves taking grain roughness into account was chosen to reflect the conditions at the study site. This value is referred to as the grain roughness Shields parameter ($\theta_{2.5}$), considers the grain roughness of a flat bed of sand as $2.5d_{50}$ (Nielsen 1979), and employs a friction factor ($f_{2.5}$) developed by Swart (1974). Formulations for $\theta_{2.5}$ and $f_{2.5}$ are given by Equations 4.13 & 4.14:

$$\theta_{2.5} = \frac{0.5 f_{2.5} (u_b)^2}{(G_s - 1) g d_{50}} \tag{4.13}$$

$$f_{2.5} = exp\left[5.213\left(\frac{2.5d_{50}}{A}\right)^{0.194} - 5.977\right] \tag{4.14}$$

where u_b is the horizontal bottom orbital velocity under waves, and A is the orbital amplitude. Bottom orbital velocities and amplitudes were estimated using linear wave theory via significant wave height (H_s) and peak period (T_p) measurements from an Acoustic Wave and Current (AWAC) buoy located in 4.5 m of water at the study site. It is acknowledged that these velocities contributing to stresses on the bed are computed for a submerged area offshore of the beach environment where the samples were collected. However, this estimate was chosen as a conservative estimate due to difficulties in estimating bed shear stresses under swash and the ability to use data available at the site as direct inputs into the relation (Nielsen 2018).

4.4. Results

Figure 4.3 shows the measured significant wave height from the AWAC buoy over the course of the week (US Army Corp of Engineers 2022). During a storm event on October 11th, significant

wave heights were greater than 2 m, and gradually calmed over the next five days reaching heights of less than 1 m by October 15th (Figure 4.3). Peak period mostly fluctuated between 7-10 seconds with a decreasing trend towards the end of the week.

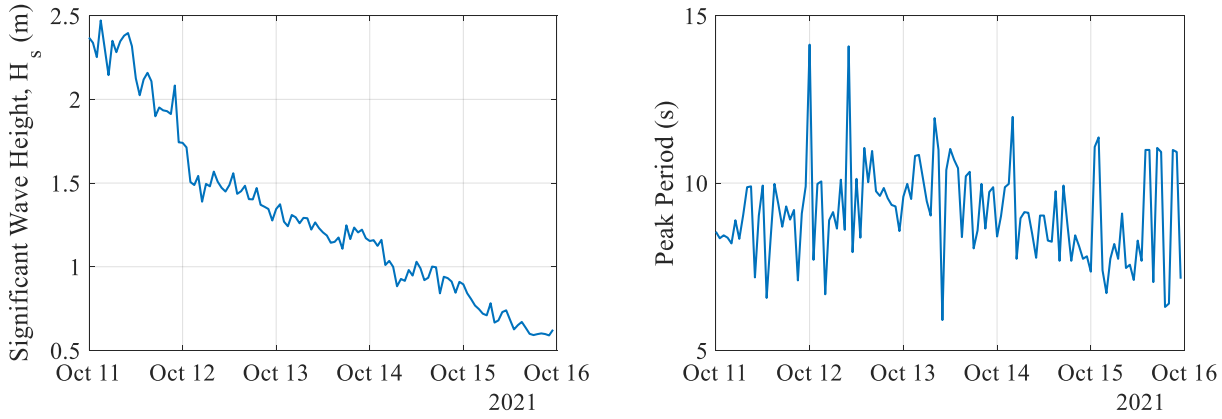

Figure 4.3: Significant wave height (left) and peak period (right) versus time over the course of the survey week.

Figure 4.44, left, depicts a histogram of the sample median grain sizes (d_{50}) for all samples taken over the course of the week. Samples were taken around low tide on all days. A majority of the samples had a d_{50} less than 0.43mm, classifying as a fine sand via ASTM 6913 (Dashed lines, Figure 4.4). Figure 4.4, right, shows the crosshore variation of d_{50}. On the x-axis, zero indicates the dune toe, and the swash zone was located near the 25-30m station depending on the low tide level on a given day. As seen from the figure, d_{50} exhibited little variation in the crosshore until the lower intertidal zone where grain size and variability increased.

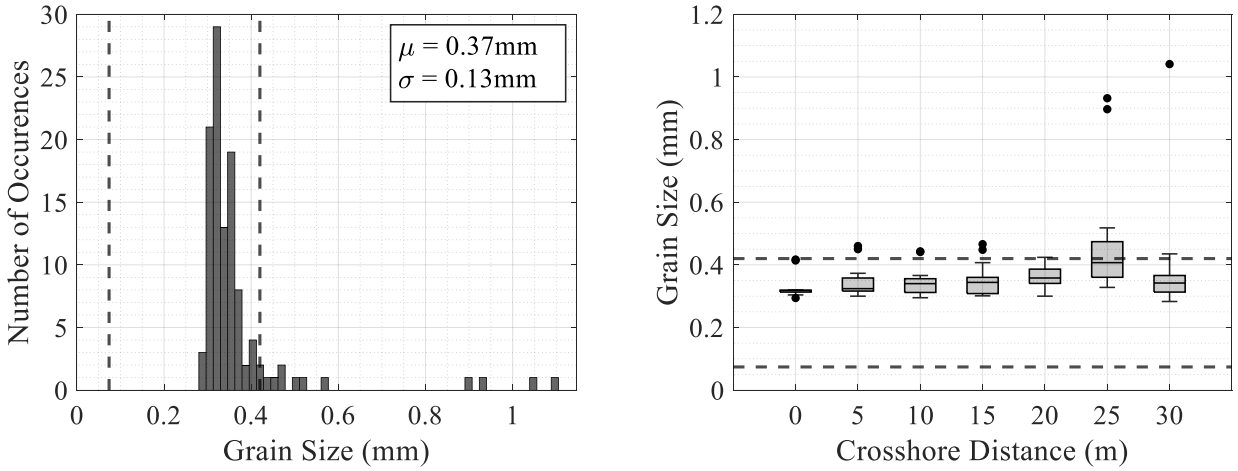

Figure 4.4: Histogram of sample d_{50} (left), and crosshore variation of d_{50} (right).

The results of the theoretical incipient motion modelling are shown in Figure 4.5. Grain sizes from the 120 push cores were used to calculate θ and θ_{cr}. Additionally, wave heights and periods from the time corresponding to each sample were used to estimate the bottom velocities to obtain θ. As seen in Figure 4.5, θ (blue dots) was greater than the critical values for all stations over the course of the survey. This result implies that particle motion would be initiated for every sample under the given forcing. The diamonds represent θ_{cr} from the results of the JET analysis. These data points implied a critical Shield's parameter nearly an order of magnitude greater than the theoretical analysis. Still, only one of the critical values from the JET was above one of the blue dots representing the in-situ forcing.

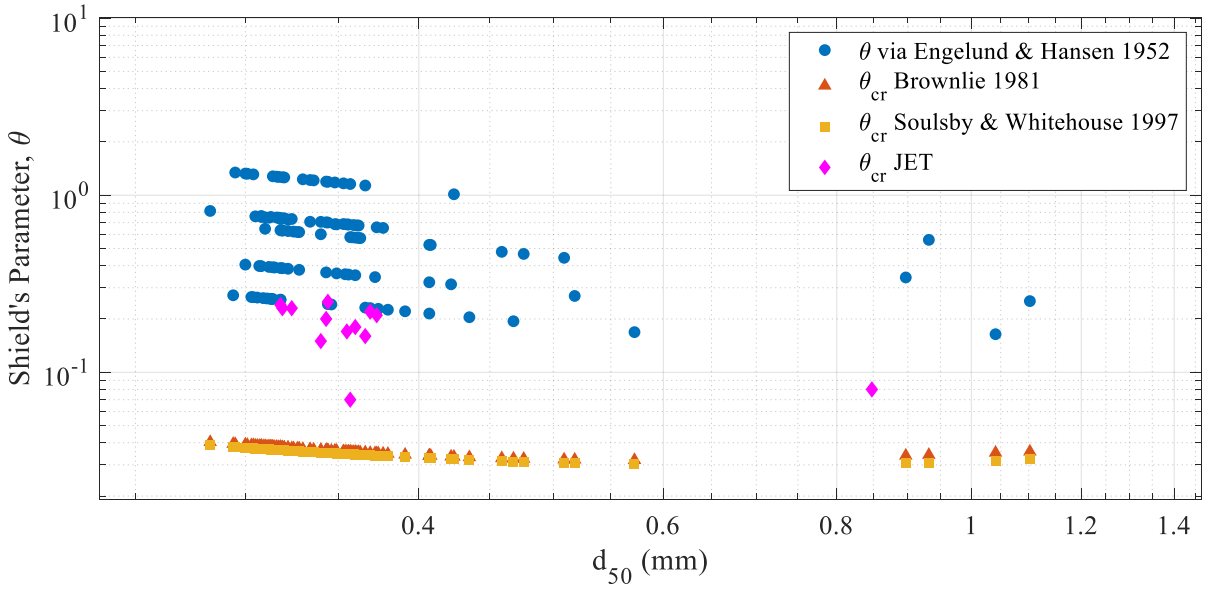

Figure 4.5: Critical Shield's parameter (red and yellow symbols) determined using Brownlie (1981) and Soulsby & Whitehouse (1997), respectively, and in-situ Shield's parameter compared for median grain sizes and wave data collected.

Figure 4.6 shows the relationship between Firmness Factor, $qsbc$, and both void ratio and bulk density. In the plot, the color of each data point differs with the measured moisture content. Firmness Factor (top) and $qsbc$ (bottom) both correlate with each of the two properties through a negative relationship with void ratio and a positive relationship with bulk density. Additionally, samples with higher densities (high bulk unit weight, low e), $qsbc$, and FF consistently had higher water contents, as these denser, stiffer samples were found in and near the swash zone (Figure 4.6).

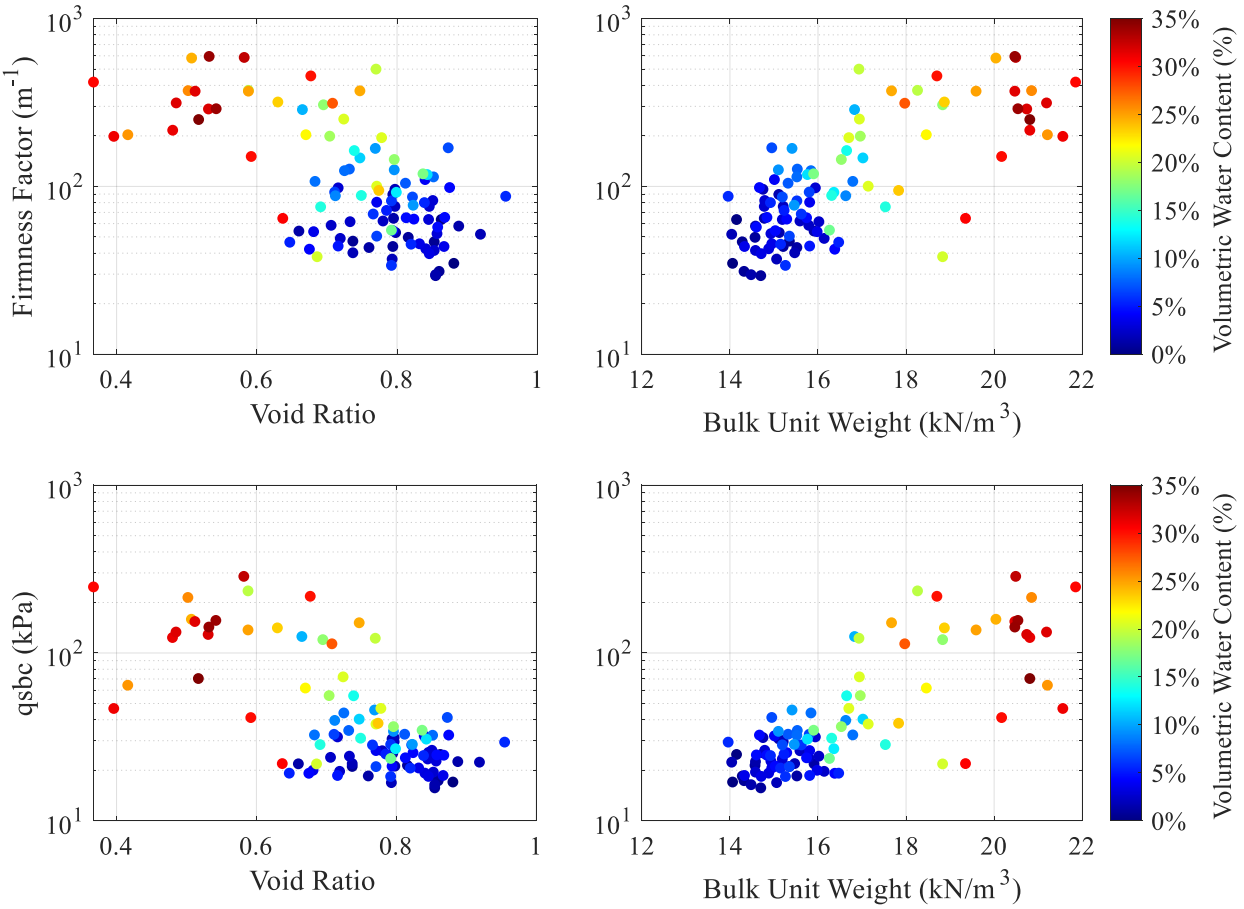

Figure 4.6: Firmness Factor versus void ratio (left) and bulk unit weight (right), with warmer colors of the data points indicating higher moisture content, and vice-versa.

Figure 4.7 displays morphological change over the course of the survey from ground-based LiDAR measurements. For each transect, the four stations closest to the waterline are shown as these were the stations below the high tide line, and thus, were being acted upon by wave energy. The data points show elevation over time for each transect. Transect A experienced deposition on the upper stations (A4 & A5) from October 11th through the 13th, followed by erosion of the seaward stations (A6 & A7) in the later part of the week (Figure 4.7, left). Transect B was relatively stable (bed level changes < 10cm) compared to the other two (bed level changes 20-50cm), but did experience slight deposition, especially on October 15th (Figure 4.7, middle). Transect C experienced erosion of the seaward stations, followed by deposition from October 13th through the 15th (Figure 4.7, right). The variation between transects in close proximity (~200m spacing) could be due to the presence of beach cusps (see Figure 4.1) on the order of 5m in the alongshore direction, and the position of the transect in relation to the cusp. Beach cusps are a common occurrence at this site,

typically forming in the days following storm events, with a mean spacing of 12.4 to 38.8 m (Holland 1998).

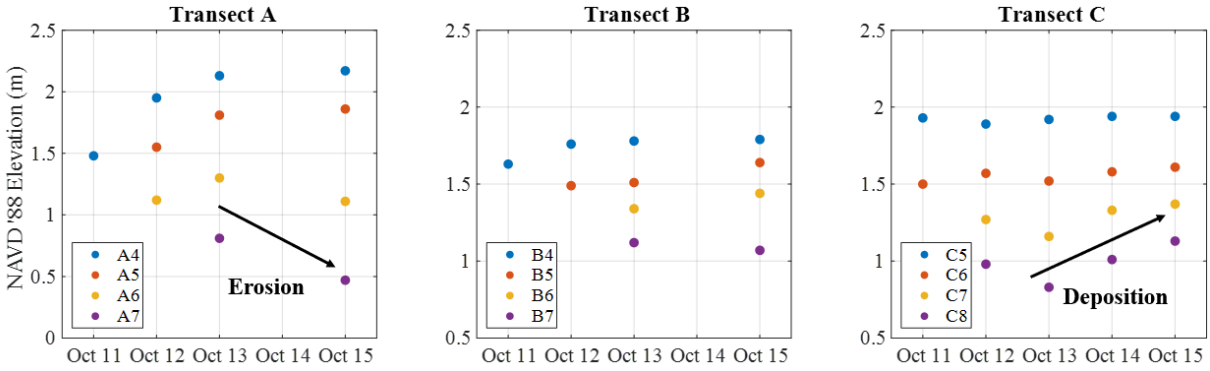

Figure 4.7: Elevation data for intertidal stations over time for Transect A (left), Transect B (middle), and Transect C (right).

Once the general patterns in morphologic change were ascertained, specific stations were selected and general trends in bed-level change (erosion or deposition) were compared to corresponding changes in the measured sediment properties over the same time period (Table 4.1). For stations that experienced deposition, void ratio increased, while $qsbc$, and firmness factor decreased. Trends in sediment properties were less apparent for sites that eroded, with a decrease in void ratio being the only consistent metric. *qsbc* and *FF* increased significantly with erosion at site A6. It should also be noted that there was no observed relationship between the magnitude of changes in sediment properties and the magnitude of elevation change (Table 4.1).

Table 4.1: Changes in sediment properties compared to trends in bed-level for select stations.

Station	**Period**	**Trend**	**ΔElevation (cm)**	**Δe**	**Δ$qsbc$**	**ΔFF**
A4	10/11-10/13	Deposition	+64	3%	-29%	-33%
C6	10/13-10/15	Deposition	+10	40%	-75%	-66%
C7	10/13-10/15	Deposition	+21	79%	-48%	-53%
A6	10/13-10/15	Erosion	-19	-18%	473%	300%
C7	10/12-10/13	Erosion	-11	-32%	-84%	-66%

Figure 4.8 depicts changes in void ratio, with corresponding erosion/depositional behavior for all sites where LiDAR and sediment property measurements were available consistently over the course of the survey (28 sites). The x-axis is the initial void ratio, and the y-axis shows the percent change in void ratio over a 24-hour period between surveys. The two colors separate the data into sites that experienced erosion (orange) and sites that experienced deposition (blue) over the same

time period. Of the selected sites, 22 were depositional and 6 were erosional. 14 of the depositional sites had an increase in void ratio (loosening) and 8 had a decrease in void ratio (densification). All 8 of the depositional sites that showed a decrease in e had initial void ratios greater than the maximum dry void ratio (Figure 4.8, black dashed line), meaning that the very loose soil structure was being held together by partial saturation. Additionally, all the densification was small in magnitude, all less than 15% changes. Of the six erosional sites, 4 showed an increase in e, and two showed a decrease. A similar analysis was conducted using FF and $qsbc$, but no discernable trends were observed in the data. Finally, e, γ_{bulk}, FF, and $qsbc$ were compared to the detachment rate coefficient, k_d, from the JET experiments (Figure 4.9).

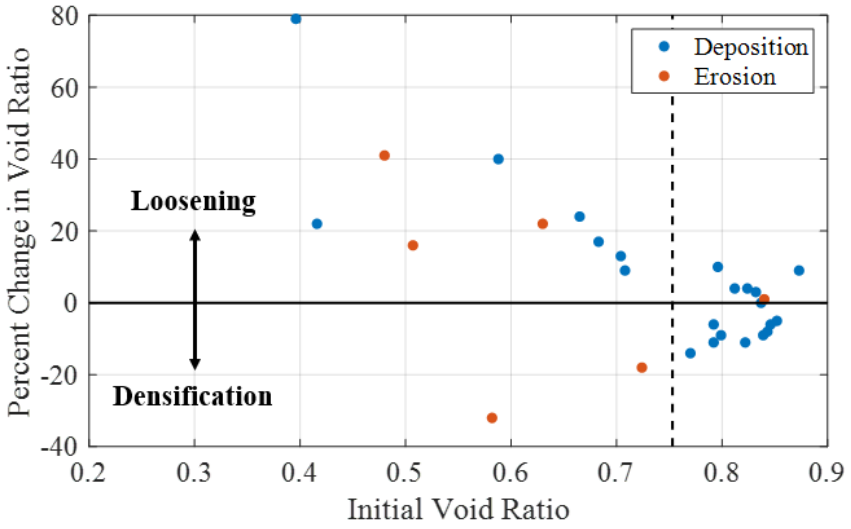

Figure 4.8: Changes in void ratio from initial condition separated by erosion/deposition behavior. The x-axis shows the initial void ratio, points above zero are increasing void ratio or loosening, and points below zero on the y-axis are decreasing void ratio or densification.

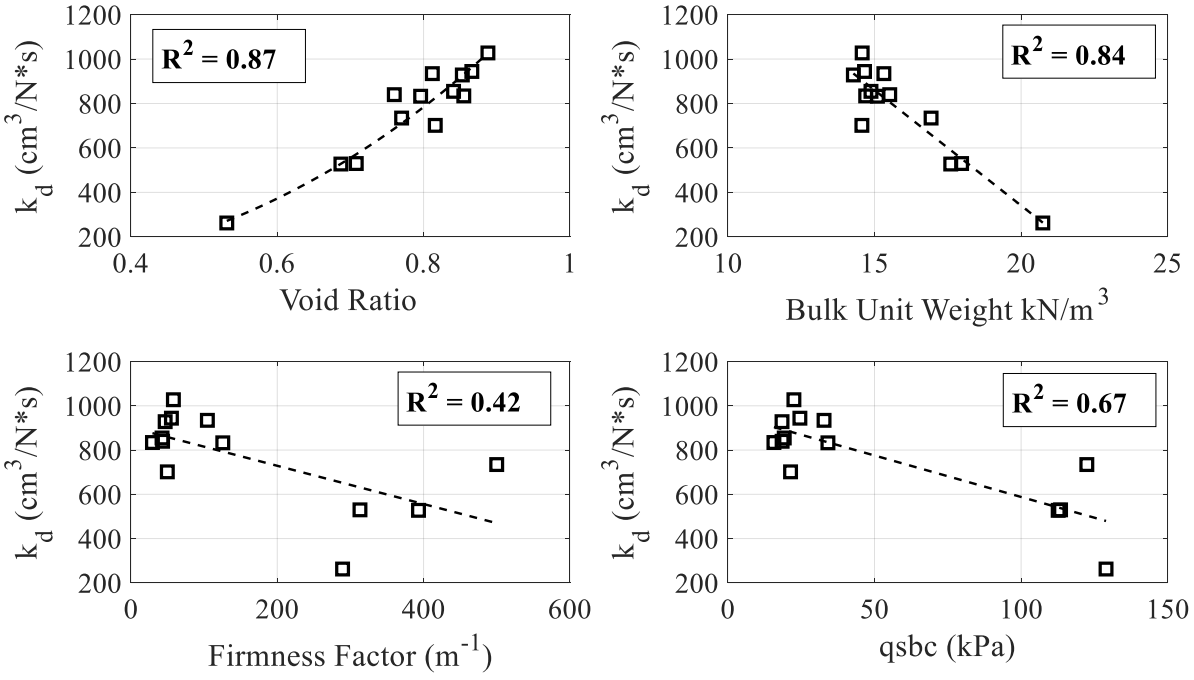

Figure 4.9: Detachment rate coefficient from the JET versus void ratio (top left), bulk unit weight (top right), firmness factor (bottom left), and qsbc (bottom right).

For the directly measured sediment properties, increasing void ratio and decreasing bulk unit weight correlated well with increasing k_d (Figure 4.9, top). Both properties were similarly well-correlated with k_d, with $R^2 = 0.87$ for e and $R^2 = 0.84$ for γ_{bulk}. Penetrometer measurements, FF and $qsbc$, were both negatively correlated with k_d (Figure 4.9, bottom). Although these relationships are less well-defined than the sediment properties, $qsbc$ provided a stronger correlation than FF, with $R^2 = 0.67$ and $R^2 = 0.43$, respectively. These four properties were also compared to τ_c from the JET experiments, but no significant correlation was observed.

4.5. Discussion

The modelled values of θ_{cr} and $\theta_{2.5}$ suggested that motion would be initiated under the hydrodynamic forcing for all stations sampled (Figure 4.5). θ_{cr} from the JET was nearly an order of magnitude higher than the other two grain size-based methods, representing an upper bound solution for θ_{cr}, but still predicted motion for all samples but one. This result is consistent with theory and the observations, as sand is the easiest particle size to move on the Shields curve, and geomorphological change was observed throughout the survey period (Shields 1936). Having the estimates of θ_{cr} from the JET is a useful addition to the analysis, as this test method is capturing

the in-situ properties and variability in each physical sample more thoroughly than grain size based estimates. As mentioned previously, $\theta_{2.5}$ is an estimate of the Shields parameter based on wave data from 4.5 m water depth, and likely does not reflect the true shear stresses on the bed under breaking waves and swash. The methodology for estimating θ in-situ is likely conservative, as the Madsen and Grant (1976) formulation is a more conservative estimate than the general form of Shields by an order of magnitude. This implies that the blue dots in Figure 4.5 should be higher and thus further in magnitude from the estimates of θ_{cr}. Additionally, swash bore velocities have been observed to travel at up to 3 m/s, higher than the maximum measured orbital velocity of 1.5 m/s (Nielsen 1992, Puleo et al. 2000), which would serve to further increase θ. It can be concluded that the presented methodology provides a conservative estimate of general initiation of motion, and thus, sediment mobility at this sandy beach. However, it provides little information on the actual geomorphodynamics since erosion, deposition, and fairly unchanged conditions have been observed at the different locations throughout the short survey period.

Based on the trends in Figure 4.7, five stations were selected as an initial analysis to determine relationships between sediment properties, sediment strength, and observed bed level change (Table 4.1). The only property to show consistent trends with erosion/deposition was packing state, quantified by void ratio in this case. It should be noted that the erosion seen at site C7 did not correlate with an increase in strength as with A6 (Table 4.1). This is likely due to pore pressure induced variations in sediment strength associated with swash processes on a wave-by-wave basis (Turner and Nielsen 1997). Void ratio is just one way to describe the packing state of sediment, and it should be mentioned that porosity, density, and unit weight can all be assumed to be related to geomorphological change as they are directly related to void ratio. At stations where deposition was observed, void ratio increased, and where erosion was observed, void ratio decreased. Figure 4.8 confirms this trend for depositional areas. 14 out of 22 stations that saw deposition also saw a corresponding increase in void ratio (loosening) over the same time period. The remaining 8 stations that saw a decrease in void ratio (densification), but all of those locations had initial void ratios greater than the maximum dry density (Figure 4.8, dashed line), and decreases in void ratio less than 15%. These sites where the initial packing state could be described as “very loose” due to the effects of partial saturation saw both increases and decreases in void ratio despite all having deposition. However, since the changes in void ratio were small (less than 15%), this result implies that the sediment would still be considered “loose” even after a small

amount of densification. Therefore, there would likely be only small changes to the erodibility, which is tied to the packing state (Figure 4.9). There were only six available stations that saw erosion, and there was no clear trend in the data. Still, it is hypothesized that as deposition is tied to increases in e, erosion is tied to decreases in e. This result is consistent with Heathershaw (1981), who observed an inverse relationship between packing state and bed-level change, with denser sediment (lower e) being correlated with decreases in bed-level. Additionally, Dean and Dalrymple (2004) noted that repeated swash and backwash cycles could reduce porosity and leave behind less erodible sediment. Packing state parameters were also related to k_d from the JET. Figure 4.9 shows clear relationships between the detachment rate coefficient, k_d, and void ratio/bulk unit weight (Figure 4.9, top). Additionally, k_d had a negative correlation with FF and $qsbc$, albeit a weaker relationship than with the sediment properties. Lower k_d indicates less erodible sediment (in terms of erosion rate), and higher k_d indicates more erodible sediment (Hanson 1991). Denser, stronger sediments are less erodible than looser, weaker sediments (Figure 4.9). While this is intuitively and theoretically expected, this relationship may offer a quantitative measure how erodibility is affected by packing state and sediment strength. It should be noted, the value of k_d is dependent on the chosen solution methodology, in this case a linear regression of the erosion rate vs. shear stress data, which is supported by the results of Wahl (2021). The outputs of this model will be used for comparison amongst results at the study site, and not in-relation to the magnitude of erodibility parameters in comparison to other sediments. While thus study was conducted over a narrow range of grain sizes and packing states, specifically for beach sands, the results highlight the variability in erodibility present even over a small range of properties, which is often overlooked in studies relating soil properties over a larger range of soil types (see National Academy of Science and Engineering 2019). The results show that there are relationships between geotechnical sediment properties, local morphodynamics, and erodibility, and support the hypothesis that these properties should be included in future models of beach evolution.

Figure 4.10 summarizes the relationships described in the previous section with relation to time before or after morphological change. At a given location, before any change is induced by hydrodynamic forcing, the packing state affects the erodibility, with denser sediments being less erodible than looser sediments. When a forcing event occurs, less sediment will be mobilized in denser areas than in looser areas. The subsequent effect on sediment dynamics and beach morphodynamics will depend on the strength of the forcing (i.e., wave heights, tide range,

currents), the existing morphology, and swash and backwash processes (Dean and Dalrymple 2004). Once morphologic change has occurred, areas experiencing deposition will typically see increases in void ratio, leaving behind looser, more erodible sediment. Some sites that are "very loose" as an initial condition ($e > e_{max}$) may see slight decreases in void ratio, but these changes will be small in magnitude, and thus have a small effect on erodibility. It is hypothesized that erosional areas will see densification and decreases in erodibility, which is supported by literature, but needs more field data for full validation in this context. This may suggest feedback loops between geomorphological change (erosion vs. deposition) and changes in surficial sand density (densification vs. loosening) that could be interrupted and lead to exacerbated responses by extreme hydrodynamic events.

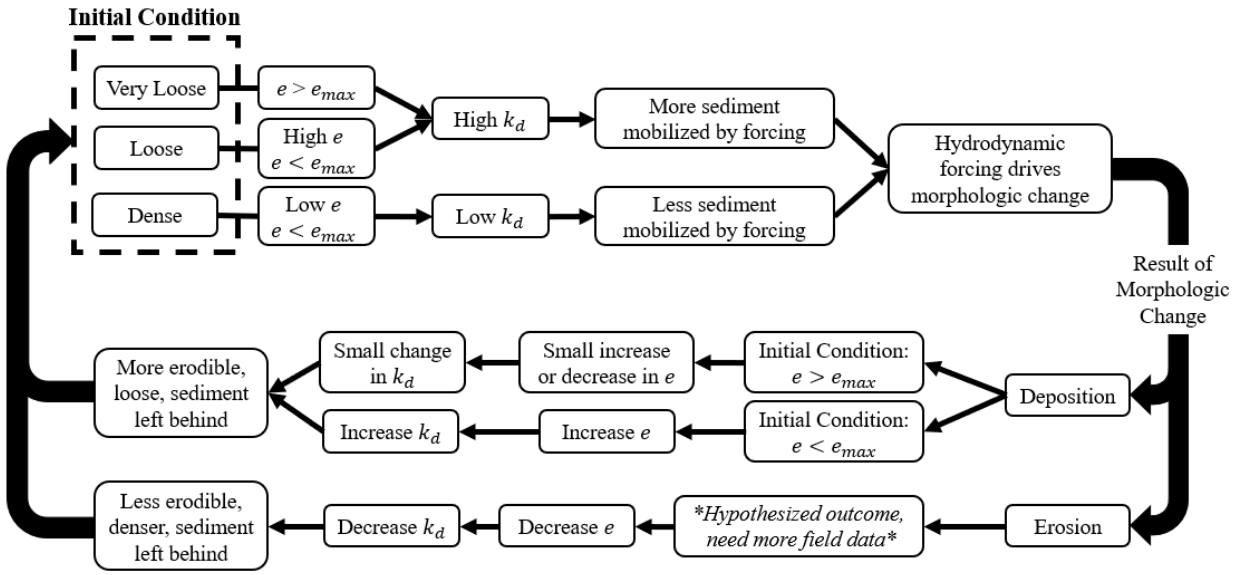

Figure 4.10: Summary flow chart of the relationships between packing state, erodibility, and sediment dynamics before and after morphological change.

Figure 4.9 shows a weaker relationship between FF and k_d, with the trend showing a tendency for lower FF (within the sandy sediments) to indicate less erodible sediment, and vice-versa. This result can be understood more clearly when considered in the context of Figure 4.6. In Figure 4.6, it can be seen that there is a clear relationship between FF,$qsbc$, e, and γ_{bulk}, with the general trend being increasing density with increasing FF and $qsbc$. However, there is significant spread in the data. As seen from the color gradient, the result is also highly sensitive to changes in water content, with an increase in water content corresponding to an increase in FF and $qsbc$. However, this is likely due to increasing water content causing increased viscous effects due to high-strain

rate, artificially increasing a_{max} (Martin et al. 2009). The modified strain rate factor (Equation 4.3) represents a first step towards accounting for these effects, but the relationship breaks down at water contents greater than 25% by volume, which could explain why spread in the data was greater at these high water contents (Figure 4.6, bottom).. Improvements in understanding partially saturated strain-rate effects on PFFP measurements, specifically at high water contents, could help reduce the spread in these data. If packing state metrics of beach sands can be quantitively obtained from PFFP measurements, it would follow that PFFP data would be related to erodibility and morphodynamics as discussed previously in this section.

4.6. Conclusions

The goal of this study was to measure geotechnical sediment properties in a sandy intertidal beach environment, and investigate the relationships between those properties, erodibility, and local geomorphodynamics. These relationships were tested using a field dataset collected at the USACE FRF in Duck, North Carolina, in October 2021 and JET erosion testing of obtained soil samples. Measurements included moisture content, grain size, density, and sediment strength via PFFP deployments. Morphological change was recorded from terrestrial LiDAR and hydrodynamics were measured using an offshore AWAC buoy. Theoretical sediment mobility modelling and laboratory erodibility testing were also performed. It should be highlighted that variations in sediment properties were tested within mostly one sediment type, fine sand with d_{50} ranging from 0.3 to 0.43 mm, and bulk densities and void ratios ranging from 14 kN/m^3 to 22 kN/m^3 and from 0.39 to 0.96, respectively, exploring small-scale variations in packing state and associated strength and relationship with erodibility and geomorphodynamic change. Key takeaways are listed below:

- A Shield's approach using just grain size showed sediment mobility for all stations, but was too simplistic for the limited range in sediments to provide further information on geomorphodynamics which ranged from erosion over little change to deposition.
- Void ratio was positively correlated with detachment coefficient, k_d, from the JET, indicating that denser sediments are less erodible than looser sediments. Thus, the packing state correlated to the amount of sediment that is mobilized by hydrodynamic forcing with denser areas mobilizing less sediment and vice-versa.
- Void ratio increased and bulk density and strength decreased with sediment deposition. While there was less of an apparent trend for erosional areas, it is hypothesized that erosion

leads to decreases in void ratio. More field data and better consideration of swash processes is needed to validate this.

- Portable free fall penetrometer sediment strength estimates related to bulk unit weight, void ratio, and water content. There was significant spread in the data, which could be mitigated by focusing future work on understanding strain-rate behavior in partially saturated emerged environments with particular emphasis on zones of high water content.

Overall, the results show that sediment properties, namely packing state in the form of void ratio changes with geomorphodynamics and affects sediment erodibility.

4.7. Acknowledgements

The authors would like to thank Julie Paprocki, Matthew Florence, Saurav Shrestha, Jonathan Moore, and the scientists and staff at the USACE FRF for their support in data collection efforts. These data were collected as part of the During Nearshore Event Experiment (DUNEX), which was facilitated by the U.S. Coastal Research Program (USCRP). We thank USCRP for their support of this effort through funding for logistics and coordination. This material is based upon work supported by the National Science Foundation under Grant CMMI-1751463. Any opinions, findings, and conclusions or recommendations expressed in this material are those of the author(s) and do not necessarily reflect the views of the National Science Foundation.

References

Akal, T., & Stoll, R. D. (1995). Expendable penetrometer for rapid assessment of seafloor parameters. Oceans Conference Record (IEEE), 3. https://doi.org/10.1109/oceans.1995.528858

Albatal, A., & Stark, N. (2017). Rapid sediment mapping and in situ geotechnical characterization in challenging aquatic areas. Limnology and Oceanography: Methods, 15(8). https://doi.org/10.1002/lom3.10192

Albatal, A., Stark, N., & Castellanos, B. (2020). Estimating in situ relative density and friction angle of nearshore sand from portable free-fall penetrometer tests. Canadian Geotechnical Journal, 57(1). https://doi.org/10.1139/cgj-2018-0267

Albatal, A., Wadman, H., Stark, N., Bilici, C., & McNinch, J. (2019). Investigation of spatial and short-term temporal nearshore sandy sediment strength using a portable free fall penetrometer. Coastal Engineering, 143. https://doi.org/10.1016/j.coastaleng.2018.10.013

Al-Madhhachi, A. T., Hanson, G. J., Fox, G. A., Tyagi, A. K., & Bulut, R. (2013). Measuring soil erodibility using a laboratory "mini" jet. Transactions of the ASABE, 56(3). https://doi.org/10.13031/trans.56.9742

American society for testing and materials ASTM. (2017). Standard Test Methods for Particle-Size Distribution (Gradation) of Soils Using Sieve Analysis (D6913 / D6913M-17). ASTM International, 04(Reapproved 2009).

Bender, F. A. M., Ekman, A. M. L., & Rodhe, H. (2010). Response to the eruption of Mount Pinatubo in relation to climate sensitivity in the CMIP3 models. Climate Dynamics, 35(5). https://doi.org/10.1007/s00382-010-0777-3

Bender, M. A., Knutson, T. R., Tuleya, R. E., Sirutis, J. J., Vecchi, G. A., Garner, S. T., & Held, I. M. (2010). Modeled impact of anthropogenic warming on the frequency of intense Atlantic hurricanes. Science, 327(5964). https://doi.org/10.1126/science.1180568

Briaud, J. L., Ting, F. C. K., Chen, H. C., Cao, Y., Han, S. W., & Kwak, K. W. (2001). Erosion Function Apparatus for Scour Rate Predictions. Journal of Geotechnical and Geoenvironmental Engineering, 127(2). https://doi.org/10.1061/(asce)1090-0241(2001)127:2(105)

Briaud, J.-L. (2013). Geotechnical Engineering: Unsaturated and Saturated Soils. John Wiley & Sons.

Brilli, N. C., & Stark, N. (2020). Variations in Sediment Strength across a Sandy Peninsula. Proceedings of Geo-Congress 2020, Minneapolis, Minnesota, 769–788. https://doi.org/10.1061/9780784482810.080

Brownlie, W. B. (1981). Prediction of Flow Depth and Sediment Discharge in Open Channels. California Institute of Technology, W. M. Keck Laboratory of Hydraulics and Water Resources, Report, KH-R-43A.

Cao, Z., Day, R., & Egashira, S. (2002). Coupled and Decoupled Numerical Modeling of Flow and Morphological Evolution in Alluvial Rivers. Journal of Hydraulic Engineering, 128(3). https://doi.org/10.1061/(asce)0733-9429(2002)128:3(306)

Chow, S. H., Bienen, B., & Randolph, M. F. (2018). Rapid penetration of piezocones in sand. Cone Penetration Testing 2018 - Proceedings of the 4th International Symposium on Cone Penetration Testing, CPT 2018.

Dalrymple, R. A. (1992). Prediction of Storm/Normal Beach Profiles. Journal of Waterway, Port, Coastal, and Ocean Engineering, 118(2). https://doi.org/10.1061/(asce)0733-950x(1992)118:2(193)

Daly, E. R., Fox, G. A., Al-Madhhachi, A. T., & Miller, R. B. (2013). A scour depth approach for deriving erodibility parameters from jet erosion tests. Transactions of the ASABE, 56(6). https://doi.org/10.13031/trans.56.10350

Davidson-Arnott, R. G., MacQuarrie, K., & Aagaard, T. (2005). The effect of wind gusts, moisture content and fetch length on sand transport on a beach. Geomorphology, 68(1–2). https://doi.org/10.1016/j.geomorph.2004.04.008

Dayal, U., & Allen, J. H. (1973). Instrumented Impact Cone Penetrometer. Canadian Geotechnical Journal, 10(3). https://doi.org/10.1139/t73-034

Dayal, U., Allen, J. H., & Jones, J. M. (1975). Use of an impact penetrometer for the evaluation of the in-situ strength of marine sediments. Marine Geotechnology, 1(2). https://doi.org/10.1080/10641197509388155

Dean, R. G., & Dalrymple, R. A. (2004). Coastal Processes with Engineering Applications. In Coastal Processes with Engineering Applications. https://doi.org/10.1017/cbo9780511754500

Erikson, L. H., Larson, M., & Hanson, H. (2007). Laboratory investigation of beach scarp and dune recession due to notching and subsequent failure. Marine Geology, 245(1–4). https://doi.org/10.1016/j.margeo.2007.04.006

Hanson, G. J. (1990). Surface erodibility of earthen channels at high stresses. Part II - Developing an in situ testing device. Transactions of the American Society of Agricultural Engineers, 33(1). https://doi.org/10.13031/2013.31306

Hanson, G. J. (1991). Development of a jet index to characterize erosion resistance of soils in earthen spillways. Transactions of the American Society of Agricultural Engineers, 34(5). https://doi.org/10.13031/2013.31831

Hanson, G. J., & Cook, K. R. (1997). Development of excess shear stress parameters for circular jet testing. Paper - American Society of Agricultural Engineers, 2.

Hanson, G. J., & Cook, K. R. (2004). Apparatus, test procedures, and analytical methods to measure soil erodibility in situ. Applied Engineering in Agriculture, 20(4).

Heathershaw, A. D., Carr, A. P., Blackley, M. W. L., & Wooldridge, C. F. (1981). Tidal variations in the compaction of beach sediments. Marine Geology, 41(3–4). https://doi.org/10.1016/0025-3227(81)90082-7

Holland, K. T. 1998. "Beach cusp formation and spacings at Duck, United States." Continental Shelf Research, 18 (10). https://doi.org/10.1016/S0278-4343(98)00024-7.

Jones, B. M., Hinkel, K. M., Arp, C. D., & Eisner, W. R. 2008. "Modern erosion rates and loss of coastal features and sites, Beaufort Sea coastline, Alaska." Arctic, 61 (4). https://doi.org/10.14430/arctic44

Kiptoo, D., Stark, N., Massey, G., Wright, C., & Friedrichs, C. T. (2020). Strain Rate Effects in Soft Estuarine Soils using Portable Free Fall Penetrometers. Proceedings of Ocean Science Meeting, San Diego, California.

Knutson, T. R., McBride, J. L., Chan, J., Emanuel, K., Holland, G., Landsea, C., Held, I., Kossin, J. P., Srivastava, A. K., & Sugi, M. (2010). Tropical cyclones and climate change. In Nature Geoscience (Vol. 3, Issue 3). https://doi.org/10.1038/ngeo779

Lucking, G., Stark, N., Lippmann, T., & Smyth, S. (2017). Variability of in situ sediment strength and pore pressure behavior of tidal estuary surface sediments. Geo-Marine Letters, 37(5). https://doi.org/10.1007/s00367-017-0494-6

Madsen, O. S., & Grant, W. D. (1976). Sediment Transport in the Coastal Environment. MIT Dep Civ Eng Ralph M, Parsons Lab Water Resource Hydrodyn Rep, 209.

Martin, B. E., Chen, W., Song, B., & Akers, S. A. (2009). Moisture effects on the high strain-rate behavior of sand. Mechanics of Materials, 41(6). https://doi.org/10.1016/j.mechmat.2009.01.014

Masselink, G., Kroon, A., & Davidson-Arnott, R. G. D. (2006). Morphodynamics of intertidal bars in wave-dominated coastal settings - A review. Geomorphology, 73(1–2). https://doi.org/10.1016/j.geomorph.2005.06.007

Masselink, G., & Short, A. D. (1993). The effect of tide range on beach morphodynamics and morphology: a conceptual beach model. Journal of Coastal Research, 9(3).

Mulukutla, G. K., Huff, L. C., Melton, J. S., Baldwin, K. C., & Mayer, L. A. (2011). Sediment identification using free fall penetrometer acceleration-time histories. Marine Geophysical Research, 32(3). https://doi.org/10.1007/s11001-011-9116-2

National Academy of Sciences Engineering and Medicine. 2019. *Relationship Between Erodibility and Properties of Soils*. Washington, D.C.: The National Academic Press.

Nielsen, P. (1979). Some basic concepts of wave sediment transport. Technical University of Denmark, Lyngby, Institute of Hydrodynamics and Hydraulic Engineering Series Paper, 20.

Nielsen, P. (1992). Coastal Bottom Boundary Layers and Sediment Transport. World Scientific Publishing, Advanced Series on Ocean Engineering.

Nielsen, P. (2018). Bed shear stress, surface shape and velocity field near the tips of dam-breaks, tsunami and wave runup. Coastal Engineering, 138. https://doi.org/10.1016/j.coastaleng.2018.04.020

Puleo, J. A., Beach, R. A., Holman, R. A., & Allen, J. S. (2000). Swash zone sediment suspension and transport and the importance of bore-generated turbulence. Journal of Geophysical Research: Oceans, 105(C7), 17021–17044. https://doi.org/10.1029/2000jc900024

Reeve, B., Stark, N., & Mewis, P. (2018). Cross-shore variation in sediment strength at a sandy beach. Coastal Engineering Proceedings, 36. https://doi.org/10.9753/icce.v36.sediment.83

Sallenger, J. (2000). Storm impact scale for barrier islands. Journal of Coastal Research, 16(3).

Sassa, S., & Watabe, Y. (2007). Role of suction dynamics in evolution of intertidal sandy flats: Field evidence, experiments, and theoretical model. Journal of Geophysical Research: Earth Surface, 112(1). https://doi.org/10.1029/2006JF000575

Shafii, I., Briaud, J. L., Chen, H. C., & Shidlovskaya, A. (2016). Relationship between soil erodibility and engineering properties. Scour and Erosion - Proceedings of the 8th International Conference on Scour and Erosion, ICSE 2016. https://doi.org/10.1201/9781315375045-134

Shields, I. A. (1936). Anwendung der Aehnlichkeitsmechanik und der Turbulenzforschung auf die Geschiebebewegung. [English title: Application of similarity principles and turbulence research to bed-load movement]. Preussische Versuchsanstalt Für Wasserbau Und Schiffbau, 26.

Simon, A., Thomas, R. E., & Research Associate, P. (2010). Comparison and Experiences with Field Techniques to Measure Critical Shear Stress and Erodibility of Cohesive Deposits. 2nd Joint Federal Interagency Conference.

Soulsby, R. L., & Whitehouse, R. J. S. (1997). Threshold of sediment motion in coastal environments. Proceedings Pacific Coasts and Ports 1997 Conference, 1(c).

Stark, N., Coco, G., Bryan, K. R., & Kopf, A. (2012). In-situ geotechnical characterization of mixed-grain-size bedforms using a dynamic penetrometer. Journal of Sedimentary Research, 82(7). https://doi.org/10.2110/jsr.2012.45

Stark, N., Hay, A. E., & Trowse, G. (2014). Cost-effective geotechnical and sedimentological early site assessment for ocean renewable energies. 2014 Oceans - St. John's, OCEANS 2014. https://doi.org/10.1109/OCEANS.2014.7003004

Stark, N., & Kopf, A. (2011). Detection and quantification of sediment remobilization processes using a dynamic penetrometer. OCEANS'11 - MTS/IEEE Kona, Program Book. https://doi.org/10.23919/oceans.2011.6106914

Stark, N., Kopf, A., Hanff, H., Stegmann, S., & Wilkens, R. (2009). Geotechnical investigations of sandy seafloors using dynamic penetrometers. MTS/IEEE Biloxi - Marine Technology for Our Future: Global and Local Challenges, OCEANS 2009. https://doi.org/10.23919/oceans.2009.5422460

Stark, N., McNinch, J., Wadman, H., Graber, H. C., Albatal, A., & Mallas, P. A. (2017). Friction angles at sandy beaches from remote imagery. Geotechnique Letters, 7(4). https://doi.org/10.1680/jgele.17.00053

Stark, N., Radosavljevic, B., Quinn, B., & Lantuit, H. (2017). Application of portable free-fall penetrometer for geotechnical investigation of arctic nearshore zone. Canadian Geotechnical Journal, 54(1). https://doi.org/10.1139/cgj-2016-0087

Stephan, S., Kaul, N., & Villinger, H. (2015). Validation of impact penetrometer data by cone penetration testing and shallow seismic data within the regional geology of the Southern North Sea. Geo-Marine Letters, 35(3). https://doi.org/10.1007/s00367-015-0401-y

Stoll, R. D., & Akal, T. (1999). XBP - Tool for rapid assessment of seabed sediment properties: Instrumented with accelerometers, new expendable probes measure the impact signature of the ocean bottom. In Sea Technology (Vol. 40, Issue 2).

Stoll, R. D., Sun, Y. F., & Bitte, I. (2007). Seafloor properties from penetrometer tests. IEEE Journal of Oceanic Engineering, 32(1). https://doi.org/10.1109/JOE.2007.890943

Swart, D. H. (1974). Offshore Sediment Transport and Equilibrium Beach Profiles. Delft Hydraulics Laboratory Publication No. 131.

True, D. G. (1976). Undrained vertical penetration into ocean bottom soils [Ph.D Dissertation]. University of California-Berkeley.

Turner, I. L., and P. Nielsen. 1997. “Rapid water table fluctuations within the beach face: Implications for swash zone sediment mobility?” Coastal Engineering, 32 (1). https://doi.org/10.1016/s0378-3839(97)00015-x.

US Army Corp of Engineers. 2022. “FRF Data.” Coastal Hydraulics Lab (CHL) Data Server. Accessed October 22, 2022. https://chldata.erdc.dren.mil/thredds/catalog/frf/catalog.html

Wahl, T. L. (2021). Methods for analyzing submerged jet erosion test data to model scour of cohesive soils. Transactions of the ASABE, 64(3). https://doi.org/10.13031/TRANS.14212

Wardinski, K. M., Guertault, L., Fox, G. A., & Castro-Bolinaga, C. F. (2018). Suitability of a Linear Model for Predicting Cohesive Soil Detachment during Jet Erosion Tests. Journal of Hydrologic Engineering, 23(9). https://doi.org/10.1061/(asce)he.1943-5584.0001690

Zambrano-Cruzatty, L., Yerro, A., & Stark, N. (2019). Influence of Shear Strength and Moisture Content on Aeolian Sand Erosion. Proceedings of Geo-Congress 2019, Philadelphia, Pennsylvania. https://doi.org/10.1061/9780784482155.001

Zhang, K., Douglas, B. C., & Leatherman, S. P. (2004). Global warming and coastal erosion. Climatic Change, 64(1–2). https://doi.org/10.1023/B:CLIM.0000024690.32682.48

Chapter 5: Assessing Variations in Sediment Properties and Erodibility in Harrison Bay, Alaska using a Portable Free-Fall Penetrometer

The contributions of the authors to the composition of this manuscript are delineated as follows:

Nicola Brilli:
- Participated in the field survey in Harrison Bay, Alaska
- Conducted all laboratory analysis of gravity core samples
- Performed literature review; processed and analyzed field data; prepared figures, tables, and draft of manuscript
- Revised manuscript based on suggestions of co-authors

Nina Stark:
- Co-primary investigator of this study
- Initiated research idea and co-developed the refined research questions
- Planned and participated in the field survey in Harrison Bay, Alaska
- Reviewed and edited the draft manuscript

Emily Eidam:
- Co-primary investigator of this study
- Initiated research idea and co-developed the refined research questions
- Planned, supervised, and participated in the field survey in Harrison Bay, Alaska serving as Chief Scientist
- Reviewed and edited the draft manuscript

Jaap Nienhuis:
- Participated in the field survey in Harrison Bay, Alaska
- Provided recommendations and suggestions on numerical modelling
- Reviewed and edited the draft manuscript

Caroline Cooper:
- Performed numerical modelling of the site in Delft3D
- Reviewed and edited the draft manuscript

Celso Castro-Bolinaga:
- Provided laboratory space and equipment for Jet Erosion Tests
- Reviewed and edited the draft manuscript

Assessing Variations in Geotechnical Sediment Properties and Erodibility in Harrison Bay, Alaska

Nicola C. Brilli[1] , Nina Stark[2], Ph.D., Emily Eidam[3], Ph.D., Jaap Nienhuis[4], Ph.D., Caroline Cooper[5], Celso Castro-Bolinaga, Ph.D[6]

[1]Virginia Tech, Department of Civil and Environmental Engineering, Blacksburg, VA 24060; e-mail: nickb96@vt.edu

[2]Virginia Tech, Department of Civil and Environmental Engineering, Blacksburg, VA 24060; e-mail: ninas@vt.edu

[3]Oregon State University, College of Earth, Ocean, and Atmospheric Sciences, Corvallis, OR 97333; email: emily.eidam@oregonstate.edu

[4]Utrecht University, Department of Geoscience, Utrecht, Netherlands; email: j.h.nienhuis@uu.nl

[5]University of North Carolina at Chapel Hill, Department of Earth, Marine, and Environmental Sciences, Chapel Hill, NC 27514; email: coopcr@email.unc.edu

[6]North Carolina State University, Dept. of Biological and Agricultural Engineering, Raleigh, NC 27606; e-mail: cfcastro@ncsu.edu

The authors of the following manuscript intend to submit it to Geo-Marine Letters

5.1. Abstract

Geomechanical data of Arctic nearshore and offshore seabed sediments are still rare. Two field surveys were conducted in Harrison Bay, Alaska in the summer of 2021 and 2022. These surveys involved portable free-fall penetrometer deployments, grab sampling, gravity coring, and chirp sonar for seabed investigation and bathymetric surveying. The goals of this study were to test geomechanical seabed surface sediments in-situ using a portable free fall penetrometer (PFFP), relate those properties to erodibility parameters from a Jet Erosion Test, and demonstrate the potential use of geomechanical seabed mapping to better inform numerical models of shelf morphological evolution in an Arctic environment. Deriving the Firmness Factor from the PFFP data, a classification scheme was developed with a $FF = 450\, m^{-1}$ threshold differentiating cohesive and non-cohesive sediments at a threshold fines content of 30%. Strength properties were then calculated for cohesive or non-cohesive sediments, respectively. For non-cohesive sediments, the packing state in the form of relative density was related to the detachment coefficient, k_d, with the critical shear stress being determined via empirical relations. Three categories were developed for cohesive sediments: an undrained shear strength separator of $s_u = 2$ kPa correlated well with groupings of k_d obtained from JET tests performed on gravity core samples, and the third category for the least erosive sediments was developed for s_u values greater than 20 kPa. These categories highlighted and related variability in erodibility and sediment strength across the entire bay and a smaller 13 km transect, with the most erodible zone likely associated with active sediment transport due to bluff erosion and surficial sediment reworking from ice gouging. Relevance for numerical modelling of Arctic geomorphology is discussed through an initial and limited sensitivity study using a cross-shelf morphodynamic model in Delft3D.

5.2. Introduction

Arctic coastal and nearshore environments are being heavily impacted by climate change. Warming temperatures have led to decreases in seasonal sea ice thickness and extent, leading to a longer, more spatially expansive open water season (Overeem et al. 2011, Barnhart et al. 2016, Mioduszewksi et al. 2018). These increased temperatures have also led to increases in humidity, precipitation, seasonal river discharge, and permafrost thaw rates (Overeem & Syvitski 2010, Box et al. 2019). Sea ice acts as a natural protection for Arctic coastlines by reducing wave action. Diminishing sea ice allows for more fetch, which increases the duration and energy of wind-waves attacking the coastline. Shorelines composed of permafrost bluffs are especially susceptible to

increased wave energy, as waves impart both mechanical and thermal energy into eroding the coastline through a process called thermal abrasion (Aré 1988). Exacerbating this issue are increases in permafrost thaw and ground ice melt, leading to slumping and block failure (Lantuit & Pollard 2008, Hoque & Pollard 2009, Günther et al. 2015). These factors have led to high rates of coastal erosion in the Arctic (Jones et al. 2008, Frederick et al. 2016) The rate of shoreline retreat is expected to increase as the aforementioned drivers of erosion will continue to strengthen with climate change, leaving Arctic coastlines and communities more vulnerable with time (Ford et al. 2006, Jones et al. 2009, Nielsen et al. 2022).

A consequence of increases in coastal erosion, river discharge, and permafrost block failure and slumping is an increase in sediment supply to nearshore and continental shelf systems (Rachold et al. 2000). The sediment will then be mobilized, transported, and deposited, but the ultimate fate of freshly introduced sediments is still often uncertain. Will it stay in the nearshore and shallow continental shelf areas, where it could potentially be reworked by waves and currents to rebuild the coastline, or will it be permanently transported off the shelf into deep ocean basins? The presence of pack-ice closer to shore in the winter months promotes offshore transport, while open-water summer months allow for more onshore transport and deposition on the inner shelf (MacDonald et al. 2015, Forest et al. 2016). Sediment entrainment in sea ice provides a mechanism for exporting sediment into deep ocean basins (Nürnberg et al. 1994). Additionally, coastal morphology plays an important role in determining transport mechanisms. A study in the Canadian Beaufort Sea found that coastline backed by bluffs favored offshore directed sediment transport during storms more than low-lying barrier island systems where overtopping allowed a more onshore directed component (Héquette et al. 2001). It has also been suggested that decreases in ground-ice and permafrost will increase delta progradation rates and decrease the offshore transport of riverine supplied sediment (Piliouras et al. 2021). Still, the relationship between sediment dynamics, hydrodynamics, and climate change is a complex interaction that is still under investigation and further complicated by often limited information about detailed seabed sediment properties (Macdonald et al. 2015, Wegner et al. 2015, Osborne and Forest 2016).

A key variable affecting nearshore sediment dynamics is sediment properties. Specifically in Arctic environments, grain size of sediments is a controlling but highly variable factor in erosion rates, with coarse-grained (fines content < 50%) deposits having lower erosion rates than fine-grained deposits (fines content > 50%) (Reimnitz et al. 1985). Spatial and vertical variations in

sediment types can result from varying and changing riverine sediment inputs and bluff erosions, along with ice gouging driven reworking of seabed sediments (Reimnitz et al. 1977, Barnes et al. 1980, Barnes et al. 1984). Sediment properties, including but not limited to grain size, directly affect erodibility (See Chapter 4) (Shields 1936, Shafii et al. 2016, National Academy of Sciences Engineering and Medicine 2019).Thus, it follows that high variability in sediment properties would lead to a commensurate degree of variability in the erodibility of these sediments. Measuring in-situ sediment properties, critical shear stress, and erosion rates for surficial seabed sediments would be an important step towards improving the understanding and prediction of sediment dynamics in Arctic nearshore environments. Enhancing the ability to quantify variations in sediment properties and erodibility could improve numerical models of shelf morphology (Malito et al. 2022). However, in-situ measurements of seabed sediments in shallow Arctic areas are difficult due to logistics of fieldwork in remote areas, accessibility of and operation in shallow-water, and presence of sea ice preventing thorough vessel surveying for most of the year. Portable free-fall penetrometers (PFFPs) provide a potential solution to these challenges, particularly where only surface sediments are investigated. Lightweight, rugged, and easily deployable from small vessels, PFFPs have been used for rapid seabed characterization, measurement of in-situ geotechnical properties, and investigation of sediment transport and mobilization (Akal and Stoll 1995, Hay et al. 2014, Stark et al. 2014, Albatal and Stark 2017, Lucking et al. 2017). Additionally, PFFPs have been used in Arctic nearshore areas for characterization of seabed bearing strength, pore pressure response, and identification of sediment layering (Stark et al. 2015, Stark et al. 2017, Brilli et al. 2022). Relating PFFP measurements to erodibility would make Arctic geomechanical seabed characterization significantly more feasible, and thus, increase data availability (Stark et al. 2022).

A combination of PFFP deployments and physical samples over a large spatial area will be used to develop a regional sediment classification model for determining cohesive vs. non-cohesive sediments, whereby PFFP data can be used in lieu of physicals to provide insights on geotechnical properties of surficial seabed sediments (Mulukutla et al 2011, Albatal and Stark 2017). Thus, the goals of this study are to use PFFP measurements in a highly variable Arctic nearshore environment to develop a regional sediment classification model to understand the variability of geomechanical sediment properties, i.e., strength properties and erodibility, and explore the

relevance of these measurements in the context of local geomorphodynamics and for numerical modelling of Arctic nearshore and shallow water environments.

5.2.1. Regional Context

Two field surveys were conducted in July/August 2021 & 2022 in Harrison Bay, Alaska, an embayment opening up to the Beaufort Sea, approximately 70 km west of the town of Prudhoe Bay, Alaska (Figure 5.1). Harrison Bay is part of the Alaskan Beaufort Shelf, a 600 km long section continental shelf on the northern Alaskan coast of the Arctic Ocean, with shelf widths of 50 to 100 km (Norton & Weller 1984). The bay is shallow (water depths < 20 m), and was chosen due to the presence of riverine sediment input from the Colville delta in the south, bluff erosion on the west side of the bay, and a wide variety of mixed sediment types on the seabed both laterally across the bay and vertically in the strata due to diverse sediment inputs and ice gouging processes reworking the seafloor (Barnes and Reimnitz 1974, Reimnitz et al. 1977, Barnes et al. 1980, Jakobsson et al. 2020). To the east of the bay, the coastline is dominated by sand and gravel barrier islands fronting shallow lagoons. Sea ice covers the area between October and June, with an average yearly thickness of 2.4 m, and landfast ice can range in extent from 1 km to 50 km (Norton & Weller 1984, Barnhart et al. 2014). Sea ice acts to shelter the bay from storms, preventing wave generation, and thus sediment transport is constrained to the open water season in the summer.

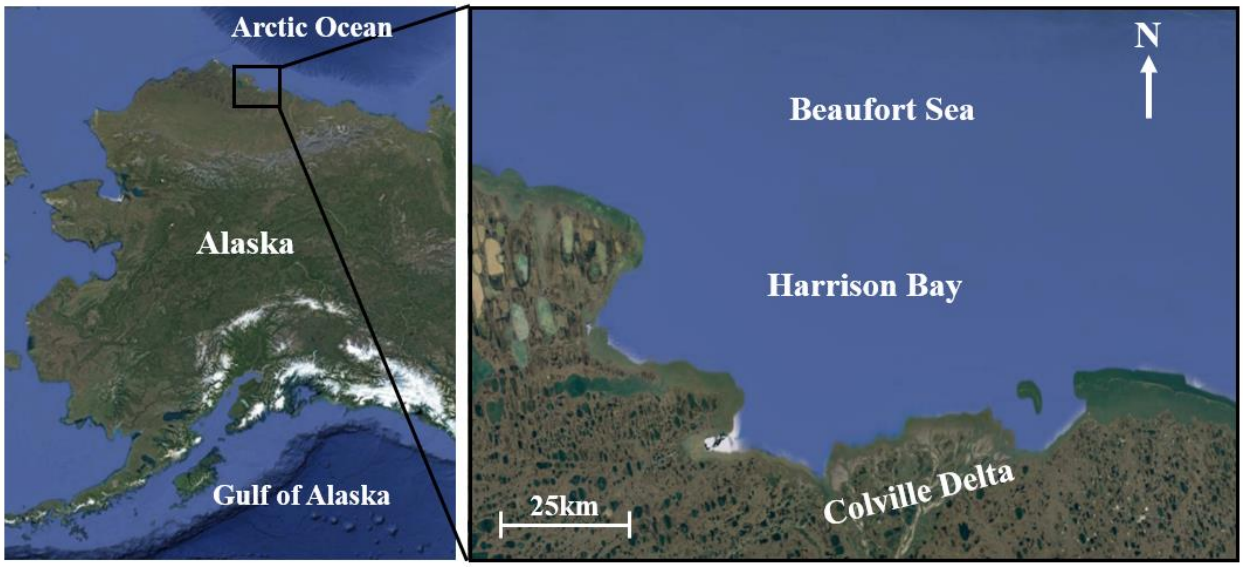

Figure 5.1: Google Earth satellite image Harrison Bay, Alaska. (by Terrametrics; lower left corner: N70°14’54.79” W149°41’42.64”)

5.3. Methods

During the survey in July/August 2021, co-located physical sampling and PFFP deployments were conducted at 71 unique sites across Harrison Bay (red dots, Figure 5.2). Samples were collected with a Shipek surface sampler, and 3 to 10 PFFP deployments were performed at each site.

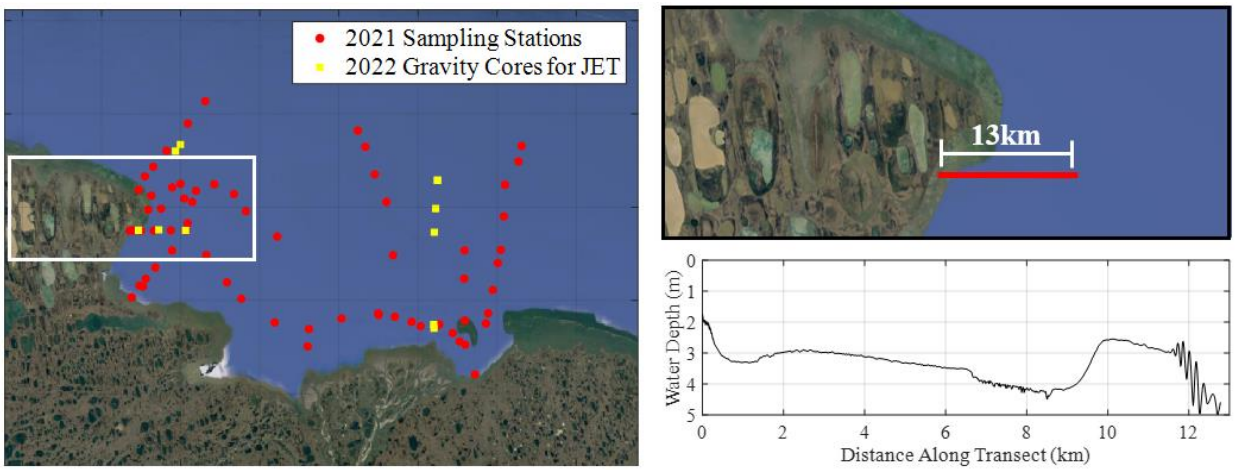

Figure 5.2: Layout of physical sampling and PFFP locations from 2021 (red dots, left), gravity core locations from 2022 (yellow squares, left), white box indicates location of high density PFFP transect from 2022 (top right) and transect bathymetry (bottom right).

In the subsequent 2022 survey, 10 gravity core samples were collected from sites across the bay in order to perform laboratory Jet Erosion Tests (JET) on local sediments to obtain near in-situ erodibility parameters (Figure 5.2) (Hanson 1991). The gravity core samples were also co-located with PFFP deployments, which were used to correlate erodibility parameters with PFFP data. Also in 2022, a 13km long transect line was surveyed off the west side of Harrison Bay, with PFFP deployments approximately every 50 meters, totaling 160 deployments (Figure 2, top right). These data, along with multibeam echosounder bathymetry (MBES) (Figure 2, bottom right) was used to assess the importance of smaller-scale variations in sediment properties and erodibility.

5.3.1. PFFP Data Analysis

The PFFP *blueDrop*, used for these surveys measures 63.1cm long, 8.75 cm in diameter, has a mass of 7.71 kg, and a streamlined body shape (Figure 5.3). The probe is equipped with five vertical accelerometers ranging from $\pm 2g$ to $\pm 250g$, and two $\pm 55g$ horizontal tilt accelerometers, where g is gravitational acceleration.

Figure 5.3: PFFP, *blueDrop*, in use during the field survey in Harrison Bay

All accelerometers record continuously at 2kHz. The device is deployed easily from a range of vessels, secured with a rope attached to the tail section (Figure 5.3), free-falls through the water column, impacts the seabed, and is brought to a stop be the resistance of the sediment. Ease of deployment, self-contained recording over a wide range of accelerations, and less than 1 cm resolution in the vertical sediment profile make this tool ideal for rapid and spatially extensive geotechnical site investigation (Stark et al. 2014, Albatal and Stark 2017).

The acceleration record from impact with the seabed until the soil resistance brings the probe to a stop can be single and double integrated to give profiles of velocity and penetration depth, respectively. Typically, stiffer soils will elicit a stronger deceleration response and softer soils will have a weaker response, reflected in the magnitude of the maximum deceleration recorded by the probe (a_{max}). However, the measured soil strength from PFFP deployments is highly dependent on the rate of strain experienced by the soil, or the impact velocity (v_i) in the case of the PFFP (Dayal and Allen 1973, Dayal et al. 1975). This strain rate dependence means that a_{max} is dependent on v_i and the soil strength properties. Mulukutla et al. (2011) proposed the Firmness Factor (FF) as an attempt to normalize the deceleration record using the impact velocity to give a velocity-independent metric proxy of soil stiffness using the raw PFFP data. This parameter has been used to normalize PFFP measurements for different diameter cones as well as sediment classification and rapid site characterization (Mulukutla et al. 2011, Albatal and Stark 2017). The

Firmness Factor is given by Equation 5.1, and was used in this study for the purpose of differentiating cohesive and non-cohesive sediments:

$$FF = \frac{a_{max}}{v_i g t_p} \tag{5.1}$$

where t_p is the penetration time from impact until stop and g is gravitational acceleration. Once sediments were classified as cohesive or non-cohesive, the geotechnical properties were characterized following a methodology similar to that proposed by Jaber (2022). For non-cohesive sediments, this means obtaining the relative density (D_r), and for cohesive sediments this involves obtaining the undrained shear strength (s_u). These engineering properties will then be used to define relationships between sediment properties and erosion parameters.

For coarse-grained (non-cohesive) sediments, the acceleration record has also tied to packing state in the form of D_r. It should be noted that packing state can also be described by void ratio (e), porosity (n), and bulk density (ρ_b). Albatal et al. (2020) performed laboratory tests on a medium quartz sand by dropping a PFFP into a sediment bed over a range of fixed D_r, and developed an empirical estimate of D_r (as a %) using only a_{max} (in g) from the PFFP (Equation 5.2):

$$D_r = -14.66 * 10^{-3}(a_{max}) + 2.66(a_{max}) - 25.17 \tag{5.2}$$

Determination of s_u requires first determining the bearing strength. Estimating bearing strength from the PFFP requires applying Newton's 2nd law to the acceleration profile to convert the deceleration response to a sediment resistance force. This sediment resistance force is then divided by the area of the tip to give a dynamic bearing capacity (q_{dyn}). This measure is likewise influenced by the aforementioned strain-rate effects. A wide range of possible impact velocities leads to a wide range of possible measured strengths. Thus, it is advantageous to normalize the bearing strength to a much slower rate of strain where these effects are minimal, like a Cone Penetration Test (Stoll et al. 2007, Chow et al. 2018, White et al. 2018). This is accomplished by dividing q_{dyn} by a strain rate correction factor (f_{sr}), given by Equation 5.3:

$$qsbc = \frac{q_{dyn}}{f_{sr}} \tag{5.3}$$

where $qsbc$ is the quasi-static bearing capacity, an estimate of the bearing capacity without strain-rate effects. There are multiple formulations for f_{sr}, the most common being the logarithmic form (Peck 1962, Mitchell 1964). and the power law (Randolph 2004). For the purposes of this study, the power law will be used as this formulation was the basis of the cohesive methodology proposed by Jaber (2022) for estimating s_u, and is given by Equation 5.4:

$$f_{sr} = \left(\frac{v_{dyn}}{v_{ref}}\right)^{\beta} \tag{5.4}$$

where, v_{dyn} is the non-linear dynamic velocity profile, v_{ref} is the reference velocity at which strain rate effects are no longer observed, typically taken as 2 cm/s to reflect CPT measurements, and β is a soil-type dependent strain rate factor. β will be taken as 0.035-0.085 for this study (Randolph and Hope 2004, Jaber 2022). Once $qsbc$ is determined via Equation 5.4, s_u can be calculated via Equation 5.5:

$$s_u = \frac{qsbc}{N_{kt}} \tag{5.5}$$

where, N_{kt} is a cone factor. Again, per the methodology in Jaber (2022) and previous literature on selection of CPT cone factors, N_{kt} will be taken as a value of 10 for this study (Lunne et al. 2002, Robertson and Cabal 2010, Mayne and Peuchen 2018).

5.3.2. Jet Erosion Test (JET)

Erodibility parameters were determined using a laboratory mini JET setup at North Carolina State University. The JET was originally developed for characterizing erodibility of cohesive soils both in-situ and in the laboratory (Hanson 1990, Hanson 1991, Hanson and Cook 2004). Tests were performed on 11 gravity core samples, trimmed to 10-12 cm sections. To run the test, a head tank was set at 2.1 meters, and a jet of water was projected onto the top of the sample through a nozzle for a fixed period of time, scouring the sample. After each individual trial, a point gauge was lowered into the scour hole to measure its depth. The test was run for time periods of 5 s, 15 s, 30 s, 60 s, 120 s, and 300 s, and each time period was tested consecutively until no more erosion was observed for that time interval. Sample preparation before testing (left), during testing showing the point gauge and test setup (middle), and post-testing with complete scour-hole (right) are shown in Figure 5.4.

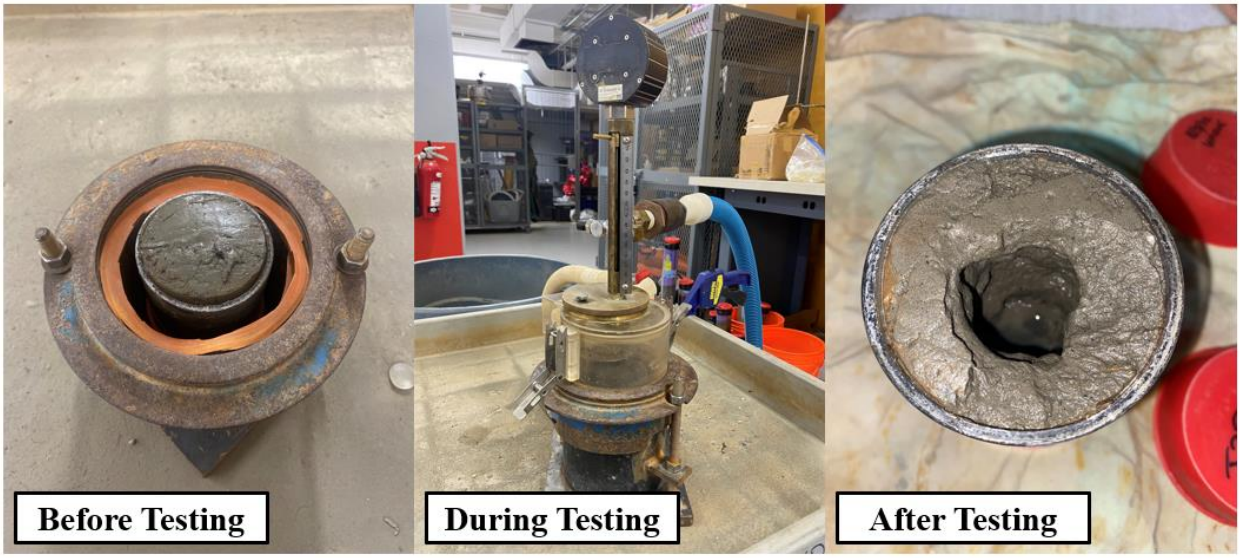

Figure 5.4: Sample prepared for testing (left), Mini-JET test with sample inside (middle), sample after testing showing scour hole (right).

Once the test is complete, the scour depth and time intervals are converted into erosion rates (E), and head height, nozzle characteristics, fluid properties, and time-varying scour depth give the applied shear stress on the sample (τ) (Hanson and Cook 1997). Erodibility parameters can then be determined by fitting the measured E and τ data to the excess shear equation given by Equation 5.6 (measured parameters shown in bold):

$$\boldsymbol{E} = k_d(\boldsymbol{\tau} - \tau_c)^n \tag{5.6}$$

where, k_d is the detachment coefficient, τ_c is the critical shear stress, and n is a fitting parameter typically assumed as unity. There are multiple solutions for obtaining k_d and τ_c from JET data (Hanson 1991, Simon et al. 2010, Daly et al. 2013, Al-Madhhachi et al. 2013, Wahl 2021). For the purposes of this study, parameters were obtained by performing a least-squares linear fit to the raw E and τ data, with k_d and τ_c being the fitting coefficients. This approach has been shown to be a simple approach that is also on par with the results of more complicated methods (Wardinski et al. 2018, Wahl 2021). Goodness of fit was quantified using a Normalized Objective Function, which has been used previously for JET data (Fox et al. 2006, Al-Madhhachi et al. 2013).

For both cohesive and non-cohesive sediments, the detachment coefficient, k_d, describes the erosion rate of the sediment once erosion has been initiated ($\tau > \tau_c$), and has units of erosion rate per unit of excess shear stress. Higher k_d indicates more erodible sediment. A companion study

was conducted using JET tests on beach sand (see Chapter 4, Figure 4.9) and found strong correlation ($R^2 = 0.87$) between k_d and void ratio, e, via an empirical power-law relationship given by Equation 5.7:

$$k_d \left(\frac{\text{cm}^3}{\text{N} - \text{s}} \right) = 1396 e^{2.5861} \tag{5.7}$$

Since D_r is related to e by Equation 5.8, and D_r can be directly estimated from PFFP measurements (Equation 5.2), it follows that k_d can also be obtained from PFFP measurements for non-cohesive sediments at this site.

$$D_r = \frac{e_{max} - e}{e_{max} - e_{min}} \tag{5.8}$$

Minimum (e_{min}) and maximum (e_{max}) void ratios were computed for the coarse-grained sediments at this site from samples obtained via Shipek sampling during the 2021 survey (ASTM D4254-00, ASTM D4253-16). Using these values, Equation 5.9 can be used to convert D_r from Equation 5.2 into void ratio and then Equation 5.7 gives k_d.

$$e_{max} = 0.72, e_{min} = 0.43 \rightarrow e = 0.72 - 0.29 D_r \tag{5.9}$$

Applying the range of possible void ratio values at the site into Equation 5.2 gives a range of k_d for sand at the site from 150-600 $\text{cm}^3/\text{N} * \text{s}$.

5.4. Results

The results from physical samples taken during the 2021 survey show the variability of seabed sediments at the site. Figure 5.5 shows the fines content for all sites sampled during the 2021 survey (see Figure 5.2). Brighter colored dots represent finer sediments and darker colors represent coarser sediments. Of the 66 individual sites where physical samples were collected during the 2021 survey, 25 classified as coarse-grained (fines > 50%), and 41 classified as fine-grained, with the only real spatial trend being a coarser deposit off the west coast surrounded by majority fine sediments (Figure 5). Further only 6 sites had fines contents less than 12%, the traditional United Soil Classification System (USCS) cutoff for a clean sand, meaning that a vast majority of the sites would be considered mixed sediments. As seen from the figure, the west side of the bay is dominated by fine sediments with a coarse grained area approximately 10 km offshore of the western coast. Fine-grained sediments were predominantly found on the eastern side of the bay,

closer to shore, with the exception of a sand bank located along the middle line heading offshore. The southern area near the Colville Delta was more mixed than any other area in the field site.

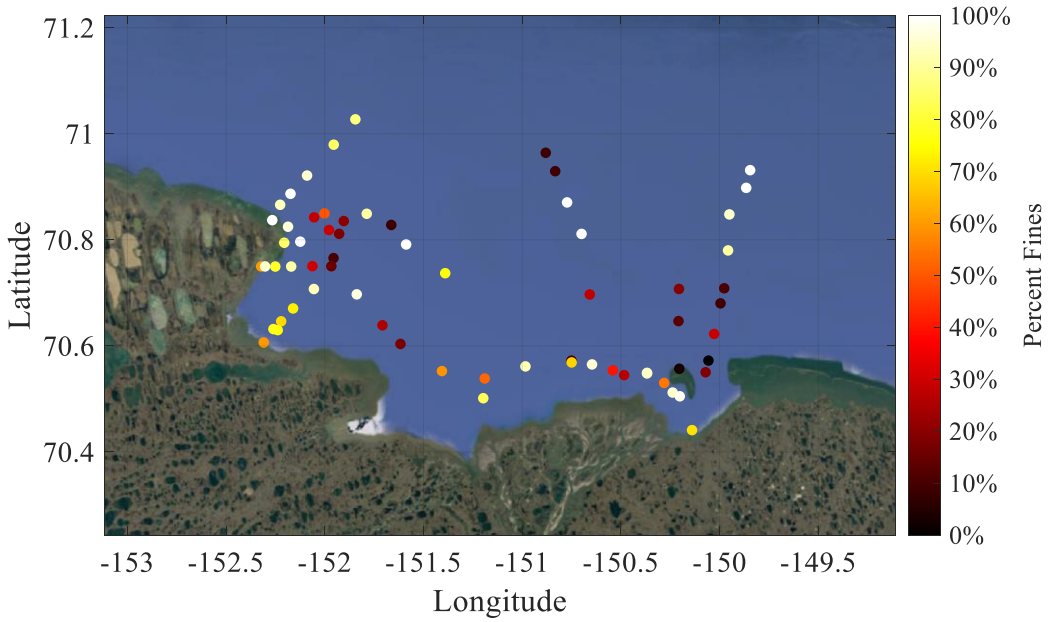

Figure 5.5: Spatial distribution of fines contents across Harrison Bay, Alaska. Brighter colors indicate finer sediments and darker colors indicate coarser sediments.

While there is no clear consensus on the fines content that determines the boundary between cohesive and non-cohesive behavior, 30% fines content has been used repeatedly in both geotechnical and sediment dynamics literature as a cutoff, and as such will be adopted here (van Ledden et al. 2004, Yang et al. 2005, van Rijn 2020). Figure 5.6 shows 179 PFFP deployments (2-3 deployments from each of the 66 sites) distinguished by $FF = 450\ \mathrm{m}^{-1}$ in two groups with red indicates deployments that were associated with samples having fines content greater than 30%, and blue having fines contents less than 30%. As seen from the figure, a threshold value of $FF = 450\ \mathrm{m}^{-1}$ accurately predicts all 125 deployments with $FF < 450\ \mathrm{m}^{-1}$ as having fines content greater than 30%, and 50 out of 55 deployments with $FF > 450\ \mathrm{m}^{-1}$ as having fines content less than 30%. The five samples that were incorrectly classified are likely due to heavily overconsolidated mud.

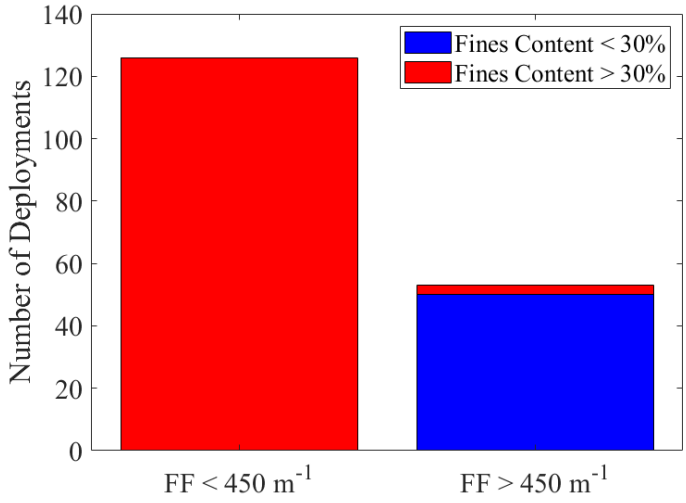

Figure 5.6: Distribution of deployments with greater than 30% fines (red) and fines less than 30% (blue), with the left column consisting of deployments with FF greater than 450 $\mathbf{m^{-1}}$ and the right column deployments greater than 450 $\mathbf{m^{-1}}$.

Table 5.2 shows the results of the JET analysis from the gravity core samples taken during the 2022 survey. Samples from the same site labelled "#1" and "#2" indicate a gravity core sample that was longer than the 12cm that can be accommodated by the JET mold and was sectioned into 12cm increments for testing. Samples labelled "#1" indicate the uppermost sample, and subsequent numbers are consecutive in depth. τ_c values ranged between 3 Pa and 16 Pa, and k_d values ranged from 3 – 120 $\frac{\mathrm{cm}^3}{\mathrm{N-s}}$.

Table 5.1: Results of JET tests on gravity core samples from the 2022 survey.

Site	$\boldsymbol{\tau_c}$ **(Pa)**	$\mathbf{k_d}\left(\frac{\mathbf{cm^3}}{\mathbf{N-s}}\right)$
WP571 #1	4.83	3.57
WP692 #1	5.68	52.08
WP852 #2	4.77	121.65
WP915 #1	16.07	5.13
WP915 #2	12.09	6.25
WP1006 #1	3.93	39.99
WP1012 #1	7.71	125.15
WP1017 #1	10.76	28.54
WP1017 #2	15.56	3.03
WP1021 #1	10.10	15.26
WP1021 #2	6.27	10.84

Erodibility parameter from the JET were then compared to s_u values from co-located PFFP deployments. A negative power law relationship between k_d and s_u is apparent for the tested

samples (Figure 5.7). Further, it was observed that samples having s_u less than 2 kPa, had k_d values $> 20\ \frac{\text{cm}^3}{\text{N-s}}$, and samples with s_u greater than 2 kPa had $k_d < 20\ \frac{\text{cm}^3}{\text{N-s}}$(dashed line, Figure 5.7). Thus, this value served as the first threshold for erodibility classification based on PFFP measurements, which is presented in the following sections. Parameters from the PFFP (s_u, FF, a_{max}) were also compared with τ_c from the JET tests, and no suitable relationships were found between PFFP measurements and τ_c for the data available at this site.

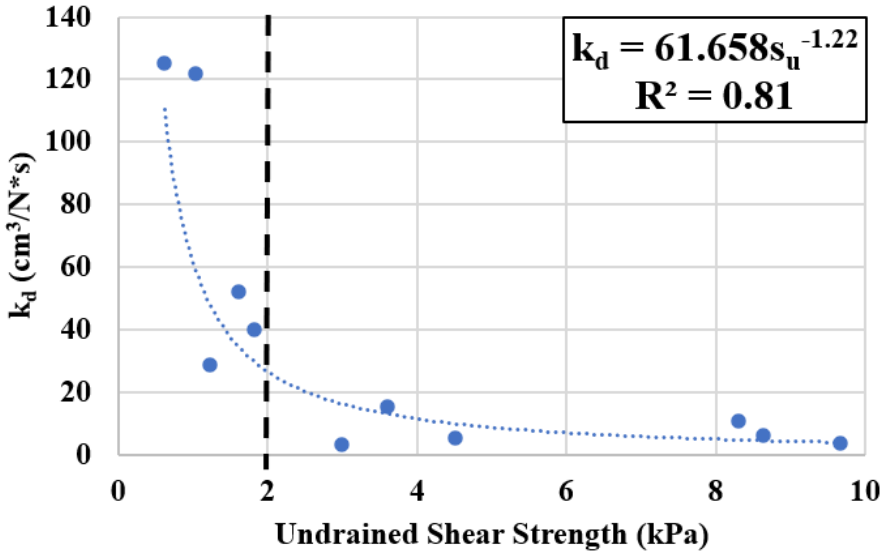

Figure 5.7: Relationship between $\boldsymbol{s_u}$ and $\boldsymbol{k_d}$ for locations where gravity core samples used for JET testing and PFFP deployments were co-located.

Based on the previously developed criteria for differentiating cohesive vs. non-cohesive sediments, and relationships between s_u and k_d, the following erodibility categories based on PFFP measurements are suggested (Table 5.2). Category SAND is defined as any deployment with $FF > 450\ m^{-1}$. This category is the most erodible of the four and encompasses non-cohesive sediments with erodibility parameter k_d falling between 150-600 $\frac{\text{cm}^3}{\text{N-s}}$, based on D_r from the PFFP. While there was no direct data available to make a prediction for τ_c, the results detailed in Chapter 4 and specifically Figure 4.5 showed that τ_c was less important for determining erosion behavior of sandy sediments (Section 4.5). Category C1 – C3 are based on s_u for cohesive sediments with $FF < 450\ \text{m}^{-1}$. C1 & C2 reflect the delineation made in Figure 5.7, with the addition of a buffer of 1 kPa due to a small number of data points and to reflect uncertainty in the measurements. C1 sediments have a slightly smaller range of τ_c values based on the results displayed in Table 5.1.

Finally, category C3 included deployments with s_u greater than 20 kPa. These sediments fell well outside of the sample data bounded by Figure 5.7, and thus no specific ranges will be given for erodibility parameters, with this category simply being described as "least erosive".

Table 5.2: Breakdown of erosion categories for cohesive sediments at the Harrison Bay site based on the results of the field and laboratory measurements.

Erosion Category	**Criteria**	**Determination of τ_c**	**Determination of k_d**
SAND	$FF > 450\ \mathrm{m}^{-1}$	No data for this study	$150 - 600\ {}^{\mathrm{cm}^3}/_{\mathrm{N-s}}$
C1	$s_u < 2 - 3$ kPa	$3 - 10$ Pa	$> 20\ {}^{\mathrm{cm}^3}/_{\mathrm{N-s}}$
C2	$s_u = 3 - 20$ kPa	$3 - 15$ Pa	$< 20\ {}^{\mathrm{cm}^3}/_{\mathrm{N-s}}$
C3	$s_u > 20$ kPa	Least erodible	

Using the criteria from Table 3, the PFFP deployments from the 2021 survey were converted into their corresponding Erosion Categories (Figure 5.8). The west side of the bay shows a lot of variability in with a mixture of C1 and C2 zones along with a large zone of SAND. Sediments seem to be more erodible offshore with most offshore sediments classifying as C1 with the exception of a small area of SAND sediments in the middle of the bay. In the South near the Colville Delta, the least erodible sediments were found, with mostly C2 and C3 sediments, as well as SAND and C1 sediments sparsely populated within those areas.

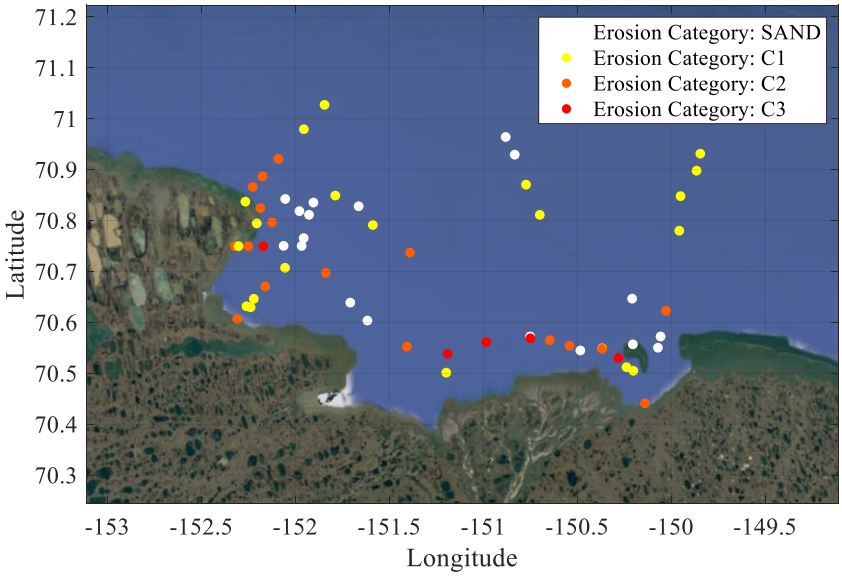

Figure 5.8: Distribution of Erosion Categories across Harrison Bay including the non-cohesive category (NC), and the three cohesive categories (C1-C3).

A similar approach was taken for the 13 km transect displayed in Figure 5.2. First, FF was calculated for each of the 160 PFFP deployments, and they were separated based on cohesive and non-cohesive behavior (Figure 5.9, top). As seen in the figure, a majority of the transect classified as cohesive, with the shoal beginning at approximately 10 km classifying as non-cohesive. The series of sand waves starting at 11.5 km also classified as non-cohesive, except for select deployments in the trough that classified as cohesive.

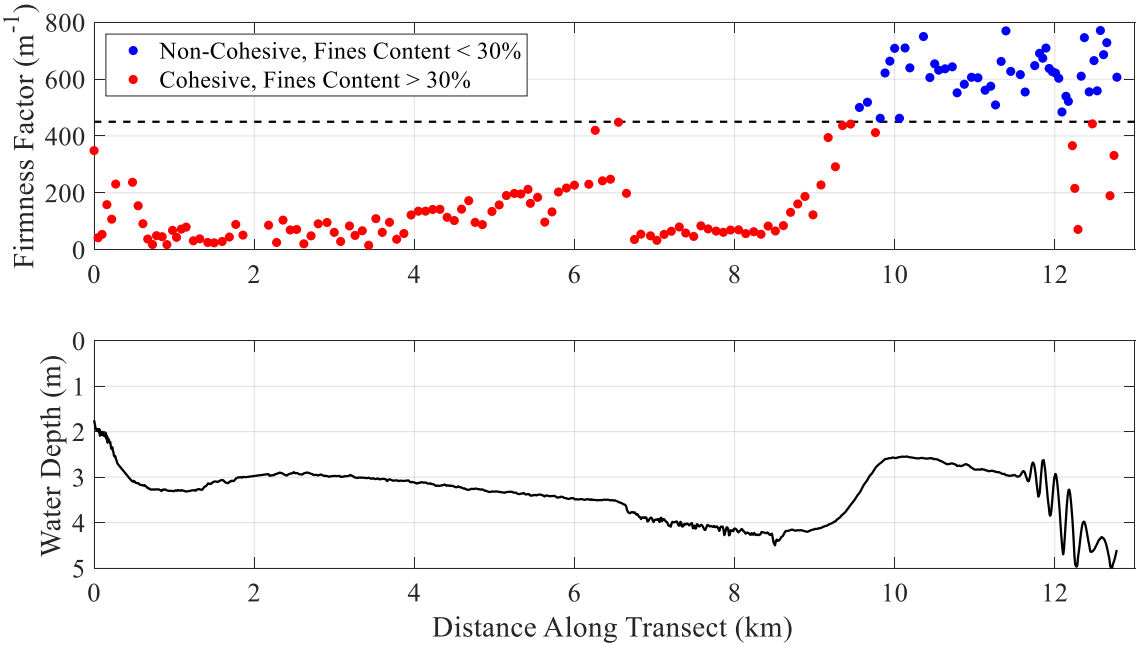

Figure 5.9: Application of the Firmness Factor classification to a smaller 13km transect off the west coast of Harrison Bay from PFFP deployments (top), bathymetry is shown in the bottom panel.

Figure 5.10, top, shows s_u on the left y-axis (only applicable for C classes), and D_r on the right y-axis (only applicable for the NC class), with the colors indicating which erosion category each value of s_u fell into. D_r values ranged from 60-90%, representing overall relatively dense sands which may suggest limited recent mobility. These values of D_r are in line with the work by Albatal et al. (2020), who developed the correlation and applied it to nearshore deployments in similar water depths. There was significant variability in s_u across the transect with values ranging from less than 1 kPa to 50 kPa, representing very soft to very stiff fine-grained seabed surface sediments. This is a wider range of s_u then presented by Jaber (2022), who derived s_u from PFFP measurements for s_u < 10 kPa. The work in that study was focused on soft estuarine and coastal sediments, but Harrison Bay additionally features stiffer, overconsolidated muddy sediments. This

variability is also reflected in the erosion categories. The x-axis on the bottom panel of Figure 5.10 translates each category onto a line for better visualization with the bathymetry. The initial depression from 0.5-2 km contained weak, highly erodible sediments, with strength increases and erodibility decreasing across a flatter, sloping bed until a second depression around 7 km, where the sediment became soft and erodible again in a zone filled with ice scours. This was followed by a sharp increase in s_u (decrease in erodibility) until the sediment transitioned to non-cohesive at which point the shoal was dominated by highly erodible SAND sediments, with the exception of less erodible C2 & C3 sediments in the troughs of the sand waves starting at 11.5 km.

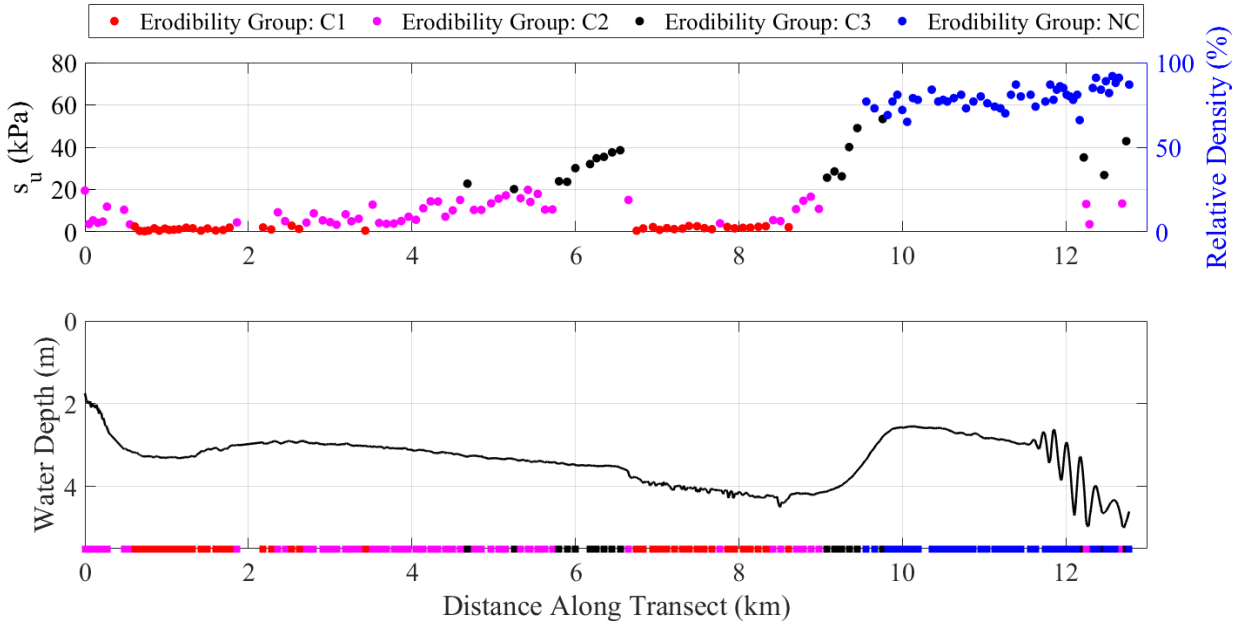

Figure 5.10: Application of Erosion Categories to the same transect from Figure 9 using the PFFP deployments (top). Bottom panel again contains bathymetry along with colored sections to visualize erodibility zones more easily.

5.5. Discussion

The results of this study show that surficial seabed sediments in Harrison Bay, Alaska, are highly variable in both geomechanical properties and erosion behavior. The observed surficial sediment variability was also noted by Barnes (1980) and is likely due to a wide variety of sediment inputs, and ice gouging causing reworking of the uppermost sediment layers (Barnes and Reimnitz 1974, Reimnitz et al. 1977, Barnes et al. 1984). The variability in sediment properties and erodibility in Arctic environments has important implications for applied engineering applications in these areas such as for the protection of buried pipelines and for improving numerical models of shelf morphodynamics in response to climate change (Nematzadeh and Shiri 2020, Hashemi et al. 2022,

Malito et al. 2022). However, remote fieldwork logistics, coupled with limited access to Arctic nearshore areas due to sea ice most of the year, make sediment characterization from physical samples, erodibility assessment from in-situ coring, and geotechnical strength estimation a difficult proposition. This highlights the utility of the proposed framework, where the PFFP was used to differentiate cohesive and non-cohesive sediments, and furthermore, to distinguish different categories of erodibility (Figure 5.6 and Table 5.3).

5.5.1. Sediment and Erodibility Classification Scheme based on PFFP Measurements

The methodology presented in the results (Section 5.4) for using PFFP measurements to classify sediment behavior type and erodibility behavior is summarized in Figure 5.11. The first step is to calculate FF directly from the PFFP data (Equation 1). Distinguishing cohesive vs. non-cohesive sediments (Figure 5.6) is important as these two groups behave differently in terms of sediment properties, strength, and erodibility (National Academy of Science and Engineering 2019). While there is no consensus agreement on 30% fines being a unique cutoff between cohesive and non-cohesive behavior, it is widely recognized as an acceptable value here (van Ledden et al. 2004, van Rijn 2020). Values as low as 10% and as high as 40% have also been suggested as thresholds, but 30% will be adopted here to stay consistent (Yang et al. 2005, Jacobs et al. 2011). $FF = 450\ \mathrm{m}^{-1}$ represented a reliable threshold for cohesive and non-cohesive sediments based on this fines content of 30% with 96% of tests classifying correctly. The five observed outliers can be explained by the presence of heavily consolidated, stiff cohesive sediments. This type of regional sediment mapping using FF and other parameters from PFFP deployments has been demonstrated before (Mulukutla et al. 2011, Albatal et al. 2017), but this is the first application of this type of analysis to an Arctic environment, and further serves the purpose of laying the foundation for deriving erodibility categories as proposed in Table 5.2 with measurements being faster and easier to perform than grab sampling or coring.

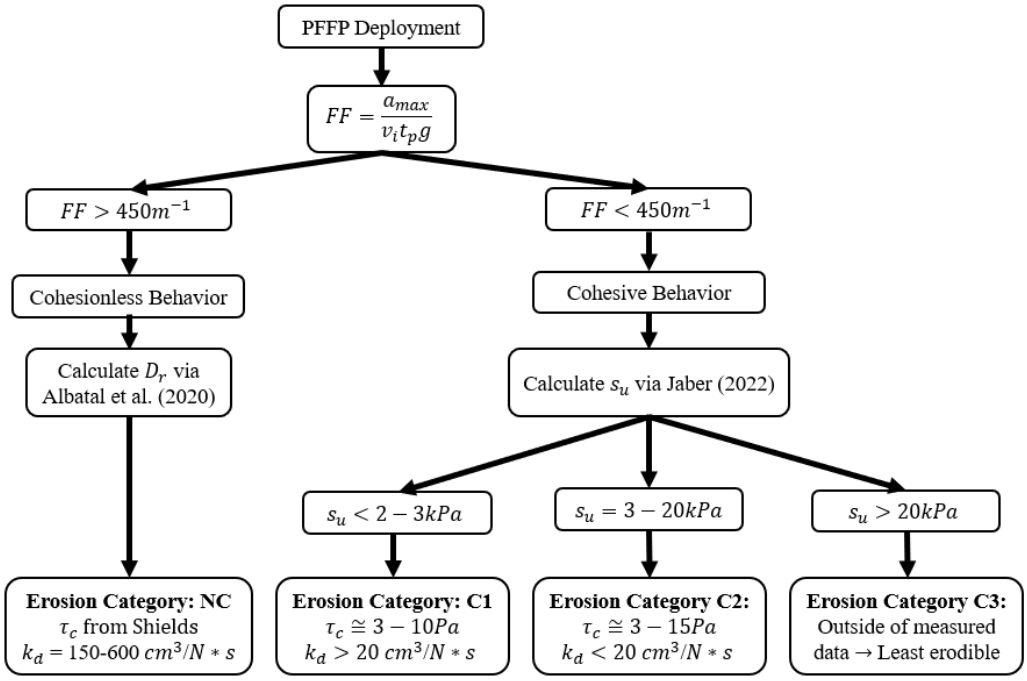

Figure 5.11: Flowchart describing data analysis and breakdown of erosion categories based on geotechnical sediment properties.

Following the left side of the flow chart, the next step is to calculate D_r from Albatal et al. (2020) (Equation 2) and using this value to compute k_d via Equations 7-9. There were no direct comparisons made between erodibility parameters and geotechnical properties for non-cohesive sediments at this site as there were no undisturbed in-situ samples of sandy sediments taken for JET testing. Gravity corers cannot sample in cohesionless soils. Data available from JET tests on high quality in-situ cohesionless samples from a companion study (Chapter 4, specifically in Figure 4.9) and laboratory tests on sand from grab samples allowed for a range of k_d values to be computed for the non-cohesive stations in Harrison Bay. For the SAND classification, it is suggested to obtain τ_c via empirical relation. While no in-situ data is available from this site, van Rijn (2020) suggested that empirical relations can give a reasonable estimate of initiation of motion (Shields 1936, Brownlie 1981, Soulsby and Whitehouse 1997, van Rijn 2007).

For sediments classifying as cohesive, s_u is calculated from Equations 3-5. The three categories C1-C3 are then differentiated using the relationship in Figure 5.7, showing a correlation between k_d and s_u. A first threshold value was chosen at s_u = 2-3 kPa, as samples with s_u less than this value had k_d less than 20 $\frac{\mathrm{cm}^3}{\mathrm{N-s}}$. s_u = 20 kPa was selected as an upper threshold, as it was outside

of the range of s_u presented in Figure 5.7 (0-10 kPa), with 20 kPa being selected to add conservatism to the model test over a limited range of s_u. There were no relationships found between τ_c and PFFP parameters for the cohesive sediments. Thus, the range presented in Table 5.2 and Figure 5.11 represent the range of values directly from the JET measurements in Table 5.1. While typical suggested values of τ_c for cohesive sediments are typically less than 1 kPa, the values from the JET are in line with previous studies showing τ_c up to 20 kPa (Kamphuis and Hall, 1983). Further, the method of erosion for the JET is mass erosion, whereby large amounts of material are removed, requiring higher stresses to initiate the larger amounts of erosion than particle erosion, where the required stresses are much lower (Hanson and Cook 2004, Winterwerp et al. 2012, van Rijn 2020).

5.5.2. Application of Classification Methodology in the Context of Local Geomorphodynamics

Analyzing the erosion categories in the context of the local site conditions offers further insights. Figure 5.8 suggests that Harrison Bay is overall highly variable in sediment properties including erodibility. The west side of the bay features a majority of fine sediment (Figure 5.5) classifying as a mix of C1 and C2. This suggests that while the fines contents may be similar, the sediments feature different strength and a different mobilization behavior. Zooming in to the 13 km transect detailed in Figures 5.9 and 5.10 further illustrates this point. Specifically, the zones of C1 material in the depressions located at 0-2 km and 7-9 km can be understood in the context of local sediment transport and ice processes. The start of the transect is located less than 1 km offshore, and the shoreline on this side of the bay is marked by bluff erosion. Hequette et al. (2001) suggested that coastal bluffs induce wave energy reflection, especially during storm events, which can drive offshore directed bottom currents. Freshly eroded unconsolidated bluff sediments and organics would be transported offshore by this process and deposited in the depression at 0-2 km, explaining why this zone was primarily comprised of soft, highly erodible sediments. Further, the zone of sharp transition (over an ~100 m distance) from the least erodible C3 sediments into a zone of soft C1 sediments marked by small bathymetric undulations (on the order of 5-30 cm) can be explained by ice gouging processes. Reimnitz et al. (1977) found that ice gouging of the seabed could completely rework bottom sediments in the upper 20 cm, which is directly in line with the magnitude of scours seen in Figure 5.10. The sharp transition from C3 to C1 sediments over a short spatial extent can be explained by the knickpoint commonly found on the inner edge of ice gouging zones, typically comprised of coarser sediments (Reimnitz and Kempema 1984). The

addition of coarser particles to sediments with cohesive behavior would account for the sharp increase in s_u and decrease in erodibility (Torfs et al. 2000). Even over a small area of the bay, there are large variations in sediments properties and erodibility. The proposed framework in Figure 5.11 allowed to assess the erodibility behavior of Arctic seabed sediments in the context of local sediment transport and sea ice processes, highlighting the utility of this methodology as a robust tool for understanding local sediment dynamics over a range of spatial scales.

5.6. Conclusions

Understanding sediment dynamics in Arctic environments is key to understanding how these systems will respond to climate change. A key question in the area of sediment dynamics is the quantitative relationship between sediment strength properties (that can be easily measured in-situ) and erodibility. Portable free fall penetrometer (PFFP) measurements in the form of firmness factor were able to create a classification scheme for cohesive vs. non-cohesive sediments, and beyond that for four erodibility categories. The main findings are summarized as follows:

1. A reliable regional sediment classification scheme was developed using $FF = 450\ \mathrm{m}^{-1}$ as a threshold for differentiating cohesive ($FF < 450\ \mathrm{m}^{-1}$) and non-cohesive ($FF > 450\ \mathrm{m}^{-1}$) sediments with 96% accuracy.

2. As with packing state for non-cohesive sediments (see Chapter 4), s_u shows a clear relationship with k_d obtained from JET tests, highlighting a relationship between geotechnical properties and erodibility parameters. This is particularly important, as s_u is easily obtainable from PFFP deployments.

3. A dual sediment strength characterization and erodibility classification framework was developed using PFFP measurements and divided into four erosion categories. The non-cohesive SAND category obtains τ_c from empirical relations and k_d from PFFP estimates of D_r. Three cohesive sediment categories (C1-C3) were differentiated using derived s_u relationship with k_d. τ_c varied from 5-15 Pa and was obtained from direct measurements from the JET. The estimates of s_u less than 2-3 kPa yielded the most erodible category (C1) with $k_d > 20\ \frac{\mathrm{cm}^3}{\mathrm{N-s}}$. Deployments with s_u between 3 and 20 kPa represented category C2, with $k_d < 20\ \frac{\mathrm{cm}^3}{\mathrm{N-s}}$, and the final category C3 was the least erosive sediment with $s_u >$ 20 kPa.

4. This framework was applied to PFFP deployments across the entire bay and for a 13 km transect near a permafrost bluff shoreline. The results highlighted the in-situ variability of sediment strength and erodibility in Harrison Bay. Analysis of the smaller transect showed how this framework could associate erodibility with local sediment dynamics and ice gouging processes.

This work provides a framework for characterizing erodibility in highly variable seabed conditions, which can be measured with a single tool capable of providing useful insights for both site characterization and improving future modelling efforts to predict Arctic response to climate change.

5.7. Acknowledgements

The authors would like to thank Captain Mike Fleming for his support and guidance for both field surveys, as well as Dan Duncan and Josephine Hall for their support in data collection efforts. This material is based upon work supported by the National Science Foundation under Grants OPP-1912863, OPP-1913195, and CMMI-1751463. Any opinions, findings, and conclusions or recommendations expressed in this material are those of the author(s) and do not necessarily reflect the views of the National Science Foundation.

References

Akal, T., & Stoll, R. D. (1995). Expendable penetrometer for rapid assessment of seafloor parameters. Oceans Conference Record (IEEE), 3. https://doi.org/10.1109/oceans.1995.528858

Albatal, A., & Stark, N. (2017). Rapid sediment mapping and in situ geotechnical characterization in challenging aquatic areas. Limnology and Oceanography: Methods, 15(8). https://doi.org/10.1002/lom3.10192

Al-Madhhachi, A. T., Hanson, G. J., Fox, G. A., Tyagi, A. K., & Bulut, R. (2013). Measuring soil erodibility using a laboratory “mini” jet. Transactions of the ASABE, 56(3). https://doi.org/10.13031/trans.56.9742

Aré, F. E. (1988). Thermal abrasion of sea coasts (part I). Polar Geography and Geology, 12(1). https://doi.org/10.1080/10889378809377343

ASTM. (2006). ASTM D4254-00: Standard Test Methods for Minimum Index Density and Unit Weight of Soils and Calculation of Relative Density. ASTM Standards, I(Reapproved 2006).

ASTM D4253-16. (2006). Standard Test Methods for Maximum Index Density and Unit Weight of Soils Using a Vibratory Table. ASTM International, 00(200).

Barnes, P. W., Rearic, D. M., & Reimnitz, E. (1984). Ice Gouging Characteristics and Processes. In The Alaskan Beaufort Sea. https://doi.org/10.1016/b978-0-12-079030-2.50015-0

Barnes, P. W., & Reimnitz, E. (1974). Sedimentary processes on arctic shelves off the northern coast of Alaska.

Barnes, P. W., Reimnitz, E., Ross, R., & Survey, U. S. G. (1980). Nearshore surficial sediment textures: Beaufort Sea, Alaska. In Open-File Report. https://doi.org/10.3133/ofr80196

Barnhart, K. R., Overeem, I., & Anderson, R. S. (2014). The effect of changing sea ice825on the physical vulnerability of Arctic coasts. Cryosphere, 8(5). https://826doi.org/10.5194/tc-8-1777-2014

Barnhart, K. R., Miller, C. R., Overeem, I., & Kay, J. E. (2016). Mapping the future expansion of Arctic open water. Nature Climate Change, 6(3). https://doi.org/10.1038/nclimate2848

Box, J. E., Colgan, W. T., Christensen, T. R., Schmidt, N. M., Lund, M., Parmentier, F. J. W., Brown, R., Bhatt, U. S., Euskirchen, E. S., Romanovsky, V. E., Walsh, J. E., Overland, J. E., Wang, M., Corell, R. W., Meier, W. N., Wouters, B., Mernild, S., Mård, J., Pawlak, J., & Olsen, M. S. (2019). Key indicators of Arctic climate change: 1971-2017. In Environmental Research Letters (Vol. 14, Issue 4). https://doi.org/10.1088/1748-9326/aafc1b

Brownlie, W. B. (1981). Prediction of Flow Depth and Sediment Discharge in Open Channels. California Institute of Technology, W. M. Keck Laboratory of Hydraulics and Water Resources, Report, KH-R-43A.

Chow, S. H., Bienen, B., & Randolph, M. F. (2018). Rapid penetration of piezocones in sand. Cone Penetration Testing 2018 - Proceedings of the 4th International Symposium on Cone Penetration Testing, CPT 2018.

Daly, E. R., Fox, G. A., Al-Madhhachi, A. T., & Miller, R. B. (2013). A scour depth approach for deriving erodibility parameters from jet erosion tests. Transactions of the ASABE, 56(6). https://doi.org/10.13031/trans.56.10350

Dayal, U., & Allen, J. H. (1973). Instrumented Impact Cone Penetrometer. Canadian Geotechnical Journal, 10(3). https://doi.org/10.1139/t73-034

Dayal, U., Allen, J. H., & Jones, J. M. (1975). Use of an impact penetrometer for the evaluation of the in-situ strength of marine sediments. Marine Geotechnology, 1(2). https://doi.org/10.1080/10641197509388155

Deltares. (2014). Delft3D User Manual.

Ford, J. D., Smit, B., & Wandel, J. (2006). Vulnerability to climate change in the Arctic: A case study from Arctic Bay, Canada. Global Environmental Change, 16(2). https://doi.org/10.1016/j.gloenvcha.2005.11.007

Forest, A., Osborne, P. D., Curtiss, G., & Lowings, M. G. (2016). Current surges and seabed erosion near the shelf break in the Canadian Beaufort Sea: A response to wind and ice motion stress. Journal of Marine Systems, 160. https://doi.org/10.1016/j.jmarsys.2016.03.008

Fox, G. A., Sabbagh, G. J., Chen, W., & Russell, M. H. (2006). Uncalibrated modelling of conservative tracer and pesticide leaching to groundwater: Comparison of potential Tier II exposure assessment models. Pest Management Science, 62(6). https://doi.org/10.1002/ps.1211

Frederick, J. M., Thomas, M. A., Bull, D. L., Jones, C. A., & Roberts, J. D. (2016). The Arctic Coastal Erosion Problem. Sandia Report, SAND2016-9.

Günther, F., Overduin, P. P., Yakshina, I. A., Opel, T., Baranskaya, A. v., & Grigoriev, M. N. (2015). Observing Muostakh disappear: Permafrost thaw subsidence and erosion of a ground-ice-rich Island in response to arctic summer warming and sea ice reduction. Cryosphere, 9(1). https://doi.org/10.5194/tc-9-151-2015

Hanson, G. J. (1990). Surface erodibility of earthen channels at high stresses. Part II - Developing an in situ testing device. Transactions of the American Society of Agricultural Engineers, 33(1). https://doi.org/10.13031/2013.31306

Hanson, G. J. (1991). Development of a jet index to characterize erosion resistance of soils in earthen spillways. Transactions of the American Society of Agricultural Engineers, 34(5). https://doi.org/10.13031/2013.31831

Hanson, G. J., & Cook, K. R. (1997). Development of excess shear stress parameters for circular jet testing. Paper - American Society of Agricultural Engineers, 2.

Hanson, G. J., & Cook, K. R. (2004). Apparatus, test procedures, and analytical methods to measure soil erodibility in situ. Applied Engineering in Agriculture, 20(4).

Hashemi, S., Shiri, H., & Dong, X. (2022). The influence of layered soil on ice-seabed interaction: Soft over stiff clay. Applied Ocean Research, 120. https://doi.org/10.1016/j.apor.2021.103033

Héquette, A., Desrosiers, M., Hill, P. R., & Forbes, D. L. (2001). The influence of coastal morphology on shoreface sediment transport under storm-combined flows, Canadian Beaufort Sea. Journal of Coastal Research, 17(3).

Hoque, M. A., & Pollard, W. H. (2009). Arctic coastal retreat through block failure. Canadian Geotechnical Journal, 46(10). https://doi.org/10.1139/T09-058

Jaber, R. (2022). Investigation of the Relationships Between Geotechnical Sediment Properties and Sediment Dynamics Using Geotechnical and Geophysical Field Measurements [Ph.D. Dissertation]. Virginia Tech.

Jacobs, W., le Hir, P., van Kesteren, W., & Cann, P. (2011). Erosion threshold of sand-mud mixtures. Continental Shelf Research, 31(10 SUPPL.). https://doi.org/10.1016/j.csr.2010.05.012

Jakobsson, M., Mayer, L. A., Bringensparr, C., Castro, C. F., Mohammad, R., Johnson, P., Ketter, T., Accettella, D., Amblas, D., An, L., Arndt, J. E., Canals, M., Casamor, J. L., Chauché, N., Coakley, B., Danielson, S., Demarte, M., Dickson, M. L., Dorschel, B., … Zinglersen, K. B. (2020). The International Bathymetric Chart of the Arctic Ocean Version 4.0. Scientific Data, 7(1). https://doi.org/10.1038/s41597-020-0520-9

Jones, B. M., Arp, C. D., Jorgenson, M. T., Hinkel, K. M., Schmutz, J. A., & Flint, P. L. (2009). Increase in the rate and uniformity of coastline erosion in Arctic Alaska. Geophysical Research Letters, 36(3). https://doi.org/10.1029/2008GL036205

Jones, B. M., Hinkel, K. M., Arp, C. D., & Eisner, W. R. (2008). Modern erosion rates and loss of coastal features and sites, Beaufort Sea coastline, Alaska. Arctic, 61(4). https://doi.org/10.14430/arctic44

Kamphuis, J. W., & Hall, K. R. (1983). Cohesive Material Erosion by Unidirectional Current. Journal of Hydraulic Engineering, 109(1). https://doi.org/10.1061/(asce)0733-9429(1983)109:1(49)

Lantuit, H., & Pollard, W. H. (2008). Fifty years of coastal erosion and retrogressive thaw slump activity on Herschel Island, southern Beaufort Sea, Yukon Territory, Canada. Geomorphology, 95(1–2). https://doi.org/10.1016/j.geomorph.2006.07.040

Lesser, G. R., Roelvink, J. A., van Kester, J. A. T. M., & Stelling, G. S. (2004). Development and validation of a three-dimensional morphological model. Coastal Engineering, 51(8–9). https://doi.org/10.1016/j.coastaleng.2004.07.014

Lucking, G., Stark, N., Lippmann, T., & Smyth, S. (2017). Variability of in situ sediment strength and pore pressure behavior of tidal estuary surface sediments. Geo-Marine Letters, 37(5). https://doi.org/10.1007/s00367-017-0494-6

Lunne, T., Powell, J. J. M., & Robertson, P. K. (2002). Cone Penetration Testing in Geotechnical Practice. In Cone Penetration Testing in Geotechnical Practice. https://doi.org/10.1201/9781482295047

Macdonald, R. W., Kuzyk, Z. Z. A., & Johannessen, S. C. (2015). The vulnerability of Arctic shelf sediments to climate change. In Environmental Reviews (Vol. 23, Issue 4). https://doi.org/10.1139/er-2015-0040

Malito, J., Eidam, E., & Nienhuis, J. (2022). Increasing Wave Energy Moves Arctic Continental Shelves Toward a New Future. Journal of Geophysical Research: Oceans, 127(9). https://doi.org/10.1029/2021JC018374

Mayne, P. W., & Peuchen, J. (2018, June). CPTu bearing factor Nkt for undrained strength evaluation in clays. Proceedings of Cone Penetration Testing 2018 (CPT ’18). https://www.researchgate.net/publication/326838102

Mioduszewski, J., Vavrus, S., & Wang, M. (2018). Diminishing Arctic sea ice promotes stronger surface winds. Journal of Climate, 31(19). https://doi.org/10.1175/JCLI-D-18-0109.1

Mitchell, J. K. (1964). Shearing Resistance of Soils as a Rate Process. Journal of the Soil Mechanics and Foundations Division, 90(1). https://doi.org/10.1061/jsfeaq.0000593

Mulukutla, G. K., Huff, L. C., Melton, J. S., Baldwin, K. C., & Mayer, L. A. (2011). Sediment identification using free fall penetrometer acceleration-time histories. Marine Geophysical Research, 32(3). https://doi.org/10.1007/s11001-011-9116-2

National Academy of Sciences Engineering and Medicine. (2019). Relationship Between Erodibility and Properties of Soils. The National Academic Press. https://doi.org/10.17226/25470

Nematzadeh, A., & Shiri, H. (2020). The influence of non-linear stress-strain behavior of dense sand on seabed response to ice gouging. Cold Regions Science and Technology, 170. https://doi.org/10.1016/j.coldregions.2019.102929

Nielsen, D. M., Pieper, P., Barkhordarian, A., Overduin, P., Ilyina, T., Brovkin, V., Baehr, J., & Dobrynin, M. (2022). Increase in Arctic coastal erosion and its sensitivity to warming in the twenty-first century. Nature Climate Change, 12(3). https://doi.org/10.1038/s41558-022-01281-0

Norton, D. & Weller, G. (1984). The Beaufort Sea: Background, History, and Perspective. https://doi.org/10.1016/B978-0-12-079030-2.50007-1.

Nürnberg, D., Wollenburg, I., Dethleff, D., Eicken, H., Kassens, H., Letzig, T., Reimnitz, E., & Thiede, J. (1994). Sediments in Arctic sea ice: Implications for entrainment, transport and release. Marine Geology, 119(3–4). https://doi.org/10.1016/0025-3227(94)90181-3

Osborne, P. D., & Forest, A. (2016). Sediment dynamics from coast to slope - Southern Canadian Beaufort Sea. Journal of Coastal Research, 1(75). https://doi.org/10.2112/SI75-108.1

Overeem, I., Anderson, R. S., Wobus, C. W., Clow, G. D., Urban, F. E., & Matell, N. (2011). Sea ice loss enhances wave action at the Arctic coast. Geophysical Research Letters, 38(17). https://doi.org/10.1029/2011GL048681

Overeem, I., & Syvitski, J. P. M. (2010). Shifting discharge peaks in arctic rivers, 1977-2007. Geografiska Annaler, Series A: Physical Geography, 92(2). https://doi.org/10.1111/j.1468-0459.2010.00395.x

Peck, G. (1962). Bearing Theories Related to Model Tests on a Remoulded Clay [M.Eng. Thesis]. McGill University.

Piliouras, A., Lauzon, R., & Rowland, J. C. (2021). Unraveling the Combined Effects of Ice and Permafrost on Arctic Delta Morphodynamics. Journal of Geophysical Research: Earth Surface, 126(4). https://doi.org/10.1029/2020JF005706

Rachold, V., Grigoriev, M. N., Are, F. E., Solomon, S., Reimnitz, E., Kassens, H., & Antonow, M. (2000). Coastal erosion vs riverine sediment discharge in the Arctic shelf seas. International Journal of Earth Sciences, 89(3). https://doi.org/10.1007/s005310000113

Randolph, M. (2004). Characterisation of soft sediments for offshore applications. Proc. 2nd Int. Conf. on Site Characterisation, Porto, 1.

Randolph, M., & Hope, S. (2004). Effect of cone velocity on cone resistance and excess pore pressures. In T. Matsui, Y. Tanaka, & M. Mimura (Eds.), Proceedings of the IS Osaka - Engineering Practice and Performance of Soft Deposits. Yodogawa Kogisha Co. Ltd.

Reimnitz, E., Barnes, P. W., Toimil, L. J., & Melchior, J. (1977). Ice gouge recurrence and rates of sediment reworking, Beaufort Sea, Alaska. Geology, 5(7). https://doi.org/10.1130/0091-7613(1977)5<405:IGRARO>2.0.CO;2

Reimnitz, E., Graves, S. M., Barnes, P. W., & Survey, U. S. G. (1985). Beaufort Sea coastal erosion, shoreline evolution, and sediment flux. In Open-File Report. https://doi.org/10.3133/ofr85380

Robertson, P. K., & Cabal, K. L. (2010). Guide to Cone Penetration Testing for Geotechnical Engineering. Gregg Drilling & Testing, Inc.

Shafii, I., Briaud, J. L., Chen, H. C., & Shidlovskaya, A. (2016). Relationship between soil erodibility and engineering properties. Scour and Erosion - Proceedings of the 8th International Conference on Scour and Erosion, ICSE 2016. https://doi.org/10.1201/9781315375045-134

Shields, I. A. (1936). Anwendung der Aehnlichkeitsmechanik und der Turbulenzforschung auf die Geschiebebewegung. [English title: Application of similarity principles and turbulence research to bed-load movement]. Preussische Versuchsanstalt Für Wasserbau Und Schiffbau, 26.

Simon, A., Thomas, R. E., & Research Associate, P. (2010). Comparison and Experience with Field Techniques to Measure Critical Shear Stress and Erodibility of Cohesive Deposits. 2nd Joint Federal Interagency Conference.

Soulsby, R. L., & Whitehouse, R. J. S. (1997). Threshold of sediment motion in coastal environments. Proceedings Pacific Coasts and Ports 1997 Conference, 1(c).

Stark, N., Hay, A. E., & Trowse, G. (2014). Cost-effective geotechnical and sedimentological early site assessment for ocean renewable energies. 2014 Oceans - St. John's, OCEANS 2014. https://doi.org/10.1109/OCEANS.2014.7003004

Stark, N., Quinn, B., Ziotopoulou, K., & Lantuit, H. (2015). Geotechnical investigation of pore pressure behavior of muddy seafloor sediments in an arctic permafrost environment. Proceedings of the International Conference on Offshore Mechanics and Arctic Engineering - OMAE, 1. https://doi.org/10.1115/OMAE2015-41583

Stark, N., Radosavljevic, B., Quinn, B., & Lantuit, H. (2017). Application of portable free-fall penetrometer for geotechnical investigation of arctic nearshore zone. Canadian Geotechnical Journal, 54(1). https://doi.org/10.1139/cgj-2016-0087

Stark, N., Staelens, P., Hay, A. E., Hatcher, B., & Kopf, A. (2014). Geotechnical investigation of coastal areas with difficult access using portable free-fall penetrometers. Proceedings of the CPT, 14, 12–14.

Stoll, R. D., Sun, Y. F., & Bitte, I. (2007). Seafloor properties from penetrometer tests. IEEE Journal of Oceanic Engineering, 32(1). https://doi.org/10.1109/JOE.2007.890943

van Ledden, M., van Kesteren, W. G. M., & Winterwerp, J. C. (2004). A conceptual framework for the erosion behavior of sand-mud mixtures. Continental Shelf Research, 24(1). https://doi.org/10.1016/j.csr.2003.09.002

van Rijn, L. C. (2007). Unified View of Sediment Transport by Currents and Waves. II: Suspended Transport. Journal of Hydraulic Engineering, 133(6). https://doi.org/10.1061/(asce)0733-9429(2007)133:6(668)

van Rijn, L. C. (2020). Erodibility of Mud–Sand Bed Mixtures. Journal of Hydraulic Engineering, 146(1). https://doi.org/10.1061/(asce)hy.1943-7900.0001677

Wahl, T. L. (2021). Methods for analyzing submerged jet erosion test data to model scour of cohesive soils. Transactions of the ASABE, 64(3). https://doi.org/10.13031/TRANS.14212

Wardinski, K. M., Guertault, L., Fox, G. A., & Castro-Bolinaga, C. F. (2018). Suitability of a Linear Model for Predicting Cohesive Soil Detachment during Jet Erosion Tests. Journal of Hydrologic Engineering, 23(9). https://doi.org/10.1061/(asce)he.1943-5584.0001690

Wegner, C., Bennett, K. E., de Vernal, A., Forwick, M., Fritz, M., Heikkilä, M., Łącka, M., Lantuit, H., Laska, M., Moskalik, M., O'Regan, M., Pawłowska, J., Promińska, A., Rachold, V., Vonk, J. E., & Werner, K. (2015). Variability in transport of terrigenous material on the shelves and the deep Arctic Ocean during the Holocene. In Polar Research (Vol. 34, Issue 1). https://doi.org/10.3402/polar.v34.24964

White, D. J., O'Loughlin, C. D., Stark, N., & Chow, S. H. (2018). Interpretation of free fall penetrometer tests in sands : An approach to determining the equivalent static resistance. Cone Penetration Testing 2018, June.

Winterwerp, J. C., van Kesteren, W. G. M., van Prooijen, B., & Jacobs, W. (2012). A conceptual framework for shear flow–induced erosion of soft cohesive sediment beds. Journal of Geophysical Research: Oceans, 117. https://doi.org/10.1029/2012JC008072

Yang, S., Lacasse, S., & Sandven, R. (2005). Determination of the Transitional Fines Content of Mixtures of Sand and Non-plastic Fines. Geotechnical Testing Journal, 29(2). https://doi.org/10.1520/GTJ14010

Chapter 6: Conclusions and Outlook

6.1. Conclusions

The following subsections specifically detail the conclusions of this work in relation to the research hypotheses proposed in Chapter 1.

6.1.1. Geotechnical properties of in-situ coastal and nearshore sediments such as relative density, moisture content, and bearing capacity can be measured in an easily deployable, and spatially rapid manner.

Advances were made in the measurement capacity of each property mentioned in this hypothesis, specifically for beach environments (Chapter 3). Relative density was measured successfully in an intertidal environment using small tubes of know volume of approximately 10cm pushed into the beach face and carefully dug out (Figure 3.2). This sampling technique served the dual purpose of allowing for density sampling as well as the collection of a physical sample for grain size analysis (Figure 3.5). Moisture content was found to be measurable using commercially available sensors. However, these sensors must be properly calibrated to mitigate the effects of seawater on the measurements. A simple laboratory calibration proved effective at reducing these effects and was applied to field data (Appendix B). Bearing capacity estimates obtained from PFFP measurements in partially saturated intertidal environments were derived using a velocity dependent strain rate correction factor (Figure 3.13). This factor provided estimates of bearing capacity that closely matched results obtained from a partially saturated bearing capacity theory for a majority of the crosshore profile with the exception of the swash zone (Figure 3.14).

6.1.2. Geotechnical properties of foreshore and nearshore continental shelf sediments vary in response to local geomorphodynamics along the crosshore beach profile and across other morphologic features. Quantifying these variations is key to understanding the complex relationships between sediment properties, morphology, and hydrodynamics.

Large variations in sediment properties occur along the crosshore intertidal beach profile (Chapters 3 & 4). Moisture content increases from dry to fully saturated from dune to swash (Figure 3.7), relative density is highest at the dune and swash and tends to be very loose in the intertidal zone (Figure 3.6). Moisture content variability is tied to tides and meteorological effects, and relative density was highest at the dune and swash, highlight how local hydrodynamics and geomorphology drive variations in sediment properties. Firmness factor and $qsbc$ obtained from PFFP measurements were correlated with void ratio, bulk density, and moisture content. While

there was spread in the data, the results indicated that PFFP deployments could be used as another tool for quantifying variations in these properties (Figure 4.6). Void ratio was also correlated with morphodynamic change in beach bed level in response to hydrodynamic forcing. In areas where deposition was observed, if the initial void ratio classified the sediment as loose, the sediment typically remained loose, whereas sediments that were initially dense transitioned from a dense state to a looser state as deposition occurred. It is also postulated that the opposite trend is true for erosion areas, where initially loose sand will densify, and dense areas will remain dense. These trends are summarized in the flowchart shown in Figure 4.10. These results show the ability to quantify variations in sediment properties (using sampling and the PFFP) and why measuring these variations is important. In nearshore areas and continental shelf systems, PFFPs can be used for rapid sediment classification in terms of strength, soil behavior, and erodibility (Figure 5.6). The ability to quantify variations in all these properties over large areas will significantly improve our ability to implement accurate sediment property information into numerical models, an important step in characterizing the in-situ properties of a site.

6.1.3. Considering geotechnical properties as significant variables in erodibility relations can improve our understanding and prediction of coastal morphodynamics.

Geotechnical properties were found to be related to erodibility (Chapters 4 & 5). For sandy beaches and non-cohesive submerged sediments, packing state in the form of void ratio and relative density was correlated with k_d, an erosion parameter that describes the erosion rate once sediment motion has been initiated (Figure 4.8). Additionally, k_d was found to be well correlated with FF and $qsbc$ from PFFP measurements (Figure 4.8). It was shown that beach areas with high initial void ratios had higher values of k_d, meaning more sediment was available to be mobilized during hydrodynamic forcing, and vice versa with low void ratios. For mixed sediment nearshore environments, s_u from a PFFP was strongly correlated with k_d (Figure 5.7). Further, using the relationships found for sandy sediments combined with the s_u relationships for cohesive sediments, a categorical framework was developed to determine different levels of erodibility from only PFFP measurements (Figure 5.11). The results introduce new relationships between sediment properties and erodibility developed during the study and highlight the possible variability of geomechanical properties including erodibility of seafloor sediments that is rarely reflected in to-date's predictions or modelling of sediment dynamics (Appendix G).

6.2. Outlook

This work represents an advancement in the measurement capability of geotechnical sediment properties in coastal/nearshore environments. Specifically, advancements have been made in assessing both sediment strength properties and erodibility parameters, and the results of this work have shown the importance quantifying these properties in-situ by demonstrating significant variability in coastal and offshore environments. This study showed how PFFP's can be used to estimate aspects of erodibility. This ability is a large step forward in the area of coastal field research as it will allow for rapid characterization of sites both in terms of sediment properties, but also in terms of erodibility. As seen in the results section of Chapter 3, PFFP estimates of bearing capacity using a new type of modified strain rate correction correlated well with a partially saturated bearing capacity model. The exception were sites in the swash zone where high water contents caused further strain rate effects due to undrained drainage conditions. Similar issues related to drainage have been addressed for fully saturated submerged sediments using strain-rate correction factors, but the effects of partial saturation at high water content serves to further exacerbate these effects. Improving swash zone strain-rate correction would give the PFFP the distinction of being able to measure sediment strength from the dune toe past the depth of closure without interruption, and currently the only area where these measurements are unreliable is in the swash zone. Continuing on PFFP improvements in beach environments, there was a positive correlation between density, $qsbc$, and moisture content, although there was large spread in the data. Reducing the spread in this data would allow for prediction of density and/or moisture content from PFFP beach deployments, which would then allow for direct prediction of k_d from the PFFP, saving time and sampling effort required to measure densities in-situ. To summarize, further areas of research for PFFP measurements on beaches include better characterization of strain-rate effects due to partial saturation in the swash zone and using PFFP deployments to predict in-situ packing state parameters and/or moisture content. Understanding how swash and backwash processes change sediment properties on a wave-by-wave basis through induced pore pressure changes is an area of active research and could be key to better understanding of PFFP data analysis in this zone (Turner and Nielsen 1997, Florence 2022). Finally, τ_c was not found to be related to any PFFP measurements on the beach or in the nearshore for both sands and mixed sediments. While this is less important for sandy areas as results showed initiation of motion was secondary to erosion rates, modelling analysis showed that τ_c was a more controlling parameter for long-term

morphological evolution. The research highlighted in section 1.2.3 showed examples of soil properties related to τ_c, suggesting that combining PFFP measurements and laboratory measures of τ_c which also measure soil properties could close this gap (National Academy of Science and Engineering 2019). Focusing future research on relating PFFP measurements to τ_c would give the PFFP the ability to give a complete picture of sediment properties prior to erosion, the initiation of motion, and the behavior once erosion has begun.

References

Florence, M. (2022). Wave Induced Vertical Pore Pressure Gradients at Sandy Beaches. [Ph.D. Dissertation]. Virginia Tech.

National Academy of Sciences Engineering and Medicine. (2019). *Relationship Between Erodibility and Properties of Soils*. The National Academic Press. https://doi.org/10.17226/25470

Turner, I. L., & Nielsen, P. (1997). Rapid water table fluctuations within the beach face: Implications for swash zone sediment mobility? *Coastal Engineering*, *32*(1). https://doi.org/10.1016/s0378-3839(97)00015-x

Appendix A: Data Repository Information

A.1. Dataset Citation

This appendix contains information related to the repository where all data data and the results of the analysis conducted in this research are stored. The datasets related to the field surveys in Duck, NC have been submitted to the Virgina Tech Data Repository (VTechData). This dataset is officially published and can be accessed using the following DOI link:

https://doi.org/10.7294/22329502

The datasets collected in Harrison Bay, AK will be published on the Arctic Data Center (https://arcticdata.io/catalog/data). Once published this dataset will be available using the following DOI link: https://doi.org/10.18739/A2JD4PQ9T with the citation:

Nicola Brilli, Nina Stark, & Emily Eidam. (2023). Alaskan Beaufort Shelf Sediment Study – Harrison Bay: Geotechnical Properties from a Portable Free-Fall Penetrometer and Erodibility Assessment, 2021-2022. Arctic Data Center. doi:10.18739/A2JD4PQ9T.

A.2. ReadMe File (VTechData)

Title of Dataset: Data Associated with Influence of Geotechnical Properties on Sediment Dynamics, Erodibility, and Geomorphodynamics in Coastal Environments Based on Field Measurements
Author(s): Nicola Brilli, Nina Stark, Celso Castro-Bolinaga
Categories: Civil Geotechnical Engineering
Group: Civil and Environmental Engineering
Item Type: Dataset
Keywords: Geotechnical properties, Erodibility, Free-Fall Penetrometer, Field Measurement Techniques, Sand Beaches
Description: Field and laboratory data collected for the purpose of geotechnical site characterization and erodibility assessment at a field site in Duck, NC. Files in this dataset include raw and processed data, summary spreadsheets, and codes needed to replicate results.
Funding: CAREER: Improving the Understanding of Coastal Erosion during Extreme Events and with Sea Level Rise through Geotechnical Investigation
Resource Title: Will be added after manuscript is accepted
Resource DOI: Will be added after manuscript is accepted
Other References:
License: CC0 1.0 Universal (CC0 1.0) Public Domain Dedication
Publisher: University Libraries, Virginia Tech
Location: 1. The U.S. Army Corps of Engineers Field Research Facility (USACE FRF) site in Duck, North Carolina. The coordinates are: 36.182101°N, 75.751282°W
Corresponding Author Name: Nicola Brilli
Corresponding Author E-mail Address: nickb96@vt.edu

Files/Folders in Dataset and Description of Files
Each sub folder details the field and laboratory data from a specific field survey. README files are included in each folder to describe the contents.
[DUNEX 2019 - Duck NC] - All data related to the DUNEX field survey in October 2019.
[DUNEX 2021 - Duck NC] - All data related to the DUNEX field survey in October 2021.

A.3. ReadMe File (Arctic Data Center)

Title of Dataset: Alaskan Beaufort Shelf Sediment Study – Harrison Bay: Geotechnical Properties from a Portable Free-Fall Penetrometer and Erodibility Assessment, 2021-2022
Author(s): Nicola Brilli, Nina Stark, Emily Eidam
Abstract: This dataset comprises the geotechnical data from a series of surveys conducted in Harrison Bay, Alaska in July/August of 2021 & 2021. The contribution of this specific dataset to the overall project goals was connecting geotechnical sediment properties to erodibility parameters in an Arctic coastal environment. During the 2021 survey, geotechnical sediment properties from a portable-free fall penetrometer (PFFP) were related to physical sampling to develop a regional sediment classification scheme, and the data collected during the 2022 survey aimed to connect the results from the previous year to laboratory-based erodibility parameters from the Jet Erosion Test (JET), which was conducted on gravity core samples taken from the site. The attached repository contains both raw and processed data, and the specifics of the file structure can be found in the readMe.txt file.
Keywords: Geotechnical, Portable Free-fall Penetrometer, Jet Erosion Test, Harrison Bay, Erosion
Geographic Description: Harrison Bay, Alaska
Bounding Coordinates:
North: 71.003770 degrees
South 70.324847 degrees
East: -149.874718 degrees
West: -152.410185 degrees
Date Range: July 28th – August 9th, 2021 & August 2nd – August 7th, 2022
Funding: Collaborative research: Arctic Shelf sediment fate - an observational and modeling study of sediment pathways and morphodynamic feedbacks in a changing polar environment
National Science Foundation Award #: OPP-1912863
National Science Foundation Award #: OPP-1913195
Ethical Research Practices: All necessary permits were obtained for location access and survey activities in both 2021 and 2022. Permits included access to Prudhoe Bay West Dock where the survey vessel was anchored. PI Eidam completed National Transportation Safety Council training to operate a vehicle through the secure area, and all members of the survey team obtained access cards through Hilcorp. All COVID regulations in place were followed when applicable. Additionally, even though the survey took place in federal waters, PI Eidam obtained a draft development permit from the North Slope Borough in good faith with regard to the survey activities in the area. Polar bears, whales, and other sensitive marine life were avoided throughout the course of the survey.

Appendix B: A Simple Laboratory Calibration for Mitigating Seawater Effects on Soil Moisture Sensors

The contributions of the authors to the composition of this manuscript are delineated as follows:

Nicola Brilli:
- Collected field data
- Conducted laboratory analysis
- Processed/analyzed field and laboratory data, prepared figures, and draft of manuscript
- Revised manuscript based on suggestions of co-authors

Nina Stark:
- Co-developed research questions and methodology
- Assisted in planning of field data collection
- Reviewed and edited the draft manuscript

Britt Raubenhiemer:
- Co-developed research questions and methodology
- Assisted in planning of field data collection
- Reviewed and edited the draft manuscript

Steve Elgar:
- Co-developed research questions and methodology
- Assisted in planning of field data collection
- Reviewed and edited the draft manuscript

Bennet Korka:
- Conducted laboratory analysis
- Reviewed and edited the draft manuscript

A Simple Laboratory Calibration for Mitigating Seawater Effects on Soil Moisture Sensors

Nicola C. Brilli[1] , Nina Stark[2], Ph.D., Britt Raubenhiemer[3], Ph.D., Steve Elgar[4], Ph.D., Bennet Korka[5]

[1]Virginia Tech, Department of Civil and Environmental Engineering, Blacksburg, VA 24060; e-mail: nickb96@vt.edu

[2]Virginia Tech, Department of Civil and Environmental Engineering, Blacksburg, VA 24060; e-mail: ninas@vt.edu

[3]Woods Hole Oceanographic Institute, Applied Ocean Physics and Engineering, Woods Hole, MA 02543, email: braubenhiemer@whoi.edu

[4]Woods Hole Oceanographic Institute, Applied Ocean Physics and Engineering, Woods Hole, MA 02543, email: elgar@whoi.edu

[5]Virginia Tech, Department of Civil and Environmental Engineering, Blacksburg, VA 24060; e-mail: bkorka@vt.edu

The authors of this extended abstract submitted it to the Proceedings of the 37th International Conference on Coastal Engineering, Sydney, Australia, December 4-9th, 2022

B.1. Extended Abstract

INTRODUCTION

The importance of moisture content for sediment dynamics in coastal environments is well documented, particularly in reference to aeolian sediment transport (Davidson-Arnott, 2005). Tidally-induced changes in moisture content in partially saturated environments, such as beaches, cause significant changes in surface shear strength through the development of suction stresses, which can affect erodibility (Sassa and Watabe, 2007). Thus, the accurate measurement of moisture content in these environments is important for determination of strength properties and for predicting sediment transport. Most moisture sensors work by measuring dielectric permittivity, the ability to carry electric charge, of the substrate, which is proportional to the moisture content. However, most moisture sensors are not calibrated for seawater, which has a higher dielectric permittivity than freshwater, causing overestimation of the moisture content. Therefore, the goal of this study is to develop and demonstrate a laboratory calibration scheme to account for this overestimation, and thus to allow for more accurate measurements of moisture content in coastal environments.

METHODS

To keep density constant a fixed amount of sediment was mixed with the desired volume of water to reach the target water content for each test. The sediment was compacted into a plastic container of known volume, burying the sensor and packing completely around it. Sensor readings were taken to give the measured moisture content. Afterwards, the full sample was weighed and dried to obtain the true moisture content. The tests were repeated by varying the moisture content from 0%-35%, with 35% moisture by volume being experimentally determined as fully saturated. Each of the 4 full sets of tests was run at a constant salinity and changing the salinity between sets of tests from fresh (0 PSS) to 30 PSS in increments of 10 PSS.

LABORATORY RESULTS

The true freshwater moisture content was represented best by a linear fit to the measured water content (blue line in Figure B.1). Salinities in the 10-20 PSS range behaved similarly as freshwater up until approximately 15% true moisture content by volume, beyond which the moisture content was overestimated by the sensor, and thus a bilinear fit gave the best results (green and yellow

curves in Figure B.1). At a salinity of 30 PSS, the moisture contents consistently were overestimated by the sensor, and a polynomial fit was selected to represent the calibration (red curve in Figure B.1).

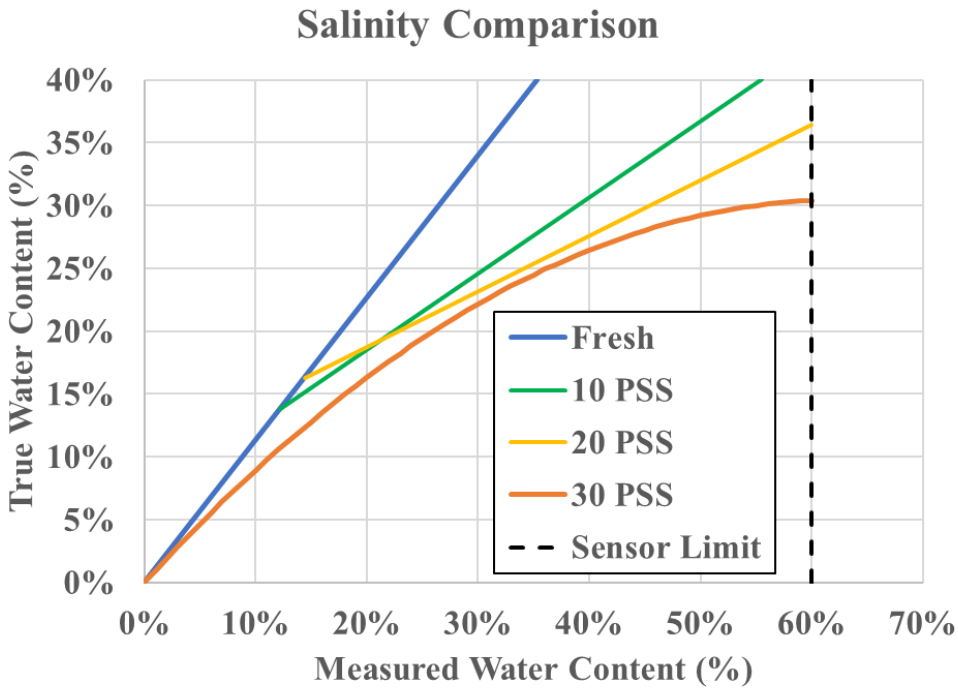

Figure B.1: True water content versus measured water content for different salinities (listed in the legend).

FIELD RESULTS

In addition to the laboratory calibration, a field data set was collected in December 2020 in Duck, NC. A vertical array of four sensors was buried in the beach over a 2-day period to observe the tidally induced change in groundwater level. For a 6-hour time series of data over one tidal cycle, the surface sensor (Figure B.2, blue curve) measured a series of wave runup events at high tide, and the sensor at 20 cm depth (Figure B.2, red curve) also measured the tidally induced groundwater fluctuations. The two deepest sensors at 40 and 60 cm were relatively constant (green and black curves, Figure B.2), implying that they were permanently below the water table and fully saturated. However, based on the soil properties the theoretical range of water contents at which the soil is fully saturated (the dashed area in Figure B.2). shows the overestimation of water content caused by seawater.

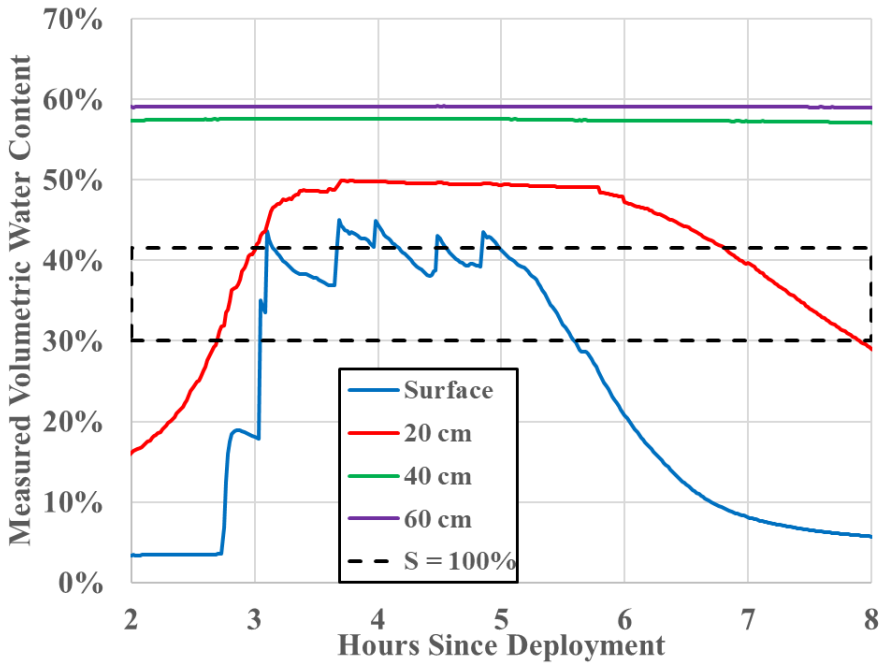

Figure B.2: Measured volumetric water content for a vertical array of buried moisture sensors versus time.

These values were determined using the theoretical minimum and maximum void ratios for the sand found at the site, having been determined via ASTM D4253 and ASTM D4254. With the range of possible void ratios, minimum and maximum gravimetric water content at saturation was computed via:

$$w = \frac{Se}{G_s} \tag{B.1}$$

where w is the gravimetric water content, S is the degree of saturation (assumed equal to 1 for full saturation), e is the void ratio, and G_s is the specific gravity of the sediment, taken as 2.65 for the quartz sand found at the site. Gravimetric water content differs from volumetric water content (measured by the sensor) in that it represents the water content as the weight of water for a given weight of sediment, rather than using the volume of water in a given volume of sediment, air, and water. The two types of water content are related by:

$$\theta = \frac{w\rho_b}{\rho_w} \tag{B.2}$$

where θ is the volumetric water content, ρ_b is the bulk density of the sediment, obtained using the measured void ratios, and ρ_w is the density of water. Using this analysis, the minimum

volumetric water content for saturation was found to be $\theta = 30\%$, and the maximum was found to be $\theta = 41.5\%$. The upper bound value of θ also can be thought of as the maximum water content the soil theoretically can sustain (maximum possible pore volume).

The knowledge of the range of possible water contents for full saturation highlights the main problem with overestimation of water contents due to seawater. A majority of the measurements lie above the upper bound (dashed line in Figure B.2), suggesting that the in-situ water content is higher than the maximum possible water content, which is not realistic. Without proper calibration, these data do not depict a physically possible scenario, and are therefore of little use. The same timeseries of data, with the calibration from Figure 1 applied. (Figure B.3) provides a more realistic depiction of the in-situ water contents.

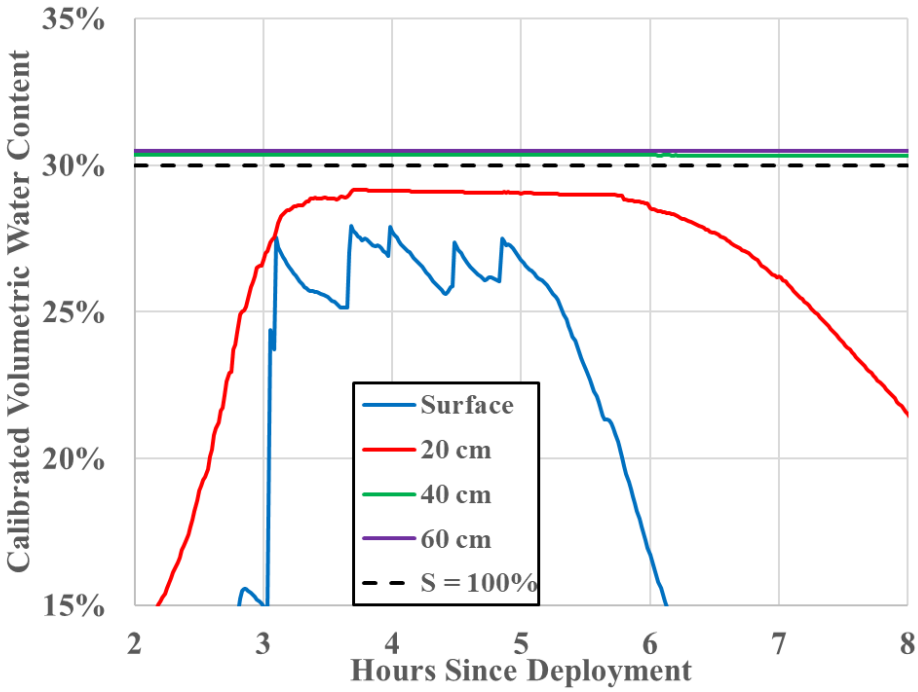

Figure B.3: Calibrated volumetric water content for a vertical array of buried moisture sensors versus time.

The surface and 20 cm depth sensors are below the lower bound dashed line, suggesting that they are not fully saturated and are measuring tidal and wave-induced fluctuations in water level (Figure B.3, red and blue curves). Additionally, the 40 and 60 cm depth sensors (Figure B.3, green and purple curves), which were believed to be below the permanent water table due to being constant value over the tidal cycle, now fall within the range of possible water contents for full saturation

(above lower bound dashed line). This example using a field data set highlights the necessity and usefulness of calibrating moisture sensors for the effects of seawater. The calibration scheme was successful in mitigating the overestimation of moisture content in field observations in a saline environment.

CONCLUSIONS

A calibration scheme that mitigates the overestimation of moisture content in the presence of saline water was developed in the laboratory and used with field data. The results suggest it is possible to collect accurate moisture content in coastal environments. Future work will use this calibration scheme to gain a better understanding of geomorphodynamics in beach environments by studying the relationship between moisture content, other sediment strength properties, and hydrodynamically-induced bed-level change.

ACKNOWLEDGEMENTS

This work was funded by the National Science Foundation (CMMI, EAR, PO), the U.S. Coastal Research Program., and a Vannever Bush Faculty Fellowship. The authors also thank the staff at the USACE FRF for support in field data collection.

REFERENCES

ASTM D2453-16. Standard Test Methods for Maximum Index Density and Unit Weight of Soils Using a Vibratory Table. ASTM International, West Conshohocken, PA.

ASTM D2454-00. Standard Test Methods for Minimum Index Density and Unit Weight of Soils and Calculation of Relative Density. ASTM International, West Conshohocken, PA.

Davidson-Arnott, MacQuarrie, Aagaard (2005). The effect of wind gusts, moisture content and fetch length on sand transport on a beach. Geomorphology, vol. 68.

Sassa, Watabe, (2007). Role of suction dynamics in evolution of intertidal sandy flats: Field evidence, experiments, and theoretical model. Journal of Geophysical Research: Earth Surface., vol. 112.

Appendix C: Variations in Sediment Properties on the Alaskan Beaufort Shelf using a Portable Free-Fall Penetrometer

The contributions of the authors to the composition of this manuscript are delineated as follows:

Nicola Brilli:
- Participated in the field survey in Harrison Bay, Alaska
- Conducted laboratory analysis
- Processed/analyzed field and laboratory data, prepared figures, and abstract/presentation
- Revised submission based on suggestions of co-authors

Nina Stark:
- Co-developed research questions and methodology
- Assisted in planning of field data collection
- Reviewed and edited the submission drafts

Emily Eidam:
- Planned and participated in the field survey in Harrison Bay, Alaska as Chief Scientist
- Co-developed research questions and methodology
- Reviewed and edited the submission drafts

Dan Duncan:
- Participated in the field survey in Harrison Bay, Alaska
- Reviewed and edited the submission drafts

Josephine Hall:
- Participated in the field survey in Harrison Bay, Alaska
- Reviewed and edited the submission drafts

Variations in Sediment Properties on the Alaskan Beaufort Shelf using a Portable Free-Fall Penetrometer

Nicola C. Brilli[1] , Nina Stark[2], Ph.D., Emily Eidam[3], Ph.D., Dan Duncan[4], Josephine Hall[5]

[1]Virginia Tech, Department of Civil and Environmental Engineering, Blacksburg, VA 24060; e-mail: nickb96@vt.edu

[2]Virginia Tech, Department of Civil and Environmental Engineering, Blacksburg, VA 24060; e-mail: ninas@vt.edu

[3]Oregon State University, College of Earth, Ocean, and Atmospheric Sciences, Corvallis, OR 97333; email: emily.eidam@oregonstate.edu

[4]University of Texas Institute of Geophysics, Jackson School of Geosciences, Austin, TX 78704; email: dduncan@ig.utexas.edu

[5]University of North Caroline at Chapel Hill, Department of Earth, Marine, and Environmental Sciences, Chapel Hill, NC 27514; email: jhall1@unc.edu

The authors of this abstract submitted it to the Proceedings of the Ocean Sciences Meeting 2022, Honolulu, HI, February 24th – March 4th, 2022

C.1. Abstract

Changing environmental conditions in the Arctic have led to decreased seasonal sea ice, which increases open water available to generate wind-driven wave energy and currents. Additionally, sediment input into continental shelf systems is increasing from bluff erosion and higher river sediment yields. Part of understanding how these environmental changes will drive changes in local sediment dynamics is collecting information on the geotechnical properties of the seabed sediments and characterizing the local sediment variability. This study aims to provide a first step towards that goal, using a data set collected in July/August 2021 on the Alaskan Beaufort Shelf. Portable free-fall penetrometers (PFFP's) are a robust tool for in-situ geotechnical testing as they are lightweight, rapidly deployed, and cost-efficient. A PFFP was deployed approximately 600 times at 78 unique locations throughout the study area, with 5-25 deployments at each location. The study sites included stations along four offshore directed transects, a focused area around the Coville Delta, as well as broader mapping of the nearshore areas of the Beaufort Sea in Harrison Bay. Physical samples from a Shipek grab sampler were collected at 71 of the sites. Additionally, two transect lines off the Coville Delta and western Harrison Bay were surveyed with continuous PFFP deployments (one deployment approximately every 10-30 meters) to obtain information about smaller scale spatial variations in sediment properties in areas of high sediment input. Initial results show a wide distribution of sediments throughout the bay, including areas of clean sand of various densities, mixed sediments, and consolidated mud. Maximum measured decelerations for sands were on the order of 50-100g, and for muds on the order of 10-30g, where g is gravitational acceleration. Additionally, peat and sediments with high organic content were found in areas close to shore where bluff erosion was present.

Appendix D: Effects of Sediment Strength on Sediment Transport Mechanisms and Morphology of a Dynamic Sandy Spit

The contributions of the authors to the composition of this manuscript are delineated as follows:

Nicola Brilli:

- Participated in the field survey in Yakutat, Alaska
- Processed and analyzed field data, prepared figures, tables, and draft of abstract
- Revised manuscript based on suggestions of co-authors

Nina Stark:

- Lead primary investigator of this study
- Initiated research idea and co-developed the refined research questions
- Planned and supervised the field survey in Yakutat, Alaska
- Reviewed and edited the draft abstract

Effects of Sediment Strength on Sediment Transport Mechanisms and Morphology of a Dynamic Sandy Spit

Nicola C. Brilli[1] and Nina Stark[2], Ph.D.

[1]Virginia Tech, Department of Civil and Environmental Engineering, Blacksburg, VA 24060; e-mail: nickb96@vt.edu

[2]Virginia Tech, Department of Civil and Environmental Engineering, Blacksburg, VA 24060; e-mail: ninas@vt.edu

The authors of this abstract submitted it to the Proceedings of the 11th Symposium on River, Coastal, and Estuarine Morphodynamics, Auckland, New Zealand, November 16-21st, 2019

D.1. Extended Abstract

INTRODUCTION

In August 2018, a field survey was conducted off the coast of Point Carrew, a sandy spit near Yakutat, Alaska. The spit forms as strong longshore transport NW along the Gulf of Alaska reaches a peninsula at the mouth of Yakutat Bay (Yehle, 1971). Wave refraction around the peninsula deposits the sediment towards the Ankau estuary in the NE (Figure D.1). After an unknown event in 1997 caused 400,000 meters2 to erode, the spit has been steadily accreting at a rate of ~32,000 meters2/yr. A portable free fall penetrometer (PFFP) was deployed along seven transects in the nearshore zone of the spit to determine sediment strength. Using the method developed by Albatal et al. (2019), friction angles (ϕ) and relative densities (Dr) of the surficial seabed sediments were determined. The goal of this paper is to use the obtained strength and packing properties to draw conclusions about the dynamic morphology of the spit by studying their effect on and response to sediment transport processes.

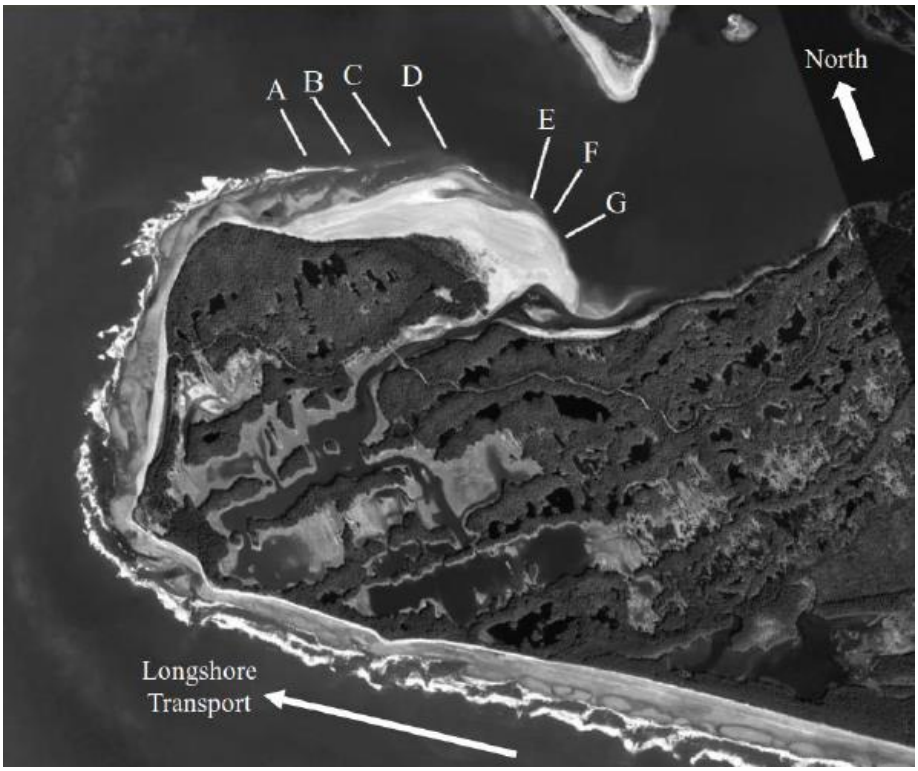

Figure D.1: Site layout (Lettered line = transects) Source: Google Earth (59°32'23.42"N, 139°49'18.09"W)

RESULTS

The deceleration profile produced by the PFFP yields a maximum deceleration and an estimate of bearing capacity (Stark et al. 2012). Relative density is obtained via direct correlation from the deceleration record, and the friction angle is back calculated using the bearing capacity (Albatal et al 2019). The results show higher friction angles and relative densities for transects (E-G) than transects (A-D). Average ϕ and Dr values in the middle of transects A-D were 45° and 23% respectively compared to 53° and 55% for transect E-G.

The area of A-D (N side of the spit) is the location with the highest deposition rate (20,000 meters2/yr) because this side is exposed to the refracting waves and longshore transport. The combination of wave energy and large tidal range (~3m) leads to the formation of intertidal bars (Masselink et al. 2006). Despite the net deposition on the sub-aerial body of the spit, storms, tides, and waves constantly rework the sediment in the intertidal zone, producing these dynamic bars and contributing to high sediment mobility. In contrast, the high accretion rate to the North serves to protect the area of transect E-G thus it receives much lower wave energy and experiences lower deposition rates (2,500 meters2/yr). This prevents the formation of an intertidal bar system, which leaves sediment in this area relatively undisturbed by hydrodynamic processes. Seismic activity would act to consolidate and densify the sediment everywhere on the spit, contributing to high ϕ and DR values. This may be reflected in the results from transects E-G, which are mostly protected from hydrodynamic forcing.

CONCLUSIONS

Transects A-D are subject to constant reworking of surficial sediment and deposition processes by waves and sediment transport as seen by the presence of an intertidal bar system, which is the reason for the lower ϕ and DR values. These processes likely work in a feedback loop by which the lower ϕ and DR sediments are more mobile and enhance sediment transport, and the stronger, stiffer sediments are more resistant to transport mechanisms.

ACKNOWLEDGEMENTS

The authors would like to thank the City and Borough of Yakutat, specifically Rhonda Coston and Irving Grass. Funding was provided by NSF award CMMI-1751463.

REFERENCES

A. Albatal, N. Stark, and B. Castellanos. (2019). Estimating in-situ relative density and friction angle of nearshore sand from portable free fall penetrometer tests. *Canadian Geotechnical Journal*.

G. Masselink, A. Kroon, and R. G. D. Davidson-Arnott, "Morphodynamics of intertidal bars in wave-dominated coastal settings — A review," *Geomorphology,* vol. 73, no. 1, pp. 33-49, 2006/01/01/ 2006.

Stark, N., Wilkens, R., Ernstsen, V. B., Lambers-Huesmann, M., Stegmann, S., & Kopf, A. (2012). Geotechnical properties of sandy seafloors and the consequences for dynamic penetrometer interpretations: quartz sand versus carbonate sand. *Geotechnical & Geological Engineering*, *30*(1), 1-14.

Yehle, L.A. (1971). *Reconnaissance Engineering Geology of the Yakutat Area, Alaska, With Emphasis on Evaluation of Earthquake and Other Geologic Hazards*, Geological Survey Professional Paper No. 1074, prepared for USGS

Appendix E: Geotechnical Investigation of Spatiotemporal Variations at a Sand Beach characterized by Active Erosion and Sediment Remobilization Processes

The contributions of the authors to the composition of this manuscript are delineated as follows:

Nina Stark:

- Lead primary investigator of this study
- Initiated research idea and co-developed the refined research questions
- Planned, supervised, and participated in the field survey in Yakutat, Alaska
- Processed and analyzed field data, prepared figures, tables, and draft of manuscript
- Addressed comments from co-authors & outside reviewers and prepared final manuscript

Nicola Brilli:

- Participated in the field survey in Yakutat, Alaska
- Processed and analyzed field data
- Reviewed and edited the draft manuscript
- Reviewed and edited the response to reviewer comments and the final version of the manuscript

Geotechnical Investigation of Spatiotemporal Variations at a Sand Beach characterized by Active Erosion and Sediment Remobilization Processes

Nina Stark[1], Ph.D. M.ASCE., and Nicola Brilli[2], S.M. ASCE

[1]Virginia Tech, Department of Civil and Environmental Engineering, Blacksburg, VA 24060; e-mail: ninas@vt.edu

[2]Virginia Tech, Department of Civil and Environmental Engineering, Blacksburg, VA 24060; e-mail: nickb96@vt.edu

The authors submitted this manuscript to the Proceedings of the 10th International Conference on Scour and Erosion (ICSE-10), Virtual, October 18-21st, 2021

Reference:
Stark, N., & Brilli, N. C. (2021). Geotechnical Investigation of Spatiotemporal Variations of Moisture Contents in Intertidal Beach Sands and Effects on Coastal Erosion Processes. *Proceedings of the 10th International Conference on Scour and Erosion (ICSE-10)*.

E.1. Abstract

Intertidal beach environments are subject to a number of processes affecting spatiotemporal variations of moisture contents: tides, waves, groundwater level, rainfall, and possibly surge during and after storm events. At sandy beaches with a limited range of grain sizes, grain shapes, and mineralogies, moisture content can represent a key factor governing in-situ strength and erodibility. Here, a first insight is provided into a large field data set comprising geotechnical and environmental data collection from multiples sites. This conference contribution focuses on a subset of measurements collected at the beach of Ocean Cape, Yakutat, Alaska, characterized by a medium sand and an energetic wave climate. The beach features a complex morphology, sometimes exhibiting a ridge-runnel profile and a large cobble to boulder beach step. Co-located measurements of moisture contents, topography, and soil strength are presented, providing a new perspective on the variability of geotechnical properties at a sandy beach of complex geomorphology and active erosion and sediment remobilization processes.

INTRODUCTION

Intertidal beach environments are affected by a complex interaction of hydrodynamics, geomorphodynamics, and sediment dynamics on different temporal and spatial scales. These processes are interlinked as water levels govern the location of the swash zone and waves in the intertidal zone, etc. Local geomorphology impacts groundwater pathways, as well as wave and actual water levels through overall beach slope and presence of more complex geomorphological features such as ridge-runnel systems and even smaller features such as ripples and cusps. Vice versa, the presence of certain geomorphological features can be associated with certain combinations of hydrodynamic conditions and led to summaries of conceptual beach models (e.g., Masselink and Short 1993).

The variability of sediments in the intertidal zone of sand beaches has been observed within one beach system as well as in comparison of different beaches, and there is general consensus on the importance of those local sediment properties on sediment transport processes (Medina et al. 1994; Gallagher et al. 2011, 2016; and others). However, most studies and models relating sediment properties with geomorphodynamics consider sediment particle properties only. The most prominent property is grain size and particle density, being used, for example, for estimating the Shields parameter (Shields 1936; VanRijn 2007). Other models and concepts utilize the particle fall velocity, if actually measured, also accounting for particle shape, and being mostly introduced with focus on sediment transport and deposition (Wright and Short 1984). However, the importance of sediment properties as a bulk material have been stressed increasingly regarding remobilization and post-deposition behavior. For example, VanRijn (2007) highlights the effects of biological and organic materials, cohesive particle-particle interaction on the critical bed shear stress for initiation of motion, and particle packing. Kirchner et al. (1990) stress effects of friction angles of coarse-grained sediments on critical bed shear stress, and Erikson et al. (2007) discuss the role of friction angles regarding beach scarp and dune recession. Moisture content of sands has been identified as a key parameter governing wind erosion of sands at beaches (e.g., Van Dijk et al. 1996; Davidson-Arnott et al. 2005; Darke and Neuman 2008).

In-situ friction angles also control the shear strength of sandy soils for dry or fully saturated sands (e.g., Briaud 2013). For partially saturated sands, an apparent cohesion adds to the shear strength through suction between the sand particles and depends on the moisture content (e.g., Briaud 2013). Friction angles can potentially vary spatially and temporally at beaches through

particle size and shape re-distributions as well as packing and resulting bulk density. Moisture contents are expected to respond rapidly to hydrodynamic conditions as well as rainfall and air humidity, and are also affected by sediment conditions. Therefore, rapid and significant variations in surficial shear strength are expected at sandy beaches and are likely affecting local erosion processes (Sassa et al. 2014; Manning and Stark 2019; Sassa and Yang 2019). However, a more detailed understanding and more observations of variations in shear strength at sandy beach environments are needed to implement such geotechnical properties effectively into sediment transport and erosion models and predictions.

A large field data set including moisture content measurements, sediment sampling, in-situ testing of sediment strength, and measurements of beach topography, was collected at multiple locations throughout the last years. This conference contribution will focus on a subset of measurements collected at Ocean Cape, Yakutat, Alaska, characterized by a medium sand beach comprised of predominantly quartz sand with a significant amount of heavy minerals and an energetic wave climate. The beach also features a complex morphology, sometimes exhibiting a ridge-runnel profile and including a large cobble to boulder beach step.

REGIONAL CONTEXT

Yakutat is located in Southeast Alaska (Figure E.1). Most of its offshore directed beaches are composed of quartz sands with a significant amount of heavy minerals (Wright 1972). The area is characterized by an energetic wave climate, reaching significant wave heights of up to 10 m at Cannon Beach just south of the survey site (Tschetter et al. 2016). The energetic wave climate is reflected by the thin and fairly steep beach at Ocean Cape, observations of berm erosion leading to tree removal, and breaking waves. The beach of Ocean Cape features a cobble-sand beach toe with an abundance of large boulders. Beach scarp evolution as well as a ridge-runnel system have been observed by the authors occasionally from 2014-2019, but not consistently. Therefore, there is clear evidence for local erosional processes and active geomorphodynamics. Ocean Cape represents the southern point of the entrance to Yakutat Bay.

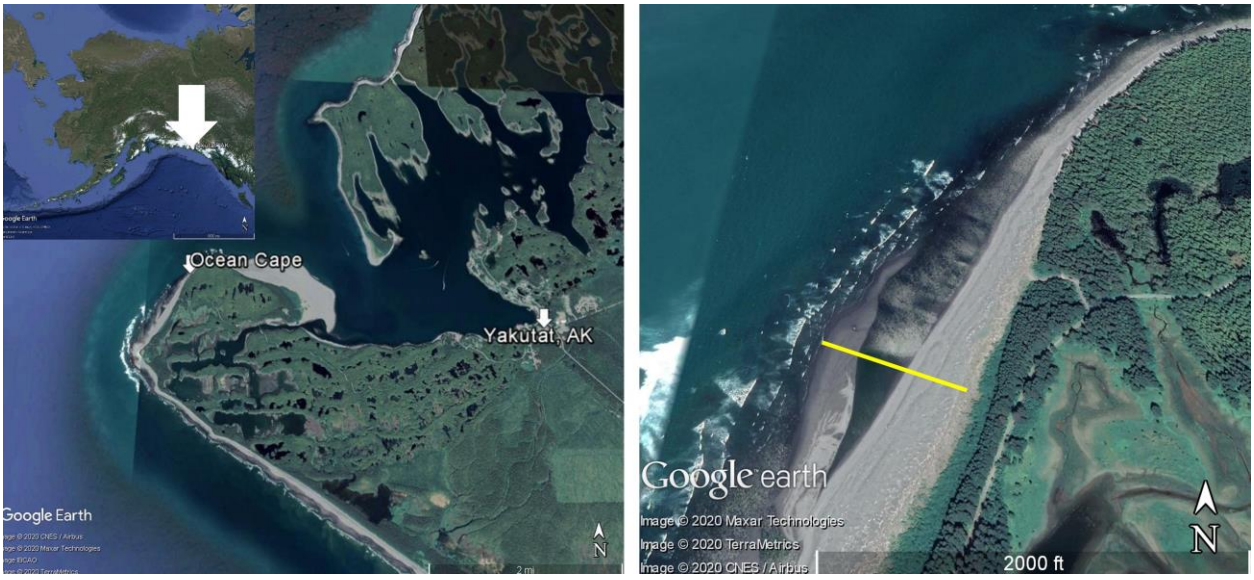

Figure E.1: Google Earth (2020) images showing the location in Alaska (top left zoom), Ocean Cape in the context of Yakutat Bay and the city of Yakutat (left), and a close up (right) with the transect location highlighted as yellow line.

METHODS

In this conference article, a data subset of a larger, multi-location field study will be presented and discussed focusing on beach-based measurements of geomorphology and soil properties at Ocean Cape collected on August 17 and 18, 2019. Measurements from August 14 and 15, 2018 will serve a temporal comparison but will not be focus of this article. Some additional details about the results from 2018 can also be found in Stark and Manning (2019).

Measurements targeted local geomorphology, sediment properties, and geotechnical soil properties. To assess local geomorphology, an optic satellite image was taken by the WorldView 3 satellite, and profiles of beach topography were collected along a cross-shore directed profile by measuring differential height approximately every 3 m along the profile. Distances between the measurement points were extended or shortened depending on obvious changes in topography. Other measuring techniques would potentially have enabled more accurate measurements of topography, but logistical restrictions led to the decision of utilizing this simple method.

Sediment samples were carefully collected using a push tube of known volume. By means of weighing, drying and re-weighing, the bulk unit weight, dry unit weight, and gravimetric water content (ratio of mass of water and mass of soil), the volumetric water content (ratio of volume of water and total volume of sample), and void ratio were determined. The relative density was

derived from the determined void ratios of the sample, and laboratory tests of minimum and maximum void ratios of the material. Samples were collected at six locations along the cross-shore profile (referred to as OC1-6 from now on), with OC1 being located most onshore and OC6 closest to the water line (Fig. 1). Moisture contents were measured in-situ at the same locations using a *Dynamax SM150* soil moisture gauge with an absolute accuracy of ± 3.0% volumetric water content.

Sediment strength was measured in three independent ways using (i) the vane shear option of the *GeoTAC Soil Saber*, (ii) the penetrometer option of the *GeoTAC Soil Saber*, and (iii) the portable free fall penetrometer *BlueDrop* by *BlueCDesigns*. The *Soil Saber* is a novel field survey tool that provides a digital measurement of soil resistance against rotation of a vane (with similar vane blade options as for a traditional laboratory mini-vane shear device) or against an approximately 5 mm wide squared bar that is being pushed into the soil. In both cases, penetration or rotation is manually controlled what may lead to some effects of variations in rotational or penetration velocity, but an effort was made to apply a consistent speed. The vane shear option was utilized despite the cohesionless soils, following the concept presented by Sassa et al. (2014) to investigate effects of apparent cohesion. The portable free fall penetrometer (FFP) was designed for subaqueous seafloor investigations. However, it has recently been used for beach surveys to provide a consistent measurement from the subaerial zone to the nearshore zone (i.e., in water) by e.g., Reeves et al. (2018). The device is dropped from approximate one meter above the ground and impacts the soil in free fall. While the device penetrates the soil at changing velocities (i.e., decreasing velocity when the device is being slowed down and eventually stopped by the soil), impact velocity can be considered constant with a consistent drop height following the physics of free fall. The device measures its own motion, and by doing so, the deceleration experienced during impact. Then, deceleration can be related to sediment resistance and strength, or serve as a direct proxy for changes in soil strength (e.g., Stark et al. 2012).

RESULTS AND DISCUSSION

Ocean Cape beach features significant longshore changes in beach width (Figure E.1 right). On the day when the multispectral satellite image was taken (July 26, 2019), the main beach width was ~ 106 m from vegetation to the sand-cobble beach toe plus another ~ 100 m intertidal beach toe in front of the beach access road. Going towards the northeast, the smallest beach width measured less than 10 m plus ~ 50 m of cobbles and boulders at the point before widening eastwards towards Point Carrew. The plane view satellite image already suggests the possibility of a ridge runnel system towards the South of Ocean Cape beach. However, the beach profile (Figure E.2) reveals the full complexity of the local geomorphology with three sets of changing from a steep beach slope of approximately 5-15° (decreasing elevation towards the water) to -2-3° (increasing elevation towards water) until reaching the flatter toe at 1-3° of beach slope.

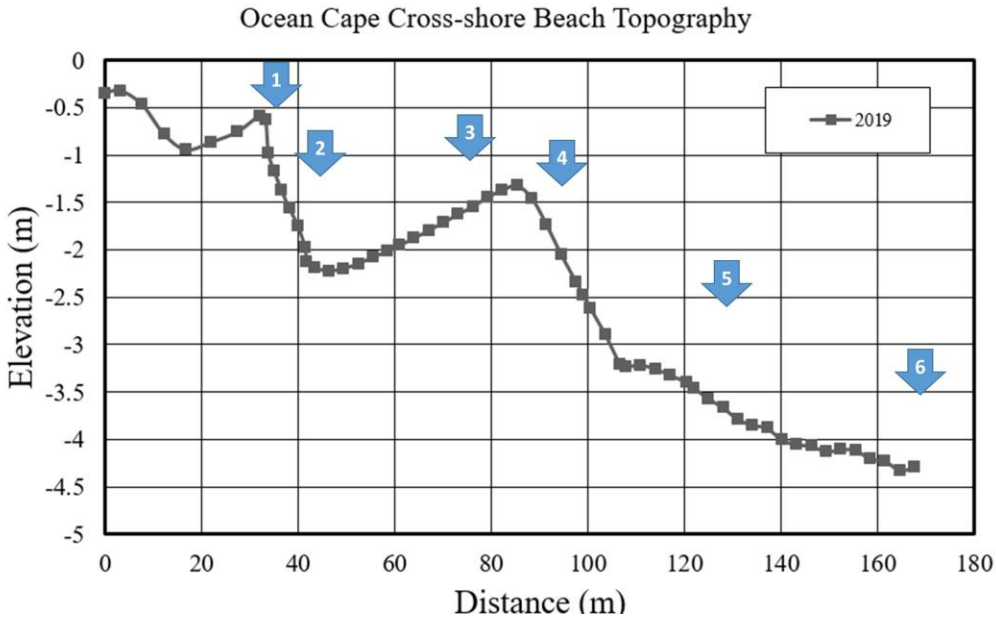

Figure E.2: Cross-shore beach topography measured in August 2019 along the transect shown in Figure E.1. Measurement locations OC 1-6 are highlighted as blue arrows.

It can easily be imagined that this complex topography has major impacts on local groundwater dynamics (Horn 2002), as well as surf and wash sediment transport (Baldock et al. 2011; Masselink et al. 2011). While a direct comparison to the 2018 topography appears difficult due to a mismatch in the longshore starting point, and the significant variations in the longshore direction, none of the measured profiles from 2018 suggested the three ridges/terraces profile as seen in 2019 (Figure E.2), but only documented the presence of one or two ridges/terraces. Similar significant variations

in beach cross-shore topography have been noted at other beaches with energetic wave climates such as Carmel, California, USA (Komar 1998). Following beach classification schemes such as by Masselink et al. (2011), this points at a reflective to intermediate barred (high tide reflective to low tide dissipative) beach with a low relative tidal range (i.e., wave breaker heights are relatively large compared to the mean spring tide range) and a low to medium dimensionless fall velocity (ratio of breaker height over sediment fall velocity of mid-beachface sediments times wave period).

Sediment grab samples confirmed a medium sand beach (median grain size d_{50} ranged from 0.25-0.30 mm) with limited variations in grain size other than the increasing abundance of cobbles and boulders towards the low water shoreline. In 2018, sediment samples appeared biased by either inconsistent filling of the tube or handling during transport to derive reliable values of bulk density. While trends in water content appeared valid, the magnitude of estimated water contents (up to <24% gravimetric water content; Manning and Stark 2019) appeared somewhat low. Therefore, sediment sampling was carried out with utmost care and special preparation of short push tubes which were filled entirely and closed in place in 2019. Figure E.3 displays the measurements of bulk density at two consecutive days. Figure E.4 shows the gravimetric moisture content for the same days determined from sampling and with the in-situ moisture gage. Differences in tidal state or weather were negligible between those dates. Thus, differences in the results were negligible.

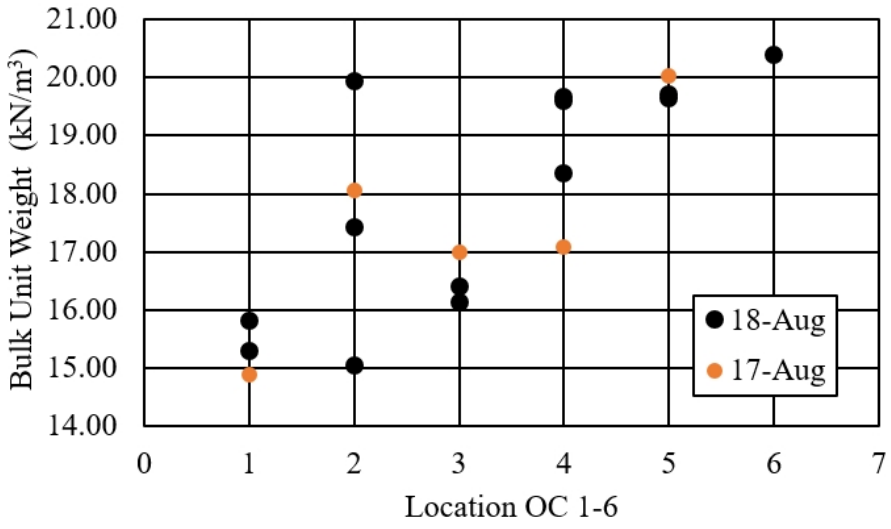

Figure E.3: Bulk unit weight of sediment samples at locations OC 1-6 (towards the ocean) on August 17 and 18, 2019.

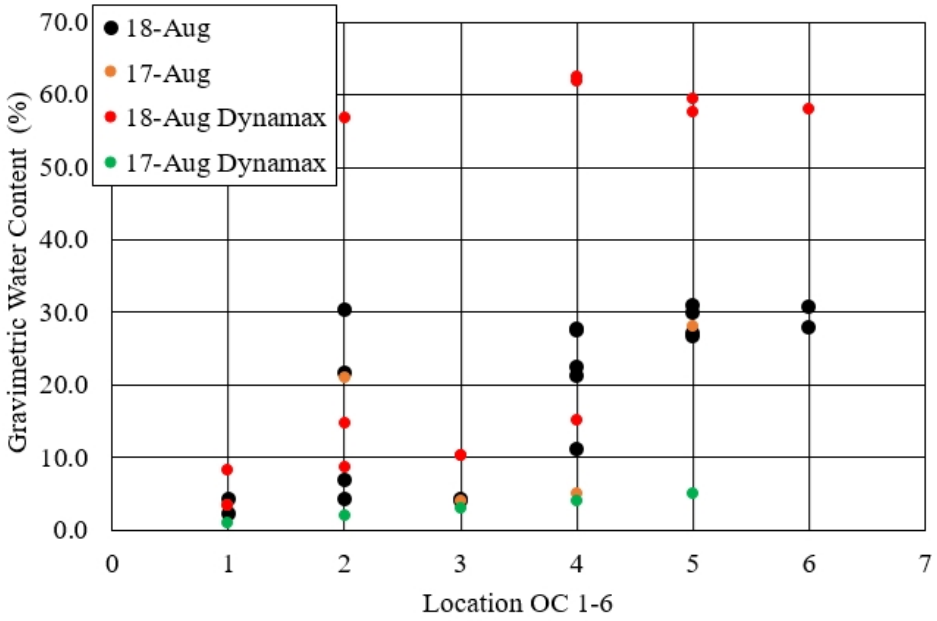

Figure E.4: Gravimetric water content of sediment samples and in-situ (Dynamax) at locations OC 1-6 (towards the ocean) on August 17 and 18, 2019.

Generally, a trend of increasing bulk density towards the shoreline can be observed. Locations OC 2 and 4, the former in the deepest runnel and OC 4 at the transition between ridge and steep slope, were affected by most variability between tests repeated in the same area (radius < 10 m) (Figure E.3). The same applies to the gravimetric moisture contents, showing the expected increase in moisture content with decreasing distance to the water and most variability at locations OC 2 and 4 (Figure E.4). Readings of the in-situ moisture gauge appeared erroneous on August 17, 2019, in response to handling issues. On August 18, the readings appeared valid and suggested that in-situ moisture contents of >50% were achieved at one location at OC 2, two locations at OC4, and at all locations at OC 5 and 6. This may suggest that even the careful sample extraction may limit the retaining of moisture contents, and that moisture contents beyond 35% can hardly be preserved unless additional mechanisms such as suction are being applied during sample extraction of cohesionless sediments. At the same time, the moisture gage readings may also generally be high due to calibration limitations associated with seawater salinity. Nevertheless, the sample data highlights the complexity in moisture contents and bulk density at a barred beach. Particle packing and bulk density is known to affect the critical shear stress needed to mobilize sediments (e.g., Bagnold 1966), and moisture content impacts significantly the potential for aeolian sediment transport (e.g., Bauer et al. 2009). Reeves et al. (2018) also hypothesized that the increase in sediment strength from the subaerial zone to the swash zone of a sandy beach was related to a

combination of moisture content and bulk density. The data collected here support noticeable and likely related trends and variations in these properties.

Results from the three different ways of measuring in-situ sediment strength of the upper 10 cm of the beachface sediments are displayed in Figure E.5. The measure of sediment strength can be expected to reflect the sand's in-situ effective friction angle, as well as potential effects of apparent cohesion from partial saturation where applicable (Briaud 2013; Sassa et al. 2014).

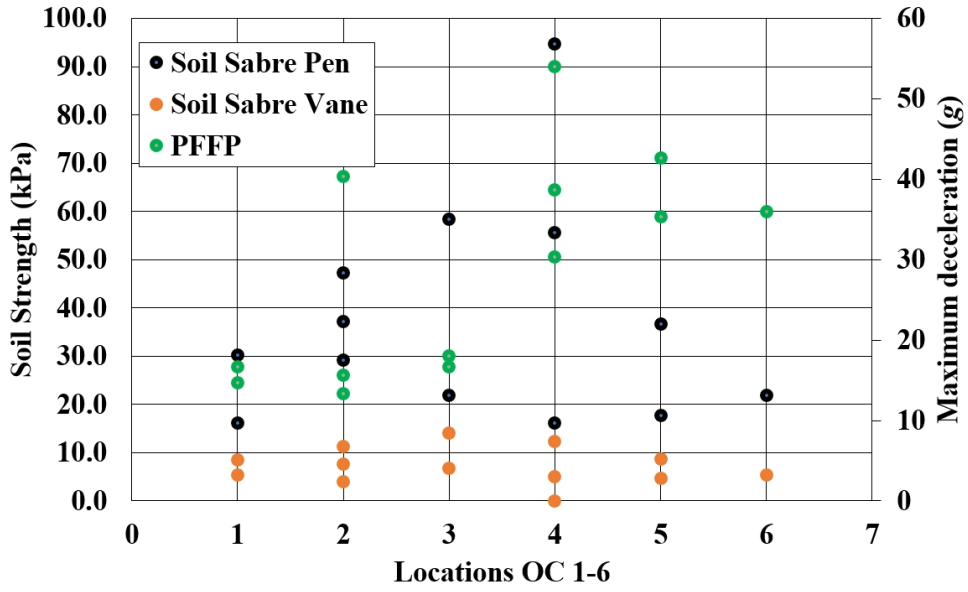

Figure E.5: Sediment strength measured using the *Soil Saber* penetrometer and vane and maximum deceleration measured by the PFFP *BlueDrop* as a proxy of sediment strength locations at OC 1-6 (towards the ocean) on August 18, 2019.

The three methods yielded noticeably different results. The maximum deceleration was used here as a measure of variations in sediment resistance to avoid effects from empirical parameters needed for further processing of the FFP data. Impact velocities were consistently ~ 5 m/s for all deployments considered here, enabling this direct comparison of changes in maximum deceleration (Stoll et al. 2007). The vane shear yielded overall lower sediment strength values than the penetrometer. Such significant differences between vane shear results and penetrometers are well known, and therefore, expected (e.g., Lunne et al. 1976). The vane shear results are not mimicking trends observed in bulk density or moisture content, but exhibit somewhat of an increase in strength towards OC 3 (low water content and moderate bulk density), and then a decrease in strength towards areas of higher moisture contents. This may suggest a closer

relationship to moisture contents which are known to affect sediment strength through an apparent cohesion in a non-linear way (Briaud 2013; Sassa et al. 2014). The Soil Saber penetrometer readings suggested most variability in strength at positions OC2 and 4, similarly to observations in bulk density and water content. However, some inconsistency between repeated tests at locations OC 3 and 5 makes it overall difficult to identify possible trends. One may argue that the data suggests a similar trend as the vane shear with an increase in strength towards OC 3-4 coming from the onshore and offshore directions. For the FFP results, most variability between repeated tests were observed again at locations OC 2 and 4. However, the FFP seemed to suggest generally weaker soils from OC 1 to 3 and significant stronger sediments from OC 4 to 6 where also water content and bulk density were higher. This matches observations by Reeves et al. (2018) and Manning and Stark (2019) at sandy beaches. The FFP is larger in size and faster in penetration than the Soil Saber penetrometer. This means a different drainage regime may apply to the different penetrometers with likely fully drained to partially drained conditions for the Soil Saber penetrometer and fully undrained to partially drained conditions for the FFP. The latter would suggest that viscosity effects of the pore water (i.e., viscosity driven strain rate effects) may add to sediment resistance instead of seeing the non-linear water content – strength behavior (Albatal et al. 2019). It can be summarized that in-situ soil strength of a sandy beach at Ocean Cape appears to be related to variations in moisture content and somewhat bulk density, but that special attention has to be given to the method of in-situ soil strength measurement and its process-based relationship to moisture contents. It is expected that these variations in geotechnical soil behavior across sandy beach environments affect local sediment erodibility, i.e., that local erodibility may vary noticeable spatiotemporally at sandy beaches even if variations in grain size are limited.

CONCLUSIONS

In current erosion prediction and assessment models often only limited geotechnical sediment properties are considered, or if so, they are considered constant. In this preliminary study, significant variations in soil strength, moisture content, and bulk density were found along a cross-shore transect of complex geomorphology and known for active erosion and sediment remobilization processes. Variations in these properties are expected to affect local erodibility and to vary on different temporal and spatial scales. Difficulties in high quality sediment sampling to preserve geotechnical soil properties of cohesionless sediments as well as differences in in-situ testing of soil strength were identified as challenges to obtain data sets that may enable an

integration of geotechnical soil properties into erosion prediction and assessment. However, the latter differences may also offer insights into soil behavior to different stresses. In conclusion, geotechnical properties of surficial beach sands can vary significantly across beaches characterized by a complex geomorphology and active erosion and sediment remobilization processes. However, no detailed guidance exists yet about best practices to measure geotechnical properties at intertidal sand beaches, and significant differences in sensitivity to different environmental conditions of the respective methods were expected and confirmed. More data sets are needed to gain a more fundamental understanding of the soil behavior and governing processes, but also more research is needed regarding the optimization of data collection strategies. The potential knowledge gained from inclusion of geotechnical processes and properties will likely contribute to the improvement of beach erosion prediction and assessment.

ACKNOWLEDGEMENTS

The authors acknowledge funding by the National Science Foundation through grant CMMI-1751463. The authors would like to thank the City and Borough of Yakutat (and particularly the late Rhonda Coston) for on site support. Field measurements were assisted by the Virginia Tech and University of New Hampshire undergraduate group of the 2019 Coastal Geotechnical Field Research Experience. Furthermore, the authors would like to acknowledge Virginia Tech graduate students Julie Paprocki and Matthew Florence. The authors would also like to acknowledge Ming Xiao for review and constructive comments that led to the improvement of this article.

REFERENCES

Albatal, A., Stark, N., & Castellanos, B. (2020). Estimating in situ relative density and friction angle of nearshore sand from portable free-fall penetrometer tests. *Canadian Geotechnical Journal, 57*(1), 17-31.

Baldock, T. E., Alsina, J. A., Caceres, I., Vicinanza, D., Contestabile, P., Power, H., & Sanchez-Arcilla, A. (2011). Large-scale experiments on beach profile evolution and surf and swash zone sediment transport induced by long waves, wave groups and random waves. *Coastal Engineering, 58*(2), 214-227.

Bauer, B. O., Davidson-Arnott, R. G. D., Hesp, P. A., Namikas, S. L., Ollerhead, J., & Walker, I. J. (2009). Aeolian sediment transport on a beach: Surface moisture, wind fetch, and mean transport. *Geomorphology*, *105*(1-2), 106-116.

Briaud, J. L. (2013). *Geotechnical engineering: unsaturated and saturated soils*. John Wiley & Sons.

Davidson-Arnott, R. G., MacQuarrie, K., & Aagaard, T. (2005). The effect of wind gusts, moisture content and fetch length on sand transport on a beach. *Geomorphology*, *68*(1-2), 115-129.

Darke, I., & Neuman, C. M. (2008). Field study of beach water content as a guide to wind erosion potential. *Journal of Coastal Research*, 1200-1208.

Erikson, L. H., Larson, M., & Hanson, H. (2007). Laboratory investigation of beach scarp and dune recession due to notching and subsequent failure. *Marine Geology*, *245*(1-4), 1-19.

Gallagher, E. L., MacMahan, J., Reniers, A. J. H. M., Brown, J., & Thornton, E. B. (2011). Grain size variability on a rip-channeled beach. *Marine Geology*, *287*(1-4), 43-53.

Gallagher, E., Wadman, H., McNinch, J., Reniers, A., & Koktas, M. (2016). A conceptual model for spatial grain size variability on the surface of and within beaches. *Journal of Marine Science and Engineering*, *4*(2), 38.

Horn, D. P. (2002). Beach groundwater dynamics. *Geomorphology*, *48*(1-3), 121-146.

Kirchner, J. W., Dietrich, W. E., Iseya, F., & Ikeda, H. (1990). The variability of critical shear stress, friction angle, and grain protrusion in water-worked sediments. *Sedimentology*, *37*(4), 647-672.

Komar, P. D. (1998). *Beach processes and sedimentation*. Prentice Hall, New Jersey.

Lunne, T., Eide, O., & Ruiter, J. D. (1976). Correlations between cone resistance and vane shear strength in some Scandinavian soft to medium stiff clays. *Canadian geotechnical journal*, *13*(4), 430-441.

Manning, M., & Stark, N. (2019). Investigating moisture contents of sandy beaches in the context of a geotechnical site characterization. *Proceedings of the 9th International*

Conference on Coastal Sediments 2019, Tampa/St. Petersburg, FL, USA 27-31 May 2019, https://doi.org/10.1142/11391.

Masselink, G., & Short, A. D. (1993). The effect of tide range on beach morphodynamics and morphology: a conceptual beach model. *Journal of coastal research*, 785-800.

Masselink, G., Hughes, M., & Knight, J. (2011). *Introduction to coastal processes and geomorphology*. Hodder Education, London, UK.

Medina, R., Losada, M. A., Losada, I. J., & Vidal, C. (1994). Temporal and spatial relationship between sediment grain size and beach profile. *Marine Geology*, *118*(3-4), 195-206.

Reeves, B., Stark, N., & Mewis, P. (2018). Cross-shore variations in sediment strength at a sandy beach. *Coastal Engineering Proceedings*, *1*(36), 83.

Sassa, S., Yang, S., Watabe, Y., Kajihara, N., & Takada, Y. (2014). Role of suction in sandy beach habitats and the distributions of three amphipod and isopod species. *Journal of sea research*, *85*, 336-342.

Sassa, S., & Yang, S. (2019). Role of geoenvironmental dynamics in the biodiversity of sandy beaches and sandflats: the ecohabitat chart and its ecological implications. *Estuarine, Coastal and Shelf Science*, *219*, 278-290.

Shields, A. (1936). Anwendung der Aehnlichkeitsmechanik und der Turbulenzforschung auf die Geschiebebewegung. *PhD Thesis Technical University Berlin*.

Stark, N., Wilkens, R., Ernstsen, V. B., Lambers-Huesmann, M., Stegmann, S., & Kopf, A. (2012). Geotechnical properties of sandy seafloors and the consequences for dynamic penetrometer interpretations: quartz sand versus carbonate sand. *Geotechnical and Geological Engineering*, *30*(1), 1-14.

Stoll, R. D., Sun, Y. F., & Bitte, I. (2007). Seafloor properties from penetrometer tests. *IEEE Journal of Oceanic Engineering*, 32(1), 57-63.

Tschetter, T., Kasper, J. L., & Duvoy, P. X. (2016). Yakutat Area Wave Resource Assessment. *Final Report to the Alaska Energy Authority*.

Van Dijk, P. M., Stroosnijder, L., & De Lima, J. L. M. P. (1996). The influence of rainfall on transport of beach sand by wind. *Earth Surface Processes and Landforms*, *21*(4), 341-352.

Van Rijn, L. C. (2007). Unified view of sediment transport by currents and waves. I: Initiation of motion, bed roughness, and bed-load transport. *Journal of hydraulic engineering*, *133*(6), 649-667.

Wright, F. F. (1972). Marine geology of Yakutat Bay, Alaska. *US Geological Survey Professional Paper*, *800*, 9-15.

Wright, L. D., & Short, A. D. (1984). Morphodynamic variability of surf zones and beaches: a synthesis. *Marine geology*, *56*(1-4), 93-118.

Appendix F: Extended Field Study of a Large Spit in an Area of High Seismicity

The contributions of the authors to the composition of this manuscript are delineated as follows:

Nicola Brilli:

- Initiated research idea and participated in the field survey in Yakutat, Alaska
- Processed and analyzed field data, prepared figures, tables, and draft of abstract
- Revised abstract and poster based on suggestions of co-authors

Nina Stark:

- Co-developed the refined research questions
- Planned and supervised the field survey in Yakutat, Alaska
- Reviewed and edited the draft abstract and poster before submission

Extended Field Study of a Large Spit in an Area of High Seismicity

Nicola C. Brilli[1] and Nina Stark[2], Ph.D.

[1]Virginia Tech, Department of Civil and Environmental Engineering, Blacksburg, VA 24060; e-mail: nickb96@vt.edu

[2]Virginia Tech, Department of Civil and Environmental Engineering, Blacksburg, VA 24060; e-mail: ninas@vt.edu

The authors of this abstract submitted it to the Proceedings of the Geological Society of America Penrose Conference: Climactic Controls on Continental Erosion and Sediment Transport, Juneau, Alaska, August 4-10th, 2019

F.1. Abstract

An extended field survey will be conducted from June-August 2019, in Yakutat, AK. The goal of this survey will be studying the evolution of a large (1 km^2) sandy spit, with specific focus on the variations in sediment strength across the spit during the study. This spit is of interest due to its location in an area of high seismic activity. Using satellite imagery, an event was identified to have eroded approximately 0.4 km^2, likely due to seismically induced liquefaction or a submarine landslide. The spit will be surveyed 2-3 times per week (with occasional offshore work), including PFFP deployments to measure sediment strength, moisture content measurements, and topographic surveying. The presentation will detail the initial results, discuss new insights on this particular site's susceptibility to large, seismically induced, erosion events, and highlight the effects of such events on sediment transport mechanisms and the morphology of the spit.

INTRODUCTION

In Summer 2018 & ‘19, field surveys were conducted at Point Carrew, a sandy spit near Yakutat, AK. The spit forms as strong longshore transport NW along the Gulf of Alaska reaches a peninsula at the mouth of Yakutat Bay [1] which combines with wave refraction around the peninsula to deposit sediment in the protected bay to the NE (Figure F.1).

Figure F.1: Regional Context: Phipps Peninsula. Samples and measurements were taken along Transect A. Google Earth Pro V 7.3.2. (6/25/2019) Yakutat, AK, 59°32'13.86"N, 139°49'14.96"W

RESEARCH QUESTIONS

1. How does sediment strength differ along a transect at the spit?

2. How does the measured crosshore strength profile compare to two other sites at the peninsula?

3. Can site-specific morphology and/or hydrodynamics explain the strength differences?

4. Does the high seismic activity in this area have any effects on the spit?

MEASUREMENT TECHNIQUES

- Topographic Profiling: A basic differential levelling method, two sticks and a level rope, local school children assisted in surveys.

- Sediment Strength: *blueDrop* portable free-fall penetrometer (PFFP) gives an estimate of in-situ bearing capacity.

Figure F.2: Yakutat middle schoolers collecting beach profiles (left), the author holding the blueDrop PFFP for beach deployments (right)

SEDIMENT PROFILE AT POINT CARREW (TRANSECT A)

- Main Body: Wind-blown sediment, consistent strengths (Figure F.3)
- Ridge-Runnel: Basin often saturated, constant reworking, lower strengths
- Intertidal/Swash: Densification due to waves, added strength due to partial saturation, large strength increase.

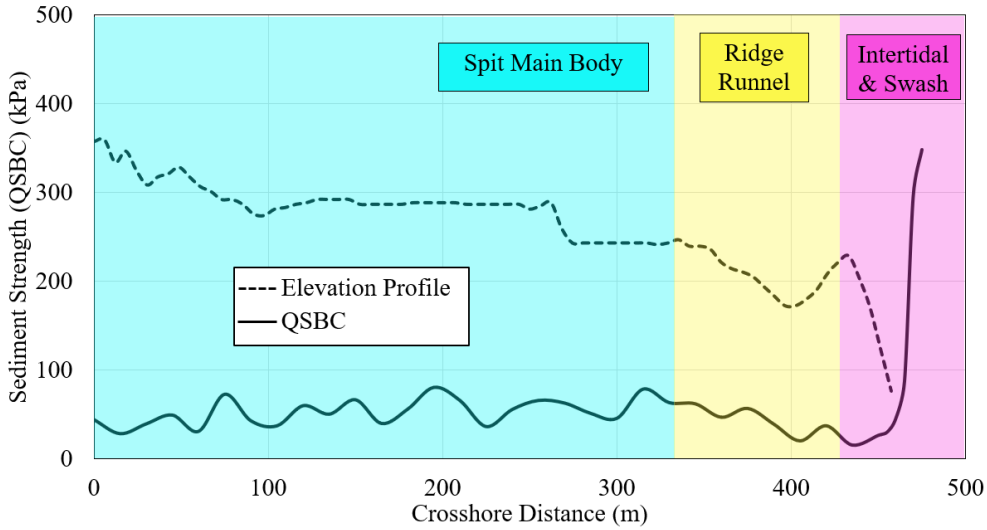

Figure F.3: Elevation & variation in sediment strength across Transect A at Point Carrew

ADDITIONAL FIELD SITES

Two additional sites with different morphologies and hydrodynamics were surveyed for comparison (Figure F.4).

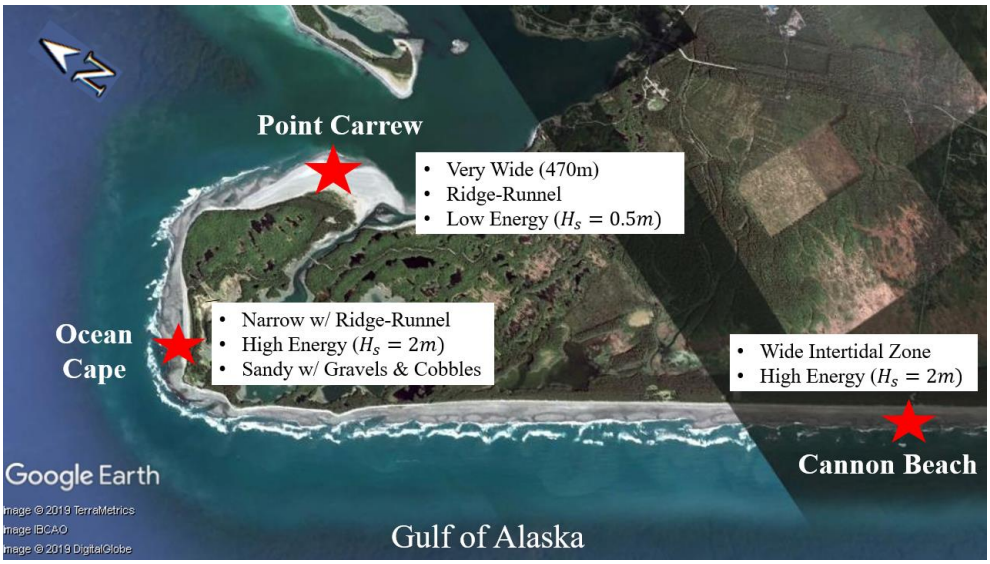

Figure F.4: Location of and descriptions of Point Carrew, Ocean Cape & Cannon Beach field sites.

STRENGTH COMPARISONS TO POINT CARREW

- Cannon Beach: Higher energy = higher strength from densification, wide intertidal + tide/partial saturation interaction = high intertidal variability.
- Ocean Cape: Ridge-runnel = similar strength decrease. Same swash zone increases due to higher energy as Cannon Beach (Figure F.5).

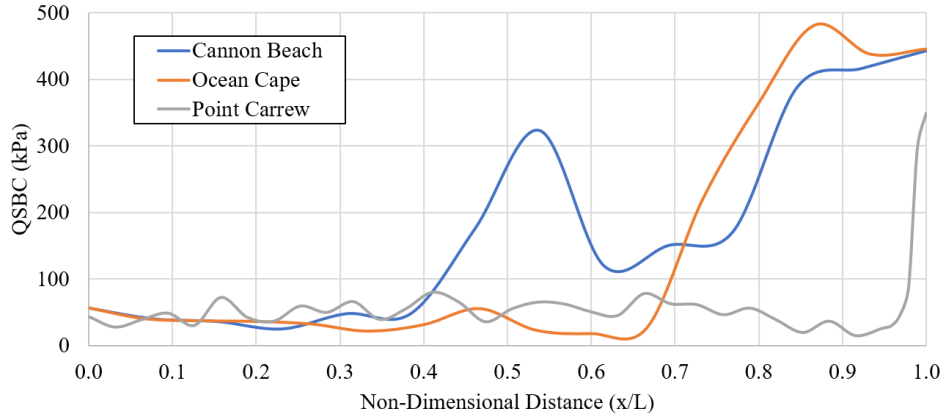

Figure F.5: Strength profiles for the three field sites plotted versus non-dimensional distance

EVIDENCE OF SIESMIC ACTIVITY

- An unidentified, likely seismic, event in 1997 caused the loss of over 400,000 meters^2 of the spit's surface area.
- Yehle (1971) reported that beach deposits in the area were susceptible to liquefaction and/or submarine landslides due to earthquakes.
- Evidence of the event remains, seen by a distinct drop in elevation at the point on the profile where the erosion occurred (Figure F.6, red).

Figure F.6: Satellite Images Detailing a Large Erosive Event (Top) Source: Google Earth, 12/30/1996 (Left) & 12/30/1997 (Right). Elevation Profile Showing the Drop Tied to the Event (Bottom).

CONCLUSIONS

- Sed. strength is consistent across the main body of the spit, as it is unaffected by tides/waves, decreases in the runnel due to reworking, and increases near the water due to densification.
- This strength profile differs from other areas of the peninsula, which is tied to differing morphologies and hydrodynamics.

- Analysis of satellite imagery revealed a large erosion event in 1997, likely tied to seismic activity in the area.

ACKNOWLEDGEMENTS

The authors acknowledge funding by the National Science Foundation through grant CMMI-1751463. The authors would like to thank Julie Paprocki, Dennis Kiptoo, and the undergraduate students of the Coastal Geotechnical Field Research Experience 2018 for support in the field. Additional thanks go the City and Borough of Yakutat, and specifically, Rhonda Coston, Irving Grass, and Jon Eriksson.

REFERENCES

[1] Yehle, L.A. (1971). “Reconnaissance Engineering Geology of the Yakutat Area, Alaska, With Emphasis on Evaluation of Earthquake and Other Geologic Hazards.” Geological Survey Professional Paper 1074. USGS.

Appendix G: Implications of Geotechnical and Erodibility Assessment in Harrison Bay, Alaska for Numerical Modelling Applications

The contributions of the authors to the composition of this manuscript are delineated as follows:

Nicola Brilli:
- Participated in the field survey in Harrison Bay, Alaska
- Conducted all laboratory analysis of gravity core samples
- Performed literature review; processed and analyzed field data; prepared figures, tables, and draft of manuscript
- Revised manuscript based on suggestions of co-authors

Nina Stark:
- Co-primary investigator of this study
- Initiated research idea and co-developed the refined research questions
- Planned and participated in the field survey in Harrison Bay, Alaska
- Reviewed and edited the draft manuscript

Emily Eidam:
- Co-primary investigator of this study
- Initiated research idea and co-developed the refined research questions
- Planned, supervised, and participated in the field survey in Harrison Bay, Alaska serving as Chief Scientist
- Reviewed and edited the draft manuscript

Jaap Nienhuis:
- Participated in the field survey in Harrison Bay, Alaska
- Provided recommendations and suggestions on numerical modelling
- Reviewed and edited the draft manuscript

Caroline Cooper:
- Performed numerical modelling of the site in Delft3D
- Reviewed and edited the draft manuscript

G.1. Overview

The work presented in Chapter highlighted the variability in seabed sediments in Harrison Bay (Figure 5.5), as well as the associated variability in erodibility (Figure 5.10). While the goal of Chapter 5 was focused on development of a classification scheme based on PFFP measurements, the variability in Figures 5.8 and 5.10 also suggests the need for appropriately characterizing erodibility in morphological models. Thus, a sensitivity analysis was conducted to determine the relative impact of changing erodibility parameters for cohesive soils on model performance, and to assess the importance of including site specific erodibility parameters in such models. Malito et al. (2022) developed a 2D cross-shelf morphodynamic model for Harrison Bay using Delft3D (Lesser et al. 2004, Deltares 2014). Model runs were performed over a 500 year timescale, and present-day wave conditions were considered. The model takes erodibility parameter inputs of τ_c and the Erosion Parameter, M, and inputs are a single value of each parameter for the sand and mud classes. M is related to k_d by multiplying k_d by τ_c and the bulk density of the substrate, ρ_b. The two parameters both describe the rate of erosion at stresses great than τ_c, but k_d does this in terms of volume and M accomplishes this in terms of mass. Table G.1 provides a breakdown of the sediment properties included in the model for each test case. See Malito et al. (2022) for full explanation model setup, domain, and hydrodynamics. As seen in Table G.1, the only parameters varied were τ_c and M for mud. Only the mud erosion parameters were varied in the test cases, as variations in cohesive erodibility parameters became more readily important for the purposes of the study, as discussed in Chapter 5.

Table G.1: Model Parameters for Delft3D sensitivity testing (changes between test cases are highlighted in bold).

	Test Case		
Model Parameters	**HB-Original**	**HB1**	**HB2**
Sand, Non-Cohesive d_{50} (mm)	0.11	0.11	0.11
Cohesive Settling Velocity (mm/s)	1	1	1
Volumetric Sand Fraction	29	29	29
Volumetric Mud Fraction	71	71	71
Sand Porosity	0.4	0.4	0.4
Mud Porosity	0.6	0.6	0.6
Sand τ_c (Pa)	0.23	0.23	0.23
Mud τ_c (Pa)	**0.5**	**5**	**5**
Sand Erosion Parameter, M $(kg/m^2/s)$	0.0001	0.0001	0.0001
Mud Erosion Parameter, M $(kg/m^2/s)$	**0.0001**	**0.25**	**1**

As seen from Table G.1, τ_c was changed from 0.5 kPa to 5 kPa, and M was changed to 0.25 $\mathrm{kg/m^2/s}$ and 1.0 $\mathrm{kg/m^2/s}$, or an equivalent k_d of 0.01 $\frac{\mathrm{cm^3}}{\mathrm{N-s}}$ to 30 $\frac{\mathrm{cm^3}}{\mathrm{N-s}}$. These changes in parameters reflect the in-situ erosion parameters from the results of the JET tests (Table 5.1). The results of this case study are presented in Figure G.1. As mentioned previously, sand parameters were not changed, as no in-situ measurements were collected for this sediment type. Model run "HB-Original" represents the control model run, and "HB1 & HB2" represent the updated values.

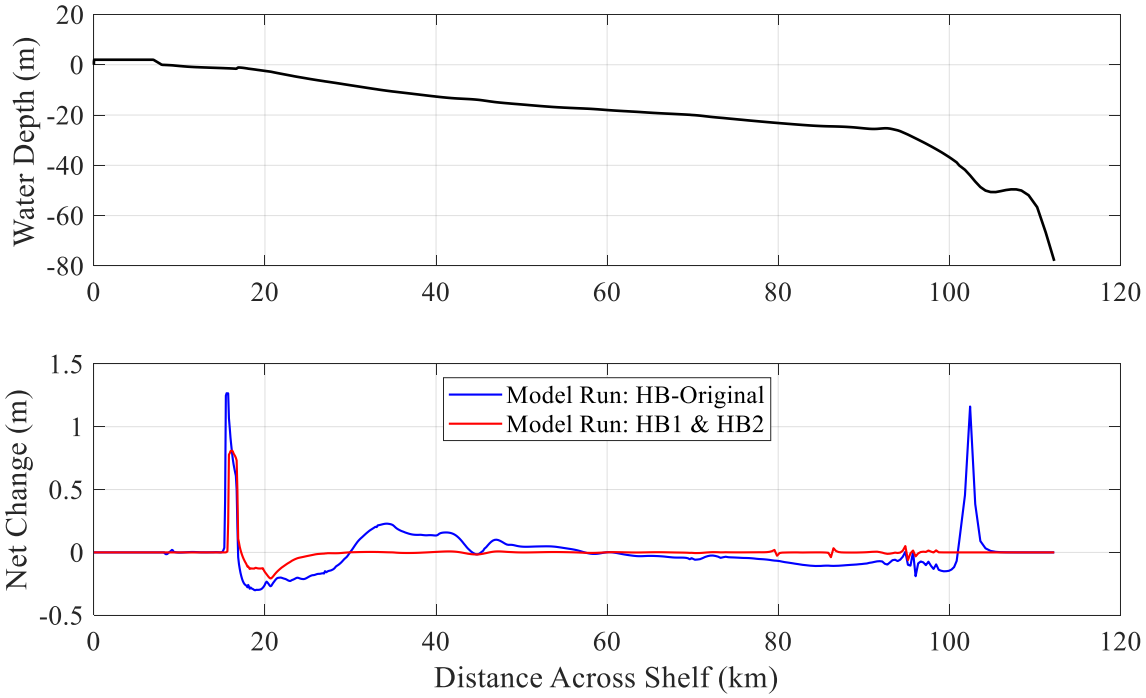

Figure G.1: Results of sensitivity analysis. Top panel shows shelf bathymetry before 500yr time-scale model runs, and bottom panel shows net changes in elevation across the shelf after the 500yr run for 3 test cases with different erodibility parameters.

The top panel of Figure G.1 shows the shelf profile, and the bottom panel shows net elevation change over the 500 year time period. The model run with updated erodibility parameters showed significantly less elevation change than the original. The depositional zone at 18 km was reduced from 1.3 m of deposition to 0.7 m, erosion around 20 km was reduced, and there was virtually no change recorded across the rest of the shelf. This lack of change is likely the result of an order of magnitude increase in τ_c and the model not considering any storms over the time period. Initiation of erosion became more difficult, coupled with calm conditions not generating the necessary flows to induce sediment transport across a majority of the shelf. Still, the differences in morphological

change in this simple example highlights the necessity of including erodibility parameters that reflect the in-situ conditions. Future modelling will test different ranges of τ_c and k_d, with the goal of eventually coupling the sediment classes in the model with the erodibility classification scheme from PFFP measurements. This ongoing work aims to improve long term morphodynamic modelling of Arctic environments by including the large degree of observed variability in sediment properties and erodibility.

REFERENCES

Deltares. (2014). Delft3D User Manual.

Lesser, G. R., Roelvink, J. A., van Kester, J. A. T. M., & Stelling, G. S. (2004). Development and validation of a three-dimensional morphological model. Coastal Engineering, 51(8–9). https://doi.org/10.1016/j.coastaleng.2004.07.014

Malito, J., Eidam, E., & Nienhuis, J. (2022). Increasing Wave Energy Moves Arctic Continental Shelves Toward a New Future. Journal of Geophysical Research: Oceans, 127(9). https://doi.org/10.1029/2021JC018374